Nonlinear Finite-Element Analysis of Casings in High-Temperature Geothermal Wells

Gunnar Skúlason Kaldal

Dissertation submitted in partial fulfillment of a
Philosophiae Doctor degree in Mechanical Engineering

Supervisor
Dr. Magnús Þór Jónsson, University of Iceland

Doctoral Committee
Dr. Magnús Þór Jónsson, Professor, University of Iceland
Dr. Halldór Pálsson, Professor, University of Iceland
Dr. Sigrún Nanna Karlsdóttir, Professor, University of Iceland

Opponents
Dr. Arve Bjørset, Professor II, Western Norway University of Applied Science
Dr. Catalin Teodoriu, Associate Professor, University of Oklahoma

Faculty of Industrial Engineering, Mechanical Engineering and Computer Science
School of Engineering and Natural Sciences
University of Iceland
Reykjavik, May 2019

Nonlinear Finite-Element Analysis of Casings in High-Temperature Geothermal Wells
Dissertation submitted in partial fulfillment of a Philosophiae Doctor degree in Mechanical Engineering

Faculty of Industrial Engineering, Mechanical Engineering and Computer Science
School of Engineering and Natural Sciences
University of Iceland
Hjarðarhagi 2-6
107, Reykjavik
Iceland

Telephone: +354 525 4000

Bibliographic information:
Gunnar Skúlason Kaldal, 2019, *Nonlinear Finite-Element Analysis of Casings in High-Temperature Geothermal Wells*, PhD dissertation, Faculty of Industrial Engineering, Mechanical Engineering and Computer Science, University of Iceland.

ISBN 978-9935-9438-7-3

Author ORCID: 0000-0003-4811-953X

Printing: Háskólaprent
Reykjavik, Iceland, May 2019

Abstract

High-temperature geothermal wells are drilled in stages and constructed of several concentric steel casings that are cemented over their entire external surface for sealing and structural support purposes. The structural integrity of such casings is essential during drilling and for safe operation after the construction phase. High pressures can in some cases cause casing failures but the most powerful mechanical force is driven by large temperature changes from an initially cooled to a hot operating well. Thermal expansion generates large stresses in the casings which are constrained by cement and therefore, in conventional high-temperature wells, permanent plastic strains are formed as the wells warm-up to production temperatures. Elevated temperatures cause material strength reduction, further increasing the risk of failures. Casing failures, e.g. collapse and axial tensile rupture, can occur during the lifetime of wells and it is important to analyze the load history of casings thoroughly to evaluate risks of such failures. With recent increasing interest in drilling deeper geothermal wells, for seeking higher enthalpy geothermal fluids, the strength of the casing becomes one of the limiting factors due to higher temperatures, pressures, and difficult corrosive conditions. The structural integrity of the casing of otherwise productive wells can determine if they are a success or not. Nonlinear material properties, large displacements and connections between multiple contacting surfaces form a structural system which in this thesis is analyzed numerically with the use of the nonlinear finite-element method (FEM). The resulting models provide tools that are used for structural analysis in support to failure analysis, well design and material selection. This thesis describes problems of casing failures and structural analysis that provide a platform for better understanding and improvements of casings in high-temperature geothermal wells.

Keywords: High-temperature geothermal wells, steel casings, thermal expansion, thermo-mechanical loads, structural analysis, nonlinear finite-element analysis.

Útdráttur

Háhitaborholur eru boraðar í áföngum og fóðraðar með stálfóðringum sem eru steyptar að utanverðu. Vegna öryggissjónarmiða verður að vera hægt að beisla jarðhitavökva jafnt í borun sem og í vinnslu eftir að framkvæmdum er lokið. Í öllum tilvikum þarf burðarþol fóðringa að vera tryggt. Á meðan borun stendur er borholum haldið köldum með hringdælingu borleðju eða ádælingu með vatni. Þegar þær hitna eftir borun getur hitastigshækkunin orðið umtalsverð. Varmaþensla veldur spennumyndun í fóðringunum vegna skorðunar steypunnar. Þegar hefðbundnar háhitaholur hitna myndast því háar spennur sem í flestum tilvikum valda varanlegum formbreytingum. Að auki veldur hátt hitastig styrktarveikingu í stáli og steypu sem leiðir til aukinnar hættu á skemmdum. Fóðringaskemmdir, s.s. gúlpmyndun og togslit, geta orðið á mismunandi stigum á líftíma borholna og er því mikilvægt að greina ítarlega álagssögu fóðringa til að skilja möguleg álagstilfelli og hættur sem fylgja. Með auknum áhuga á djúpborun til vinnslu á orkuríkum jarðvarmavökva verður burðarþol fóðringa einn af takamarkandi þáttunum vegna hærra hitastigs, þrýstings, og aukinnar efnisáraunar í formi tæringar. Afkastageta borholna ræðst ekki einungis af því að gjöfular æðar séu rofnar í borun heldur einnig af líftíma mannvirkisins. Ólínulegir efniseiginleikar, færslur og tenging á milli yfirborða í borholum mynda burðarþolskerfi sem ekki er auðleysanlegt með einföldum reikniaðferðum. Burðarþolskerfið er því leyst hér með einingaaðferðinni (e. nonlinear finite-element method) þar sem ólínuleiki kerfisins er tekinn með í reikninginn. Líkönin sem þróuð hafa verið hér er hægt er að nota til burðarþolsgreiningar á fóðringum til varnar skemmdum og til aðstoðar við hönnun og efnisval. Doktorsritgerðin lýsir fóðringaskemmdum og burðarþolsgreiningum sem byggja grunn til betri skilnings á burðarþoli fóðringa háhitaborholna.

Lykilorð: Háhitaborholur, stálfóðringar, varmaþensla, varmaálag, burðarþolsgreining, ólínulega einingaaðferðin.

To Eva, Hrafn Ingi, Sigmar Kári and Birkir Logi,

and my parents Ingibjörg Kaldal and Skúli Víkingsson.

Contents

Nomenclature

A_f	Area of the distributed surface resistance
A_p	Outside area of surface of which pressure is defined normal to
c	Specific heat (J/kg°C)
D	Outer diameter (m)
E	Young's modulus (Pa)
E_T	Tangent modulus (Pa)
F_e^{nd}	Nodal forces applied to an element
k	Foundation stiffness
K	Thermal conductivity coefficient (W/(m°C))
f_c	Compressive strength of cement (Pa)
P	Contact normal pressure (Pa)
P_{wh}	Wellhead pressure (Pa)
R^2	Coefficient of determination (-)
t	Thikness (m)
t	Time

T_i	Initial wellhead temperature (°C)
T_f	Final wellhead temperature (°C)
T_{wh}	Wellhead temperature (°C)
u_{wh}	Wellhead displacement (m)
U	Strain energy (internal work)
V	Volume
W	external work
$[B]$	Strain-displacement matrix
$[D]$	Elastic stiffness matrix (stress-strain matrix)
$[F]$	Deformation gradient
$\{F^a\}$	acceleration (D'Alembert) force vector
$\{F_e^{pr}\}$	Element pressure vector
$\left\{F_e^{th}\right\}$	Element thermal load vector
$[G]$	Matrix of shape function derivatives
$[I]$	Identity matrix
$[K_e]$	Element stiffness matrix
$\left[K_e^f\right]$	Element foundation stiffness matrix
$[M_e]$	Element mass matrix
$[N_n]$	Shape function matrix
$\{P\}$	Applied pressure vector
$[R]$	Rotation matrix
$\{\ddot{u}\}$	Acceleration vector
$[U]$	Shape change stretch matrix

$\{u\}$	Nodal displacement vector
$\{w\}$	Displacement vector
$\{w_n\}$	Motion normal to surface
$\{X_n\}$	Current geometry
$_{st}$	Subscript for steel
$_{co}$	Subscript for cement
$_{ro}$	Subscript for rock formation
α	Thermal expansion coefficient ($°C^{-1}$)
ΔT_w	Wellhead temperature change (°C)
μ	Coefficient of friction (-)
ν	Possion's ratio (-)
ρ	Density (kg/m^3)
τ_b	Contact cohesion (Pa)
τ_{max}	Maximum shear stress (Pa)
τ_{lim}	Limit shear stress (Pa)
τ	Equivalent shear stress (Pa)
σ_y	Yield strength (Pa)
$\sigma_{vm.pr}$	Von Mises stress in the production casing (Pa)
$\sigma_{vm.an}$	Von Mises stress in the anchor casing (Pa)
σ	Standard deviation (-)
$\{\epsilon\}$	Strain vector
$\{\sigma\}$	Stress vector
$[\tau]$	Matrix of Cauchy (true) stresses

Glossary

Annulus	*The void between the drill pipe and the casing, two casings or a casing and the formation.*
API	*American Petroleum Institute.*
BC (1)	*API buttress thread casing, also referred to as BTC, widely used in geothermal wells.*
BC (2)	*Boundary conditions.*
Blow-out	*Uncontrolled flow of fluid (steam) out of the well into the formation or to the surface.*
BPD	*Boiling-point depth curve.*
Burst	*Deformation because of too high net internal pressure, that can ultimately result in loss of pressure.*
Casing	*Steel pipe that is used to seal off unwanted feed zones, for well control and blow-out prevention during drilling and to be a conduit for formation fluids.*
CBL	*Cement bond log, sonic log used to assess cement quality behind casing.*

Cement *Well cement blends are often referred to as cement only. This applies both to wet cement grout as well as hardened cement.*

Collapse *Deformation in a pipe or casing because of too high net external pressure.*

CSS *Cyclic steam stimulation also known as huff and puff, where thermal stimulation is used to reduce viscosity of heavy oil in order to induce flow.*

Dope *Grease for threaded connections.*

EOB *End of build, the depth in a directionally drilled well where deviation stops.*

Free water *Free water is the residual water that is not required for cement hydration.*

Huff and puff *Refer to CSS.*

KOP *Kick-off point, the depth in the well where deviation initiates in directional drilling.*

Kill-line *Flow line in the blow-out prevention (BOP) stack intended for injecting fluids, e.g. heavy mud, for well control.*

Killing wells *The procedure of pumping water or other injection fluids into wells to control/stop flow.*

Load history *Sequence of loads, e.g. pressure, temperature, gravity or other forces, of a structure.*

MD *Measured depth.*

Multi-stage cementing *Multi-stage tools are used to cement a casing in two or more stages in order to achieve a good cement coverage.*

OCTG	*Oil country tubular goods.*
Plastic strain (plastic deformation)	*Permanent (nonrecoverable) deformation occurring at stresses beyond the yield strength of metallic materials.*
Premium connections	*Proprietary connections that have superior features such as increased strength and sealing capacity.*
RCC	*Reverse circulation cementing, a cementing method where cement is pumped into the annulus.*
Running casing	*Casing is run in hole, e.g. put into the well.*
SAGD	*Steam assisted gravity drainage, where steam is used to recover heavy oil in horizontal wells.*
Shutting-in	*Closing of wellhead valves.*
Stab-in	*A tool for allowing cementing through the casing shoe.*
Stand-off	*The distance of a drillstring, tool or casing to an external casing or the wellbore.*
Strain (elastic deformation)	*Recoverable deformation of materials occurring at stresses below the yield strength of metallic materials*
Tensile rupture	*Failure in connection or casing caused by excessive tensile loading.*
TVD	*Total vertical depth.*
Yield strength	*Tensile or compressive stress that results in first yielding of the material.*

Wellbore *A drilled hole.*

Work-over *Wells may need to be worked over, e.g. by drilling out obstacles such as scaling buildup in the well with a work-over rig.*

List of Figures

List of Tables

List of Publications

Kaldal, G.S., Jonsson, M.T., Palsson, H., Karlsdottir, S.N., and Þorbjörnsson, I., 2011. *Load History and Buckling of the Production Casing in a High Temperature Geothermal Well*, Thirty-Sixth Workshop on Geothermal Reservoir Engineering, Stanford University, Stanford, California.

Kaldal, G.S., Jonsson, M.T., Palsson, H., Karlsdottir, S.N., 2012. *Thermal and Structural Analysis of the Casing in a High Temperature Geothermal Well During Discharge*, Thirty-Seventh Workshop on Geothermal Reservoir Engineering, Stanford University, Stanford, California.

Kaldal, G.S., Jonsson, M.T., Palsson, H., Karlsdottir, S.N., 2013. *Collapse Analysis of the Casing in High Temperature Geothermal Wells*, Thirty-Eighth Workshop on Geothermal Reservoir Engineering, Stanford University, Stanford, California.

Kaldal, G.S., Jonsson, M.T., Palsson, H., Karlsdottir, S.N., 2013. *Using Probabilistic Analysis with Finite Element Modeling of High Temperature Geothermal Well Casings*, SIMS 54th conference in Bergen, Norway, 176-184.

Kaldal, G.S., Jonsson, M.T., Palsson, H. and Karlsdottir, S.N., 2015. *Structural modeling of the casings in high temperature geothermal wells*. Geothermics 55, 126 –137.

Kaldal, G.S., Jonsson, M.T., Palsson, H., Karlsdottir, S.N., 2015. *Structural Analysis of Casings in High Temperature Geothermal Wells in Iceland*, Proceedings World Geothermal Congress 2015, Melbourne, Australia.

Kaldal, G.S., Jonsson, M.T., Palsson, H. and Karlsdottir, S.N., 2016. *Structural Modeling of the Casings in the IDDP-1 Well: Load History Analysis*. Geothermics 62, 1 –11.

Kaldal, G.S., Jonsson, M.T., Palsson, H. and Karlsdottir, S.N., 2017. *Structural Analysis of the Casings in Deep Geothermal Wells*, SIMS 58th conference in Reykjavik, Iceland, 391-398.

Acknowledgements

This work was financially supported by the University of Iceland research fund, the Technology Development Fund at RANNIS - The Icelandic Centre for Research, the Innovation Center Iceland, Landsvirkjun Energy Research Fund, and GEORG - Geothermal Research Group. Their support is much appreciated. The PhD study has been focused on the geothermal experience in Iceland and has had the privilege to be in close cooperation with the local power companies and connected consulting firms. Connected with the literature the good cooperation has greatly enriched the study and its practical outcome. The author would like to thank Reykjavik Energy (OR), Our Nature (ON), HS Orka, Landsvirkjun, Iceland Drilling (Jarðboranir), Iceland GeoSurvey (ÍSOR), Mannvit and the Innovation Center Iceland for providing data, discussion and useful information for the work presented here. The author would also like to thank the Geothermal Association of Iceland (GAI) for providing a travel grant to the World Geothermal Congress 2015 in Melbourne, Australia.

Additionally the author would like to thank individually and in no particular order the following contributing people; Albert Albertsson, Guðmundur Ómar Friðleifsson, Geir Þórólfsson, Ómar Sigurðsson, Þór Gíslason, Ari Stefánsson, Bjarni Pálsson, Sveinbjörn Hólmgeirsson, Kristján Einarsson, Ásgrímur Guðmundsson, Sigurður H. Markússon, Karl E. Sveinsson, Ásbjörn Einarsson, Helgi Leifsson, Jón Búi Guðlaugsson, Einar Gunnlaugsson, Sigurður Þorvaldsson, Kristinn Ingason (and his team), Sturla F. Birkisson, Sverrir Þórhallsson, Björn Már Sveinbjörnsson, Ólafur H. Wallevik, Ingólfur Þorbjörnsson, Hjalti Páll Ingólfsson, Ali Bakhshinejad, Sunna Ó. Wallevik, Árni Ólafsson, Heimir Hjartarson, Lárus Þorvaldsson, Halldóra Guðmundsdóttir, my doctoral committee, Sigrún Nanna Karlsdóttir, Halldór Pálsson and my main supervisor Magnús Þór Jónsson.

1

Introduction

In geothermal power production, the energy from deep heat sources within the earth is extracted from its crust, with water as the main energy carrier. Wells are drilled into hydrothermal reservoirs to transfer the geothermal fluid up to the surface. Such wells are located in high-temperature geothermal fields which are defined as such if the temperature at 1000 m depth reaches beyond 200°C (Böðvarsson, 1961; Palmason, 2005; Axelsson et al., 2006). As the energy rich geothermal fluid flows upwards it boils and in most cases a mixture of steam and water is present at the wellhead (Palmason, 1980; Sveinbjornsson and Thorhallsson, 2014). In hot areas or where production has caused pressure drawdown in the system, pure steam with very little moisture is extracted. Closer to the heat source, the steam can be in a saturated, superheated or even supercritical state. The idea of targeting such high-enthalpy sources, is that fewer number of wells are needed to produce same amount of energy, leading to potentially reduced investment costs and environmental footprint.

High-temperature geothermal wells are constructed of several concentric steel casings that are fully cemented externally. The casings are thus bound together as well as to the surrounding rock formation with a cement sheath which also acts as a sealant. The structural integrity of these casings is essential for the utilization of high-temperature geothermal wells. Casing collapse can reduce the cross-section of the well significantly, leading to reduced power output and hindering accessibility, e.g. for work-over or logging tools. In worst case scenarios, failures can cause risk of steam blow-out in the well and/or to the surface. During the lifetime of a typical well, the casings are subjected to multiple thermo-mechanical loads that can cause casing failures which could be avoided if careful measures are taken in well construction and operation during its lifetime. With recent increasing interest in drilling deeper geothermal wells, the strength of the casing is one of the limiting factors when compared to conventional wells be-

cause of increased casing depths, higher pressures and temperatures and more difficult corrosive environment.

Although high pressures provide numerous design challenges, the most challenging load in geothermal wells is caused by thermal expansion driven by large temperature changes and constraints. When wells warm up after being drilled in cooled conditions, thermal stresses are produced in the casings, eventually resulting in permanent deformation. Thermal expansion and sudden boiling of enclosed annular fluids can also generate high pressures that can lead to failures. Large wellbore temperature changes and fast heating/cooling rate, e.g. while flow testing or killing producing wells with water, result in large axial stresses in the casing. Radial and hoop stresses are present as well as a result of thermal expansion when casings expand outward into the cemented annulus, while wells heat up and contract inwards if they are allowed to cool down again. The mechanical force because of thermal expansion of the casing also materializes in wellhead displacement, but wellheads are known to rise slightly during discharge (wellhead growth) and decline when they cool down. Thermal expansion, material strength reduction at elevated temperatures, corrosion and cyclic loading are among the problems that can cause structural conditions that can be detrimental to casings. Casing failures appear in numerous modes, e.g. structural and chemical in the form of corrosion. Structural failures occur mainly in the form of axial tensile rupture, collapse, burst and material yielding. Forms of corrosion such as environmental cracking, e.g. embrittlement, stress corrosion cracking, corrosion fatigue, where combination of loads and corrosive environment is required is regularly seen in geothermal applications. Failures presumably develop due to a combination of several factors, e.g. the setup of the well, material properties and impurities, as well as various loads. If one of these failures occur in the casing, flow could be restricted and logging or workover of the well can become impossible. Additionally, operating the well can become dangerous because of the risk of well blow-out between casings or out through the formation, or other catastrophic well failures. Therefore, it is important to understand comprehensively the structural system and its response to various loads during well operations.

The objective of the PhD study is to study the structure of high-temperature geothermal wells, by constructing nonlinear structural models of the cased section and to use the models to analyze various load scenarios and casing failures. The resulting models provide tools which can be used to improve well design by analyzing casing design, material selections and various expected load scenarios. The results from the study furthermore provide an insight into the structural response of high-temperature geothermal well casings to wellbore temperature and pressure loads. By including large displacements, nonlinear material properties and nonlinear connectivity between the surfaces that are in contact, e.g. between steel and cement, increased knowledge is gained on the structural integrity of casings in high-temperature geothermal wells.

Calculating the structural response of cemented steel casings, wellhead and surrounding rock formation to loads, e.g. temperature and pressure, is a complicated task. This is mainly due to the nonlinear behavior of material properties, large displacements, friction between the numerous contact surfaces that are present and small diameters compared to depth of wells. Therefore, the structural system of the cased well is analyzed numerically with the use of the nonlinear finite-element method (FEM) with ANSYS. Both thermal and structural FEM models are used. The purpose of the models is to evaluate the structural integrity of casings in conventional high-temperature geothermal wells when subjected to transient temperature and pressure loads.

The scientific contribution of this study can be summarized as:

- Accurate analysis of the structural response of high-temperature geothermal wells to transient and non-transient thermo-mechanical loads.
- Mapping of possible load scenarios and casing failure modes.
- Analysis of heat-transfer, stresses and strains and risks of casing failures by developing nonlinear FEM models of cased wells.
- Measuring and using wellhead displacement (i.e. wellhead growth) of discharging high-temperature wells to validate FEM models.

The results can be divided into three categories; data and information acquisition, wellhead displacement survey and nonlinear finite-element modeling. Some of the main results of the study are listed here:

Data and information acquisition:

1. Throughout the PhD project, information on casing failures have been collected and as a result the main failure modes of casings in high-temperature geothermal wells have been identified as collapse and coupling tensile rupture. The particular shape of casings that have collapsed during warm-up or operation of wells is of special interest.
2. The main load scenarios have been determined as;
   - Residual stresses from manufacturing,
   - Axial load during installation due to casing self weight,
   - Compressive loads during thermal recovery due to thermal expansion,
   - Intensive compressive loads during discharges due to sharp temperature changes,
   - Radial loads due to pressure from expanding liquids in casing-to-casing annulus,
   - Axial tensile load when wells are closed or quenched with cold water.
3. The load history of casings and cyclic loads have shown to be important for accurate structural evaluation of casings.

Wellhead displacement survey:

1. For wells that are initially cold at the surface, the upward wellhead displacement is very fast in the first minutes of discharge and then slows down, following exponential decay.
2. For wells that are initially hot at the surface, some or full wellhead displacement has already taken place and in some cases no displacement is observed when wells are discharged. In other cases the initial displacement was slower than was observed in initially cold wells.
3. Items 1. and 2. above indicate that stresses and strains produced as a result of thermal expansion are less severe in initially warm wells compared to initially cold wells because of lower thermal gradient between casings due to a longer warm-up period.
4. A failed discharge attempt where gas pressure was released without initiating discharge showed a downward displacement that was roughly 2.5%

of the final observed displacement when the well was later discharged successfully. This suggests that wellhead displacement (i.e. wellhead growth) is primarily governed by temperature changes of the casing rather than by wellhead pressure.

Nonlinear finite-element modeling:

1. A two-dimensional axi-symmetric model of the cased section of a well is in good agreement with the wellhead displacement survey.
2. The two-dimensional axi-symmetric model was adopted to structurally analyze the Iceland Deep Drilling Project well IDDP-1 where several casing failures were observed in a video log after the well was quenched with cold water. The main findings of the FEM analysis are:
   - Stress concentrations are seen at the locations of casing shoes and thickness changes of neighboring casings.
   - The production casing is subjected to thermal shocks during the operation history and the anchor casing is protected against these shocks, provided that the thermal insulation of the cement in between is sound.
   - After 8 hours of quenching, large thermal gradients still exist between casings and that slower cooling would be ideal if possible in such critical situations.
3. Three-dimensional collapse analysis in a section of a multiple cased well. The results show that:
   - Residual stresses, impurities and defects greatly reduce the collapse resistance of casings.
   - Non-uniform loads are more likely to produce collapses.
   - Structural support of cement increases the stability of casings and higher pressure is needed for collapse to occur than for casings without cement support. This shows the importance of cement support.
   - The collapse shape of casings with cement support resembles the ones seen in operating wells, but without cement support casings collapse completely.
4. Two-dimensional axi-symmetric model of a cemented buttress threaded coupling. The results show that:
   - At the upper and lower regions of the couplings indications of substantial cement damages are seen, this is expected since the couplings act as anchors for the casing in the cement.
   - Stress concentration is primarily seen in the first 3-4 threads of the connections.

This thesis is structured as a monologue with a collection of papers in appendix. The intention is to connect together and summarize the content of the papers and provide additional information that is not included in the papers. Following the introduction chapter, a background chapter summarizes past knowledge of structural analysis of casings. High-temperature geothermal wells, casing loads and casing failure modes are described in the following chapter. The nonlinear finite-element method is described in chapter four. Chapter five describes models and field studies. Chapters six and seven summarize the main results. In the appendix the main conference proceedings papers and journal articles are found. Papers I, II, III and V are conference papers and papers IV and VI are journal articles. The structure of topics related to papers is illustrated in Fig. 1.1.

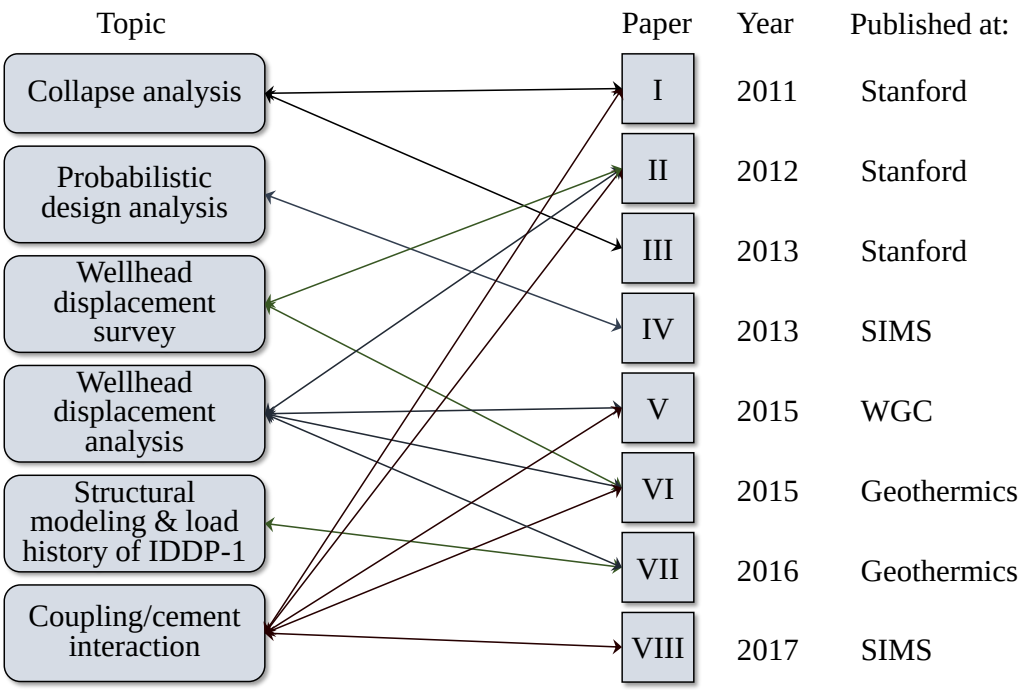

Figure 1.1: *Structure of topics related to published papers.*

The mentioned papers that are included and discussed in this thesis are:

I. Gunnar Skúlason Kaldal, Magnús Þór Jónsson, Halldór Pálsson, Sigrún Nanna Karlsdóttir and Ingólfur Þorbjörnsson, 2011. *Load History and Buckling of the Production Casing in a High Temperature Geothermal Well*, Thirty-Sixth Workshop on Geothermal Reservoir Engineering, Stanford University, Stanford, California.

II. Gunnar Skúlason Kaldal, Magnús Þór Jónsson, Halldór Pálsson and Sigrún Nanna Karlsdóttir, 2012. *Thermal and Structural Analysis of the Casing in a High Temperature Geothermal Well During Discharge*, Thirty-Seventh Workshop on Geothermal Reservoir Engineering, Stanford University, Stanford, California.

III. Gunnar Skúlason Kaldal, Magnús Þór Jónsson, Halldór Pálsson and Sigrún Nanna Karlsdóttir, 2013. *Collapse Analysis of the Casing in High Temperature Geothermal Wells*, Thirty-Eighth Workshop on Geothermal Reservoir Engineering, Stanford University, Stanford, California.

IV. Gunnar Skúlason Kaldal, Magnús Þór Jónsson, Halldór Pálsson and Sigrún Nanna Karlsdóttir, 2013. *Using Probabilistic Analysis with Finite Element Modeling of High Temperature Geothermal Well Casings*, SIMS 54th conference in Bergen, Norway, 176-184.

V. Gunnar Skúlason Kaldal, Magnús Þór Jónsson, Halldór Pálsson and Sigrún Nanna Karlsdóttir, 2015. *Structural Modeling of the Casings in High Temperature Geothermal Wells*, Geothermics.

VI. Gunnar Skúlason Kaldal, Magnús Þór Jónsson, Halldór Pálsson and Sigrún Nanna Karlsdóttir, 2015. *Structural Analysis of Casings in High Temperature Geothermal Wells in Iceland*, Proceedings World Geothermal Congress 2015, Melbourne, Australia, 19-25 April 2015.

VII. Gunnar Skúlason Kaldal, Magnús Þór Jónsson, Halldór Pálsson and Sigrún Nanna Karlsdóttir, 2016. *Structural Modeling of the Casings in the IDDP-1 Well: Load History Analysis*, Geothermics.

VIII. Gunnar Skúlason Kaldal, Magnús Þór Jónsson, Halldór Pálsson and Sigrún Nanna Karlsdóttir, 2017. *Structural Analysis of the Casings in Deep Geothermal Wells*, SIMS 58th conference in Reykjavik, Iceland, 391-398.

2

Background

In this chapter, a background is given on problems and analyses related to the subject of this thesis. The finite-element method (FEM) is a numerical method devised and refined by mathematicians, physicists and engineers for over half a century. Since the early 1960s a large amount of research has been devoted to the technique and a large number of publications on the finite-element method is available (Bathe, 1996). The "nonlinear" finite-element method is used to further describe and model nonlinear behavior, e.g. large geometrical displacements, nonlinear material properties and contact behavior between surfaces. The nonlinear finite-element method can be used to perform structural analysis that goes beyond the elastic range of materials, i.e. in plastic analysis. The method is therefore practical to use for analyzing structural problems of high-temperature geothermal wells where plastic strains can be produced in casings if loads are large enough. The method is also useful for buckling analysis which in this thesis is used for analyzing collapse of casings. Furthermore, the method is used for solving contact problems, e.g. surface connectivity and friction between surfaces which is also important for analyzing collapse of cement supported steel casings and for transfer of loads between surfaces, e.g. heat and pressure.

Maximum formation temperatures of hydrothermal geothermal systems are governed by saturation temperatures, i.e. by the boiling point depth curve (BPD) (Steingrimsson, 2013). Typical wellhead temperatures in high-temperature geothermal wells are in the range of 200-300°C, although higher temperatures are seen in some cases. For instance, reservoir temperatures in the Krafla high temperature geothermal area in Iceland typically range from 210°C to 350°C (Ragnarsson, 2003) and the wellhead temperature of the Iceland Deep Drilling Project well IDDP-1 located in that reservoir reached 450°C and 140 bar-g which is the highest recorded operational temperature in a geothermal well (Hauksson et al., 2014; Hólmgeirsson et al., 2010; Elders et al., 2012; Pálsson et al., 2014).

Temperatures are normally much lower in oil wells but in some applications, the temperatures are similar as in high temperature geothermal wells. High Pressure High Temperature (HPHT) oil wells are defined as such when expected shut-in pressures exceed 690 bar or static bottom hole temperatures are higher than 150°C (Norsok D-010, 2004). Such high wellhead pressures are however not expected in hydrothermal reservoirs.In thermal oil wells, such as Steam Assisted Gravity Drainage (SAGD) and Cyclic Steam Stimulation (CSS) wells, casings and their connections experience extreme loads due to exposure to temperatures up to 350°C (Nowinka and Dall'Acqua, 2011). Due to these high temperatures, elasto-plastic behavior needs to be considered in casing design. Although seeking different goals, synergies exist between geothermal and oil and gas applications where similar casing failures are seen.

The finite-element method has been used to generate models of casings in oil and gas for decades, mostly for premium connection design where features such as threadform and sealing surfaces are optimized. Limited research has however been devoted to structural modeling geothermal wells. Partly due to difficult dimensions, i.e. their diameter to depth ratio, and consequently models are often confined to solving specific local problems. With ever increasing computing power, modeling wells in 3D with complex geometry and solving in conjunction local and global stress and strain state is becoming more viable.

Few FEM analysis of wells have been published where the frictional characteristics between surfaces in contact are taken into account. Da Silva et al. (1990) introduced sliding interfaces between cement and formation in order to predict onset of casing failures due to compaction of high porosity chalk during reservoir depletion. They conclude that the results are sensitive to assumptions concerning the sliding along the cement/formation interface. Philippacopoulos and Berndt (2002) presented a two-dimensional FEM model of a cross section of a double cased geothermal well with the objective of evaluating the stress field of the cement. In the study, the need for further general research to focus on the transient structural response of a geothermal well was emphasized. Gretarsdottir (2007) presented an elastic two dimensional FEM model of a geothermal well where surfaces were bound together and no slippage was allowed. A three-dimensional push-out model was used and push-out test results were obtained in a laboratory. This, along with the two dimensional model, was used to estimate the displacement of the production casing at the surface due to thermal expansion. Magnusdottir (2009) presented a nonlinear two-dimensional FEM model of a

geothermal well, where the upward displacement of casings was analyzed with regards to the bonding characteristics between the production casing and cement, using contact elements. The results for no-, partial- and full separation between the surfaces, were compared and demonstrated that the defined contact behavior greatly affected the results. Ferla et al. (2009) proposed a linear axi-symmetrical model of a short well section with a casing surrounded by cement and rock, where thermal-induced stresses around a cased injection well were modeled. The model included two types of rock which showed that interbedding layers of relatively soft and stiff rock types have a major effect on the thermal stress distribution along the casing. They also analyzed casing pre-tension and its potential effect on the reduction of the thermal compressive stress, but concluded that the amount of pre-tension needed depends on the rock formation surrounding the casing.

Threaded connections have been specially analyzed with FEM models for evaluating their performance to anticipated loads. These have mainly been aimed at premium connection designs as discussed below. Johnson (1984) presented a linear FEM model of a threaded tubular connection where elastic loads were considered and gaps between elements "in connection" were defined. Since then with increasing computer processing capabilities, the potential has been increasing for solving larger and more detailed models that include nonlinearities, e.g. plasticity and contact between surfaces. Maruyama et al. (1990) examined physically the leak resistance of America Petroleum Institute (API) buttress thread coupling (BTC), API long round-thread couplings (LTC) and premium coupling for temperatures up to 354°C. The results showed that the seal limit temperatures of API BTC is 200°C and for API LTC it is 300°C, but the premium connection showed higher leak resistance where no leakage was seen for testing temperature of 354°C. They also used a FEM model of premium connections, a regular casing material grade K55 coupling, a heavy K55 coupling and a regular C95 coupling, to model the contact pressure of the connections. The conclusion was that in order to increase the contact pressure and thus the coupling sealing capacity, a heavier or higher grade coupling should be used. This was based on the results that the regular coupling looses its seal due to a greater deformation than in the couplings made of stronger material. Secondly, they recommended the use of grade C95 material that contained 0.45% molybdenum as it showed less reduction in seal interference at elevated temperatures than regular C95 material. Hilbert and Kalil (1992) used FEM models to analyze premium connections and verified the model results with strain gauge data from full-scale tests, pointing out that using combination of FEM and full scale testing can reduce cost and time and increase

confidence in connection use. In the model they used so called slide lines, as an improvement from previously used gap elements, where search algorithm was used to determine locations of nodes. Additionally, they used nonlinear stress-strain curves and large displacements, necessary when modeling response under extreme loads and failure. Dvorkin and Toscano (2003) analyzed, internal pressure, thermal, jump-out and torque loads on threaded connections with 2D axisymmetric models. Although pointing out that there is not enough available knowledge to quantitatively predict the sealing capability of a connection, they devised sealability indicators for comparing the sealing potential of different seal designs. They also showed the improvement of match between experimental and FEM results by the inclusion of dope pressure. Teodoriu and Falcone (2009) devised a FEM model of a threaded connection where a stress concentration factor was defined in order to analyze low-cycle fatigue (LCF) of the coupling. The results were then compared to full scale experiments. They showed that under extreme loads (approximately 200°C temperature variation) the LCF resistance of a N80 grade, 18 5/8 inch outer diameter casing with buttress threaded connections can be as low as 10 cycles. To ensure that the total number of cycles to failure remains higher than 100 they showed that a temperature variation of less than 80°C is required. FEM analyses are regularly used along with full scale physical testing in connection evaluation and design, e.g. in literature by Hilbert and Kalil (1992), Schwind et al. (2001) and Dvorkin and Toscano (2003), and in proprietary connection design that is not published. Guidelines for evaluating threaded connections was developed by the petroleum industry, API Recommended Practice 5C5 for Evaluation Procedures for Casing and Tubing Connections (API RP 5C5), where numerous full-scale physical tests are required to capture variations in performance due to variations in critical dimensions and material properties (Hilbert and Kalil, 1992). FEM models are progressively replacing the use of full-scale tests in the design phase of new connections and the method has been incorporated in combination with full-scale tests (Dvorkin and Toscano, 2003). The current evaluation standard (ISO13679/API5C5) excludes temperatures above 180°C and loads beyond pipe body yield (Nowinka and Dall'Acqua, 2011). A new protocol for evaluating casing connections for thermal well applications, Thermal Well Casing Connection Evaluation Protocol (TWCCEP), has been developed for wells that reach maximum temperatures of 200-350°C (Nowinka and Dall'Acqua, 2011), and has now been adopted as international standard ISO/PAS 12835:2013 Qualification of casing connections for thermal wells. The standard provides procedures for evaluating threaded casing connections for service in intermediate or production casing strings of thermal-

recovery applications, specifically SAGD and CSS, but might also be used for other extreme-service wells in which casings undergo full-body yielding as occurs in geothermal wells (ISO/PAS 12835:2013, 2013).

FEM modeling has also been used to study the effects of defects on collapse pressure of pipes, e.g. by Assanelli et al. (1998), Dvorkin and Toscano (2003), Pattillo et al. (2004), Sakakibara et al. (2008) and Netto (2009). Collapse of cemented casings that occurs during operations of wells is a different case because of the lateral and radial support the external cement sheath provides. This is to some extent comparable to horizontal soil supported pipes that have greater capacity to withstand net external pressures than pipes without support, e.g. a study by Watkins and Anderson (1999). In compact soil the cross section remains sensibly circular, until failure by wall-buckling takes place (Bulson, 1982). Likewise for burst design, the support of external cement sheath increases burst resistance of casings (Kalil and McSpadden, 2011). W. J. Rodriguez (2003) presented a plain strain model with casing and cement sheath bonded together. They varied the cement material properties of the casing-cement sheath system to analyze which cement type is best able to reduce radial and von Mises stresses in the casing. One of their result was that cement with high Young's modulus and high Poisson's ratio have the capability to compensate more stress internally in its structure and pass less stress to the surrounding media, pointing out that this would be an ideal system to reduce collapse-loading conditions to the casing, but they also note that such cement properties can be difficult to achieve. Berger et al. (2004) analyzed collapse resistance of eccentrically centered casings, voids in cement and formation, channels in the cement and declining pore pressure in voids with a 2D FEM model of a cross-section of a well with casing and cement sheath fully bonded together. The results showed that for a completely cemented annulus, eccentricity has little effect on casing collapse resistance. Voids in the formation up to 60-80° wide showed increase in von Mises stresses in the casing, depending on if soft or hard cement properties were used. They analyzed effect of pore pressure decline in the void on casing collapse resistance, resulting in more unstable casing which in turn generated higher stresses as the pore pressure declined. A void in the cement annulus showed similar results as for voids in the formation and they concluded that the location of voids is not important, they only generate unstable conditions which increase the possibility of casing collapse. Yuan et al. (2012) also analyzed the effects of voids in cement and eccentricity on stresses in the production casing and cement with a 2D FEM model of a horizontal cross-section of a well with casing, cement sheath and formation

bonded together. They similarly analyzed the elasticity of cement by comparing results from using elastic cement versus brittle cement material properties. Their main results include that alone, the casing eccentricity did not have much effect on the casing and cement under the modeling loads and geometry, and adding voids in the cement generated the worst geometric conditions. Hidayat et al. (2016) used a FEM model to analyze structural integrity of casings in thermal environment of steam injection wells where collapse of casings due to external formation pressure and thermal cycles were analyzed. The results show that the capability of casings to withstand external pressures decreases as the number of thermal cycles increase and that casings may fail under external pressure below its specified collapse strength. Casing failure as a result of expansion of trapped fluid in the annulus between casings have been discussed as a suspected cause of casing collapse (Björnsson et al., 1978; Magneschi et al., 1995; Southon, 2005). Some examples of casing collapse where the deformation (pucker or bulge) was drilled out however, show good cement behind the casing which indicates that other factors, e.g. impurities, defects, material properties and axial loads, could have greater impact than previously suspected. An examples of such casing failure is shown in section 3.4 in this thesis.

Maruyama et al. (1990) analyzed the bi-axial collapse resistance of casings under axial tensile stresses. They found that by using quenched and tempered, a perfect elastic/plastic material, e.g. L80, C95 and P110, the biaxial collapse pressure is adequately predicted by API collapse equation based on the von Mises yield criterion. They, however, showed that for work hardening material such as K55 the API collapse equation applies only for small axial tensile stresses and that the measured collapse resistance is significantly higher than those predicted by the API equation. They also showed that due to the work-hardening characteristics of a grade K55 casing, it may be superior to higher-grade casing for thermal well service where high residual axial tensile stresses may be present. Wu et al. (2008) discuss the possibility of biaxial casing collapse where thermal axial compressive stress is present during steam injection and the increased risk due to reduced collapse resistance where the casing could easily collapse by a small external pressure. Dall'Acqua et al. (2012) discuss and analyze collapse responses of casings in thermal well applications, where stresses and strains go beyond yield. One of their conclusions is that collapse behavior is clearly dependent on the assumed loading path, i.e. the sequence of temperature and external pressure. They show that low net external pressures can lead to ovalization (representing collapse) when combined with thermally-induced axial strain if the cement sheath does

not offer adequate radial support. They also show that after full-section yielding of a casing with initial external pressure, the rate of ovalization is actually lower if it is cooled from 350°C (resulting in axial tension) than in heating (resulting in axial compression). They also emphasize the importance of considering material response at a particular strain level rather than referring to a stress level. Material post-yield stiffness is also discussed and two examples are shown. Both materials share identical yield strengths which is reached at the same strain level. However, one material has a flat yield plateau and a rounded stress-strain response at higher strain levels and the other has a smaller elastic range followed by a gradual departure from the elastic curve. The former is representative of some materials at ambient or low-temperatures and the latter is typical of OCTG (Oil Country Tubular Goods) materials at elevated temperature. Therefore, they conclude that yield strength alone, listed by material grade, must not be used as a sole base for material selection.

Further discussion on geothermal well design, casing loads and failures follows in the next chapter.

3

Geothermal wells

3.1 Geothermal energy utilization

Geothermal activity is primarily found near tectonic plate boundaries of the earth. Iceland's location on an intersection between the Mid-Atlantic Ridge and the Iceland hot spot hosts favorable conditions for geothermal activity (Agustsson and Flovenz, 2005). The ridge crosses the country from southwest to northeast, as shown in Fig. 3.1, and a large number of volcanoes and associated geothermal activity is found within the zone (Ragnarsson, 2015). Geothermal energy provides about 68% of the primal energy consumption in Iceland (Orkustofnun, 2014; Ragnarsson, 2015). It is used for production of electricity and hot water for consumption and space heating. The utilization of geothermal energy divides into space heating 43%, electricity generation 41%, swimming pools 4%, snow melting 4%, and the rest is used for various industries, fish farming and greenhouses (Orkustofnun, 2014; Ragnarsson, 2015). Geothermal energy provides about 90% of space heating in Iceland (Orkustofnun, 2014) and the rest is from electricity and oil. Direct use in Iceland amounts to 26,700 TJ/year and the installed thermal power capacity is 2,035 MWt (Ragnarsson, 2015). Iceland's proportion is about 4.5% of the global thermal energy production and 3% of the global installed power capacity, but if heat pumps are excluded the proportion is 10% in energy production and 10% of the power capacity, the total being 587,000 TJ/year and 72,000 MWt, 262,000 TJ/year and 20,000 MWt excluding heat pumps (Lund and Boyd, 2015).

Geothermal power plants which are located in high-temperature geothermal areas produce electricity from steam and in some cases hot water for district heating. High-temperature areas which are found in the geothermal active zone in Iceland associated with the Mid-Atlantic Ridge. In Iceland, eight geothermal power

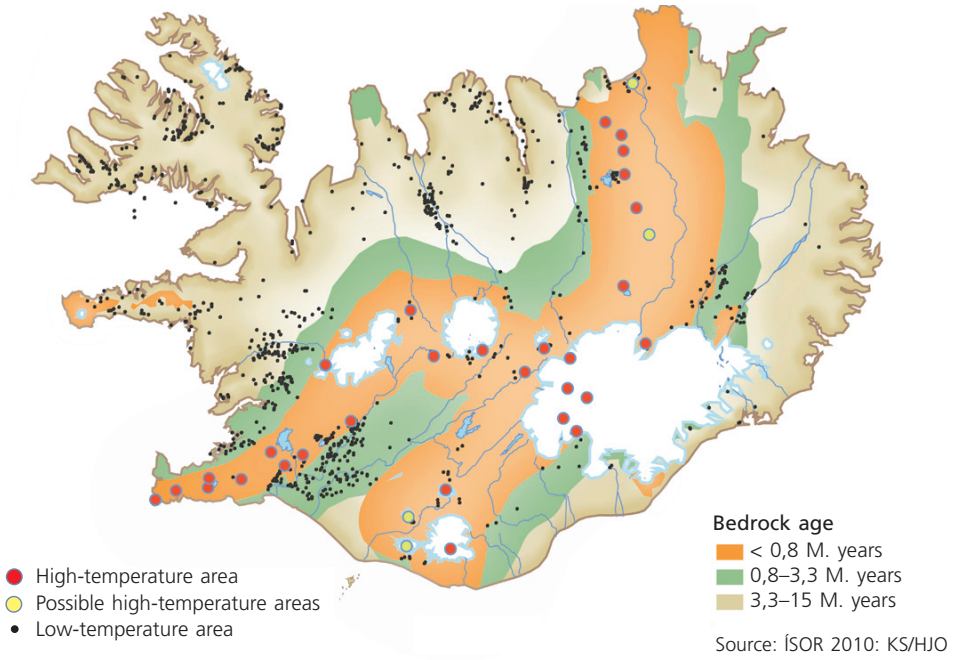

Figure 3.1: *The geothermal areas in Iceland (ÍSOR - Iceland GeoSurvey).*

plants have been built since the first one, Bjarnaflag, which was put into operation in 1969. The installed electric power capacity of the power plants is; Bjarnaflag (1969) 3 MWe, Svartsengi (1977) 74.4 MWe, Krafla (1978) 60 MWe, Nesjavellir (1998) 120 MWe, Húsavík (2000) 2 MWe (binary), Reykjanes (2006) 100 MWe and Hellisheiði (2006) 303 MWe (Ragnarsson, 2015). Construction for a new 90 MWe powerplant at Theistareykir N-Iceland began in 2015 with planned commissioning of two 45 MWe phases in late 2017 and spring 2018 (Landsvirkjun, 2016).

In 2014, electricity generation from high-temperature geothermal power plants was 5239 GWh or 29% of the total electricity generation in Iceland and the total electricity power capacity of geothermal power plants was 665 MWe or 25% of the total (Orkustofnun, 2014). Iceland provides about 7% of the global geothermal electricity generation and the installed electricity power capacity is about 5% of the global installed power capacity (Bertani, 2015).

3.2 High-temperature geothermal wells

The main purpose of high-temperature geothermal wells is to provide steam for electricity production. Thermal energy that is otherwise discarded is in some cases used to produce hot water for consumption and space heating. Condensers and heat exchangers are used to heat up cold water for this purpose. Several wells are drilled for each power plant, the number depends on the power capacity of each well and the size of the power plant. Make-up wells also need to be drilled throughout the lifetime of power plants in order to provide enough steam to keep up the power production because well productivity tends to decline with time. Geothermal power plants operate on a number of different power cycles. Single or double flash steam cycle power plants are common, but back pressure and binary plants are also found. Site-selection and targeting of geothermal wells is based on surface explorations, reservoir engineering and knowledge of the formation from past drilling. The design phase of a typical geothermal well includes several tasks, including: determining design temperatures and pressures at static and dynamic flowing conditions, minimum casing depth selections, casing diameters and clearances, minimum thickness selections, drilling program and well completion, and after completion, plan for warm-up and flow-testing. For well design purposes, the formation lithology and its conditions provide vital information on targeting, drilling procedures and wellbore integrity.

A typical casing program for a high-temperature geothermal well is displayed in Fig. 3.2. High-temperature geothermal wells are constructed of several concentric steel casings which are fully cemented externally from the casing shoe up to the surface, forming a layered structure of steel and cement sheaths, Fig. 3.3. The cement sheaths provide pressure sealing as well as structural support for the casings. The purpose of casings is to prevent collapse of the well, to seal off unwanted aquifers, for well control and blow-out prevention during drilling and to be a conduit for the geothermal fluid to flow up the well (Björnsson et al., 1978). Two main designs, specified by the outer diameter of the production casing, are used in Iceland, a regular $9^{5}/_{8}''$ or larger diameter $13^{3}/_{8}''$, both having their pros and cons. The larger type has larger wellbore cross-section allowing for higher production rates and is less affected by scaling but large diameter casings have less collapse resistance than smaller diameter casings if similar thicknesses are selected. On the other hand increase in cross-section is roughly proportional to the steam flow output, therefore the value per well can potentially be almost doubled provided that the structural integrity is ensured.

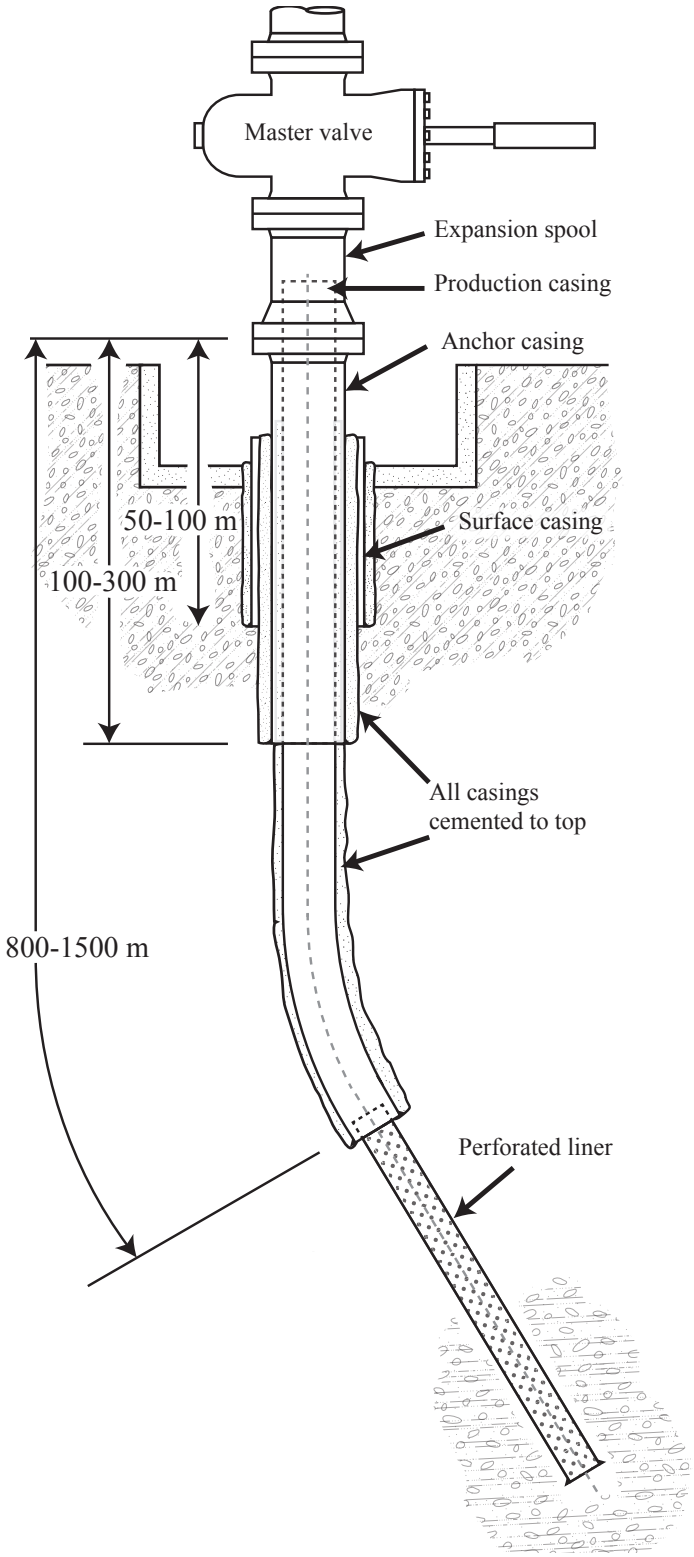

Figure 3.2: *A diagram of a typical casing program for high-temperature geothermal wells in Iceland.*

Figure 3.3: *Cross-section of cemented casings that were excavated from a high-temperature geothermal well in Reykjanes, Iceland, showing the layered structure of casings and insulating cement sheaths (figure by Sigrún Nanna Karlsdóttir).*

Depending on the setup and purpose of wells, 2-5 casing strings are used; conductor casing, surface casing, intermediate casings which are sometimes needed, anchor casing and production casing (Thorhallsson, 2008). When drilling is done, well completion involves installing a perforated liner, to prevent the formation collapsing into the well, and a wellhead of sufficient pressure class. The liner is normally installed with a hanger from the bottom of the production casing, but is in some cases skipped if the wellbore is considered strong enough. The anchor casing is defined as the casing on which the permanent wellhead is mounted but in some cases this may be the same as the production casing (NZS 2403:2015, 2015). The production casing sits inside an expansion spool below the master valve of the wellhead, or in some cases the wellhead is directly mounted onto the production casing.

The drilling process of high-temperature geothermal wells consists of several

stages. First a drilling platform is prepared for the rig and a shallow large diameter conductor casing is installed. A large diameter hole is then drilled for the surface casing which provides a platform for further drilling. The circulation fluid consists of drilling mud that is used to bring back cuttings to the surface and to cool and control the well against kicks. When the cuttings reach the surface, they are filtered out of the mud before the it is recirculated. When total circulation loss occurs and cement jobs attempting to seal the loss zone do not work, the drilling fluid is changed to water, and in most cases a large portion the well is drilled blind with no returns to the surface. Such zones when drilling for casings can later cause problems in casing integrity for example if the cement is washed away. The surface casing components, normally made of line pipes, are welded together when the casing is run in hole. Then the casing is cemented externally to the formation. Next a smaller diameter drill bit is used to drill from the bottom of the surface casing for the next casing, which in most cases is the anchor casing. Depending on depth and formation pressures, intermediate casings are in some cases needed. When the casing has been placed it is cemented. The drilling procedure is repeated until the last casing, the production casing, has been placed and cemented. For directionally drilled wells, the kick-off point (KOP) is typically located slightly below the shoe of the anchor casing and the dogleg severity in the build section is typically 1-3°/30m and end of build (EOB) when inclination reaches about 30°from vertical. In the final drilling phase, the production section of the well is drilled down to total depth (TD).

3.3 Casing design

In general, casing design is based on (i) axial tension, (ii) burst and (iii) collapse pressures. In casing design for oil and gas wells, the most important parameters are fluid pressure, casing weight, and tensile loading (Hole, 2008). In geothermal wells, however, high-temperature loading is generally the most severe (Hole, 2008). Each casing must withstand the expected loads that are likely to occur during drilling and the lifetime of the well. Standard ISO/TR 10400:2007(E) (API/TR 5C3), developed for the oil and gas industry, provides equations and calculation guidelines for the structural properties of casings, e.g. burst strength to yield, burst strength to failure, collapse strength, axial tensile strength and biaxial strength. Well design and the definition of anticipated loads is currently

outside the scope of standardization for the petroleum and natural gas industries (ISO/TR 10400:2007(E), 2007). New Zealand standard NZS 2403:2015 "Code of practice for deep geothermal wells" proposes a well design process with particular application to geothermal conditions (NZS 2403:2015, 2015). The standard includes anticipated load cases during drilling and after well completion, and provides design methodology constrained by design factors for developing proper casing programs that incorporate minimum casing shoe depths, pressure containment, well control and structural integrity design for casings. To account for strength reduction at elevated temperatures it includes design curves up to 350°C. The standard supersedes its 1991 version and major revisions include minimum depth selections according to pressure containment by assessing the fracture pressure of the formation instead of solely using the overburden pressure. It also acknowledges that casing design for axial compressive stresses due to thermal expansion needs design practices that involve plastic strain design and do therefore not include a design factor for that specific case as was done in the older version.

Table 3.1: *Specified strength requirements and material composition for common geothermal casing steel grades (API 5CT).*

	K55	L80	T95
Minimum Yield Strength (MPa)	379	552	655
Maximum Yield Strength (MPa)	552	655	758
Minimum Ultimate Tensile Strength (MPa)	655	655	724
Total elongation under load (%)	0.5	0.5	0.5
Hardness HRC max	-	23	25.4
Hardness HBW max	-	241	255
Carbon (C)	-	0.43 (max)	0.35 (max)
Manganese (Mn)	-	1.90 (max)	1.20 (max)
Molybdenum (Mo)	-	-	0.25-0.85
Chrome (Cr)	-	-	0.40-1.50
Nickel (Ni)	-	0.25 (max)	0.99 (max)
Copper (Cu)	-	0.35 (max)	-
Phosphorus (P)	0.030 (max)	0.030 (max)	0.030 (max)
Sulfur (S)	0.030 (max)	0.030 (max)	0.010 (max)
Silicon (Si)	-	0.45 (max)	-
Iron (Fe)	Balance	Balance	Balance

Casings are manufactured according to American Petroleum Institute (API) stan-

dard API 5CT (ISO 11960) *Specification for Casing and Tubing* and line pipe standard API 5L *Specification for Line Pipe*. Specification for threading, gaging and thread inspection for casing, tubing and line pipes is provided in standard API 5B. API casings are used in high-temperature geothermal wells and lower strength grades, commonly K55, L80 and T95, are selected according to guidelines in standard NACE MR0175 (ISO 15156-1) to avoid corrosion effects in H_2S environments. X-grades or other lower strength weldable carbon steel is typically selected for the outer casings, i.e. the surface casing and the conductor. Table 3.1 shows the specified tensile requirements and material composition limits for commonly selected geothermal casing steel grades. The casings come in approximately 12 m long segments and when run in hole can either be connected with threaded connections or butt-welded together. The innermost casings are cold drawn seamless steel pipes that are usually connected with threaded connections and the outer casings are formed, helically or longitudinally welded line pipes. API buttress thread casing (BC) are commonly used in geothermal wells. In some cases where increased performance and sealing properties is desired, premium connections with metal-to-metal seal and special treads have been used. Centralizers are placed on the casing, often around couplings or the casing body at intervals depending on the design of the well.

Generalized casing design steps are as follows:

1. Gather all data on the site and formation conditions, including:
   (a) Geological lithology of the formation
   (b) Temperature and pressure conditions with depth
   (c) Conditions of the formation and anticipated problem zones, such as lost circulation depths and information on loose formations
2. Define the maximum pressure and temperature profiles with depth
3. Calculate overburden and fracture profiles with depth
4. Calculate the minimum casing shoe depths with the criteria of well control for each drilling phase
5. Decide the desired open-hole diameter of the well
6. Calculate for all casings, strength against loads during casing installation, cementing and production
7. Update the design iteratively by revising the design if any changes are made

Temperature and pressure profiles in nearby wells are used to estimate likely design conditions for new wells. The expected maximum temperatures can be

different for wells within the same geothermal area and is determined by the relationship between the well and the geothermal reservoir, depths of feed zones, the temperature of the formation and how the well is operated. For high-temperature geothermal exploration where reservoir temperatures are unknown, design temperature and pressure is assumed to follow the boiling point-depth curve (BPD) for water (Björnsson et al., 1978; Thórhallsson et al., 2014). If, however, data from nearby wells is available and the reservoir temperatures are known, knowledge of the formation, pressure and temperature conditions of those prior wells are used as basis for design. Pressure logs during the warm-up period of wells are valuable as a pressure pivot point, where pressure remains constant indicates the pressure of the reservoir at that specific point and the dominant feed zone. When drilling deep into hydrothermal reservoirs, the critical point of water will be encountered at around 3500 m depth, the depth depending on the pressure balance in the system and the salinity of the geothermal fluid. Salinity effects the BPD in such way that pressure and temperature are slightly increased downhole and the critical point is reached at a greater depth (Ingason et al., 2015). If the critical point depth will be surpassed, assumptions on the conditions deeper in the system need to be made. Below the critical point the density of the fluid can for instance be assumed to be with a fixed gradient or isochor, representing pressure corresponding to changes of temperature of fixed volume of steam (Thorhallsson et al., 2010). Once maximum pressure and temperature profiles have been defined and containment pressure for depth calculated, minimum casing shoe depths can be determined. The minimum casing shoe depths varies depending on a selected criteria, which needs to be evaluated for each case. Once casing depths have been selected, structural calculations for each casing string is calculated. The calculations determine which casing sizes, connections and materials can be selected for the well. Once these design steps are complete, a casing program is proposed. These calculations include (further described in NZS2403:2015):

1. Axial tensile stress during running and cementing casing
2. Burst and collapse calculations during cementing
3. Burst and collapse during production of steam
4. Compressive thermal loading (strain)
5. Bi-axial tensile stress due to wellhead pressure
6. Helical buckling of liner

Using the inner string cementing method, casings are cemented by connecting the drill string to a stab-in near the bottom of the casing and the cement slurry is then pumped through the drill string, stab-in and float collar in the casing

shoe and up the annulus outside of the casing. While cementing deep casings, the practice in Iceland has been tending towards reverse-circulation cementing (RCC), where the cement is pumped directly to the annulus on the kill-line. The benefit of using RCC is that less cement is lost to the formation and lower load is subjected on the casing allowing for cementing deeper casings. Advantages of RCC include (Hernandez and Bour, 2010):

1. Reduced hydraulic power as gravitational force is working in favor of the slurry flow
2. Reduced downhole pressures which reduces the risk of fracturing the formation and puts less load on the casing
3. Shorter transit and thickening times of the slurry
4. Improved compressive strength development of the cement as most of the cement will not see the shoe bottomhole temperatures
5. Less cement waste, primarily because no excess cement is pumped back to the surface

Downhole temperature logs are taken after cementing in connection to cement bond logs (CBL) which indicate the cement integrity behind the casings. CBL can indicate if good hardened cement or poor cement is present, or if cement is missing behind casings. Cement blends that are used for high-temperature geothermal wells require mixing of additives to ensure longevity. API specifications recommend Portland API Class G cement blending up to 40% by weight of cement of silica flour to prevent strength retrogression and increased porosity when exposed to elevated temperatures (Hole, 2008). Special proprietary blends have been used with good results in geothermal wells. There is room for improvements, both in cement composition and in placement techniques. Innovation in cement design for high-temperature applications aims for instance at lowering frictional pressure losses of the slurry, lowering water content and improving strength characteristics.

3.4 Structural loads and load history

To understand what loads are imposed on a casing it is useful to go through its load history. It can vary from well to well, but the most critical load cases are similar and will be described in the following paragraphs. The load cases considered

here occur during drilling, installation and in well operations after completion, e.g. control of wellhead valves during production or shut-ins. Over the operating life of a geothermal well, the casing is generally subject to external loads that can be considered static or quasi-static (Teodoriu, 2015). However, during warm-up or cooling of wells, loads are transient and the resulting structural response of the well can be sensitive to the time periods of changes. Such wellbore temperature changes, e.g. during flow-testing or shut-ins, can lead to casing failures, especially if the casing is repeatedly strained beyond the yield point. The residual thermal tensile stresses that form during cooling of wells may be large enough to exceed the coupling joint strength, resulting in casing failure (Maruyama et al., 1990).

Residual stress is formed in the material during manufacturing, which is one of the effects that influence collapse resistance of casings (ISO/TR 10400:2007(E), 2007). Acceptable manufacturing processes, heat treatment, material composition and structural properties are described in API standards API 5CT and API 5L. Casings are seamless steel pipes and line pipes are larger diameter pipes that are manufactured from sheet metal that is formed, either helically or longitudinally and welded with continuous seam by electric resistance welding or other methods. Although not specifically considered a load, residual stresses are considered here as an initial condition of the material.

As casings are run in hole, casing components are welded or screwed together and lowered down into the well. The first load case of the casing consists of axial tension due to self-weight, see diagram A in Fig. 3.4. While the casing is installed, the well is kept full of water, which provides a modest counteracting buoyancy force. Friction between centralizers on the casing and the borehole wall also lowers the tensile force on top. The tensile force on the top increases with increasing length of the casing, putting the highest load on the last installed casing component that holds the whole casing. Cement, when hardened, later provides support to the casings. For directionally drilled wells, bending loads add to tensile and compressive axial loads, since one side of the casing cross-section is in tension and the other in compression. Bending loads, caused by high dogleg severity of the well, could also result in higher stresses than those formed at the top. The magnitude of the axial tensile load therefore depends on several factors, i.e. thickness and diameter of the steel casing, how many centralizers are used, the diameter of the hole, depth of the KOP, the deviation of the hole and the density of the mud/water/cement that provides the buoyancy

force.

Shortly after casings are run in hole they are cemented. Prior to cementing, the well is cooled by circulating the drilling fluid to allow cement to be pumped and preventing it being prematurely hardened. After placement of cement no circulation is available and the well slowly heats up while the cement sets. During cementing, the casing is kept full of water or mud so the differential pressure of the casing wall does not reach critical levels, i.e. exceeds the collapse resistance or exceeds the burst strength of the casing. The differential pressure is determined by the hydrostatic pressure difference between the cement slurry and water, as well as additional cement pumping pressure, see figure B in Fig. 3.4.

The temperature the cement solidifies at is the reference temperature for subsequent axial thermal stresses for each casing string. The temperature of the casing increases gradually during cementing due to warm-up from the surroundings and exothermic chemical reactions in the cement (heat of hydration). As the cement sets, wells are typically relatively colder at shallow depths and gradually warmer with depth, depending on surrounding formation conditions. The largest temper-

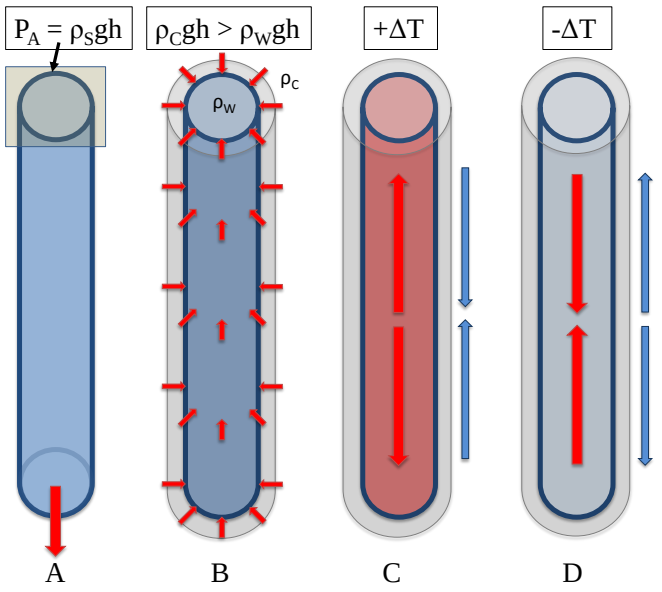

Figure 3.4: *Casing load cases. A: casing self-weight, B: differential pressures, C: thermal expansion and D: tension due to cooling.*

ature change therefore often occurs at shallow depths. However, due less constraints near the surface, the casings and the wellhead tend to move up or down with temperature changes. Smaller strains are therefore likely to form near the surface and larger below a transition zone deeper in the well where displacements of the casing are more constrained.

When the drilling is finished the rig is removed from site and the well is allowed to warm-up for the first time. After well completion the casing loads mainly consist of temperature and pressure changes within the wellbore and the formation. During this thermal recovery from drilling, the initial tensile stress in the casing is relieved and subsequent compressive thermal stress builds up, see figure C in Fig. 3.4. The intensity of stresses in the layered casing and cement structure as a result of thermal expansion depends on the temperature difference from the cementing conditions. While drilling into permeable zones in geothermal areas, using water as circulation fluid, large volumes of cold water is lost to the reservoir and full thermal recovery can typically take from 2 weeks up to 3 months (Birkisson and Hole, 2007). During this recovery period the well is initially full of water and wellhead pressure slowly builds up as the well warms-up.

During thermal recovery, wellheads can be closed to build pressure by accumulation of non-condensable gases at the top. Pressure then builds up gradually and pushes the water column in the well down into the reservoir and warms it up, thus making discharge possible when the well is opened. In some cases the water in the well prevents wellhead pressure to naturally build up to a sufficient pressure to discharge the well. Air-compressors are then used to build up wellhead pressure for same purpose as before. The disadvantage of this forced method is that the well and the wellhead remain cool while air is pumped into the well which then causes a greater thermal impact when the well is discharged. If possible, allowing wells to warm-up slowly before discharge should reduce the impact of thermal expansion. For powerful wells, shut-in conditions can lead to high wellhead pressure that puts tensile load on the wellhead and the anchor casing and if the wellhead pressure is due to saturated steam rather than gas, the pressure leads to increased temperature. Therefore, the casings and wellhead are subject to higher thermal load than in a flowing well where the wellhead pressure is lower.

Fig. 3.5 shows conceptual temperature and pressure changes during discharge. Initially the wellhead and uppermost well section is cold and a watertable is

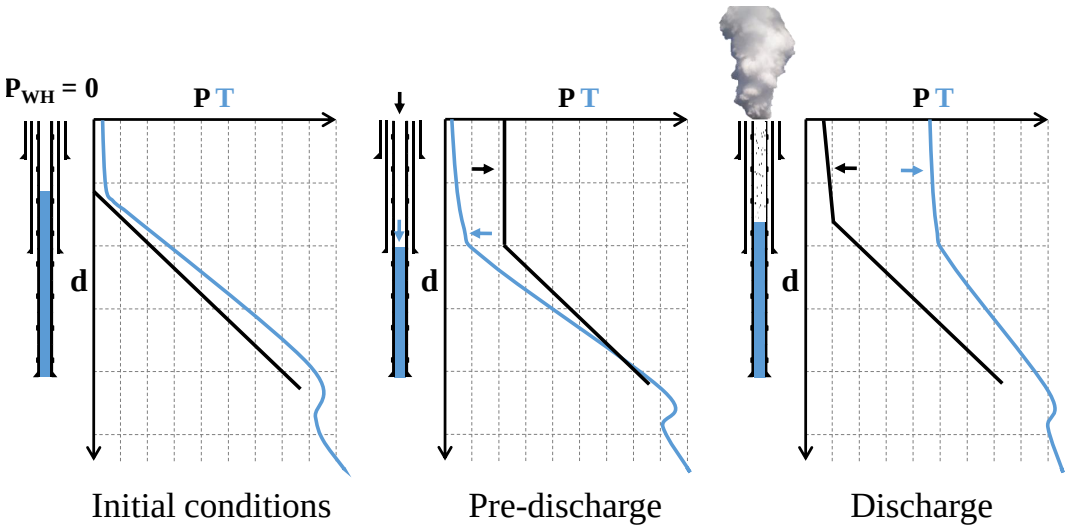

Figure 3.5: *Conceptual wellbore temperature and pressure load cases before and after discharge.*

found somewhere shallow in the well. Below the watertable the pressure increases with depth due to hydrostatic pressure of the water and temperature increases due to formation conditions. If gases accumulate or an air-compressor is used to build pressure, pre-discharge conditions are such that temperature is relatively low until the water table is reached and the wellhead pressure has pushed the water table downwards. Typically when wells are discharged, the wellhead pressure decreases rapidly and the temperature uppermost in the well increases sharply within few minutes. Wellhead valves need to be opened fast to initiate boiling and upwards momentum of the fluid in the well which then drives the discharge. The large temperature change causes thermal expansion of the casing which causes the wellhead to rise. Table 3.2 shows examples of wellhead displacements during flow-tests of selected wells in Iceland.

When wells are shut-in the wellhead temperature slowly decreases in most cases, except for powerful wells as discussed earlier. If wells are shut down (killed) with cold water the casing rapidly contracts, creating tensile forces due to the constraints of the cement, see figure D in Fig. 3.4. This occurs if stresses in the casing reach beyond the yield point during hot conditions, and cooling it down again generates tensile stress which could lead to rupture of the casing body or couplings. As post-yield permanent (plastic) strains are generated in the

compressive hot state, high tensile stresses are formed if wells cool down again, see Fig. 3.6. Thermal stresses generate similar problems in oil wells, such as CSS and SAGD operations, where steam injection is used. In these situations steam is used to heat the formation to a temperature sufficient to reduce the viscosity of the hydrocarbons which then flow back into the heat injection well (Vogel, 1966). CSS wells, in an operation involving a combination of CSS and SAGD in northwestern Alberta with maximum operating temperatures and pressures of 340°C and 14.5 MPa, see about 8 thermal cycles during their lifetime of 15 to 20 years (Dall'Acqua et al., 2012). These maximum operation values are similar for high-temperature geothermal wells, the difference is that they do not need to be cycled, except for maintenance if a workover is needed.

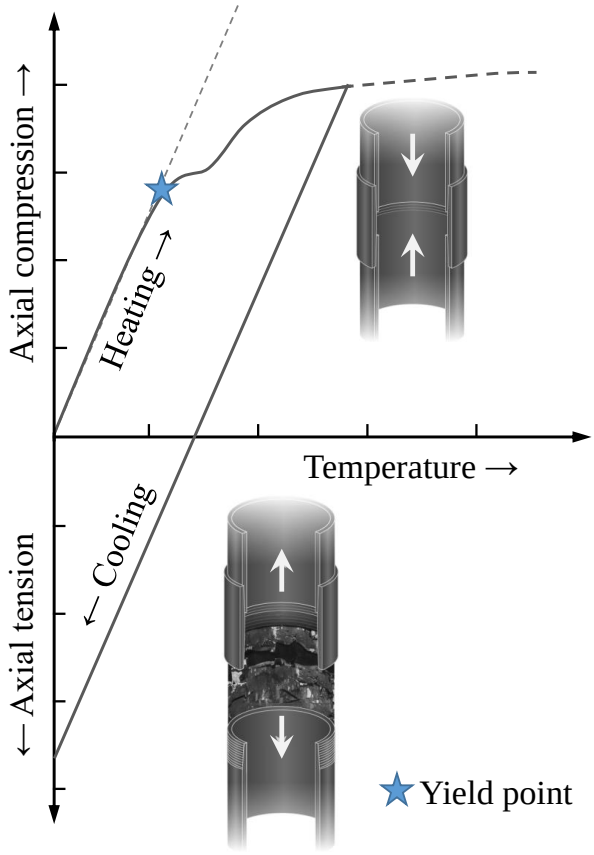

Figure 3.6: *Concept diagram describing how axial tension can be generated if hot wells cool down and have previously formed axial compressive strain. Adopted from a diagram by Rahman and Chilingarian (1995).*

Table 3.2: *Examples of wellhead displacements (u_{wh}) during discharge of selected wells in Iceland.*

Well	Year	Discharge method	u_{wh} [mm]	Time from discharge	
KJ-19	1982	Natural	20	5 hours	[1]
			45	22 days	
KJ-21	1982	Natural	22	2 hours	[2]
			33	1 day	
			68	52 days	
KJ-22	1983	Natural	27	Missing	[3]
NJ-12	1986	Wire-piston	41	11 days	[4]
NJ-13	1985	Natural	9	5 hours	[5]
NJ-14	1986	Air-pump	20	1.5 hours	[6]
NJ-16	1986	Natural	5	Missing	[7]
PG-1	2004	Air-pump	15	14 days	[8]
IDDP-1	2011	Natural	420	10 weeks	[9]

[1] Krafla, Hola KJ-19 (OS82099/JHD27), Oct. 1982
[2] Krafla, Hola KJ-21 (OS83013/JHD03), Feb. 1983
[3] Krafla, Hola KJ-22 (OS84008/JHD02), Feb. 1984
[4] Nesjavellir, Hola NJ-12 (OS85100/JHD56), Nov. 1985
[5] Nesjavellir, Hola NJ-13 (OS85101/JHD57), Nov. 1985
[6] Nesjavellir, Hola NJ-14 (OS86031/JHD09), Apr. 1986
[7] Nesjavellir, Hola NJ-16 (OS87007/JHD06), Feb. 1987
[8] Þeistareykir, Hola ÞG-01 (ISOR-2004/040), Nov. 2004
[9] Ingason et al. (2014)

Casing loads have been discussed briefly here. In essence, the main structural loads on casings are temperature changes and differential pressures. Temperature loads in the form of thermal stress in constrained conditions and reduced structural strength of materials at elevated temperatures. Pressure loads in geothermal wells materialize in high wellhead pressures which puts high tensile load on the anchor casing, and in differential pressures between the inner and outer casing wall. Temperature and pressure loads can result in casing failures that are discussed in the following section.

3.5 Casing failures

Part of this PhD study as background analysis was to quantify and map the occurrence of different casing failures. This study was then further expanded within a H2020 project GeoWell as discussed below. In the PhD study, the most common casing failure modes in high-temperature geothermal wells have been established as collapse, in the form of deformation known as puckers/bulges, and axial tensile ruptures of couplings or the threaded part of the casing. Knowledge of the number of casing failures is scarce as they are primarily found during downhole logging campaigns where there is a restriction in the well. Downhole video cameras have been used to document casing failures for greater understanding of the problem and to plan for repair of the damage. Pictures from such video logging are shown in this section.

An attempt to quantify casing failures in Iceland that was initiated in this PhD study was followed through by ÍSOR (Iceland GeoSurvey) in Horizon 2020 project GeoWell. In the study, 34 known casing failures were found in 235 high-temperature wells in Iceland. Of the total, 85% were identified as production wells, 10% as injection wells and 5% as exploration wells. Of the total, 67% of the wells were productive, 10% were insufficient producers and 11% were not productive. In 34 wells, 15% of the total, casing failures have been documented. Of those, 19 wells had casing failures of collapse and/or tensile ruptures and 15 wells had other/unknown failures, e.g. due to logging problems in the casing section. Of the 19 known failures, collapse/bulges occurred in 7 wells, tensile ruptures in 8 wells and both failures occurred in 4 wells. All of these failures occurred in production wells, except for two tensile ruptures that occurred in early exploration wells. The majority (65%) of the failures occurred in wells drilled in the past 20 years, a period where the well design has remained essentially the same.

Similar failures are seen in thermal oil wells. In one mature thermal oil project, with steam injection temperatures of 180-300°C, 35% of the steam injection wells and 49% of the "huff and puff" wells experienced failures (Maharaj, 1996). Of the failures, 85% were due to joint pullout or fracture, with offsets between parted casing ranging between 40-115 mm, and 15% were due to buckling resulting from poorly cemented casing and low cement tops. In the cyclic steam injection wells, the temperatures were more pronounced and most wells experi-

enced failure after two or three steam injection cycles (Maharaj, 1996) Another example, from Chevron's Bakersfield Cymric 1Y steam injection project, show casing failure rate of 19%, where 42% of the failures were collapses or buckling and 46% related to parted casing segments or other types of gaps causing leakage (Wu et al., 2008).

Magneschi et al. (1995) conducted a statistical research of 85 high-temperature geothermal wells in Italy. They do not mention number of failure cases, however they concluded that casing failures occur mostly in the production casing, are commonly close to the surface (h $\leq$ 250 mm). This was correlated with high free water and fluid-loss values in the cement slurry, more frequent in the casings where multi-stage cementing was used and are usually a consequence of a production test or of a temperature increase in the well. Chiotis and Vrellis (1995) list casing failures observed in seven high-temperature geothermal wells in Greece with production temperatures exceeding 300°C. Wellheads of two wells rose by 0.5 m during production test because of thermal expansion and inadequate cementing. In one well, $9^5/_8''$ production casing was severed at the joints at a depth of 69 m due to thermal stresses. In another well, a $9^5/_8''$ production casing collapsed at 6 different locations. A $7''$ tieback casing was installed to repair the damage but later failed due to collapse and possible buckling. They conclude that the major casing failures observed are caused by thermal stress while producing or cooling wells that could have been avoided through combination of slow preheating before production and proper casing design. Additionally, they conclude that burst and collapse strengths are severely reduced by axial thermal stress. Torres (2014) shows examples of casing failures observed in geothermal wells, where the casing has collapsed forming a bulge/pucker, presumably due to poor cementing at the location of a centralizer. They also name three common casing connection failures found in geothermal wells; pin compression deformation where the pin end deforms due to compression against the coupling shoulder, pin jump-in where the threads of the pin disengage and the pin displaces into the coupling and pin pull-out where previous pin jump-in is pulled out in subsequent tension. Additionally they show a full-scale test of a $10^3/_4''$ L80 casing cemented into a $13^3/_8''$ L80 casing with trapped water in the annulus. As the specimen was gradually heated up the casing collapsed precisely at the location of the trapped water.

The most severe and dangerous casing failures can cause blow-out in between casings or into the formation. Steam blow-out can be very dangerous and can

be difficult to manage. In an example from the year 1975, severe casing failures of well no. 4 in the Krafla geothermal field in N-Iceland resulted in steam blow-out which caused an catastrophic explosion and left a large crater at the well location that later got the name "Sjálfskaparvíti" which directly translates to self-made-hell (Palmason, 2005). As a result of volcanic eruption in the area the steam had become very acidic (pH of 1.8) which caused high corrosion at the wellhead, resulting in uncontrollable flow of steam from the main valve, subsequently blowing off the wellhead equipment and leaving nothing but a crater (Mortensen et al., 2009). In 1976, during drilling of well no. 9 in Krafla a surface blowout occurred near the rig, spewing mud and rocks over the drilling crew, that was later found to be caused by shallow casing rupture in nearby well no. 3 that was then abandoned and filled with gravel and cement (Mortensen et al., 2009). These rare types of failures are the most critical ones and after these incidents the casing programs in Krafla were redesigned.

In general, casing collapse occurs if the pressure difference between its external and internal surface exceeds its collapse resistance. During cementing, collapse can occur at the bottom where the pressure is highest and the casing collapses completely because of lack of annular support. However, in a producing well the collapse shape is controlled by the external support of cement and/or outer casing, and a bulge/pucker forms on the casing. Video logs of casing failures have revealed this strange collapse form. In some cases, little or no evidence of cement behind the collapse is found after it has been milled out and therefore it can be concluded that the collapse occurred due to thermal expansion of entrapped fluid behind the casing, see Fig. 3.7. In other cases, see Fig. 3.8, the cement behind the casing seems to be in good condition. This suggests that the collapse is not only related to thermal expansion of entrapped fluid but could also be caused by other factors, e.g. loss of collapse resistance due to axial compression and plastic straining of the material, both due to thermal expansion of the casing.

If no rupture occurs, collapses are not an immediate risk. The power output of the well is however proportional to the cross sectional area of the casing, therefore a collapsed casing could lead to a less productive well. Although these collapses are not a problem initially, they produce weak spots in the casing which could lead to subsequent rupture, e.g. during maintenance stops if the casing cools down and contracts. The impact of casing collapse on well integrity was seen in its most critical form in the IDDP-1 well, where the collapse of the production casing presumably caused conditions that lead to failures of two external casings,

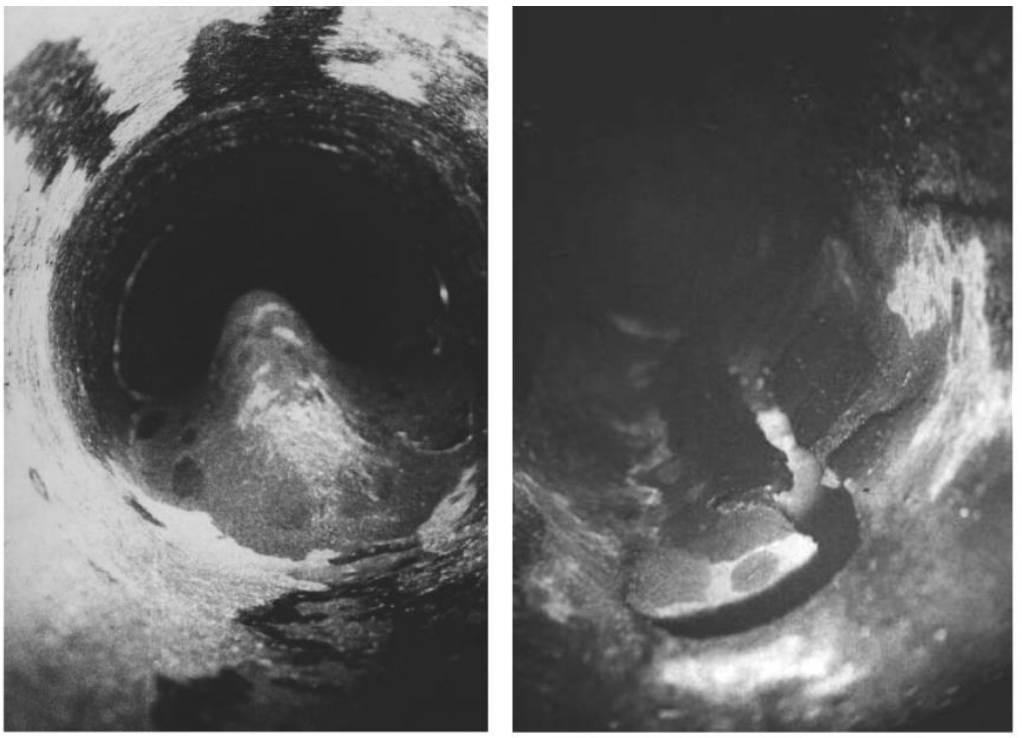

Figure 3.7: *Collapsed production casing forming a partial blockage (left). The bulge has been drilled out and no visible cement is found behind the casing suggesting collapse due to annular pressure due to expansion of entrapped boiling fluid (right) (Thorhallson, 2016).*

most likely due to high-velocity erosion after the collapse took place. This could have lead to blow out into the formation or through the annulus of the external casings. The severity of the collapse was only known after the well had been shut down (killed with water) and the collapse had been milled out. Additionally to the collapse, the production casing parted at numerous locations where in all cases the casing (pin) was pulled out of the coupling (box). This occurred when the well, initially at 450°C at the wellhead, was quenched with water. The operation history and casing failures of this special well are covered separately in section 6.4.

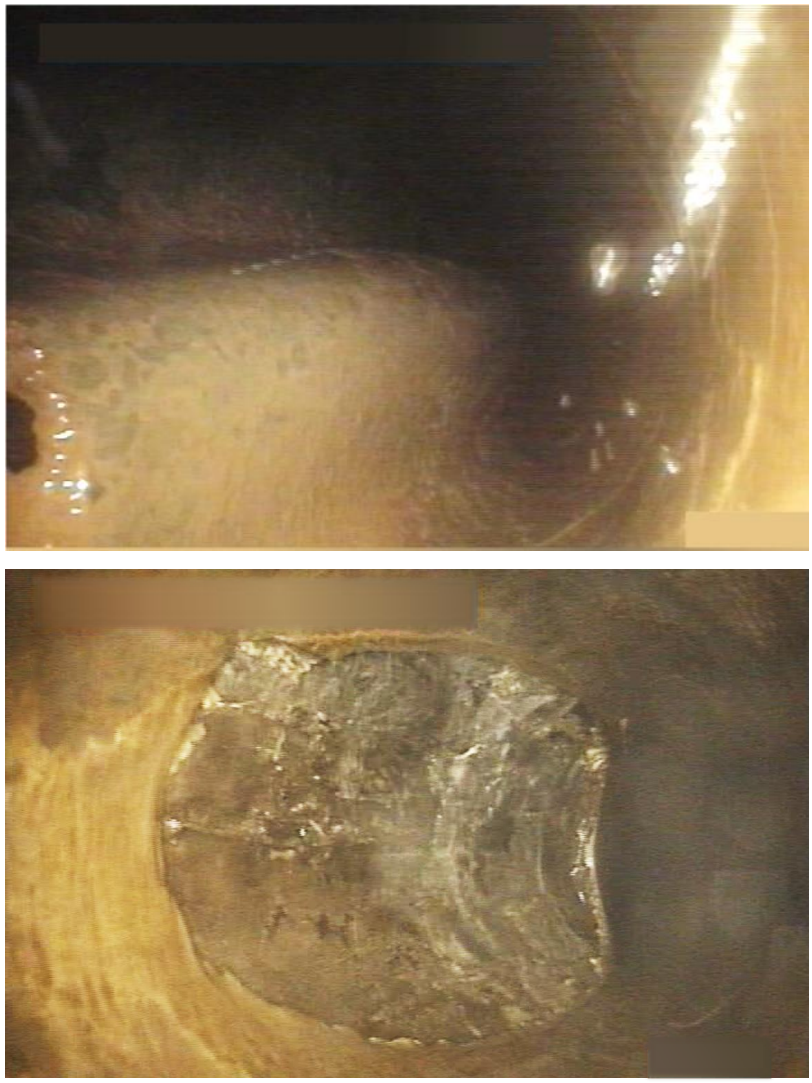

Figure 3.8: *Downhole video log by Iceland GeoSurvey (ISOR) shows collapsed production casing forming a partial blockage (top). The bulge has been drilled out and cement seems to be in good condition behind the casing (bottom) (by courtesy of ISOR and HS Orka).*

Collapse has been profoundly studied, often in connection to specific failure modes, e.g. collapse of silos, pipelines and in this case casings in high-temperature geothermal wells. Such analysis have been performed for the necessity of economical design and safety, dating back to the end of the industrial revolution where collapse resistance of tubes was studied extensively and empirical equations were devised from numerous experiments, e.g. by (Fairbairn, 1858). Since then many studies have been performed on the subject to improve empirical equations describing pipe collapse. Experiments have revealed that collapse resistance of pipes is controlled by the diameter-to-thickness ratio (D/t), material properties and is highly dependent on geometrical imperfections, e.g. average outside diameter, average wall thickness, ovality and eccentricity, as well as residual stresses from manufacturing.

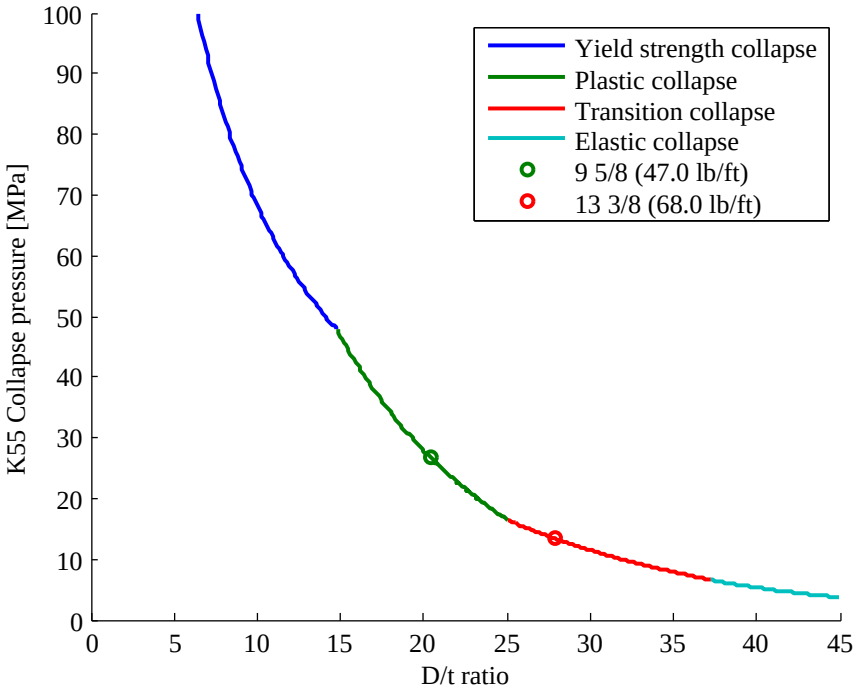

Figure 3.9: *Collapse resistance of K55 grade casing according to standard ISO/TR 10400:2007(E). Two casings are shown as an example.*

The approach taken in the ISO/TR 10400:2007(E) standard is to combine theoretical, numerical and statistical tools in order to develop collapse equations for casings (ISO/TR 10400:2007(E), 2007). Collapse resistance of K55 grade cas-

ing, calculated according to the standard, is shown in Fig. 3.9. Four zones where different equations are applied are used to calculate the collapse resistance; (i) yield strength collapse for the casings with the high relative wall thickness (low D/t ratio), (ii) plastic, (iii) transition, and finally (iv) elastic collapse for relatively thin walled casings (high D/t ratio). This applies for unsupported casings with uniform differential pressure between the inner and outer casing wall. It is worth noting that API burst and collapse design equations from the standard do not address pipe body response when axial stress in the casing exceeds the material yield strength, as the focus of standardization has been geared towards elastic designs (Dall'Acqua et al., 2012).

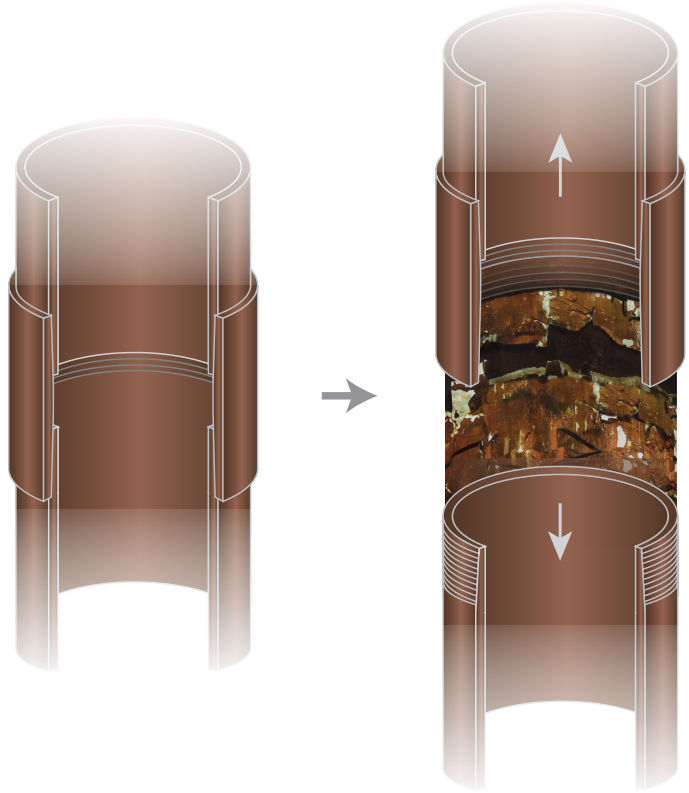

Figure 3.10: *Casing failure mode caused by thermal stresses reaching beyond yield generating permanent plastic strain in axial compression leading to tensile ruptures if wells cool down again, e.g. by pumping water into hot wells (see Fig. 3.6).*

Shutting down wells during maintenance or other stops can have multiple neg-

ative effects on the casing. Cooling during such periods generates contraction in the casing and multiple stops during the lifetime of wells lead to cyclic thermal loading. If some sections of wells cool down, e.g. uppermost in wells, the compressive forces that were generated during production could be reversed to tensile forces. If shut-in conditions lead to increase in pressure, temperature can increase as well, further straining the structure.

High temperature and thermal straining as a result of thermal expansion have been discussed here as a major structural concern for casings in geothermal wells. Another great structural concern, of chemical nature, is corrosion. The subject of corrosion is outside the scope of this thesis, but its major structural impacts are embrittlement and thickness reduction of casing material. Materials used in aggressive geothermal environment can be subjected to corrosion due to dissolved gases such as H_2S and CO_2 and in some cases HCl (Karlsdottir and Thorbjornsson, 2012). Corrosion is also dependent on key parameters, i.e. temperature, pressure, flow rate and pH level of the fluid (Karlsdottir and Thorbjornsson, 2012). Corrosion mechanisms in high-temperature geothermal environment include uniform corrosion, galvanic corrosion due to potential difference of different materials, localized pitting and crevice corrosion, hydrogen embrittlement and hydrogen induced cracking (HIC), stress corrosion cracking (SCC) and sulfide stress cracking (SSC), corrosion fatigue cracking (CFC) and flow related mechanisms of erosion corrosion and cavitation. Corrosion can in some cases be measured, one method is to estimate a corrosion rate. In geothermal wells as in hydrocarbon wells the acceptable corrosion rate is considered 0.1 mm/year reduction in material thickness (Karlsdottir, 2013; Norsok M-001, 2002). In high-enthalpy wells where the produced steam is superheated single phase steam, shut-in periods can lead to condensation of the geothermal fluid which can cause abrupt corrosion due to high concentration of corrosive substances. Hydrogen damages such as HIC can decrease the ductility and cause premature fracture of the casing when subjected to tensile stress. Studies on corrosion in geothermal environment have resulted in narrowed material selection as some materials are good candidates and other are more susceptible to corrosion and related effects. Thorbjornsson et al. (2015) discuss material selection for geothermal wells in high temperatures and pressures based on testing in geothermal environment in Iceland.

4

Nonlinear finite-element method

4.1 General description

The finite-element method (FEM) is a method for solving problems by obtaining numerical approximate solutions to partial differential equations describing the problem. The problem domain, a surface or a volume, is discretized by generating a mesh constructed of elements with nodal points. In this thesis, the method is used for heat transfer and structural analysis. The nonlinear finite-element method incorporates nonlinearities, i.e. in large geometrical displacements, material properties and due to change of status, for example in contact between surfaces. ANSYS Parametric Design Language (APDL) is a scripting language that is used to automate common tasks to build and solve models in terms of parameters (Ansys, Inc.). Documentation for ANSYS is partly used here to describe in brief some of the essential mathematical representations of the nonlinear finite-element method.

Elements are used to convert continuous areas or volumes into discrete counterparts known as a mesh. The elements are built of and connected to other elements by nodes. Specific element types exist for different types of problems for vastly wide range of applications, e.g. electrical, magnetic, heat transfer and structural modeling. An element type can be categorized into multiple groups but their main features is their shape, degree of freedom (DOF) and intended use. Two-dimensional (2-D) and three-dimensional (3-D) models require different types of elements and some elements work in both cases. In general, four element shapes are usually used: point defined by one node such as a mass element, a line element typically represented by a line or arc defined with two or three nodes, an area element with triangular or quadrilateral shape that can be a 2-D solid element or a shell and a volume element that has a tetrahedral or brick shape and

is usually a 3-D solid element. 2-D elements used in structural analysis can be classified as either plane stress or plane strain elements. Plane stress assumes that the stress state varies only in two directions X and Y and the stress in Z direction is always zero, as are the XZ and YZ shear stresses. Plane strain is a stress state also varies in X and Y directions but the strain in Z direction and in XZ and YZ shear are always zero. Therefore, plane stress elements are ideal for modeling thin structures and plane strain elements for modeling cross-sections where strain considerations in Z direction are not necessary. 2-D axisymmetric elements follow neither plane stress nor plane strain limitations, instead they assume that the structure is a full circle revolution, where radial and axial displacements can be modeled, and tri-axial stresses and strains can be analyzed. DOF determine the intended use of elements, i.e. structural, thermal, fluid, electric, magnetic or coupled field. In thermal analysis the DOF is temperature and in structural analysis DOF is displacements and rotations for some elements.

Two types of thermal analyses are possible. A steady-state analysis where temperature distribution and other thermal quantities are determined under steady-state loading conditions where heat storage effects varying over a period of time can be ignored. A transient thermal analysis where temperature distribution and other thermal quantities vary over a period of time. Structural analysis fall under numerous classifications, e.g. static analysis where displacements, stresses, etc. are solved under static loading conditions, modal analysis for determining natural frequencies and mode shapes of a structure, transient dynamic analysis to determine a structures response to arbitrary time-varying loads, linear buckling analysis for calculating buckling loads and determining buckling mode shapes, nonlinear buckling analysis for including nonlinearities, and many more.

The linear finite-element method can be used for modeling small displacements in structures and stresses that are within the elastic range of materials. Nonlinear behavior, i.e. (i) large geometrical displacements, (ii) nonlinear material properties and (iii) contact between surfaces/changing status, needs to be solved with the nonlinear finite-element method, typically using the Newton-Raphson method. In such models, large displacements/rotations, plastic strain and contact problems are solved in each load-step with multiple iterations within a defined number of substeps. Selection of the number of substeps depends on the problem each time. If surface contact is included, a minimum number of substeps needs to be used in order to get convergence in the solution.
Linear eigenvalue analysis is useful for initial assessment of buckling and col-

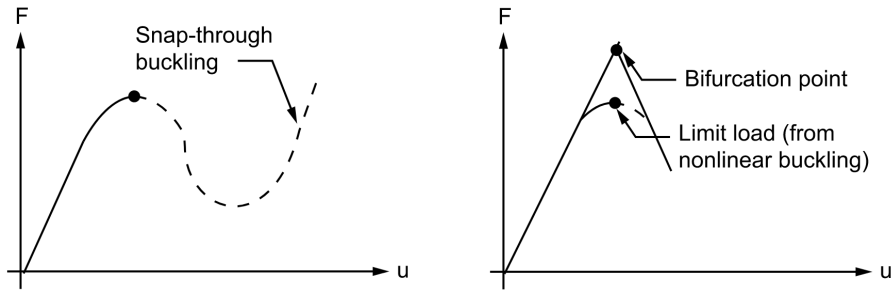

Figure 4.1: *Nonlinear load-deflection curve (left) and linear (eigenvalue) buckling curve illustrating the bifurcation point and limit load from nonlinear buckling analysis (Ansys, Inc.).*

lapse loads. The analysis estimates theoretical buckling strength or the bifurcation point of an ideal linear elastic structure. Imperfections and nonlinearities prevent most structures from achieving their theoretical buckling strength. Therefore, linear eigenvalue buckling analysis overestimates the buckling load in most cases, see Fig. 4.1.

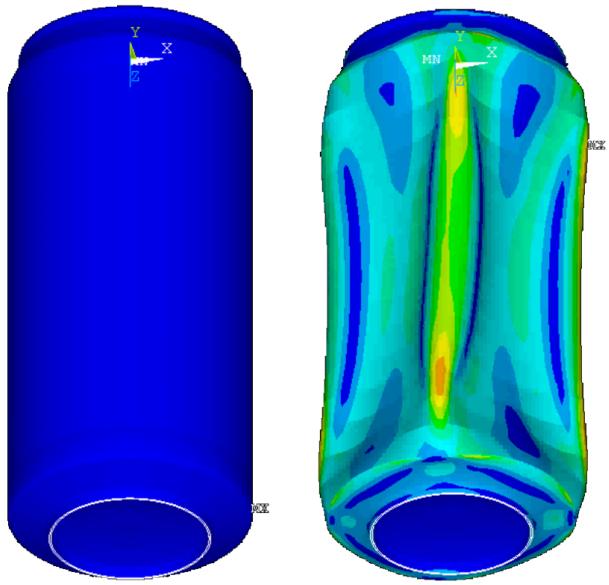

Figure 4.2: *An example of a nonlinear buckling analysis predicting limit load, post-buckling shape, displacements and stresses of a soda bottle under external pressure (showing von Mises stress distribution).*

Nonlinear buckling analysis can predict the limit load with better accuracy as well as the buckling shape, displacements, stresses and strains by incorporating nonlineatities and imperfections. Post-buckling shapes of structures can be modeled with the method as well. Fig. 4.2 shows an example of a limit load analysis by using nonlinear structural analysis.

4.2 Derivation of Structural Matrices

The principle of virtual work states that a virtual change of the internal strain energy must be offset by an indentical change in external work due to the applied loads,

$$\delta U = \delta W \tag{4.1}$$

where $U = U_1 + U_2$ is strain energy (internal work) and $W = W_1 + W_2 + W_3$ is external work. The virtual strain energy is,

$$\delta U_1 = \int_V \{\delta\epsilon\} \{\sigma\} \, dV^T \tag{4.2}$$

where $\{\epsilon\}$ is the strain vector, $\{\sigma\}$ is the stress vector and V is volume of element. Combining equations 4.1 and 4.2 gives,

$$\delta U_1 = \int_V \left(\{\delta\epsilon\}^T [D] \{\epsilon\} - \{\delta\epsilon\}^T [D] \left\{\epsilon^{th}\right\} \right) dV \tag{4.3}$$

The strains may be related to nodal displacements by,

$$\{\epsilon\} = [B] \{u\} \tag{4.4}$$

where $[B]$ is the strain-displacement matrix based on the element shape functions and $\{u\}$ is the nodal displacement vector. Combining 4.2 and 4.3 gives,

$$\delta U_1 = \{\delta u\}^T \int_V [B]^T [D] [B] \, dV \, \{u\} - \{\delta u\}^T \int_V [B]^T [D] \left[\epsilon^{th}\right] dV \tag{4.5}$$

A different form of virtual strain energy when a surface moves against a distributed resistance, as in a foundation stiffness, is written as,

$$\delta U_2 = \int_{A_f} \{\delta w_n\}^T \{\sigma\} \, dA_f \tag{4.6}$$

where $\{w_n\}$ is motion normal to the surface, $\{\sigma\}$ is stress (or pressure) carried by the surface and A_f is the area of the distributed resistance. The point-wise normal displacement is related to the nodal displacements by,

$$\{w_n\} = [N_n] \{\delta u\} \tag{4.7}$$

where $[N_n]$ is a matrix of shape functions for normal motions at the surface and the stress is,

$$\{\sigma\} = k \{w_n\} \tag{4.8}$$

where k is foundation stiffness in units of force per length per unit area. Combining equations 4.6, 4.7 and 4.8 assuming that k is constant over the area gives,

$$\delta U_2 = \{\delta u\}^{Tk} \int_{A_f} [N_n]^T [N_n] \, dA_f \, \{u\} \tag{4.9}$$

The inertial effects of the external virtual work is,

$$\delta W_1 = -\int_V \{\delta w\}^T \frac{\{F^a\}}{V} dV \tag{4.10}$$

where $\{w\}$ is a vector of displacements of a general point and $\{F^a\}$ is an acceleration (D'Alembert) force vector. According to Newton's second law,

$$\frac{\{F^a\}}{V} = \rho \frac{\delta^2}{\delta t^2} \{w\} \tag{4.11}$$

where ρ is density and t is time. The displacements within the element are related to the nodal displacements by,

$$\{w\} = [N] \{u\} \tag{4.12}$$

where $[N]$ is a matrix of shape functions. Combining equations 4.10, 4.11 and 4.12 and assuming ρ is constant over the volume,

$$\delta W_1 = -\{du\}^T \rho \int_V [N]^T [N] \, dV \frac{\delta^2}{\delta t^2} \{u\} \tag{4.13}$$

The pressure force vector formulation is,

$$\delta W_2 = \int_{A_p} \{\delta w_n\}^T \{P\} \, dA_p \tag{4.14}$$

where $\{P\}$ is the applied pressure vector and A_p is the outside area of a surface over which pressure is defined normal to, unless otherwise noted. Combining equations 4.12 and 4.14 gives,

$$\delta W_2 = \{\delta u\}^T \int_{A_p} [N_n] \{P\} \, dA_p \tag{4.15}$$

Nodal forces applied to the element can be accounted for by,

$$\delta W_3 = \{\delta u\}^T \left\{F_e^{nd}\right\} \tag{4.16}$$

where $\left\{F_e^{nd}\right\}$ are nodal forces applied to the element. Finally, combined equiations 4.11, 4.12, 4.13, 4.14, 4.15 and 4.16 give,

$$\begin{aligned}
&\{\delta_u\}^T \int_V [B]^T [D] [B] \, dV \{u\} - \{\delta_u\}^T \int_V [B]^T [D] \left[\epsilon^{th}\right] dV \\
&+ \{\delta_u\}^T k \int_{A_f} [N_n]^T [N_n] \, dA_f \{u\} \\
=& - \{\delta u\}^T \rho \int_V [N]^T [N] \, dV \frac{\delta^2}{\delta t^2} \{u\} \\
&+ \{\delta u\}^T \int_{A_p} [N_n]^T \{P\} \, dA_p + \{\delta u\}^T \left\{F_e^{nd}\right\}
\end{aligned} \tag{4.17}$$

Noting that the $\{\delta u\}^T$ vector is a set of arbitrary virtual displacements common in all of the above terms, the condition required to satisfy equation Equation 4.17 reduces to,

$$\left([K_e] + \left[K_e^f\right]\right) \{u\} - \left\{F_e^{th}\right\} = [M_e] \{\ddot{u}\} + \{F_e^{pr}\} + \left\{F_e^{nd}\right\} \tag{4.18}$$

where the element stiffness matrix is,

$$[K_e] = \int_V [B]^T [D] [B] \, dV \tag{4.19}$$

the element foundation stiffness matrix is,

$$\left[K_e^f\right] = k \int_{A_f} [N_n]^T [N_n] \, dA_f \tag{4.20}$$

the element thermal load vector is,

$$\left\{F_e^{th}\right\} = \int_V [B]^T [D] \left[\epsilon^{th}\right] dV \tag{4.21}$$

the element mass matrix is,

$$[M_e] = \rho \int_V [N]^T [N] \, dV \tag{4.22}$$

is the acceleration vector (such as gravity effects) is,

$$\{\ddot{u}\} = \frac{\delta^2}{\delta t^2} \{u\} \tag{4.23}$$

and the element pressure vector is,

$$\{F_e^{pr}\} = \int_{A_p} [N_n]^T \{P\} \, dA_p \tag{4.24}$$

4.3 Geometric nonlinearities

Nonlinear structural analysis can incorporate nonlinearities that regularly occur in structures. In small deflection and small strain analyses it is assumed that displacements are small enough resulting in insignificant stiffness changes. When strains in a material become larger than a few percent, the change in geometry due to this deformation can no longer be neglected. Large strain analysis accounts for stiffness changes that results from changes in shape and orientation of elements. The theory of large strain computation can be addressed by

definition of few basic physical quantities, motion and deformation, and the corresponding mathematical relationship. The motion derived from of applied loads acting on a body can be defined by studying a position vector in the deformed and undeformed configuration (Fig. 4.3 with states represented as $\{x\}$ and $\{X\}$, respectively, then the motion vector $\{u\}$ is calculated by:

$$\{u\} = \{x\} - \{X\} \tag{4.25}$$

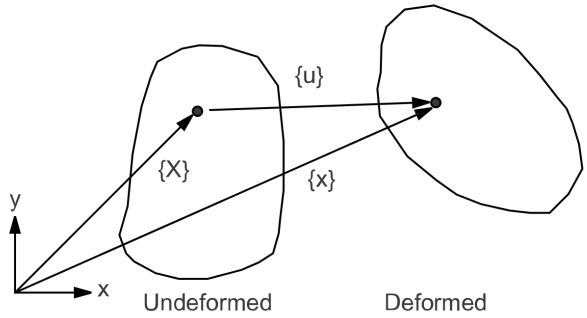

Figure 4.3: *Position vectors and motion of a deforming body (Ansys, Inc.).*

The deformation gradient is defined as:

$$[F] = \frac{\delta\{x\}}{\delta\{X\}} \tag{4.26}$$

which can be written in terms of displacement of the point via equation 4.25 as:

$$[F] = [I] + \frac{\delta\{u\}}{\delta\{X\}} \tag{4.27}$$

where $[I]$ is the identity matrix. The information contained in the deformation gradient $[F]$ includes the volume change, rotation and shape change of the deforming body, where the volume change at a point is:

$$\frac{\delta\{V\}}{\delta\{V_0\}} = det\,[F] \tag{4.28}$$

Where V_0 is the original volume and V is the current volume.

The deformation gradient can be separated into rotation and shape change:

$$[F] = [R]\,[U] \tag{4.29}$$

where $[R]$ is the rotation matrix ($[R]^T [R] = [I]$ and $[U]$ is the shape change right stretch matrix.

The element matrices and load vectors are derived using an updated Lagrangian formulation which produces equations of the form,

$$\left[K_i^T\right] \{\Delta u_i\} = \{F^a\} - \{F_i^{nr}\} \tag{4.30}$$

where the tangent matrix $[\bar{K}_i]$ has the form,

$$\left[\bar{K}_i\right] = [K_i] + [S_i] \tag{4.31}$$

$[K_i]$ is the usual stiffness matrix,

$$[K_i] = \int [B_i]^T [D_i] [B_i] \, dV \tag{4.32}$$

where $[B_i]$ is the strain-displacement matrix in terms of the current geometry $\{X_n\}$, $[D_i]$ is the current stress-strain matrix and $[S_i]$ is the stress stiffness contribution, written symbolically as,

$$[S_i] = \int [G_i]^T [\tau_i] [G_i] \, dV \tag{4.33}$$

where $[G_i]$ is a matrix of shape function derivatives and $[\tau_i]$ is a matrix of the current Cauchy (true) stresses $\{\sigma_i\}$. The Newton-Raphson restoring force is,

$$[F_i^{nr}] = \int [B_i]^T [\sigma_i] \, dV \tag{4.34}$$

4.4 Material nonlinearities

Elastic behavior is characterized by linear stress-strain relationship and recoverable strain. When surpassing yield point of materials and generating plastic

nonrecoverable strain, nonlinear material curves need to be incorporated, calling for nonlinear iterative solution methods. Plasticity theory provides a mathematical relationship of the elastoplastic response of materials. Three major components in the rate-independent plasticity theory, the yield criterion, flow rule and hardening rule.

The yield criterion determines the stress level at which yielding initiates at. For multi-component stresses, this is represented as a function of individual components, which can be interpreted as an equivalent stress:

$$\sigma_e = f\left(\{\sigma\}\right) \tag{4.35}$$

where $\{\sigma\}$ is a stress vector. When the equivalent stress is equal to the yield parameter $f\left(\{\sigma\}\right) = \{\sigma_y\}$ the material will develop plastic strains.

The flow rule determines the direction of plastic straining and is given by:

$$\left\{d\epsilon^{pl}\right\} = \lambda \left\{\frac{\delta Q}{\delta \sigma}\right\} \tag{4.36}$$

where λ is a plastic multiplier determining the amount of plastic straining, Q is a function of stress termed the plastic potential determining the direction of plastic straining.

The hardening rule describes the changing of the yield surface so that the stress state condition for subsequent yielding can be established. Two hardening rules are available, work hardening (isotropic) and kinematic hardening. In work hardening the yield surface remains centered about its initial centerline and expands in size as plastic strains develop, but kinematic hardening assumes that the yield surface remains constant in size and the surface translates in stress space with progressive yielding, as shown in Fig. 4.4. Multilinear kinematic hardening rule allows for a multilinear stress-strain curve that exhibits the Bauschinger effect, as shown in Fig. 4.5.

The Euler backward scheme is used to enforce consistency condition in implementation of plastic strain increments. The parameter σ_y is determined for the time step, the stresses are computed based on the trial strain $\{\epsilon^{tr}\}$ which is the total strain minus the plastic strain from previous time point,

$$\left\{\epsilon_n^{tr}\right\} = \{\epsilon_n\} - \left\{\epsilon_{n-1}^{pl}\right\} \tag{4.37}$$

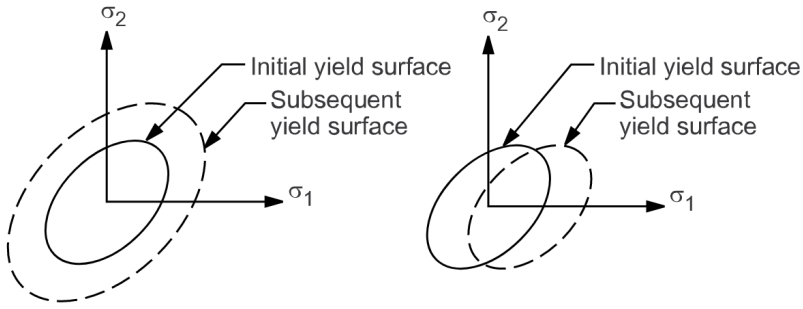

Figure 4.4: *Types of hardening rules, isotropic work hardening (left) and kinematic hardening (right)(Ansys, Inc.).*

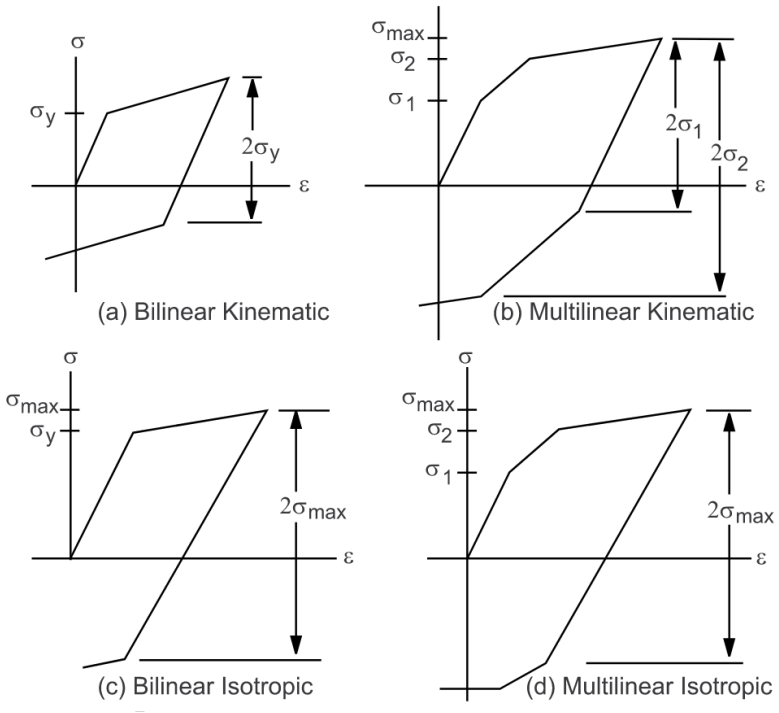

Figure 4.5: *Stress-strain behavior of different plasticity options(Ansys, Inc.).*

The trial stress is then,

$$\left\{\sigma^{tr}\right\} = [D]\left\{\epsilon^{tr}\right\} \tag{4.38}$$

The equivalent stress is evaluated by equation 4.35. If stress exceeds the material yield, the plastic multiplier λ is determined by a local Newton-Raphson iteration

procedure. The plastic strain increment is calculated by,

$$\left\{d\epsilon^{pl}\right\} = \lambda \left\{\frac{\delta Q}{\delta \sigma}\right\} \tag{4.39}$$

The current plastic strain is updated,

$$\left\{\epsilon_n^{pl}\right\} = \left\{\epsilon_{n-1}^{pl}\right\} + \left\{\Delta\epsilon^{pl}\right\} \tag{4.40}$$

and the elastic strain computed,

$$\left\{\epsilon^{el}\right\} = \left\{\epsilon^{tr}\right\} - \left\{\Delta\epsilon^{pl}\right\} \tag{4.41}$$

The stress vector is,

$$\left\{\sigma^{tr}\right\} = [D]\left\{\epsilon^{tr}\right\} \tag{4.42}$$

4.5 Surface contact

Surface contact is defined by contact-target element pairs meshed onto each surface. Their main purpose is to prevent surfaces from intersecting each other while still allowing gaps to form and tangential displacement. They also serve to transfer temperature and structural loads between the surfaces. A conductive heat transfer between two contacting surfaces is defined by:

$$q = TCC\,(T_t - T_c) \tag{4.43}$$

where q is the heat flux per area, TCC is the thermal contact conductance coefficient and T_t and T_c are the temperatures of the target and contact surfaces. Other heat transfer mechanisms, i.e. convection, radiation and heat generation due to friction, between surfaces are also supported but are not used in this study.

Using the Coulomb friction model, friction is described with a friction coefficient, μ, cohesion shear stress τ_b. The surfaces can withstand shear stresses up to a certain magnitude across its interface before relative sliding initiates, once the equivalent shear stress τ exceeds τ_{lim}, relative sliding begins.

$$\tau_{lim} = \mu P + \tau_b \tag{4.44}$$

Additionally, a maximum shear stress τ_{max} independent of the normal stress can be defined as:

$$\tau = \begin{cases} \mu P + \tau_b & \text{if } \tau < \tau_{max} \\ \tau_{max} & \text{if } \tau \geq \tau_{max} \end{cases} \tag{4.45}$$

where τ is the equivalent shear stress, τ_{max} is the maximum shear stress, μ is the isotropic coefficient of friction, τ_b is the contact cohesion and P is the contact normal pressure. Fig. 4.6 shows the graphical interpretation of the Coulomb friction model.

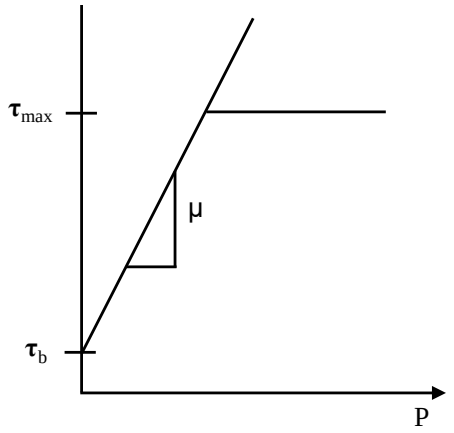

Figure 4.6: *The Coulomb friction model in Ansys (Ansys, Inc.).*

4.6 Solution procedure

The finite-element discretization process yields a set of simultaneous equations,

$$[K]\{\Delta u\} = \{F^a\} \tag{4.46}$$

where $[K]$ is a coefficient matrix, $\{u\}$ is a vector of unknown DOF values $\{F^a\}$ is a vector of applied loads. If $[K]$ is itself a function of unknown DOF values, equation 4.46 becomes a nonlinear equation that needs to be solved iteratively. The Newton-Raphson method solves nonlinear equations in an iterative process and can be written as follows:

$$\left[K_i^T\right]\{\Delta u_i\} = \{F^a\} - \{F_i^{nr}\} \tag{4.47}$$

$$\{u_{i+1}\} = \{u_i\} + \{\Delta u_i\} \tag{4.48}$$

where in a structural analysis $\left[K_i^T\right]$ is the tangent stiffness matrix, $\{u_i\}$ is the displacement vector and $\{F_i^{nr}\}$ is the restoring force vector calculated from the element stresses, and in thermal analysis $\left[K_i^T\right]$ is the conductivity matrix, $\{u_i\}$ is the temperature vector and $\{F_i^{nr}\}$ is the resisting load vector calculated from the element heat flows. $\{F^a\}$ denotes a vector of applied loads i is a subscript representing the current equilibrium iteration.

A number of iterations is taken until a converged solution is found. The algorithm for the solution procedure is such that first the tangent matrix $\left[K_i^T\right]$ is calculated and updated along with the restoring load $\{F_i^{nr}\}$ from configuration $\{u_i\}$, $\{\Delta u_i\}$ is calculated from equation 4.47 and added to $\{u_i\}$ for the next approximation $\{u_{i+1}\}$ with equation 4.48. These steps are repeated until convergence is obtained.

Convergence is obtained when the residual vector, the imbalance of the right hand side in equation 4.47, is within the force convergence criterion tolerance and/or the degree of freedom (DOF) increment is within its defined tolerance in equation 4.50,

$$\|\{R\}\| < \epsilon_R R_{ref} \tag{4.49}$$

$$\|\{\Delta u_i\}\| < \epsilon_u u_{ref} \tag{4.50}$$

where the residual vector is,

$$\{R\} = \{F^a\} - \{F^{nr}\} \tag{4.51}$$

When the load incremental step has converged the next load increment can be taken. Considering the Newton-Raphson method iteration, the major computational cost lies generally in the calculation and factorization of the tangent stiffness matrix (Bathe, 1996). If the tangent stiffness matrix is updated in each iteration, then the process is termed the full Newton-Raphson method. The stiffness matrix can be updated less frequently by using the modified Newton-Raphson method where during each iteration it can remain constant. Which method is best suited depends on the problem in question and time consuming calculations to update the tangent stiffness matrix can in some cases result in better and even faster convergence. Other method includes initial-stiffness procedure where the stiffness matrix is prevented from updating which requires higher number of iterations but in turn requires fewer matrix reformulations and inversions.

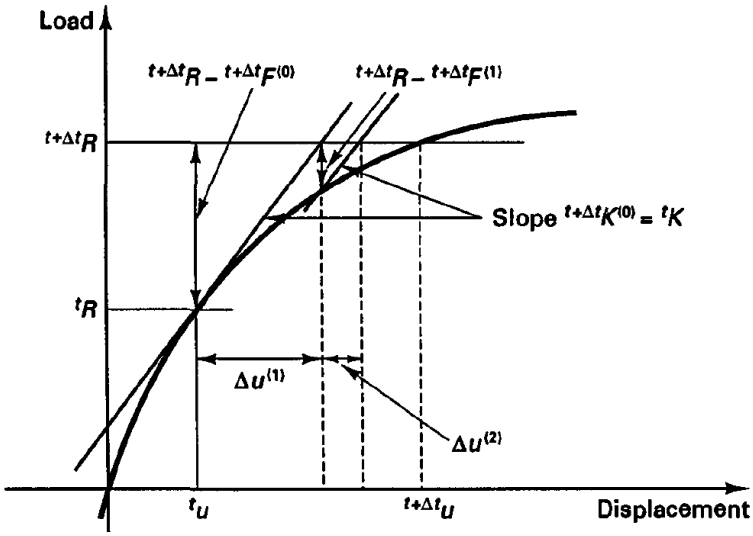

Figure 4.7: *The modified Newton-Raphson method requires fewer updates of the stiffness matrix than the full method (Bathe, 1996).*

5

Models and verification

5.1 Models

Model descriptions

In this section, the construction of models of the cased section of high-temperature geothermal wells is described. The ANSYS Parametric Design Language (APDL) is used to build and solve the models. Different well setups and load cases are analyzed by defining geometric parameters, material properties, loads and boundary conditions. Two geometries are essentially used to analyze different aspects of the structural system; (a) a 2-D axisymmetric model of the whole cased well used to model temperature, displacements, stress and strain distributions of the global structural system, and (b) a 3-D model of a section of the well which is used to model non-symmetric phenomena such as collapse. Additionally, a 2-D axisymmetric model of a buttress thread casing (BC) connection is presented.

When thermal loads are defined, the models are divided into two parts, thermal and structural, that are run in succession. Identical meshes are used for both cases using elements with suitable degrees of freedoms (DOFs). After the thermal analysis has been performed the results are used as thermal load in the structural part of the model where wellbore pressures are defined additionally. This decoupling of thermal and structural analyses is necessary due to difficulties in solving surface contact with coupled field elements that have both thermal and structural DOFs.

Casing collapse is analyzed with 3-D models where the structural support of cement and instability due to water enclosed in the cemented annulus are analyzed. The effect of geometrical defects and initial geometrical perturbations are analyzed with the model. The following cases are considered:

I. Eigenvalue collapse analysis
II. Nonlinear collapse analysis
    i. Effect of initial geometry
        a. Mode shape perturbation
        b. Ovality of casing
        c. External defect in casing
    ii. Effect of cement support
        a. Exclusion of cement
        b. Enclosed water pocket in the casing-to-casing annulus

Eigenvalue buckling analysis is used to predict the theoretical collapse strength and the collapse mode shapes of the casing. The eigenvalue analysis is a linear solution method in which nonlinear properties, i.e. nonlinear material properties and interaction of contacting surfaces, cannot be taken into account. Nonlinear buckling analysis is then used to account for such nonlinearities. The limit load of the casing is obtained and stabilization is used to track the post-buckling shape of the casing.

The geometry of the casing model is shown in Fig. 5.1. A 12 meter section of the production casing is modeled. The cement around the production casing is included in the nonlinear analysis and external casings are not included for simplification purposes. Instead boundary conditions are defined where no radial displacements are allowed at the outer boundary of the cement and axial displacements are constrained at both ends. The casing that is considered in the analysis has a $13^3/_8$ inch outer diameter, with thickness of 12.2 mm and made of K55 grade steel. One half of the casing circumference is modeled, which is possible due to the symmetry of the casing and its collapse shape. The thickness of the wall is scaled with an API manufacturing tolerance of -12,5%. Contact element pairs are used between the casing and the cement surfaces and a Coulomb friction model is used to define friction between the surfaces.

Due to the perfect geometry of the model, some imperfections or perturbations need to be introduced to create instability in the structure. Instead of applying a small radial force, which is a common practice, instability is created with randomly distributed material imperfections in the steel casing. These imperfections are included in the casing as small variations in material properties. 20% of the casing elements are randomly selected for this purpose.

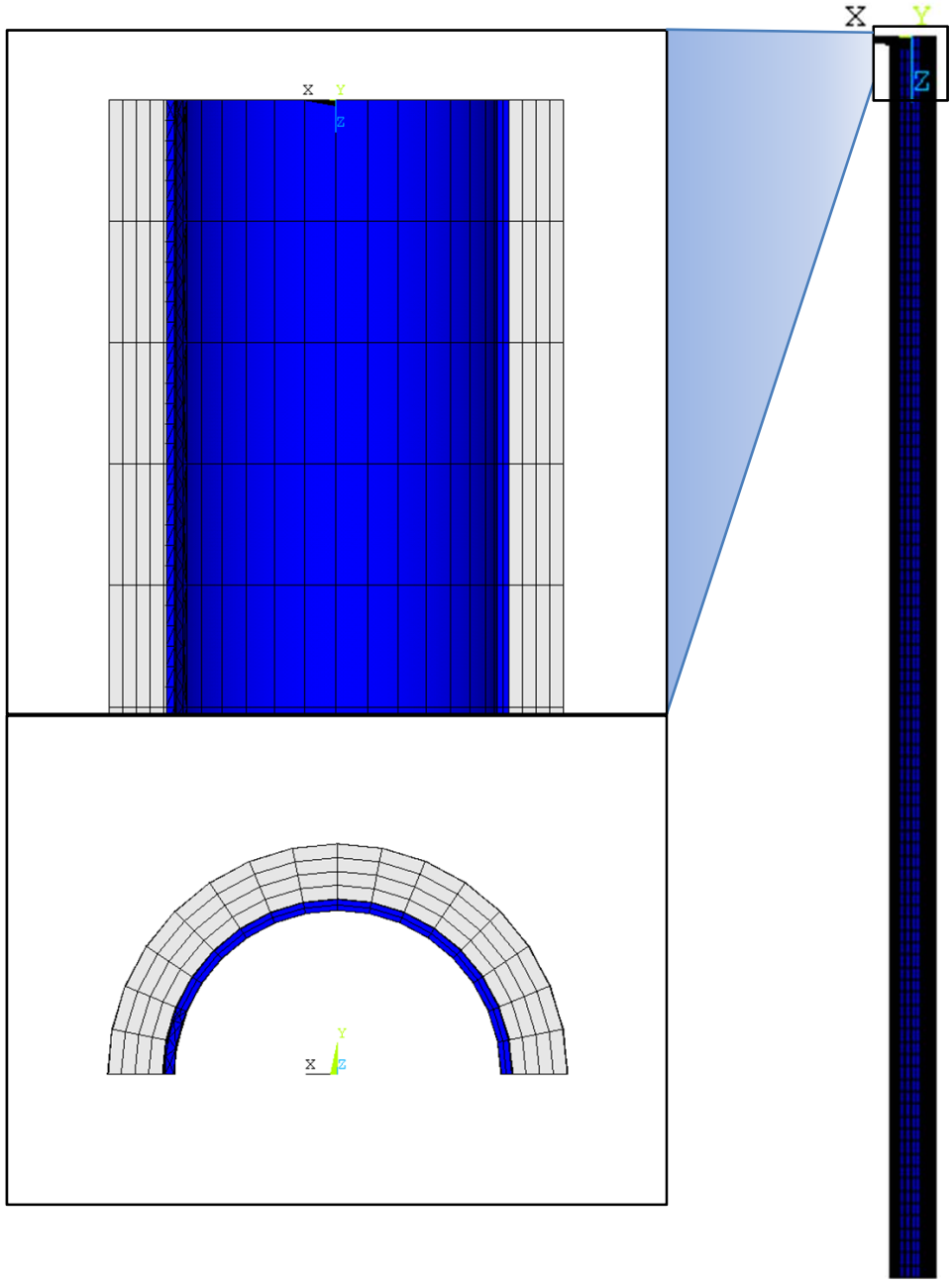

Figure 5.1: *The geometry of the innermost casing and cement of the 3D collapse model.*

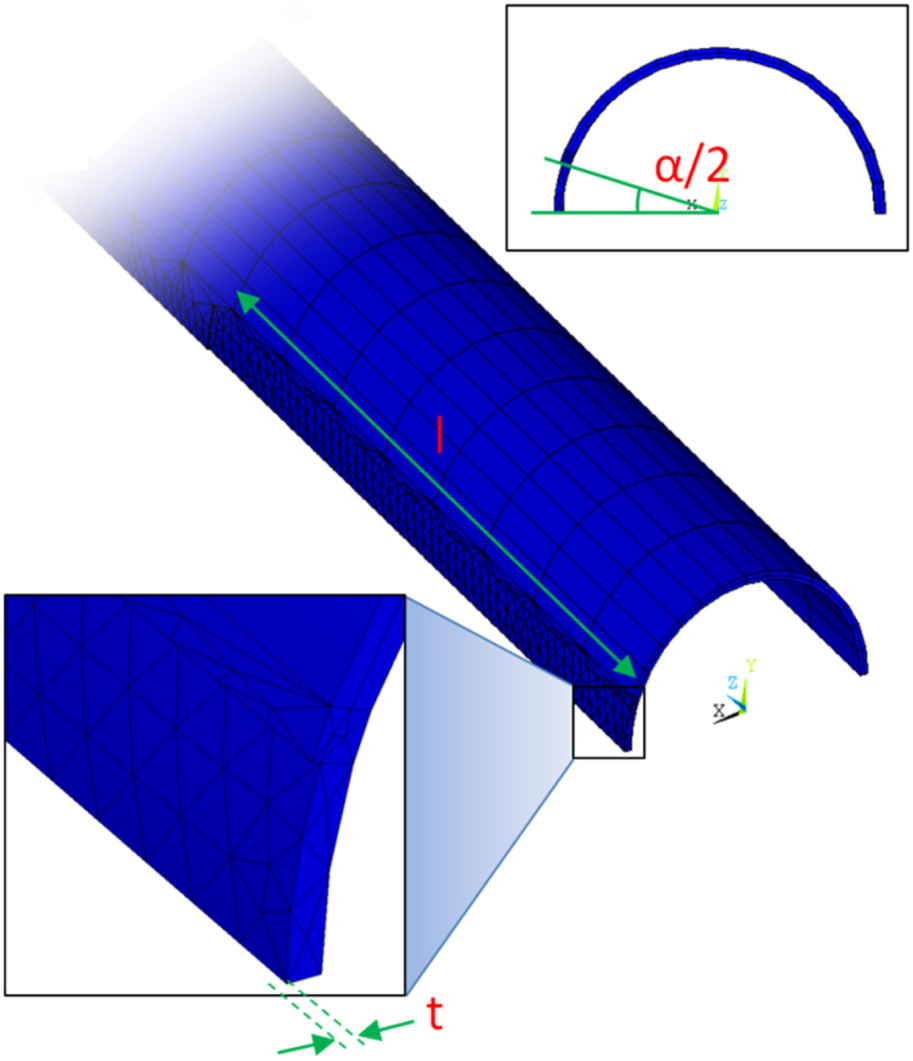

Figure 5.2: *Size and shape of an external defect in the casing.*

The effect of ovality on collapse strength of the casing is analyzed. Ovality of pipes is defined as:

$$Ovality = \frac{D_{max} - D_{min}}{D} \tag{5.1}$$

where D_{max} is the maximum outer diameter, D_{min} is the minimum outer diameter and D is the mean outer diameter. The effect of a small local defect on the outside of the production casing is also analyzed. The size and shape of the defect is controlled by three parameters; thickness, angle size and length as shown in Fig. 5.2.

The effect of enclosed water in the annulus between casings is analyzed by including a small water pocket in the cement. The water pocket is 1.6 m long and fills up half of the annulus circumference. Imperfections are randomly dispersed in the pocket, consisting of 80% water and 20% cement, as shown in Fig. 5.3.

A 2-D model that is axially symmetric around the center of the well is used to analyze the cased section of the geothermal well, i.e. the structure above the production casing shoe. Axial and radial deformations can therefore be analyzed with the model but lateral and asymmetrical deformations, e.g. bending, buckling and collapse can not. Although the angular displacements are zero, hoop strains and stresses can nevertheless be analyzed because of the revolving axial symmetry. The model, seen in Fig. 5.4, reaches from the wellhead down to the bottom of the production casing and 20 m further down where the lower boundary is located. The radial boundary of the model is located 100 m from the center of the well. To account for the anchoring effects of couplings that stick out to the cement, simplified connections with no threads are included. Additionally, a simplified wellhead, shown in Fig. 5.5, is included to account for pressure loads and the interaction between the casings and the wellhead. Sliding of the production casing inside the wellhead is therefore included if such wellhead design is being analyzed.

Geometrical sizes and material properties are easily adjusted so that different well designs can be analyzed. However, the model quickly grows in element numbers, specially if long casings are being analyzed. Despite its 2D axial symmetry and therefore greatly reduced number of elements compared to a 3D model, the model is heavy in computation time.

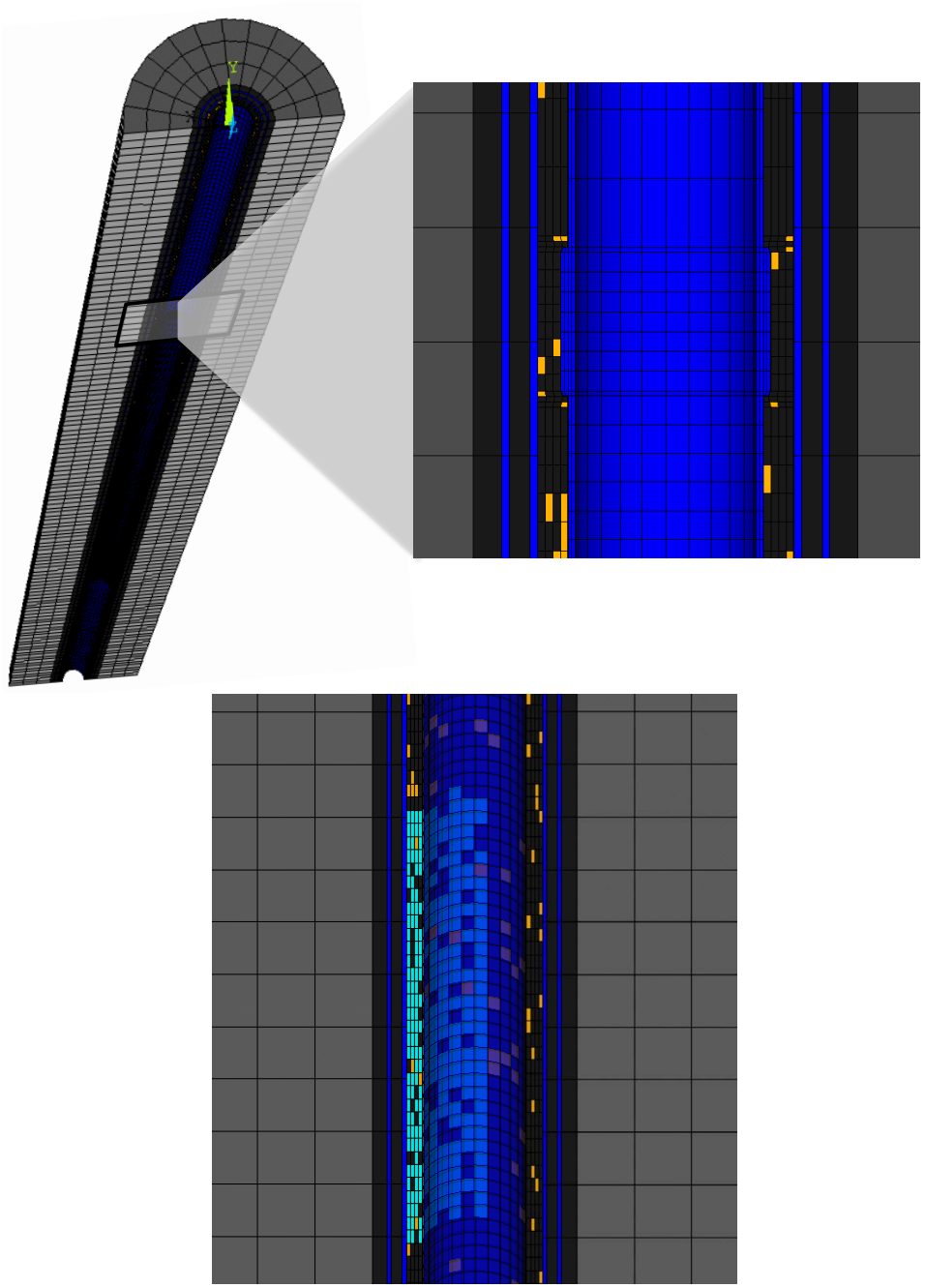

Figure 5.3: *The geometry of a model with simplified couplings and water pocket enclosed in the casing-to-casing annulus (the production casing is transparent). The water pocket is shown in cyan color and yellow elements are randomly distributed material imperfections. The water pocket is 1.6 m long and fills up half of the annulus circumference.*

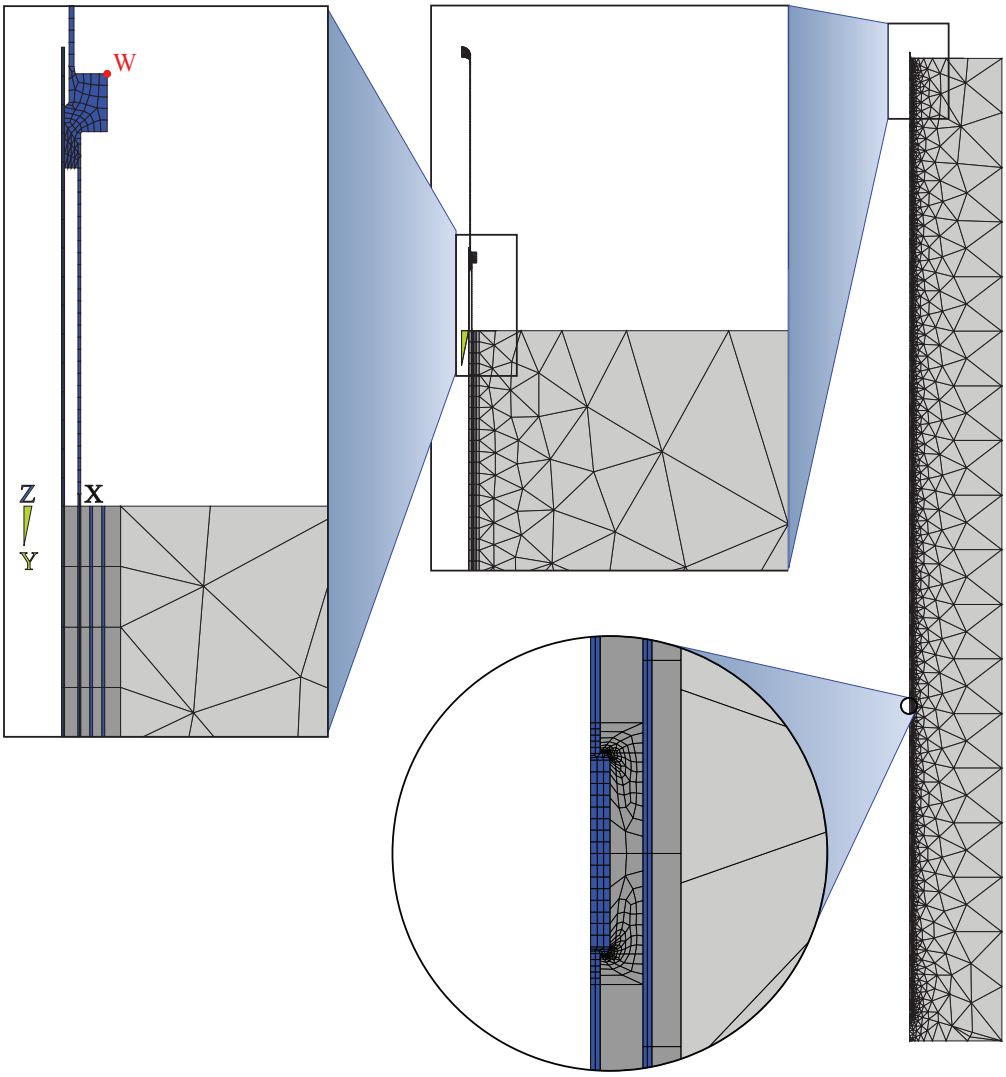

Figure 5.4: *The geometry of the 2D axi-symmetric model of the whole well. The whole model is displayed on the right and the wellhead and a simplified coupling are shown in close-ups. The wellhead displacement is monitored at the node denoted with W.*

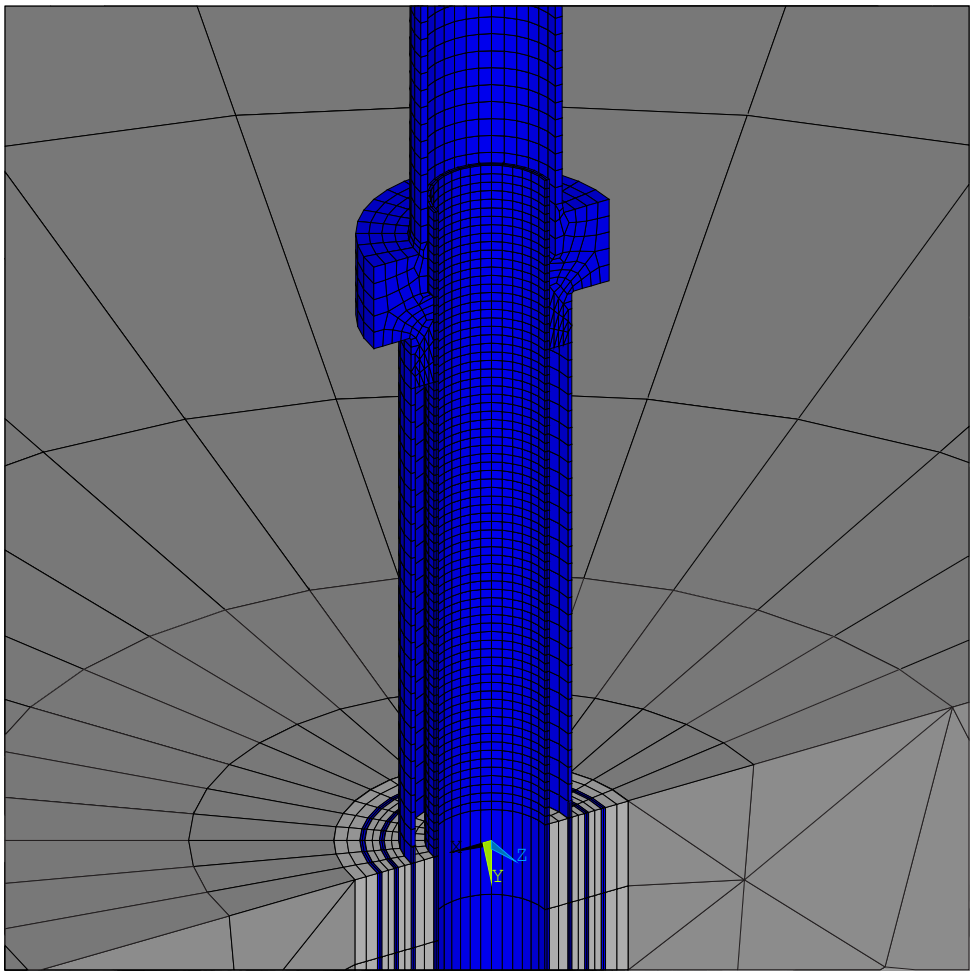

Figure 5.5: *Symmetry expansion (180°) of the simplified wellhead for the axi-symmetric model of the cased section of the well. The wellhead is fixed to the anchor casing and the production casing is allowed to slide inside the wellhead.*

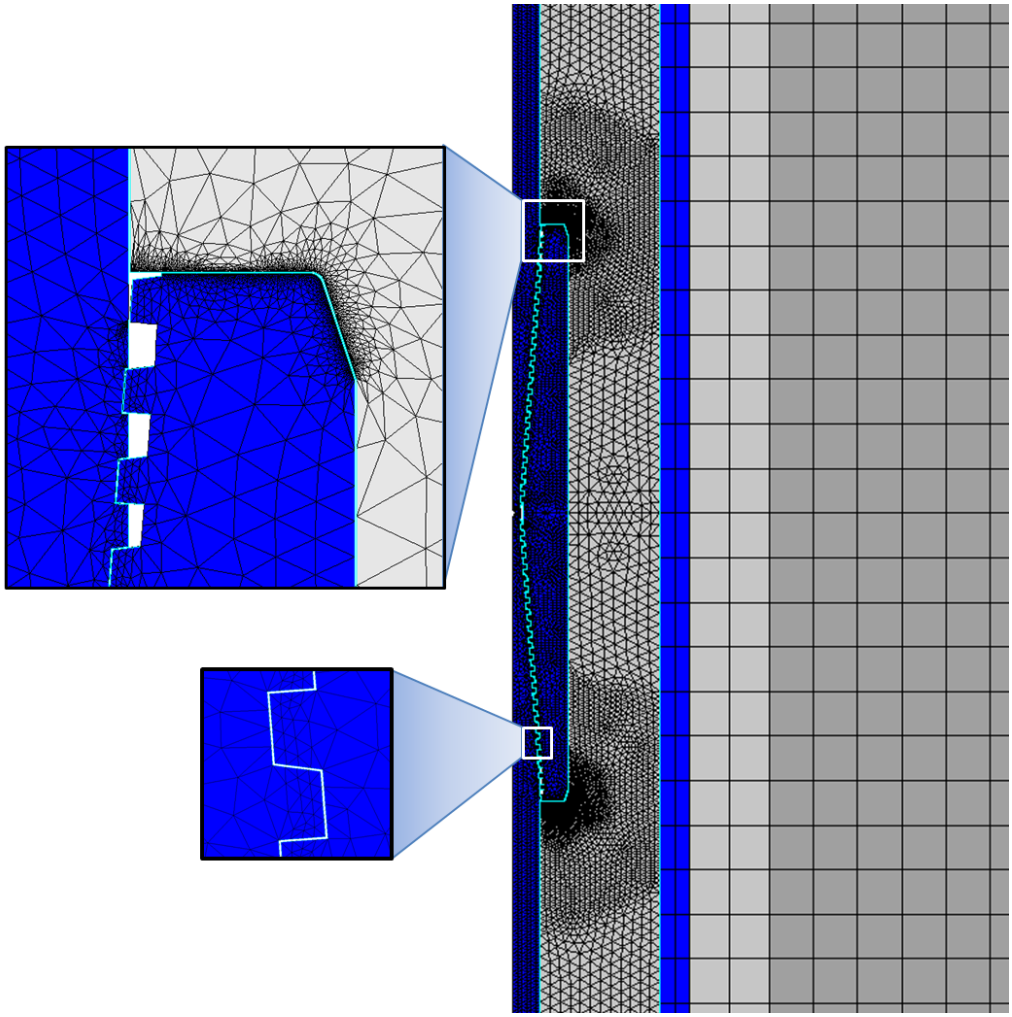

Figure 5.6: *Axisymmetric model of buttress thread casing (BC) connection.*

The simplified geometries of couplings in the global model do not capture details in the cement and the coupling. Another model is therefore constructed to analyze the coupling and its interaction with the cement in more detail. API buttress thread casing (BC) connection as used in most geothermal wells in Iceland is modeled in a two-dimensional axisymmetric model, shown in Fig. 5.6.

Elements and mesh

2-D axisymmetric elements are used in many of the models as the geometry of the well is challenging to model due to the small diameter to depth ratio and three-dimensional analysis exceeds the computation capacity fast with increased modeled depth of wells. As the elements are axisymmetric (with a full circle revolution), and follow neither plane stress nor plane strain limitations, radial and axial displacements in the well can be modeled, and tri-axial stresses and strains can be analyzed. Fig. 5.7 shows plane elements that can be used either in plane strain, plain stress or axisymmetric formulations.

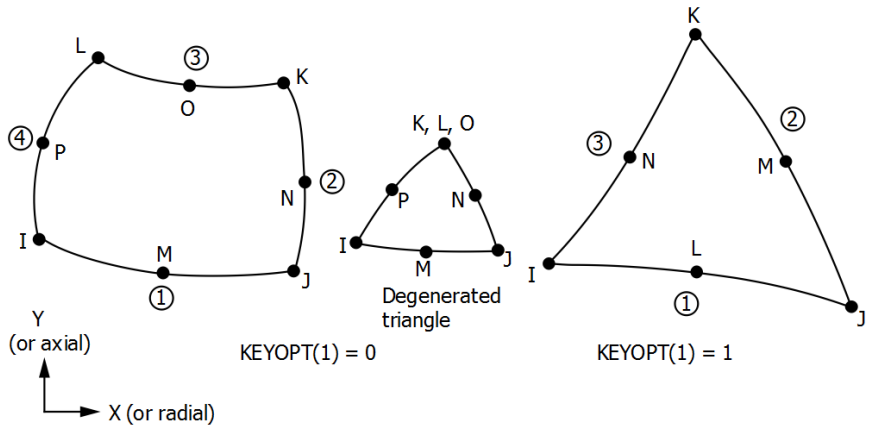

Figure 5.7: *Plane element used for axi-symmetric models (PLANE183) (Ansys, Inc.).*

Solid elements are used when modeling sections of the well in three dimensions, see Fig. 5.8. Specific boundary conditions can be defined to apply symmetric conditions and save computational time, but to capture collapse half of the circumference of the well is modeled. Contact between surfaces is defined with contact elements and the frictional characteristics are defined using the Coulomb friction model.

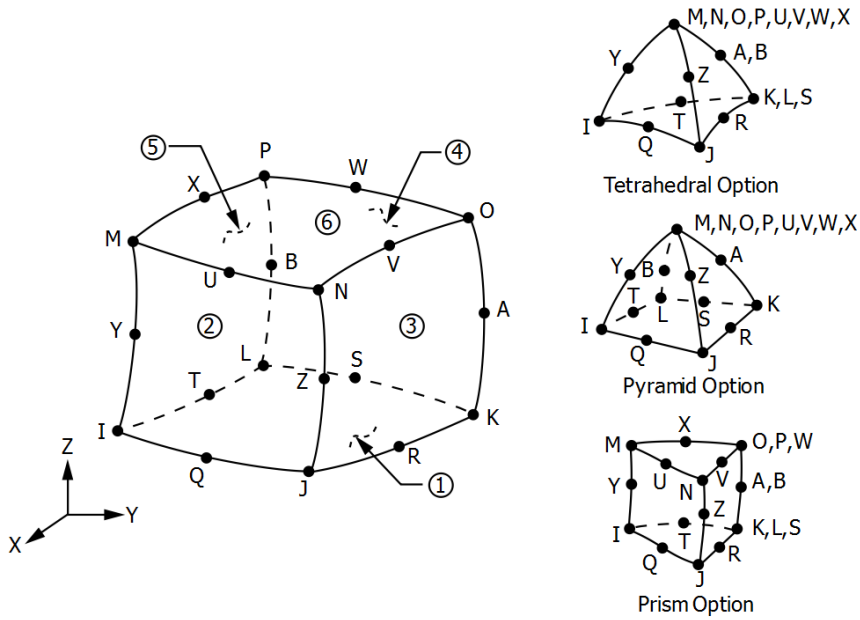

Figure 5.8: *Solid element used for three dimensional models (SOLID186) (Ansys, Inc.).*

Boundary conditions and loads

In most cases when analizing thermal loads, transient load histories are defined and in some cases static loads are defined, e.g. in collapse analyses. Fig. 5.9 illustrates how the thermal load is applied to the wellbore (inside the production casing). Interpolation is used to avoid step changes inside the wellbore, which could produce false stress intensities in subsequent structural analysis.

Transient thermal load in the axisymmetric model of the cased section of the well is defined such that the initial formation temperature, a gradient changing with depth that is estimated from temperature logs, is defined for the whole model.

Then, assumed cooling from drilling is defined and depending on the load history, warm-up of the well, flow-testing and shut-in conditions. Load steps can be added depending on what is being studied, but to model the temperature distribution these initial load steps need to be defined and solved. This is further described for case studies in the results section. Conductive heat transfer is assumed to be dominant in the formation and therefore the model is defined as such

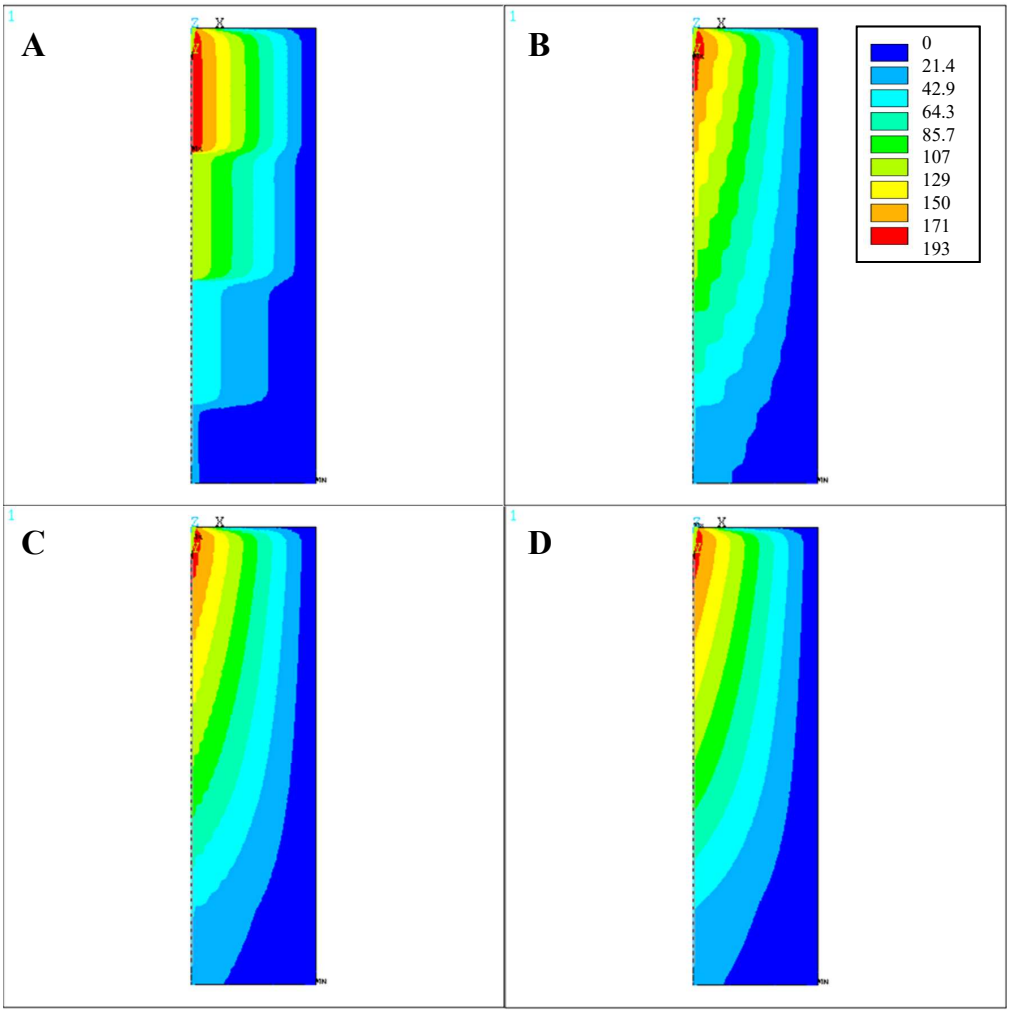

Figure 5.9: *Themperature change during discharge demonstrating load interpolation between sparse data points. (A) No interpolation, (B) 4 interpolation points, (C) 10 interpolation points and (D) 100 interpolation points. Axisymmetric model 350 m deep and 100 m wide.*

and convective phenomena disregarded. The outer boundary of the model, that is defined as 100 m away from the center of the well remains at the formation temperature. This distance is sufficient for the analyses, as the main reason for calculating the temperature distribution is to use it as thermal load for analyzing the cased well structurally.

Structural loads that are defined are gravity, temperature and pressure. Temperature is defined from the results of the thermal model as described above. Pressure loads are defined within the well at each load step. Depending on the definition of time for the load steps, the pressure can either be a step or ramp load.

Material properties

The material properties and values that are used in the models are listed in Table 5.1. Additionally, the default value used for the coefficient of friction between steel and cement is $\mu = 0.45$ and the shear stress when sliding initiates is $\tau_b = 0.46\,\mathrm{MPa}$ which is based on two separate shear strength studies of externally cemented casings. Shear strength measurements performed by Gretarsdottir (2007) showed maximum shear strength of 0.26 MPa and 0.64 MPa, for 1 day strength and 28 days strength, respectively. Similar results were obtained by Wallevik et al. (2009), where the maximum shear strength was 0.21 MPa and 0.72 MPa, for 1 day strength and 28 days strength, respectively. The steel-steel coefficient of friction between the production casing and the wellhead is not known but is chosen to be $\mu_{wh} = 0.7$, near the upper limit of the static coefficient of friction for steel-steel contact which is 0.6±0.11 according to ASM (1992b).

Table 5.1: *Material properties and default numerical values used in the model.*

Material property	Units	Steel	Cement	Rock
Young's modulus (E)	GPa	205	2.40	80.0
Poisson's ratio (ν)	-	0.30	0.15	0.31
Density (ρ)	$^{\mathrm{kg}}/_{\mathrm{m}^3}$	7850	1600	2650
Th. conductivity (K)	$^{\mathrm{W}}/_{\mathrm{m}^\circ\mathrm{C}}$	50.0	0.81	2.00
Specific heat (c)	$^{\mathrm{J}}/_{\mathrm{kg}^\circ\mathrm{C}}$	490	880	840
Th. expansion (α)	$^{1}/_{^\circ\mathrm{C}}$	12e-6	10e-6	5.4e-6
Compressive strength (f_C)	MPa	-	25e6	

Nonlinear material properties of API steel grades K55, L80, T95 and X56 are implemented in the model by using stress-strain curves, seen in Fig. 5.10, which were obtained from tensile tests by Karlsdottir and Thorbjornsson (2009). Stress-strain input to the model is in terms of true stress - true strain. The curves are therefore converted from engineering stress - engineering strain to true stress-true strain, shown in Fig. 5.11. The curves are converted with the following

equations[1]:

$$\epsilon_{true} = ln\left(1 + \epsilon_{eng}\right) \tag{5.2}$$

$$\sigma_{true} = \sigma_{eng}\left(1 + \epsilon_{eng}\right) \tag{5.3}$$

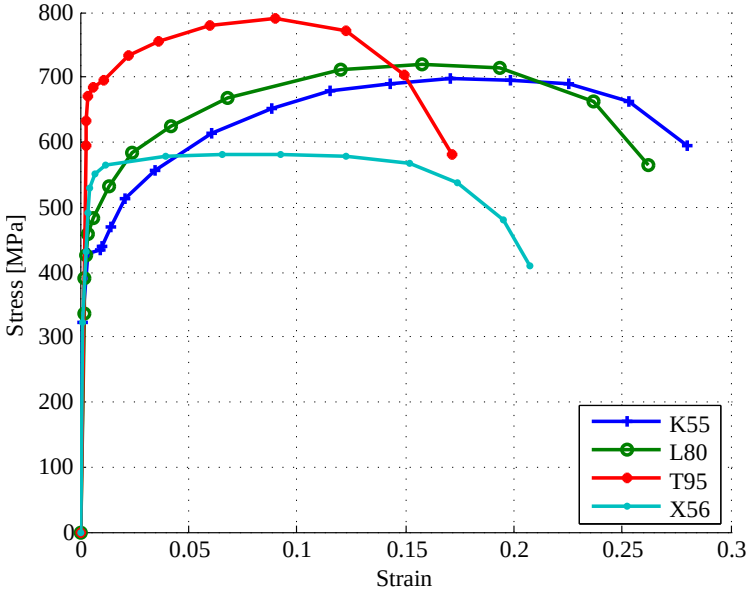

Figure 5.10: *Stress-strain curves (engineering) that are used in the model for steel grades K55, X56, L80 and T95 (Karlsdottir and Thorbjornsson, 2009).*

Since exact stress-strain curves of casing steel at elevated temperatures was not found in the literature, strength reduction is accounted for by scaling these curves according to the reduction of the young's modulus, yield strength and ultimate strength at elevated temperatures according to Snyder (1979) for papers I-V, but for paper VI the curves are scaled according to guidelines in the recently updated New Zealand standard NZS 2403:2015, "Code of Practice for Deep Geothermal Wells". The strength reduction parameters and the scaled true stress-true strain curves for API grade K55 at elevated temperatures using NZS 2403:2015 is shown in Fig. 5.12.

In the model the thermal expansion coefficient of steel is temperature dependent as is shown in Fig. 5.13. As a reference, the thermal expansion coefficients of spheroidal graphite (SG) cast iron (with a minimum tensile strength of 600 MPa)

[1] Ansys, Inc.

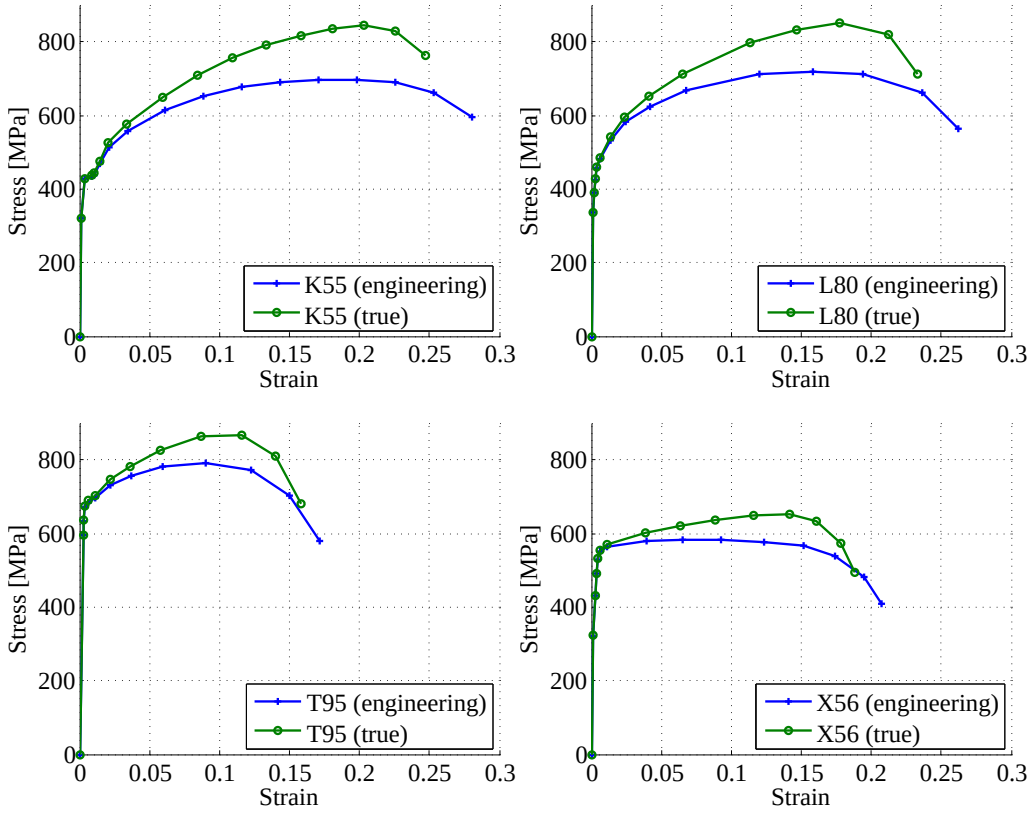

Figure 5.11: *Stress-strain curves of K55, L80, T95 and X56 grade casing steel (Karlsdottir and Thorbjornsson, 2009) converted to true stress - true strain, as is the input in the model.*

and AISI-SAE grade 1040 are shown. The cement is assumed to yield plastically above its maximum compressive strength. It is however arguable how this should be defined due to the question of the post-failure compressibility of the cement in tri-axial stress state. In the model, the Young's modulus of the cement after it has reached the maximum compressive strength is reduced by 50%, see Fig. 5.14. A cement material model that behaves differently in compression and tension is not defined in the model due to convergence difficulties after the cement has been impaired, which normally occurs as soon as small thermal expansion occurs. Using such material model could however give better estimates of stresses and strains within the cement, but modeling of load histories of wells has proven to be difficult. The strength reduction of cement at elevated temperatures is accounted for as is shown in Fig. 5.15.

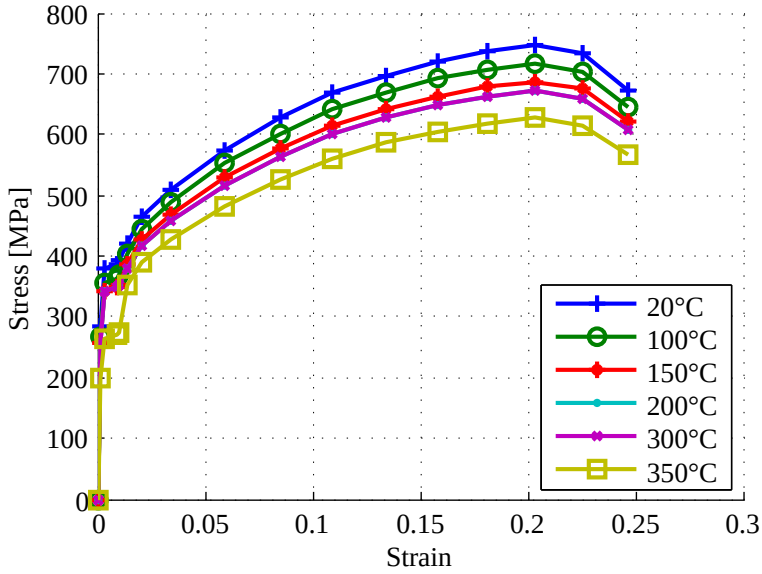

Figure 5.12: *True stress-true strain curves and strength reduction at elevated temperatures for API grade K55 according to strength reduction guidelines of New Zealand standard NZS 2403:2015 are used to scale the curves.*

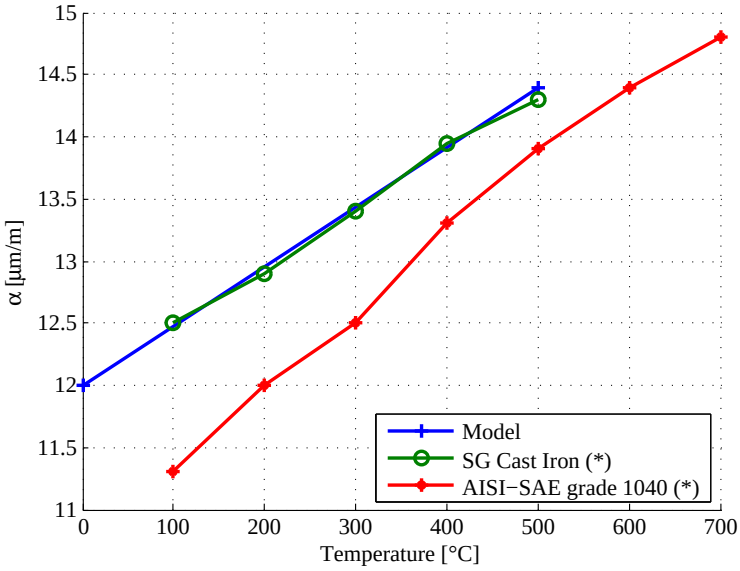

Figure 5.13: *Thermal expansion coefficient α of steel used in the model. $*$ As a reference thermal expansion coefficient for Ductile Spheroidal Graphite Cast Iron (600 MPa min tensile strength) and AISI-SAE grade 1040 is shown ASM (1992a).*

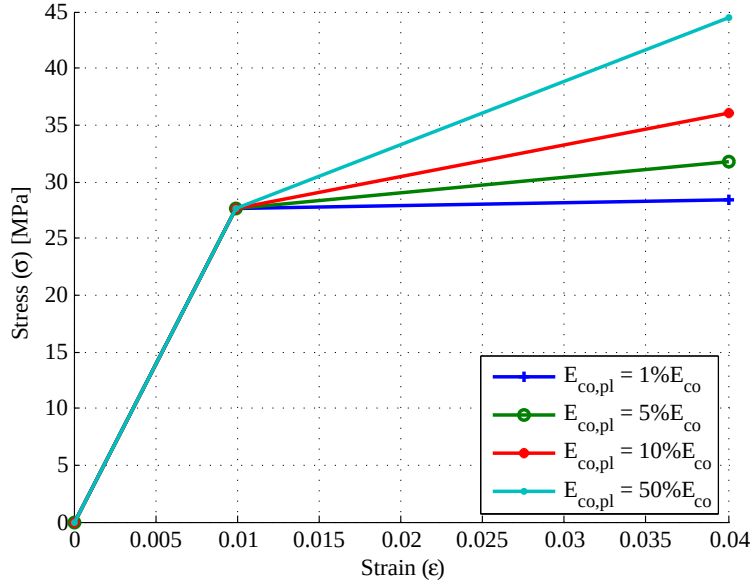

Figure 5.14: *Bilinear concrete material model with different tangent moduli E_T. In the model the default values for cement compressive strength f_C is 25 MPa and the tangent modulusis E_T is $50\%E_{co}$.*

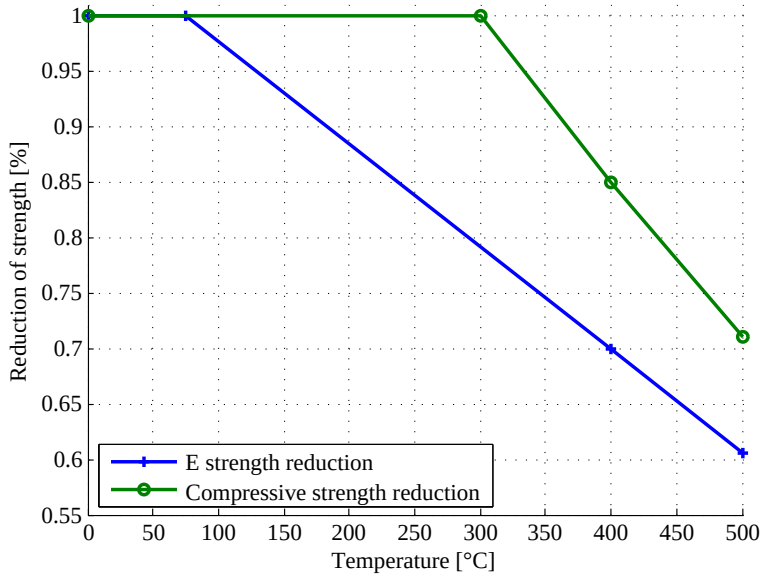

Figure 5.15: *Strength reduction of cement Young's modulus (E) and compressive strength (σ_y) at elevated temperatures based on Phan and Carino (2000).*

5.2 Model verification

Parameter sensitivity and convergence studies

Mesh convergence studies are performed on each model. Convergence studies of the axisymmetric model of the cased section of the well with respect to mesh density is shown in Fig. 5.16. Changes in axial element mesh density of the casings and cement result in increase in mesh density of the outer elements which represent the rock formation. In this case, average element length of 0.25 m proved to be adequate. This is equivalent to 100.000 elements for a test model with a 285 m deep production casing.

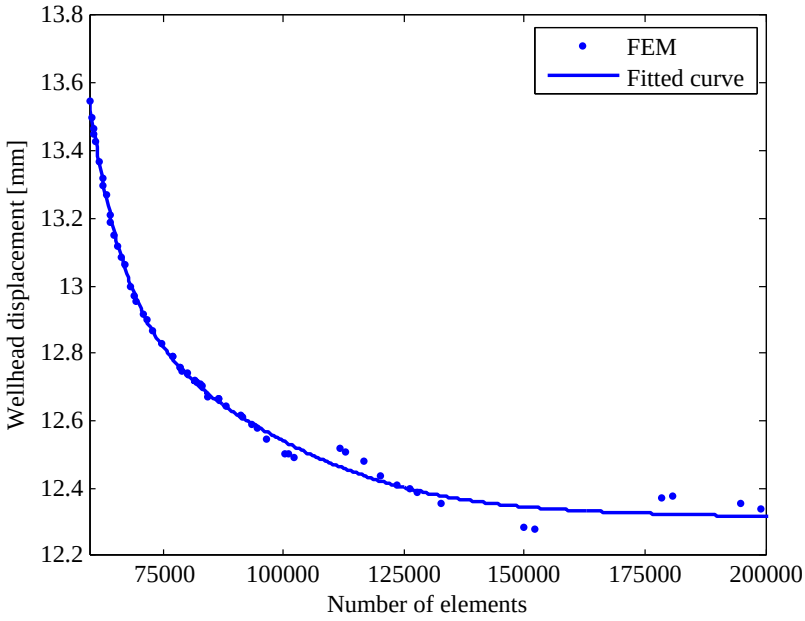

Figure 5.16: *Convergence studies of the element mesh density of the axisymmetric model of the cased section of the well.*

The precision of the solution is explored with respect to the number substeps used for the solution, see Fig. 5.18. Wellhead displacement is used here to assess the precision and the precision defined as the absolute value of the displacement results of the maximum substep solution divided by the displacement result for a specific number of substeps. The loads applied are solved in one load step. The load step is divided into substeps where solutions are calculated and the

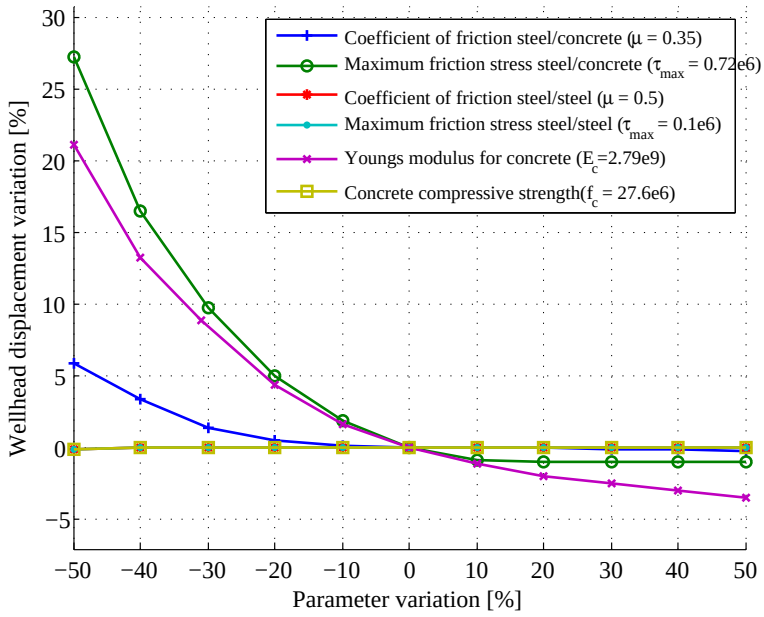

Figure 5.17: *Individual parameter sensitivity study for wellhead displacement of the axi-symmetric model of the cased section of the well during simulated discharge.*

substeps are solved with variable number of iterations depending on convergence. Sufficient number of substeps depends on the model and the precision desired. From these results 20 substeps are selected as the minimum number of substeps.

The outcome of FEM models depends highly on the accuracy of the input parameters, e.g. geometrical sizes, material properties and loads. Parameters can be evaluated individually by changing one parameter at a time as is done in Fig. 5.17. This indicates the sensitivity of parameters from a set point, i.e. all parameters share one point and are varied from that point. This method does however not capture what happens if more than one parameter is changed. However, this can be achieved by using the probabilistic approach described below.

In Fig. 5.19 thermal FEM results are compared with transient temperature data collected by Reinsch (2012) during discharge, by using a fiber optic distributed temperature sensing (DTS) cable that was installed behind the anchor casing of

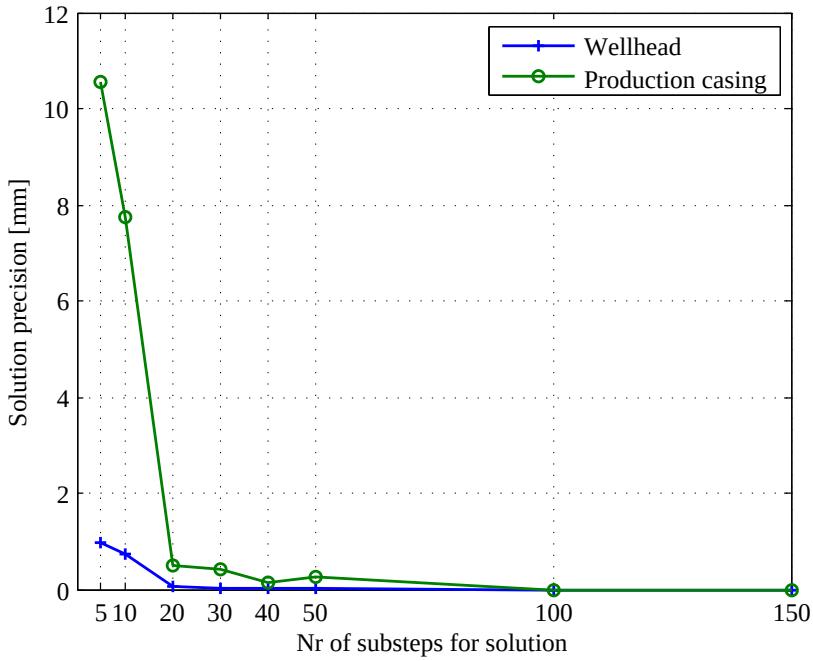

Figure 5.18: *Solution precision as a function of the number of substeps used for the solution.*

well HE-53 in Hellisheiði, SW-Iceland. By using thermal conductivities of 50 and 1 $^{\mathrm{W}}/_{\mathrm{m}^{\circ}\mathrm{C}}$ and specific heats of 490 and 880 $^{\mathrm{J}}/_{\mathrm{kg}^{\circ}\mathrm{C}}$ for the steel and cement, respectively, the modeled temperature is a bit lower than the measured values. The DTS measurements are however the maximum temperatures measured within the annulus, 229.98°C at 162.87 m depth, but the cable was installed on the outside of the anchor casing down to 261.3 m depth (Reinsch, 2012). To explain the difference, it is likely that the production casing is not centered at that depth resulting in premature temperature increase. For a casing standoff resulting in 10 mm minimum annular clearance instead of the mean 35.4 mm clearance for a centralized casing, the results match. The other approach of changing thermal conductivity of the cement is meaningless since the parameter needs to be quadrupled to get a match. Besides, in both cases, the slope of the temperature increase matches the measured data suggesting that thermal conductivity of the model is correct. Therefore, it is probable that the casing is not centralized at this depth and/or it is at a location of a connection in the production casing providing increase in heat transfer between the casings.

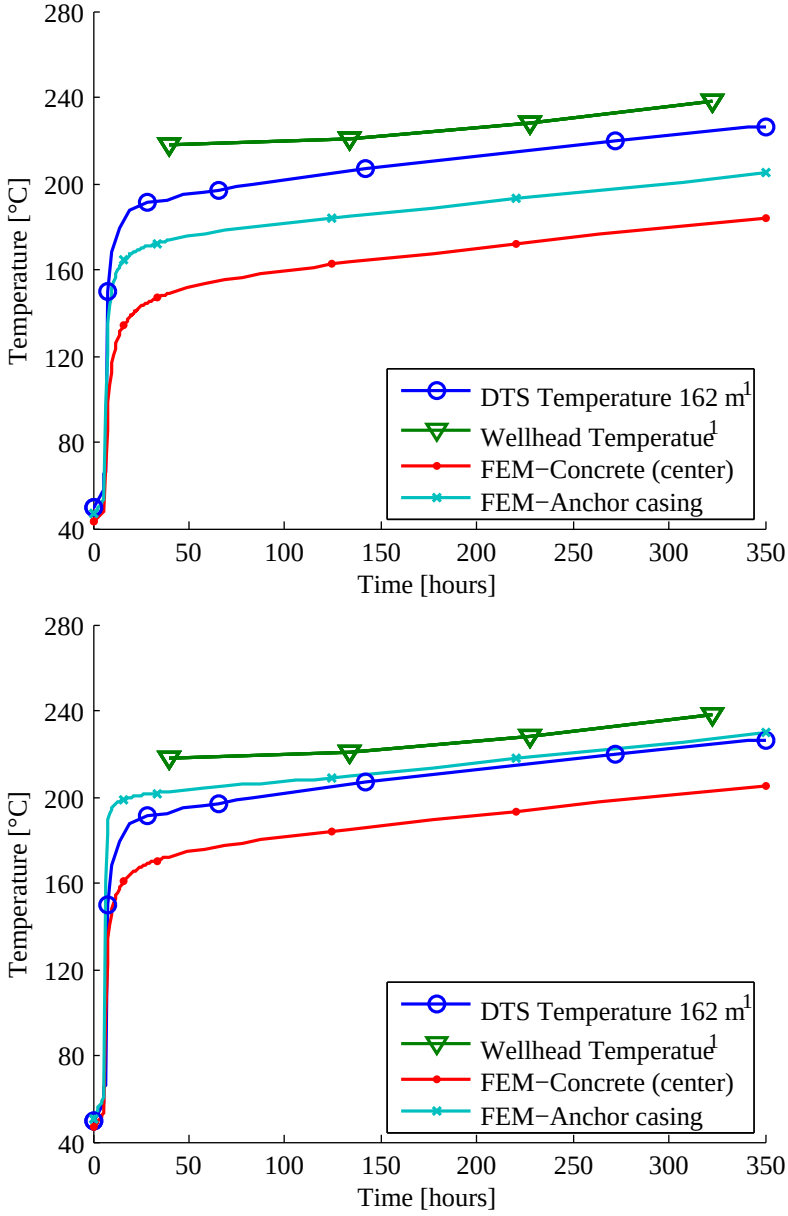

Figure 5.19: *Transient thermal analysis compared to fiber optic distributed temperature sensing (DTS) data collected at depth of 162 m external to the anchor casing in well HE-53 ([1]Reinsch (2012)). Centralized casing with 35,4 mm clearance (above) and offset casing with 10 mm clearance (below).*

To evaluate the accuracy of the results probabilistic design analysis is used. With it the uncertainties of the model results can be quantified. As opposed to deterministic analysis where input parameters are treated as constants which results in a single possible solution, a probabilistic approach where selected input parameters are assumed to contain scatter within a given range gives an estimate of the model uncertainties. Scatter plots of the input parameters versus the output results reveal the significance of the input parameters to the results of the FEM model. Empirical cumulative distribution functions (CDF) of selected results are obtained and used to estimate the uncertainty of the model.

Table 5.2: *Probabilistic design input parameters (selected means and standard deviations).*

Parameter	Units	Mean	Std
μ	-	0.45	0.15
τ_{max}	MPa	0.46	0.13
E_{co}	GPa	2.4	0.6
E_{gr}	GPa	80	20
f_c	MPa	30	7.5
ρ_{st}	$^{\mathrm{kg}}/_{\mathrm{m}^3}$	6125	150
ρ_{co}	$^{\mathrm{kg}}/_{\mathrm{m}^3}$	1600	200
α_{st}	$^{1}/_{^{\circ}\mathrm{C}}$	12e-6	1e-6
α_{co}	$^{1}/_{^{\circ}\mathrm{C}}$	10e-6	1.5e-6
σ-ϵ_{sc}	-	1	0.1

The case shown in section 6.2.1 is used for the following probabilistic design analysis. These probabilistic results are based on variation in material properties. The base case, with mean values of material properties, is first run and then the probabilistic analysis with multiple simulation loops is run employing the Monte Carlo Simulation method with Latin Hypercube Sampling, which avoids repeated samples. A reference time for the probabilistic results is 2.5 hours after the modeled discharge of the well.

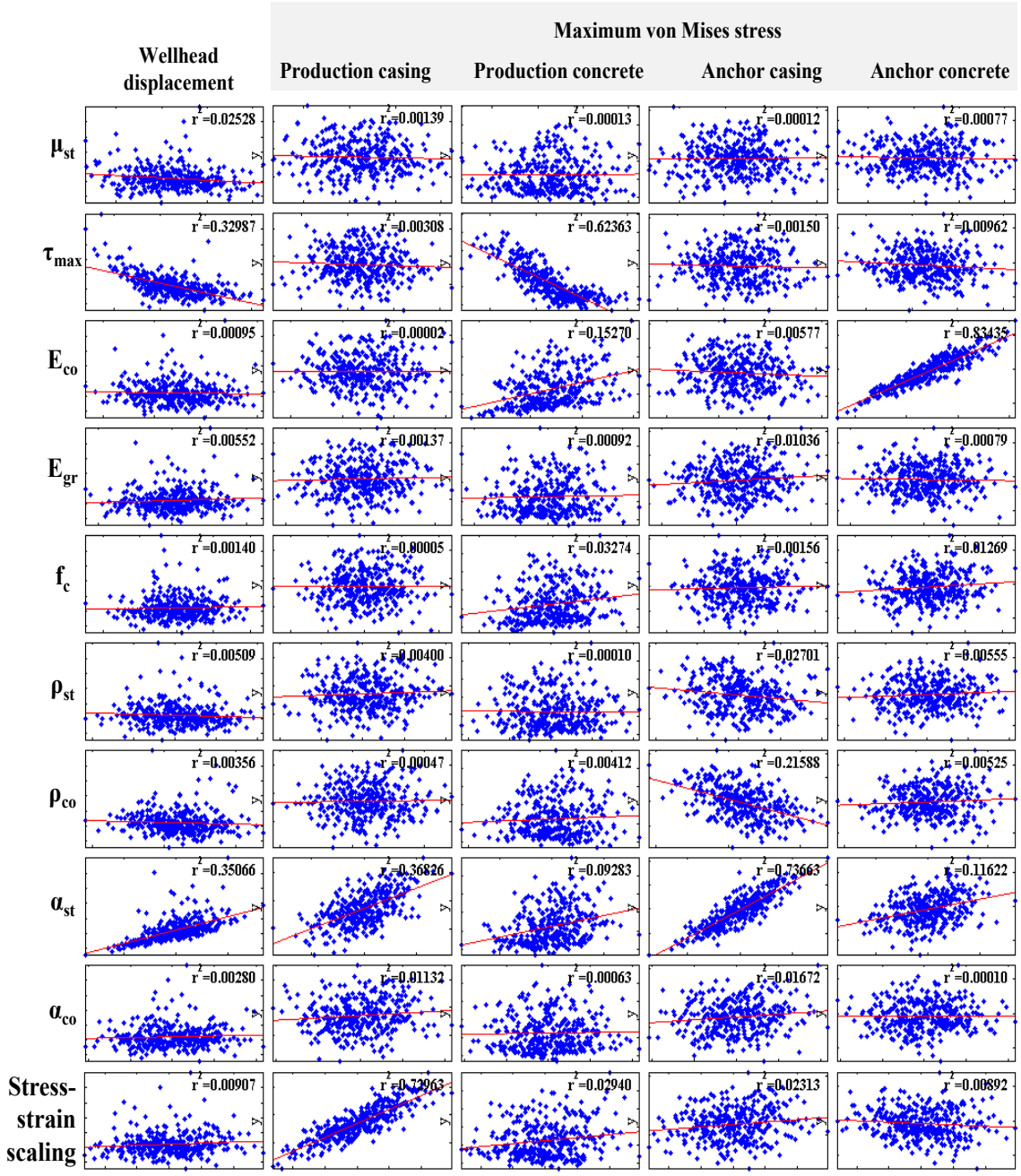

Figure 5.20: *Correlation between selected input parameters and results showing friction between casings and cement, maximum shear force before sliding, Young's modulus of cement and formation, compressive strength of cement, densities of steel and cement, thermal expansion of steel and cement and lastly scaling of stress-strain curves of the steel.*

Table 5.3: *Significant input parameters and correlation with the results with significance level of 2.5%.*

Output	Input	R^2
Wellhead displacement	μ_{st}	0.02528
	τ_{max}	0.32987
	α_{st}	0.35066
Max. von Mises stress of the production casing	α_{st}	0.36826
	σ-ϵ_{sc}	0.73963
Max. von Mises stress of cement (production casing)	τ_{max}	0.62363
	E_{co}	0.15270
	f_c	0.03274
	α_{st}	0.09283
	σ-ϵ_{sc}	0.02940
Max. von Mises stress of the anchor casing	ρ_{st}	0.02701
	ρ_{co}	0.21588
	α_{st}	0.73663
Max. von Mises stress of cement (anchor casing)	E_{co}	0.83435
	α_{st}	0.11622

Table 5.4: *Statistical summary of the output results from the probabilistic analysis. Showing mean value, standard deviation, minimum and maximum values.*

	Mean	Std	Min	Max
i.	8.43	1.52	5.19	18.1
ii.	335.6	29.73	254.6	426.5
iii.	44.86	19.55	14.11	120.6
iv.	159.2	13.69	122.3	203.1
v.	9.589	2.163	3.010	17.16

i: Wellhead displacement.

ii: Max. von Mises stress of the production casing.

iii: Max. von Mises stress of the production cement.

iv: Max. von Mises stress of the anchor casing.

v: Max. von Mises stress of the anchor cement.

400 simulations were used where chosen input parameters are varied within the specified range. Selected means and standard deviations of the selected parameters that are used as input for the probabilistic analysis is listed in Table 5.2. The standard deviation σ provides the sample range for the parameter and 99.7% of the samples should fall within 3σ from the mean provided that the number of simulation loops is sufficient. Histograms, shown in Fig. 5.21, of the input parameters show their random distribution that is defined to fall within normal distribution during the simulation loops. Histograms of the output results in Fig. 5.22 show that some of the results are close to normally distributed while others are closer to chi-squared distribution, i.e. maximum wellhead displacement and maximum stress in cement around the production casing.

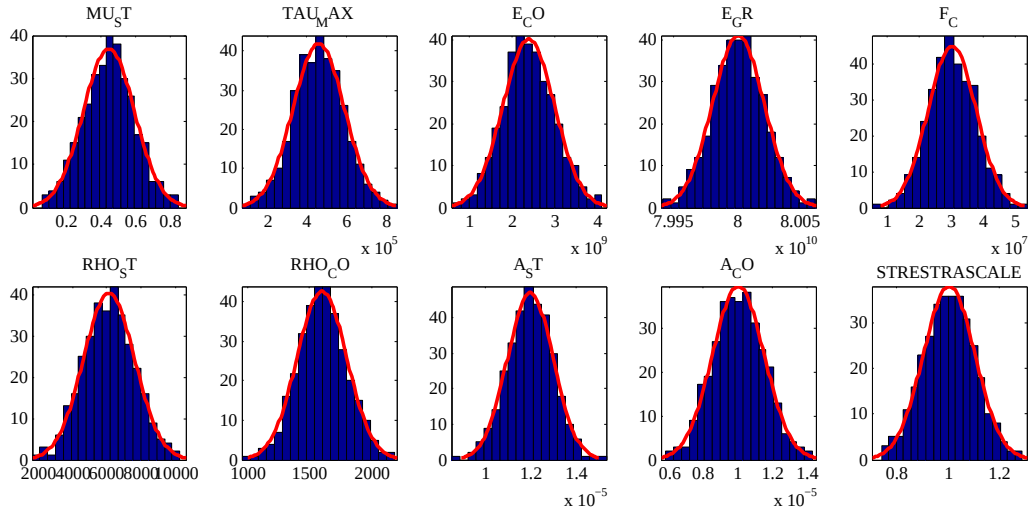

Figure 5.21: *Histograms of normally distributed input parameters.*

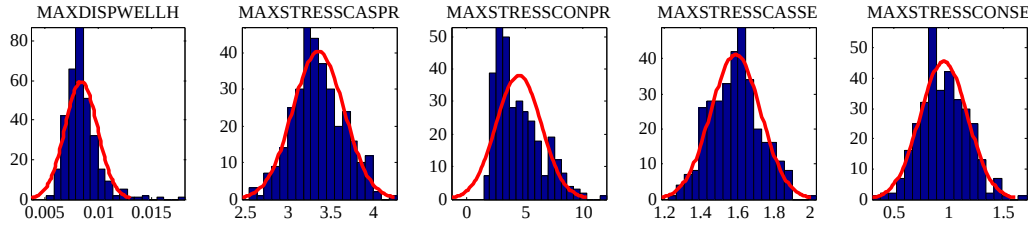

Figure 5.22: *Histograms of the selected output results from the probabilistic analysis.*

CDF plots of selected results are shown in Fig. 5.23 to 5.27. The plots are useful to discern what the probability is of a certain result, e.g. Fig. 5.23 shows 50% probability that the wellhead displacement will be lower than 8 mm, 95% probability that it will be lower than 11 mm and 99% probability it will be lower than 14 mm. Same for maximum stress in the production casing, shown in Fig. 5.24, the CDF plot shows 92% probability that the maximum von Mises stress will be lower than the yield point of 379 MPa for the K55 grade casing for this case.

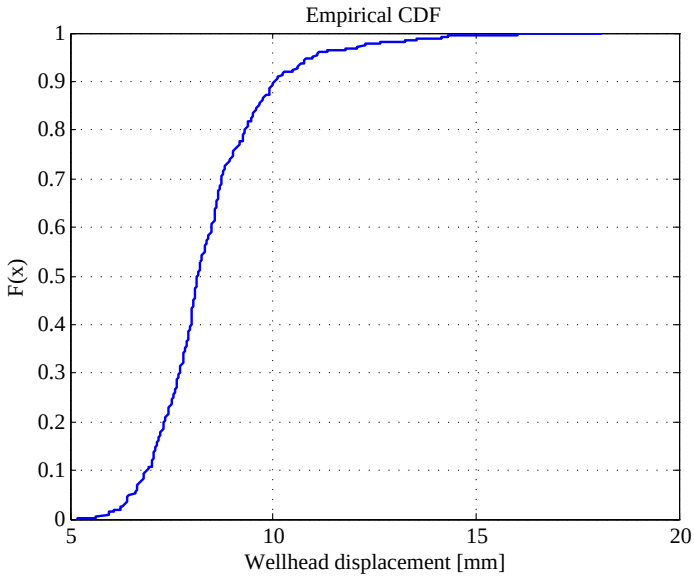

Figure 5.23: *Empirical cumulative distribution function (CDF) plot of the wellhead displacement, showing 95% probability that wellhead displacement will be lower than 11 mm.*

Fig. 5.25 shows 95% probability of maximum von Mises stress in the cement to be below 80 MPa. This high value is explained by how the stress-strain curve of cement is defined in the model by a tanget modulus after the compressive strength has been reached, see Fig. 5.14. In other perspective, the figure shows 40% probability of the stress being lower than the defined compressive strength of 25 MPa. Similarly, Fig. 5.27 shows 99% probability that the stress will be below 15 MPa and therefore below its compressive strength. The maximum von Mises stress in the anchor casing, shown in Fig. 5.26 is also much lower than in the production casing, showing 95% probability of the stress in the anchor casing being below 183 MPa and never reaching yield.

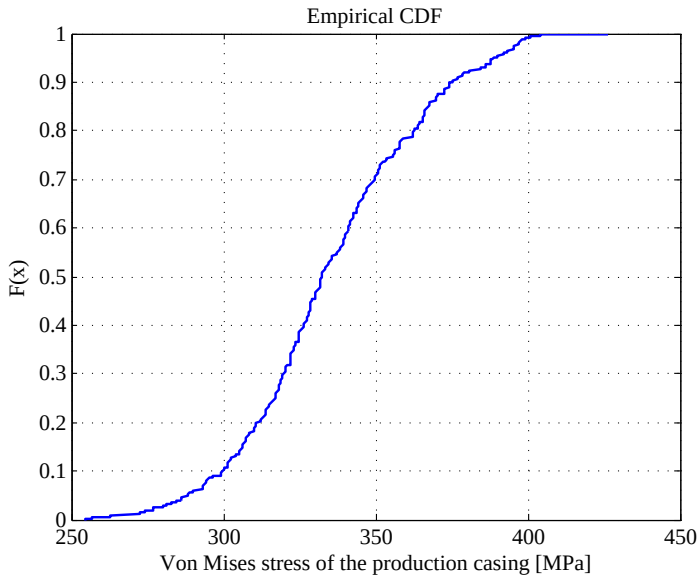

Figure 5.24: *Empirical CDF plot of the maximum von Mises stress in the production casing, showing 95% probability that the maximum stress will be lower than 385 MPa.*

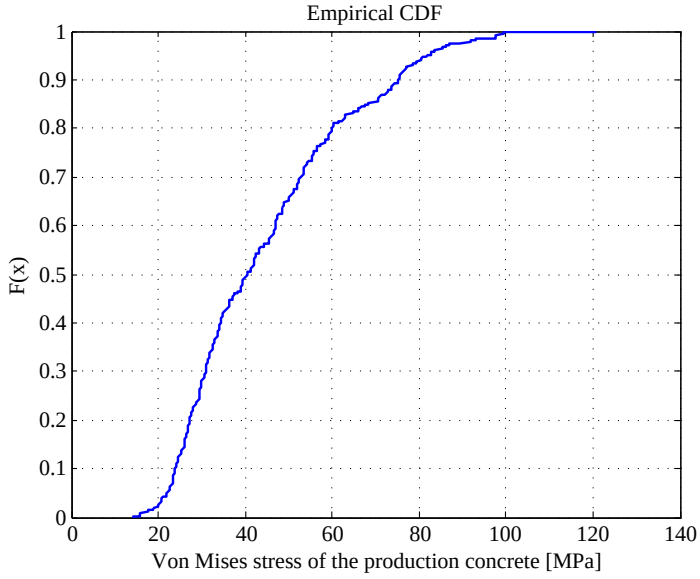

Figure 5.25: *Empirical CDF plot of the maximum von Mises stress in cement around production casing, showing 95% probability that the stress will be below 80 MPa.*

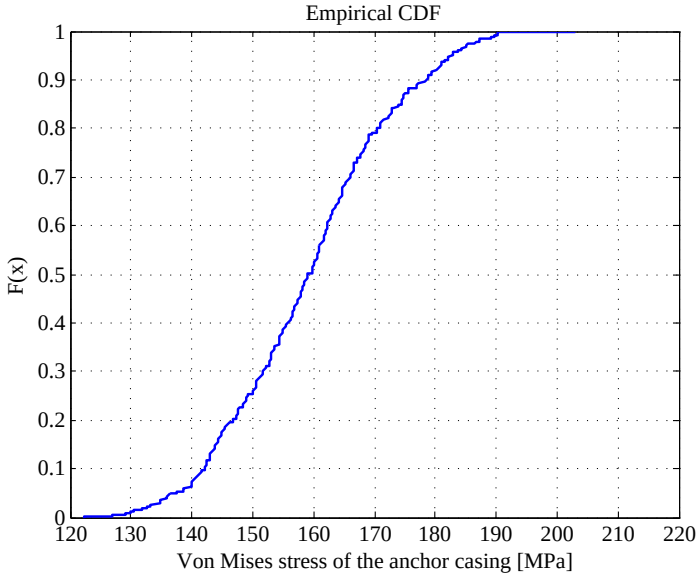

Figure 5.26: *Empirical CDF plot of the maximum von Mises stress in the anchor casing, showing 95% probability that the stress will be below 183 MPa.*

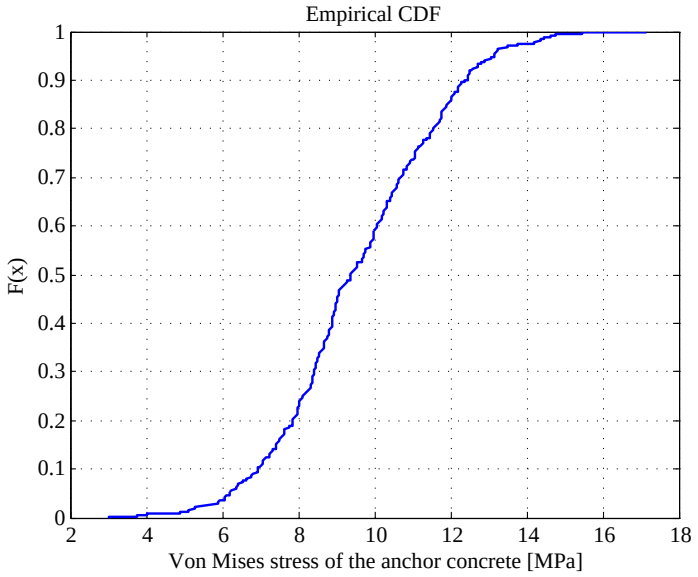

Figure 5.27: *Empirical CDF plot of the maximum von Mises stress in cement around anchor casing, showing 99% probability that the stress will be below 15 MPa.*

Measurements of wellhead displacement

Wellhead displacement measurements were conducted and compared to results from the FEM model. A change in wellhead elevation, as a product of thermal expansion of the casing, during wellbore temperature and pressure changes provides information on the structural response of the well. Monitoring wellhead displacement as wells are flow-tested is thus convenient because of the displacement that results form fast temperature and pressure changes in the well.

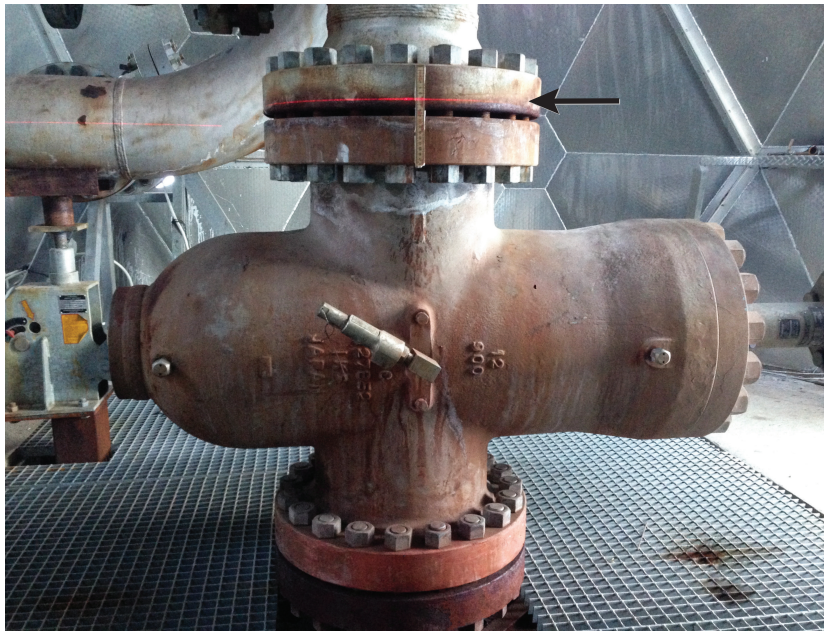

Figure 5.28: *The wellhead of well HE-46. Arrow showing the laser projected on a ruler on the top flange of the master valve.*

Recorded examples of wellhead displacements during flow-testing of wells in Iceland was shown earlier in the theses in Table 3.2. Such information of wellhead displacement during discharge is rare and for those that exist are generally rough measurements. In some cases the time period of observation is missing, but even so, the data gives a range of wellhead displacement for these types of wells. Time-series data of wellhead displacement provides additional information on the structural response of the casings to large temperature changes.

Figure 5.29: *The setup and wellhead of wells RN-22 (top left), HE-53 (top right) and RN-32 (bottom). The laser is projected on a ruler above or below the master valve. For the HE wells the setup was similar to that of HE-53.*

In this study, wellhead displacement (elevation) of five high-temperature geothermal wells was monitored while the wells were discharged. The wells are located in the Hengill and Reykjanes geothermal areas which are both located on an active volcanic ridge in SW Iceland. The monitored wells HE-13, HE-46 and HE-53 are located in the Hengill geothermal field and wells RN-22 and RN-32 are located in the Reykjanes geothermal field. The geometrical sizes of the casings of the monitored wells are listed in Table 5.5.

Table 5.5: *The casing programs of the monitored wells (measured depth of casings).*

HE-13	OD [in]	t [mm]	Length [m]
Production casing	$9^{5}/_{8}''$	12.2	775
Anchor casing	$13^{3}/_{8}''$	12.2	255
Surface casing	$18^{5}/_{8}''$	11.0	78
HE-46	D [in]	t [mm]	Shoe depth [m]
Production casing	$13^{3}/_{8}''$	12.2	1032
Anchor casing	$18^{5}/_{8}''$	11.0	337
Surface casing	$22^{1}/_{2}''$	11.0	83
HE-53	D [in]	t [mm]	Shoe depth [m]
Tieback casing	$7''$	12.6	607
Production casing	$9^{5}/_{8}''$	12.2	965
Anchor casing	$13^{3}/_{8}''$	12.2	306
Surface casing	$18^{5}/_{8}''$	11.0	70
RN-22	D [in]	t [mm]	Shoe depth [m]
Production casing	$13^{3}/_{8}''$	12.2	729
Anchor casing	$18^{5}/_{8}''$	12.3	292
Surface casing	$22^{1}/_{2}''$	12.5	74
RN-32	D [in]	t [mm]	Shoe depth [m]
Production casing	$13^{3}/_{8}''$	12.2	1077
Anchor casing	$18^{5}/_{8}''$	12.3	345
Surface casing	$22^{1}/_{2}''$	12.0	100

A laser was projected onto a ruler which was attached above the master valve, see Fig. 5.28. The reference point, where the the laser tripod was located, was 2.5-3 meters from the wellhead, depending on the setup. A digital single-lens reflex camera was then used to take high-resolution snapshots of the ruler, see Fig. 5.30, later to be interpreted thus minimizing measurement error, which with this method is estimated as ± 0.25 mm. The measurement setup for wells RN-22, RN-32 and HE-53 can be seen in Fig. 5.29. The temperature of the wellhead was measured at various locations on the wellheads using an infrared thermometer, with $\pm 2\,\%$ reading accuracy. The results of the wellhead displacement study and comparisons to the model are described in the results section below (section 6.3.1).

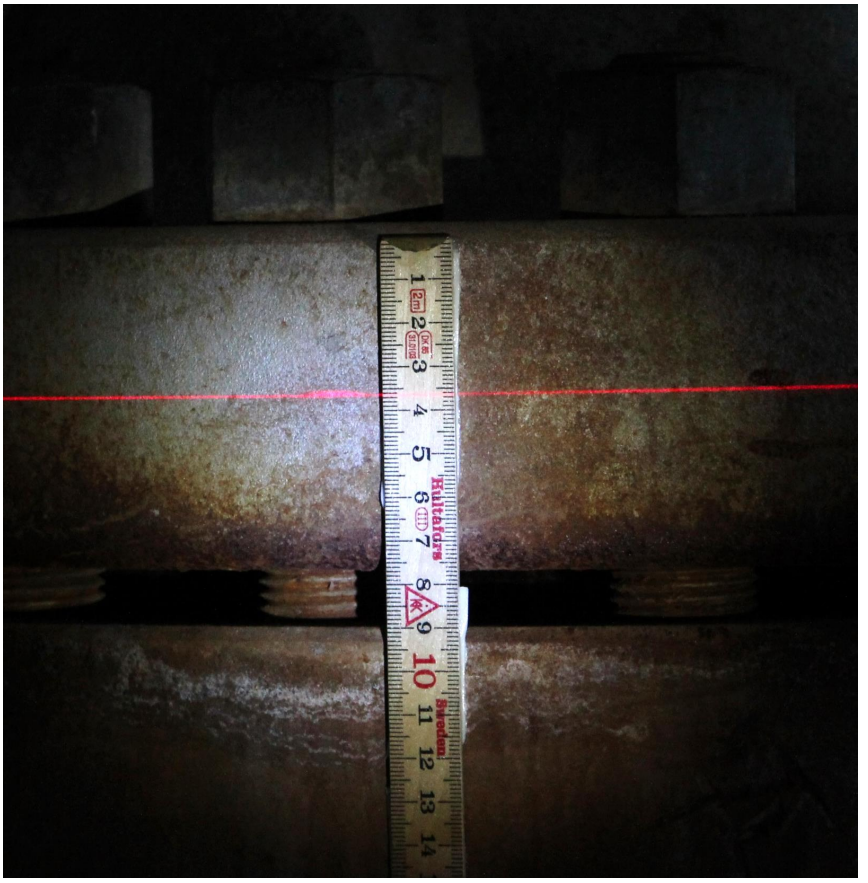

Figure 5.30: *High resolution picture of the laser projected on a ruler on wellhead flange of HE-46. Initial position of the shut-in well right before discharge.*

6

Results

6.1 Thermal analysis

In the thermal modeling, temperature is applied as initial conditions of the formation of the geothermal system near the well that is being studied, followed by wellbore condition where the temperature is applied to the inner surface of the production casing. To illustrate this, a couple of thermal analysis are presented here. In all subsequent modeling, the heat transfer is assumed to be purely conductive as only the cased section of the well is modeled and the primary goal is to provide thermal load for later structural modeling. Inside the wellbore the temperature is quasi-static in the sense that it is controlled through load steps, but the thermal solution is transient. An example of such quasi-static thermal solution is shown in Fig. 6.1.

Temperature distribution of casings, cement and formation is shown in Fig. 6.2, where discharge of a cold well that immediately becomes 450°C hot (step load) is modeled. Although this is an unlikely scenario, since wells normally need time to warm-up after being drilled, it provides a worst case thermal load. An initial condition of the analysis is the formation temperature. As the temperature is purely conductive the steady state (SS) conditions are not reached even after 100 years of constant production. In the second load case, also shown in Fig. 6.2, the well is assumed to be quenched with cold water after constant production of 1 year (step load).

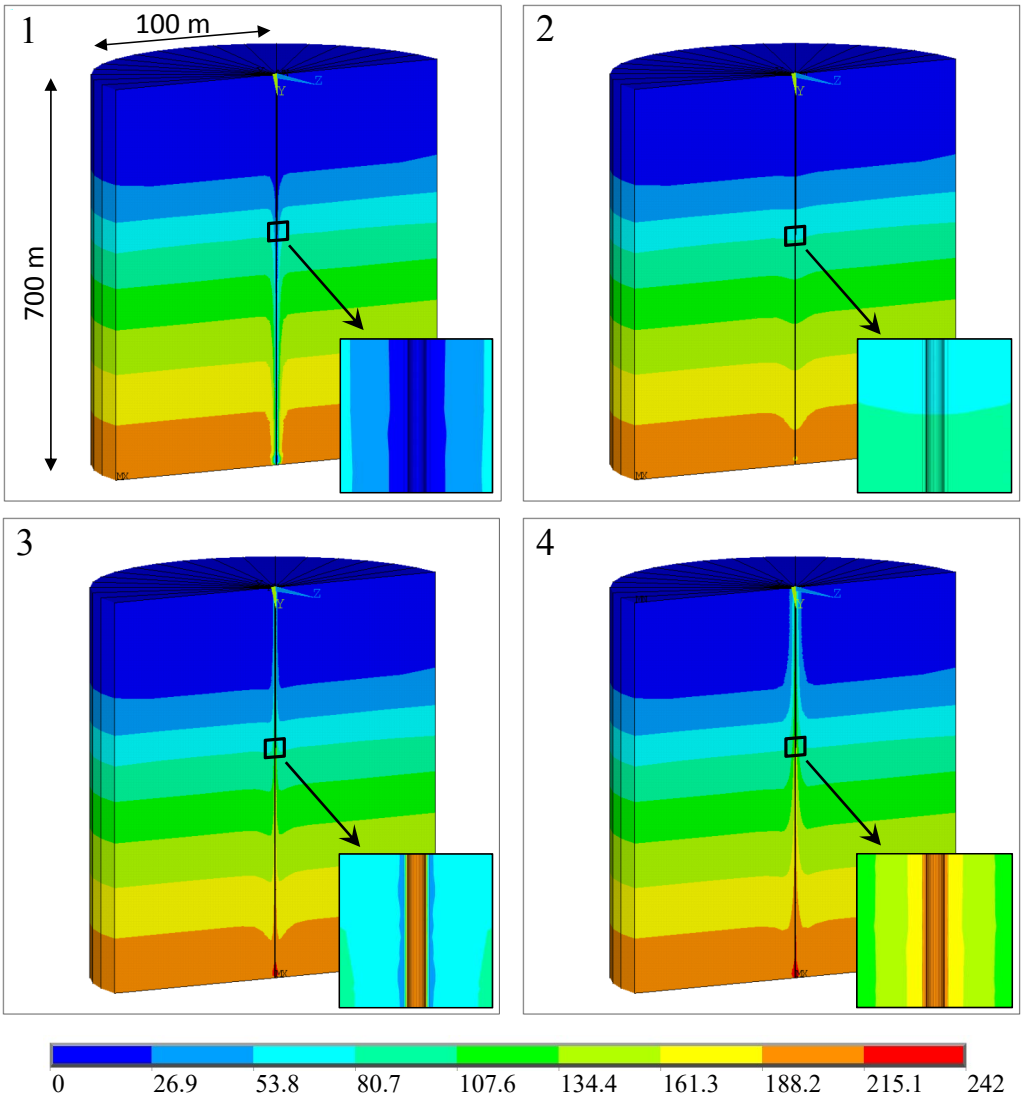

Figure 6.1: *Transient thermal analysis of a typical simplified load history (°C). 1. Cooling due to drilling, 2. Warm-up, 3. Discharge (12 minutes), 4. Discharge (3 months).*

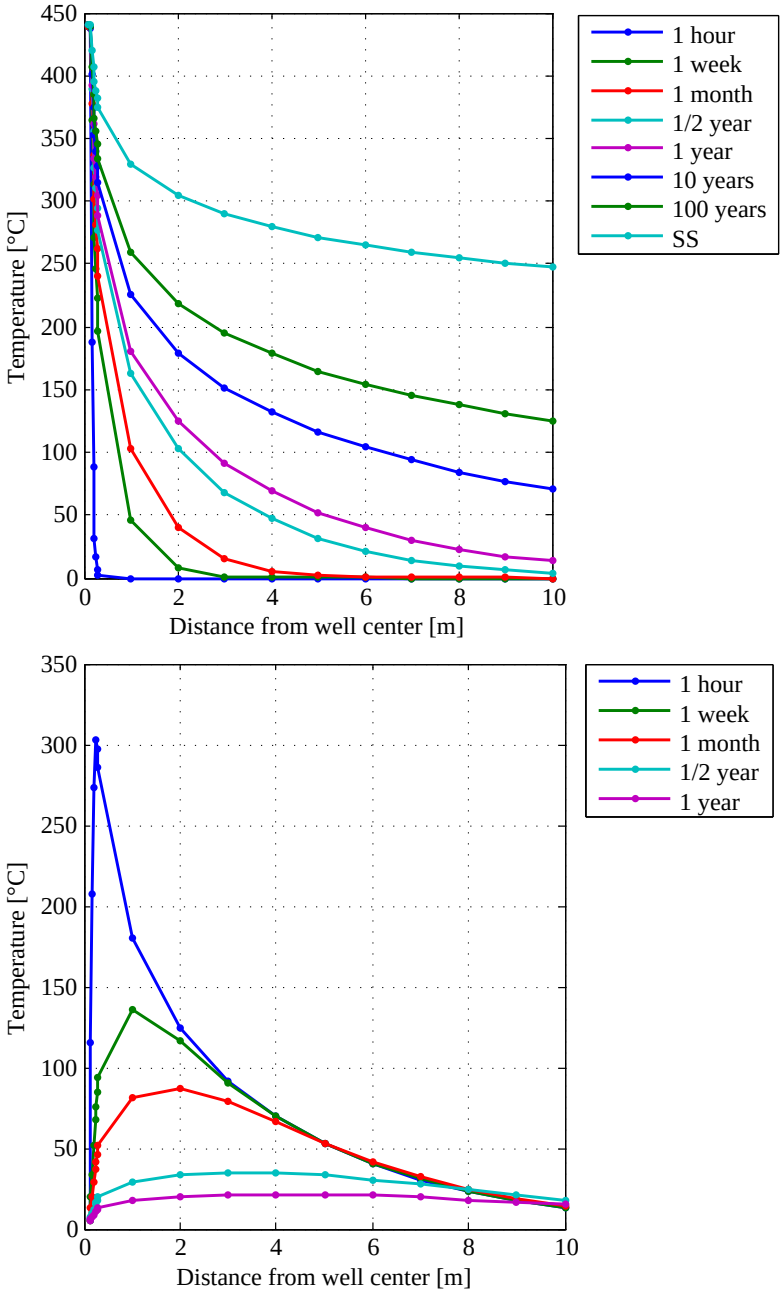

Figure 6.2: *Model results of temperature at 100 m depth for discharge (above) and cooling after one year of production (below), IDDP-1 temperature case.*

6.2 Structural analysis

6.2.1 Axisymmetric model of multiple casings

Results of the axisymmetric model are shown further in case studies below in section 6.3.1 where it is compared to surface measurements and section 6.4 where it is used to model the load history of the IDDP-1 well.

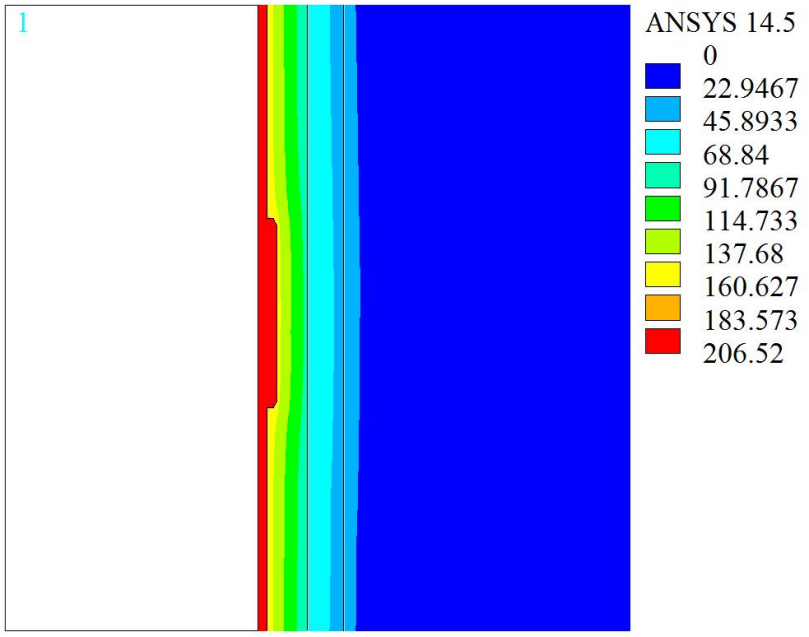

Figure 6.3: *Temperature distribution 2.5 hours after discharge, assuming uniform 200°C temperature load inside the wellbore.*

The axisymmetric model can be used to model various casing programs and load cases by parametric input. In all cases, transient thermal analysis is first performed and the results used as load along with wellbore pressure in the structural model. For the results shown here the discharge is simulated by assuming a uniform 200°C inside the wellbore. The temperature distribution after 2.5 hours at the second highest coupling of the production casing is shown in Fig. 6.3. At this time, a thermal gradient exists between the casings where the production casing is at ∼200°C and the anchor casing is at ∼70°C.

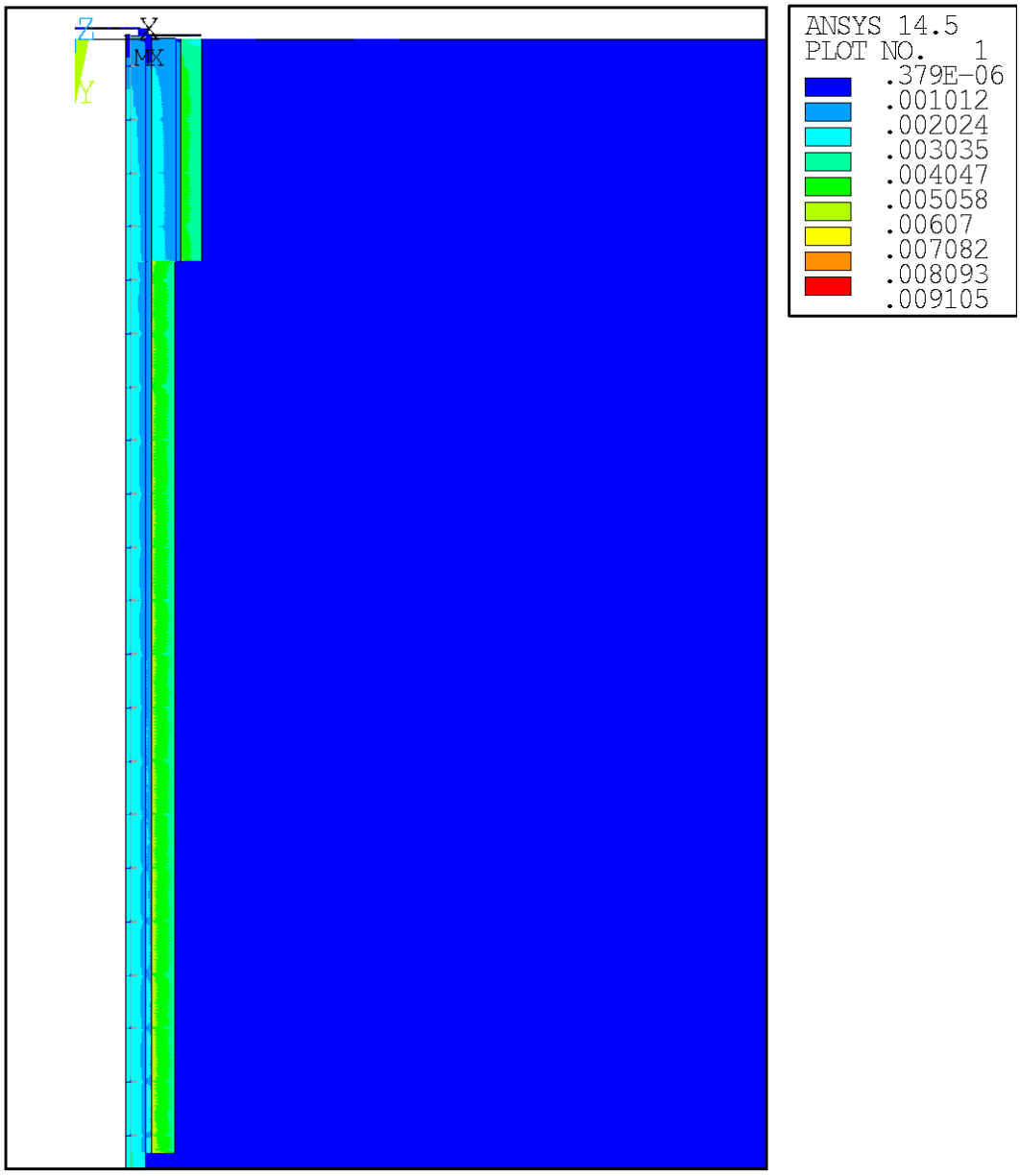

Figure 6.4: *Total strain in the cased well down to the anchor casing shoe during discharge. X-axis is scaled 100:1. Couplings in production casing are clearly visible. Cement between casing and formation shows greater strain than between casings.*

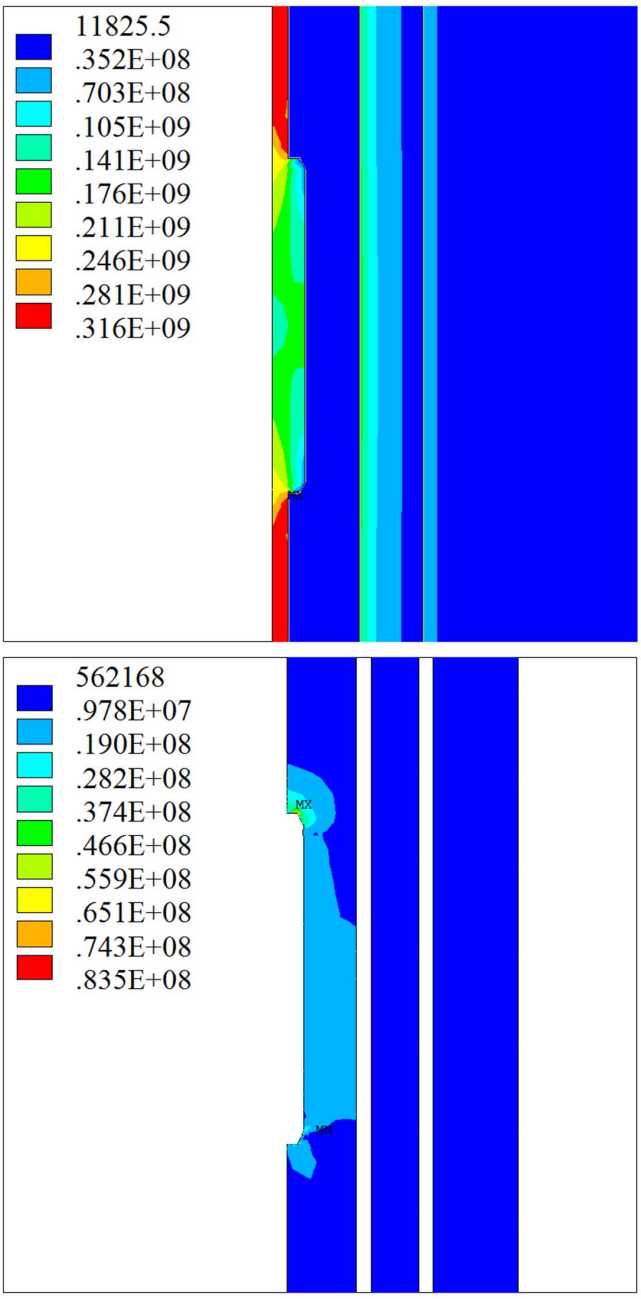

Figure 6.5: *Stress (von Mises) near the second highest coupling (Pa) in casing and cement.*

Fig. 6.4 shows total strain in the cased section of the well down to the shoe of the anchor casing. Connections of the production casing are clearly visible but in this case the anchor casing is without connections (welded). Strain of cement outside of casings to the formation is higher than in the cement between casings.

Von Mises stress results in the casing and cement at the second highest coupling are shown in Fig. 6.5. As no threads are modeled, the highest stresses in the casings are located where the couplings meet the casing. As the couplings are simplified and no threads are included the highest stresses occur due to the sharp change in thickness but in reality the highest stresses in the casings would be expected to be in the first threads where the thickness of the casing is reduced as shown later in section 6.2.2. In this case the highest stress in the casing is 316 MPa. The highest stress in the cement occurs at the upper surface of the second highest coupling, 83 MPa. This is a potential weak spot in the cement, needing further attention.

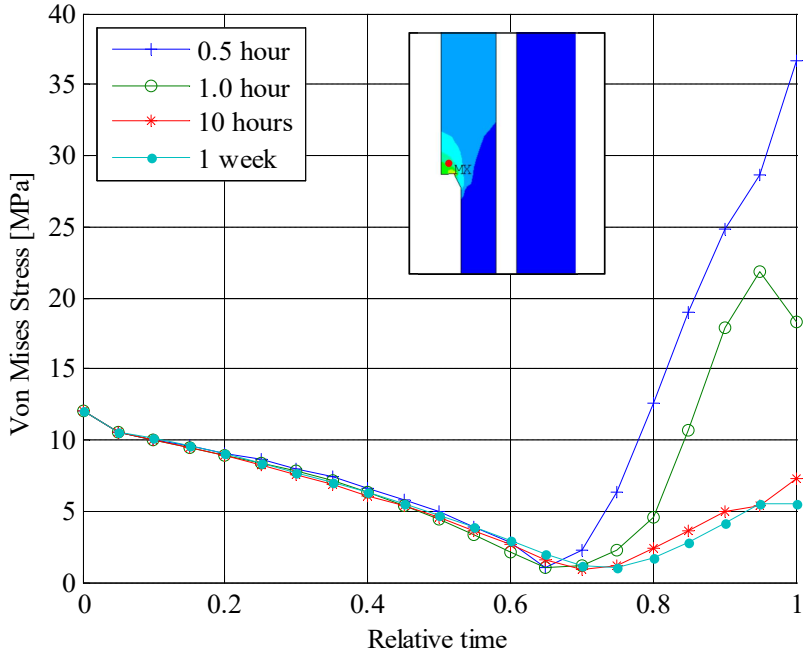

Figure 6.6: *Effect of cooling time on stress in cement near the uppermost coupling.*

The effect of cooling time on stress forming in the cement near the uppermost coupling in the production casing is shown in Fig. 6.6. This assumes that 20°C cold water is used to kill the 200°C well. The results indicate that cooling for $^1/_2$ hour leads to high compressive stress of 36 MPa but the compressive strength of the cement is defined as 25 MPa. Reduction in stress is seen for 1 hour and at 10 hours the residual stress is at manageable 8 MPa. No change is seen when cooling for longer time. Quenching with cold water is analyzed for the case study of the IDDP-1 well in section 6.4.

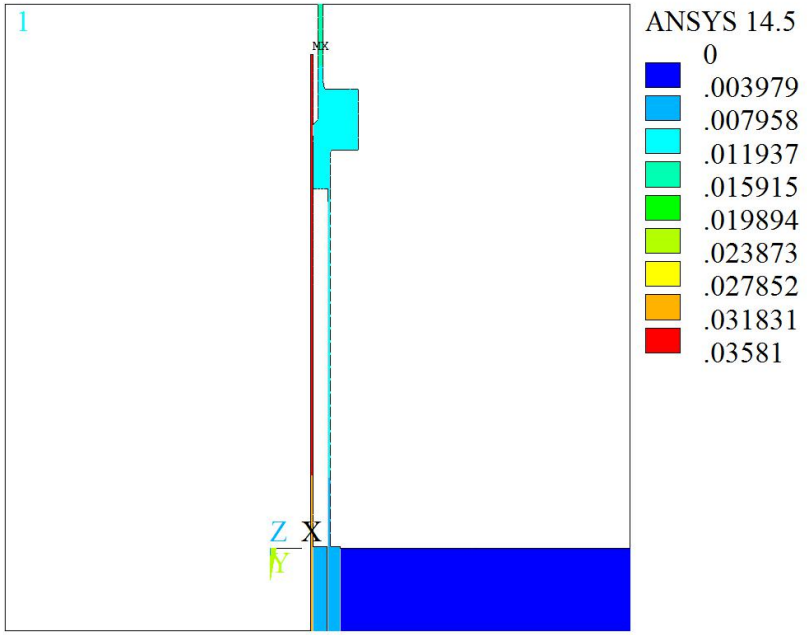

Figure 6.7: *Displacement of the production casing and the wellhead (meters).*

Wellhead displacement is shown in Fig. 6.7. For this case the displacement of the production casing is 35.8 mm and the wellhead displacement is 11.7 mm.

Three different casing programs are compared to understand what effect diameter of casings and number of casings has on wellhead displacement. Three cases are considered, the two common profiles used in Iceland, the large profile with a $13^3/_8''$ production casing, the regular profile with $9^5/_8''$ production casing and the casing program of IDDP-1, consisting of a $13^3/_8''$ production casing and two additional external casings. The temperature, shown in Fig. 6.1, is the same for

in all three cases. The casing programs are listed in Table 6.1 and the results are listed in Table 6.2.

Table 6.1: The well programs used in the analysis. The casing program of IDDP-1 is shortened for the comparison.

Well program	Casing	OD [in]	t [mm]	depth (m)
Large profile	Production casing	$13^{3}/_{8}''$	12.2	700
	Anchor casing	$18^{5}/_{8}''$	12.3	250
	Surface casing	$22^{1}/_{2}''$	12.7	50
Regular profile	Production casing	$9^{5}/_{8}''$	11.0	700
	Anchor casing	$13^{3}/_{8}''$	12.2	250
	Surface casing	$18^{5}/_{8}''$	11.6	50
IDDP-1	Production casing	$9^{5}/_{8}''$	13.8	740
	Anchor casing	$13^{3}/_{8}''$	13.1	735
	Intermediate casing 2	$18^{5}/_{8}''$	13.0	730
	Intermediate casing 1	$24^{1}/_{2}''$	13.0	254
	Surface casing	$32^{1}/_{2}''$	13.0	87

The large casing profile shows $\sim$2 mm higher wellhead displacement than the regular profile. However, the IDDP-1 profile shows double displacement compared to the regular and large profile. This is due to the increased change for displacement because of more number of thermally expanding casings. The maximum von Mises stress in the production casing is in similar range for all three cases.

Table 6.2: Wellhead rise during discharge - comparison of well profiles (identical loading)

Casing program	Nr. of casings	Nr. of nodes nodes	Production casing rise [mm]	Wellhead rise [mm]	Max von Mises stress in casing [MPa]
Large	3	228451	19.3	15.2	372.2
Regular	3	204801	17.4	13.7	358.4
IDDP-1	5	251228	36.4	33.1	335.4

6.2.2 Buttress connection in cement

In the axi-symmetric model of the cased section of a well, where simplified couplings are included to account for their anchoring effect in the cement, large stresses are seen near the uppermost couplings of the production casings, see Fig. 6.8.

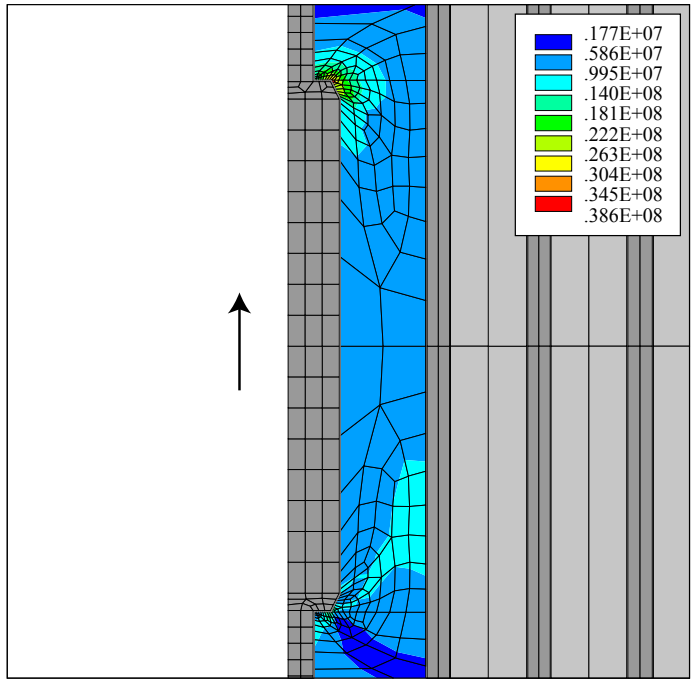

Figure 6.8: *High stress develops in the cement near the topmost coupling of the production casing using the large axi-symmetric model of the whole well with simplified connections. Casings are shown in dark gray and external cement in gray.*

Tensile strength of buttress thread casing (BC) connection is analyzed and compared to API mechanical rating. The casing chosen for this analysis has an outer diameter of $13^3/_8''$ and nominal weight of 68 lb/ft. The results show that if 700 m casing hangs (in air) from the connection the stress is well below the yield strength of the K55 material. However, compared to 5000 m casing hanging from the connection, equal to 4960 kN tensile force, yield is reached in the casing. This is in agreement with the API mechanical rating of the K55 casing which

has pipe body yield strength of 4760 kN, the tensile strength of API BC coupling is however 5780 kN.

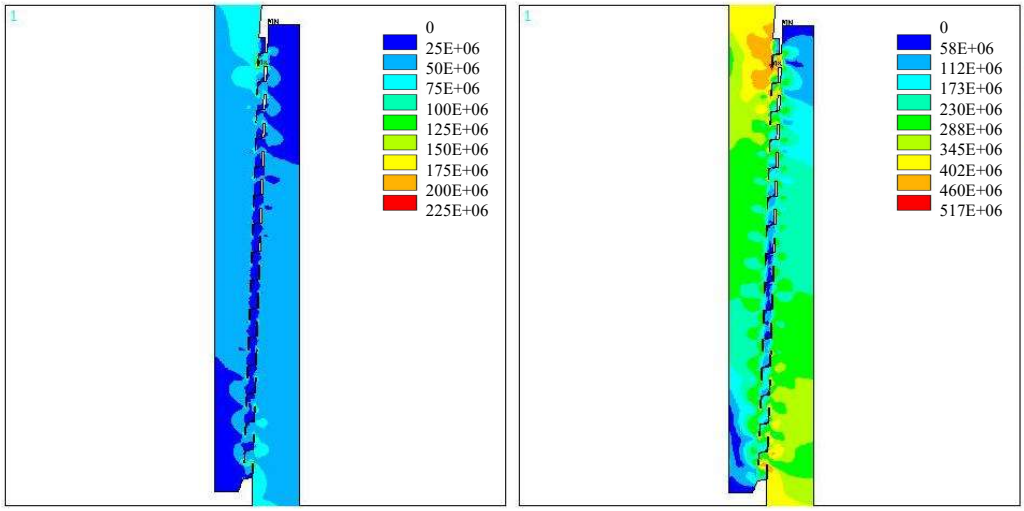

Figure 6.9: *Structural modeling of buttress thread casing (BC) connection during installation assuming casing hanging free in air, 700 m (left) and 5000 m (right) of casing hanging from the connection. Von Mises stress (Pa).*

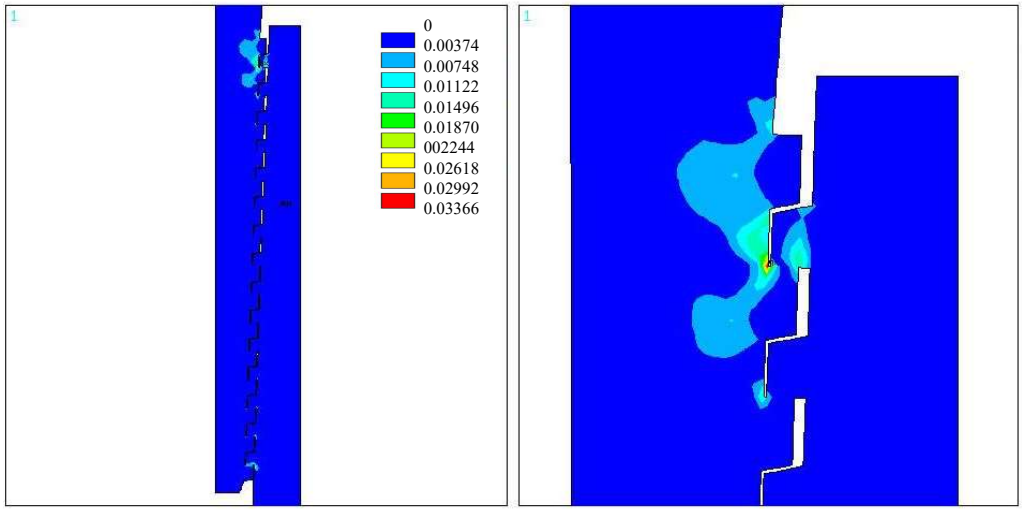

Figure 6.10: *Structural modeling of buttress thread casing (BC) connection during installation assuming 5000 m of casing hanging free in air, plastic strain (von Mises) forms in the first threads of the casing (K55grade).*

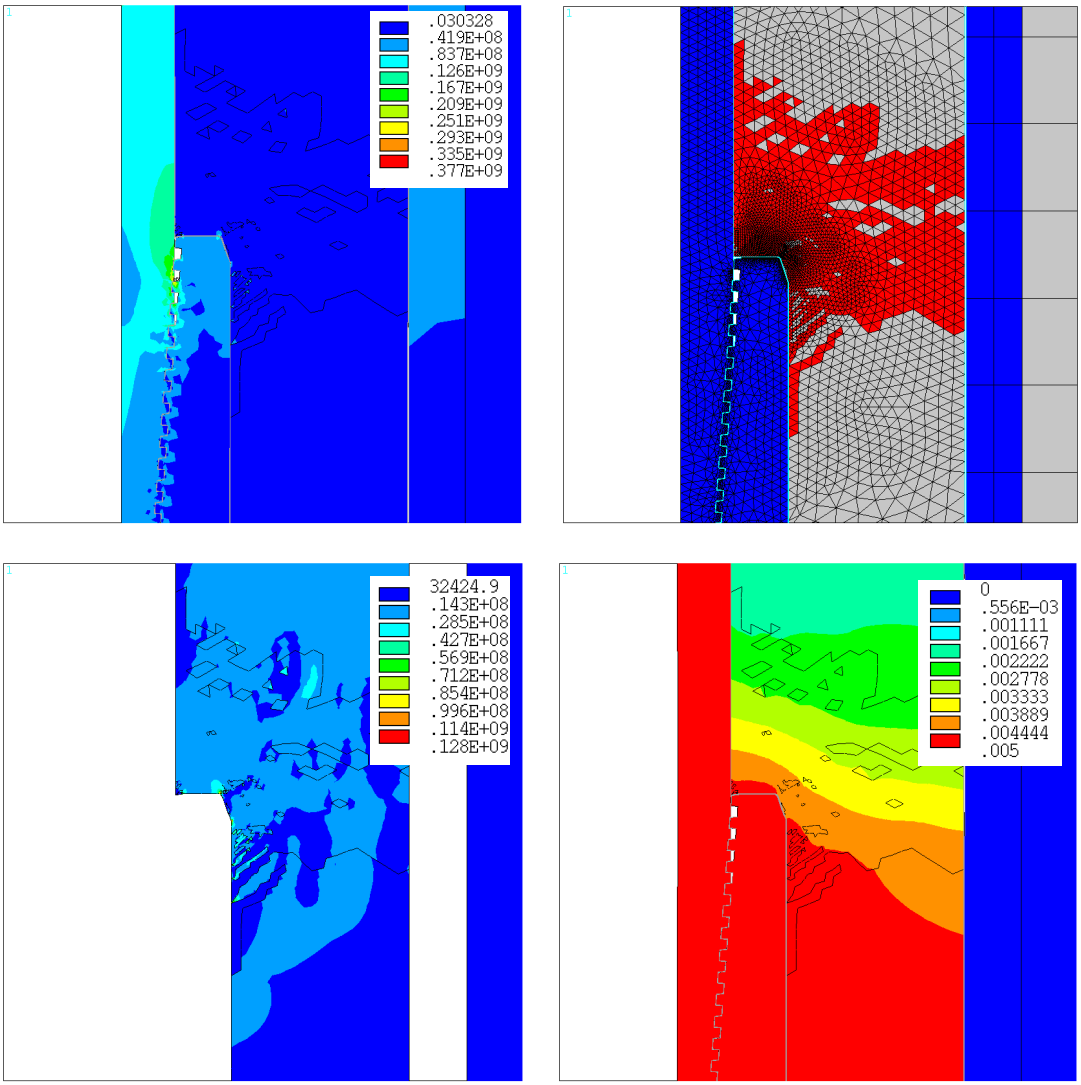

Figure 6.11: *Model of the topmost coupling of the production casing showing high stress in cement surrounding the coupling (5 mm upward displacement of the production casing). Von Mises stress (top left), von Mises stress in cement (bottom left), cement elements that have exceeded the compressive strength of the cement shown in red (top right) and displacement due to upwards casing displacement of 5 mm (bottom right).*

Cement, external casings and formation are now added to the model, to analyze stresses in the coupling and surrounding cement which the coupling is anchored in. The topmost coupling of the production casing is analyzed assuming 5 mm upward displacement of the production casing as a result of thermal expansion of the casing during discharge.

In this case, the cement is modeled elastically, thus the stress is linear according to the Young's modulus. In each step the cement elements are checked if they have exceeded the compressive and tensile strength. The tensile strength is assumed to be 10% of the compressive strength. The elements that have exceeded the strength of the cement are given diminished material properties to simulate damage. These elements are colored red in the top right corner in Fig. 6.11. Using this approach the large production casing displacement of 5 mm generates a cement damage through its full thickness. Although this might be an overestimation or simplification, the analysis indicates that cement damage could be substantial near the topmost couplings of the production casing where the casing displacement is not as restricted as deeper in the well.

6.2.3 Collapse of casings

To understand the collapse of casings and the effect of annular support on the collapse resistance as well as collapse shape, several analyses are performed. First, an eigenvalue buckling analysis is used to predict the theoretical collapse strength of a perfectly round casing (with API thickness manufacturing tolerance of -12.5%). The load on the casing is uniform external pressure. The casing that is studied has an outer diameter of $13^3/_8''$ and the thickness is 12.2 mm. Since this is a linear analysis, contact between surfaces can not be included and therefore the analysis is limited to the casing only.

Table 6.3: *Theoretical collapse strength of the modeled casing using eigenvalue buckling analysis. The calculated API collapse resistance of this casing is 13.4 MPa.*

Mode shape nr.	Theoretical collapse strength [MPa]	% of API collapse resistance
1	14.4	107.1
2	14.5	107.9
3	14.5	108.4
4	14.7	109.6
5	15.1	112.4
6	15.7	117.1
7	16.7	124.9
8	18.1	135.3

The theoretical collapse strength for mode shapes 1-8 are listed in Table 6.3 and the collapse mode shapes that were obtained with the method can be seen in Figure 6.12. As seen in the table, The theoretical collapse strength of the casing is slightly higher than the calculated API collapse resistance of the casing which is 13.4 MPa.

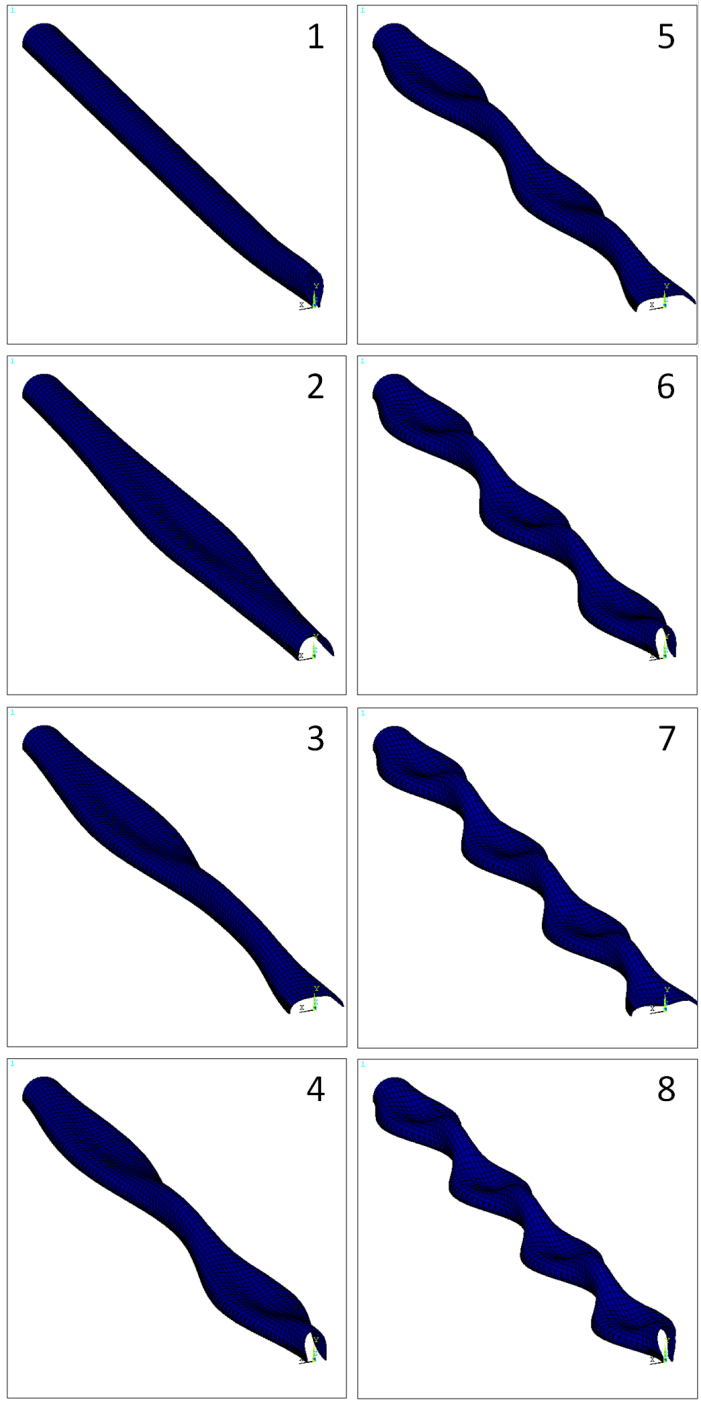

Figure 6.12: *Collapse mode shapes 1-8 of the production casing (eigenvalue buckling analysis).*

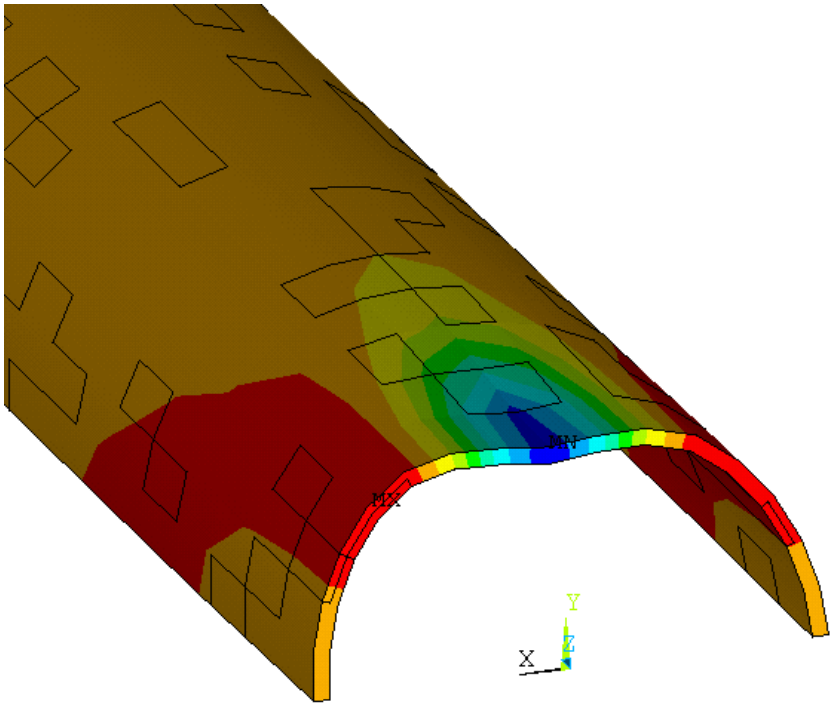

Figure 6.13: *Collapse shape after using nonlinear buckling analysis with mode shape perturbation.*

To account for nonlinearities, i.e. large displacements, in material properties and contact between surfaces, nonlinear buckling analysis is used. Because of the perfect geometry of the model, some small perturbation or instability needs to be introduced for collapse to be possible. There are several ways to do this. In all cases, small changes in material properties are randomly introduced to the casing, where 20% of the total number of elements are selected for this purpose. The first mode shape from the eigenvalue buckling analysis is used as perturbation to the initial geometry of the casing. The resulting collapse shape is displayed in Fig 6.13. Load-displacement curves are used to determine the collapse load. Since the magnitude of the mode shapes from the modal analysis is arbitrary, scaling factors are selected for slight initial deformations. The 1st mode shape is used as perturbation and scaled with values of 0.0005 and 0.001, shown in Fig. 6.14, the resulting limit loads for collapse are determined as 26.4 MPa and 21.6 MPa, respectively. This is higher than the theoretical collapse strength, i.e. the bifurcation point, that was obtained in the eigenvalue buckling analysis. The load-displacement curve for a perfectly round casing (with material impurities) is

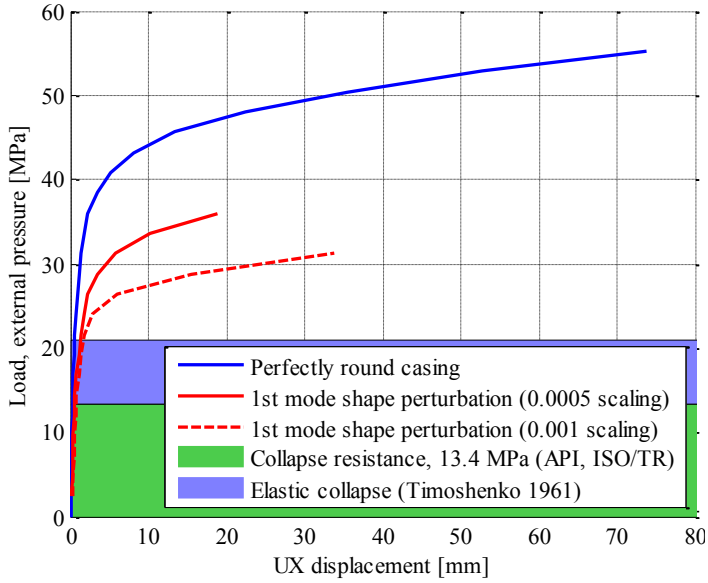

Figure 6.14: *Load-displacement curves showing the effect of initial geometry where mode shape perturbation is used.*

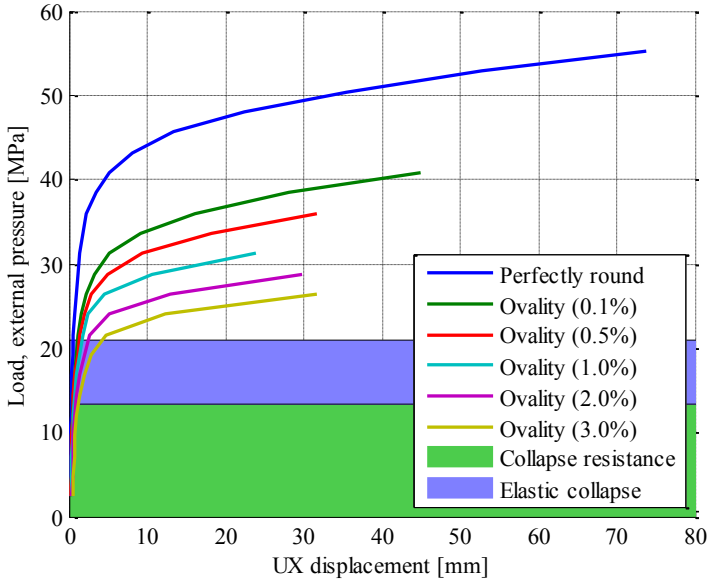

Figure 6.15: *Load-displacement curves showing the effect of ovality on collapse.*

shown for reference with collapse limit load of 38.4 MPa. Next, the effect of the initial ovality of the casing, defined in equation 5.1, on collapse resistance is analyzed. The load-displacement curves in Fig. 6.15 show that small ovality of the casing, 0.1-3.0%, reduces the collapse strength substantially. 0.1% ovality, calculated according to equation 5.1, the collapse limit load is 25.5 MPa compared to the perfectly round casing with collapse load of 38.4 MPa.

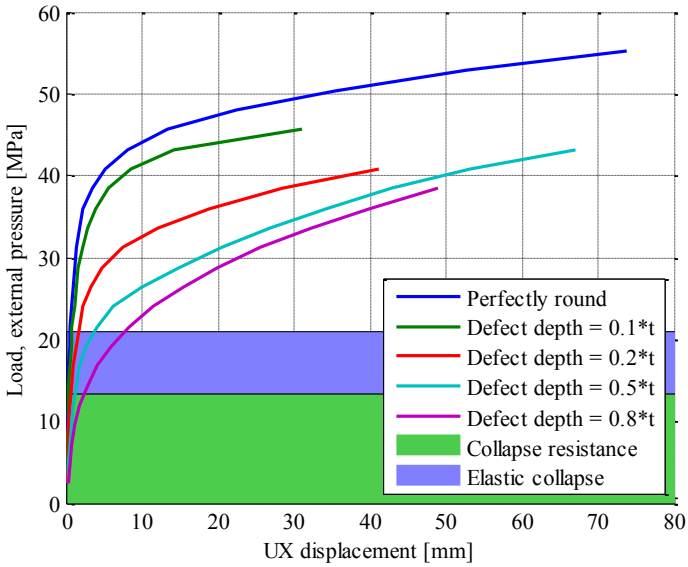

Figure 6.16: *Load-displacement curves showing the effect of external defect depth on collapse.*

Load-displacement curves showing the effect of external defect depth, 10% to the extreme 80% of the casing thickness, is shown in Fig. 6.16. Fig. 6.17 shows that at 10% defect depth the casing is unstable but the location of the defect does not control the location of the collapse. At 20-30% defect depth the collapse is located at the defect and at 40% the deformation becomes substantial. At the extreme case of 80% defect depth the collapse occurs in the defect itself in the form of plate buckling.

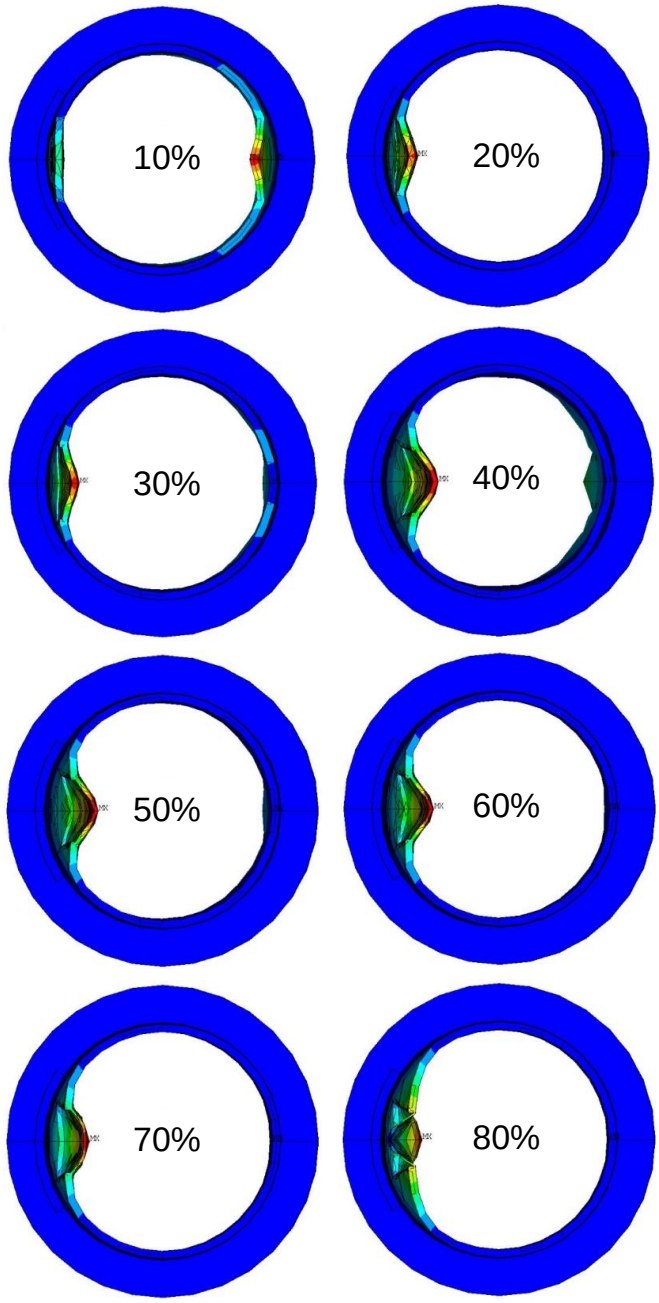

Figure 6.17: *Effect of external defect depth (percentage of casing thickness) on collapse shape. End view of the externally cemented casing.*

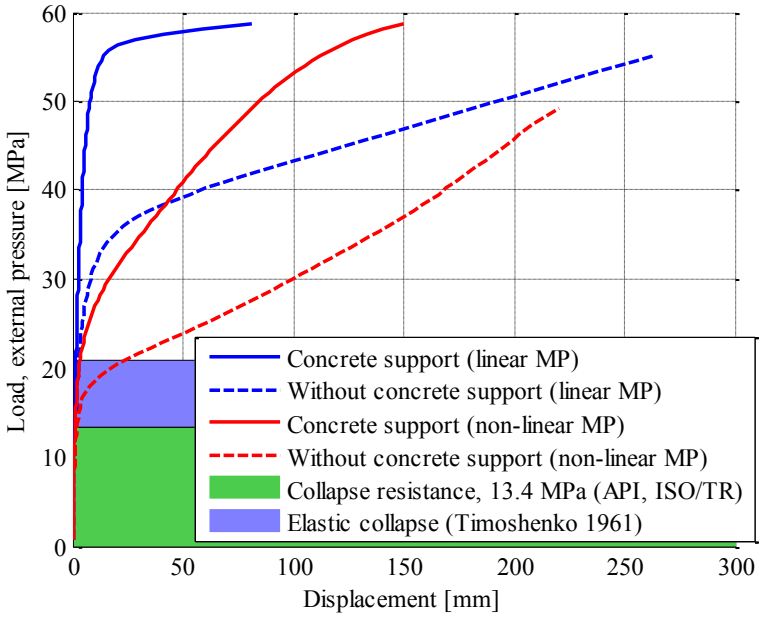

Figure 6.18: *Load-displacement curves showing the effect of structural support of cement on collapse.*

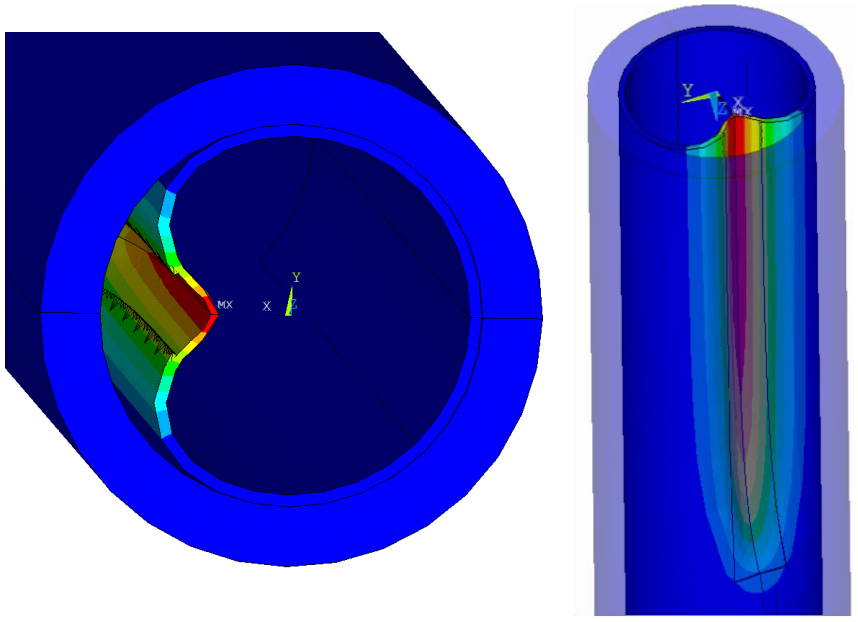

Figure 6.19: *Collapsed casing with external defect depth of 40% of the casing thickness and cement support.*

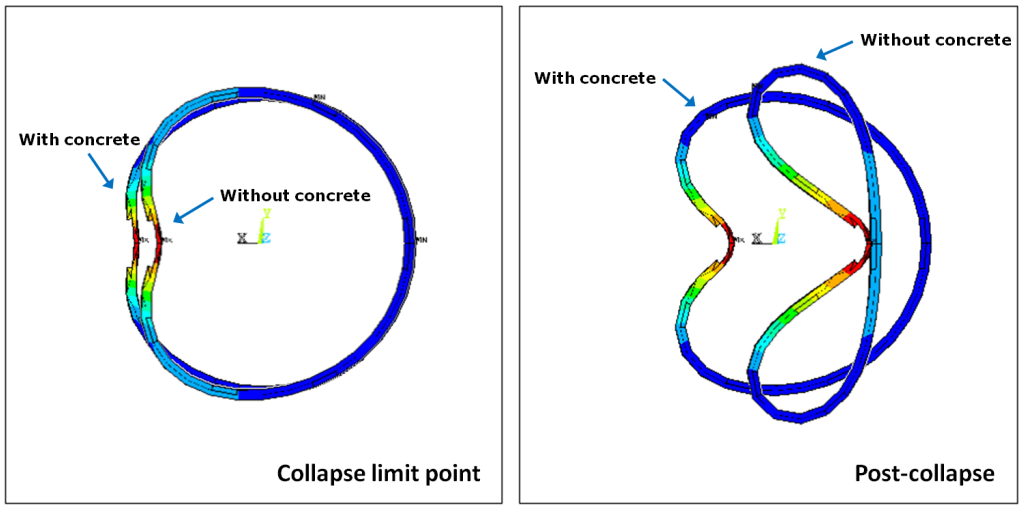

Figure 6.20: *Collapse shapes of a casing with external casing depth of 50% of the casing thickness, with and without support from cement (cement not shown). Initation of collapse (left) and post-collapse shape (right).*

Due to the buckling analysis being nonlinear, contact between surfaces and therefore the effect of cement support can be modeled. The collapse resistance of the casing is analyzed with and without cement support. Additionally, a geometric defect is added to the casing. Without the cement support the casing collapses completely, as is seen if cement slurry pressures exceed the collapse strength during cementing. When cement support is present in the model the casing only collapses partially, beginning at the location of the defect. The collapse load-displacement curves shown in Fig. 6.18 show that the cement support increases the collapse resistance of the casing. The limit load for collapse is 14.4 MPa for the unsupported casing and 18.1 MPa for the casing that is supported. In addition, the collapse shape of the supported casing resembles the collapse shapes that have been seen in wells, see Figs. 3.7 and 3.8. Using nonlinear material properties, i.e. stress-strain curves for the steel, is compared to using linear material properties, also shown in Fig. 6.18. When nonlinear material properties are used, plastic deformations take place which generates instability and leads to collapse. When linear material properties are used, on the other hand, the casing remains stable until collapse occurs elastically. According to standard ISO/TR 10400:2007(E), the D/t ratio of the casing defines a collapse region in a transition between elastic and plastic collapse, see Fig. 3.9.

Fig. 6.19 shows a collapsed casing with defect depth of 40% of the casing thickness and external cement support. Sections of the collapse and post-collapse shapes for cases with and without cement support are shown in Fig. 6.20. A summary of the collapse analysis is listed in Tab. 6.4.

Table 6.4: *Summary of the effect of initial geometry on collapse. The calculated API collapse resistance of this casing is 13.4 MPa.*

Initial geometry	Collapse limit load [MPa]	% of API collapse resistance
Without external cement support:		
Perfectly round	38.4	287
1st mode shape (0.0005)	26.4	197
1st mode shape (0.001)	21.6	161
Ovality (0.1%)	26.4	197
Ovality (0.5%)	24.0	179
Ovality (1.0%)	22.8	170
Ovality (2.0%)	21.0	157
Ovality (3.0%)	19.8	148
External defect (0.5*t)	14.4	107
With external cement support:		
External defect (0.1*t)	33.6	251
External defect (0.2*t)	25.2	188
External defect (0.5*t)	15.6	116
External defect (0.8*t)	12.0	89.6

Collapse of the production casing as a result of the presence of an annular water pocket is analyzed. The water pocket is defined as shown in Fig. 5.3. Two cases, with and without the water pocket, are compared. Table 6.5 shows maximum von Mises stress, radial displacement and axial displacement in the production casing for both cases. In the case without the water pocket, no collapse takes place despite the high temperature of 750°C and 5 MPa net external pressure. Instead the casing expands radially pushing against the cement and no debonding from the cement occurs. When the water pocket is included, collapse occurs at the location of the water pocket at 40% of the load, i.e. at about 300°C and 2 MPa net external pressure. The radial displacement of the collapsed casing can be seen in Fig. 6.21.

Table 6.5: *Maximum stress and displacements in the production casing, with and without annular water pocket.*

	W/o water pocket		With water pocket	
	Value	Location	Value	Location
Von Mises stress (MPa)	358	Casing body	440	At water pocket
Radial displacement (mm)	2.20	Near coupling	-106	At water pocket
Axial displacement (mm)	1.09	Near coupling	63.7	At water pocket

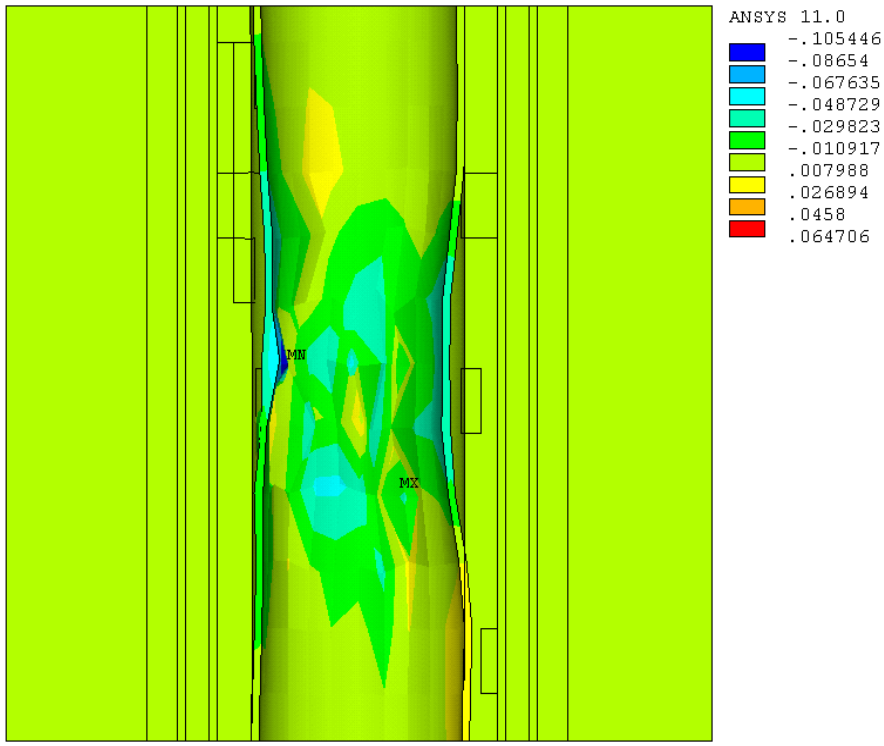

Figure 6.21: *Collapse due to annular water pocket of a $13^3/_8''$ production casing with wall thickness of 12.2 mm. The figure shows radial displacement (in meters) of the casing which collapsed at 300 and 20 bar net external pressure.*

6.3 Case study - Wellhead displacement analysis

6.3.1 Elevation measurements

Geothermal wells gradually warm up during thermal recovery from drilling (occurring over period of weeks to months). During discharges however, wellbore temperatures can change rapidly (<1 min). Large temperature changes can occur, especially close to the surface in wells that have cold gas or air mixture uppermost in the well. In such cases thermal expansion leads to upwards wellhead displacement. Wellhead elevation displacement data was gathered for 5 wells as they were discharged. In each case, the measurements lasted several hours and for 3 wells the elevation was measured again after several days of discharge.

In the survey, two types of discharges were observed; (i) from initially cold wells that needed air-pressure assistance in order to discharge and (ii) from wells that had developed wellhead pressure naturally by accumulation of non-condensable gases. In the initally cold wells, the wellhead temperature difference was large and abrupt as the wells were discharged. The wellhead displacement was therefore rapid during the first minutes after the wellhead valve was opened and then slowed down over time. But for the two initially warm wells that were observed, the lower temperature difference resulted in slower change in wellhead displacement in one well and no displacement in the other well during the observation period.

The wellhead temperature changes during discharge are shown in Fig. 6.22 and the wellhead displacement data is displayed in Fig. 6.23. Table 6.6 summarizes the wellhead temperature change, the monitored wellhead displacement and the monitoring period. All of the wells, except HE-53, showed upwards wellhead displacement shortly (<1 min) after discharge was initiated, but virtually no displacement (-0.5 mm) was seen for the wellhead of HE-53 during the observation period of three hours.

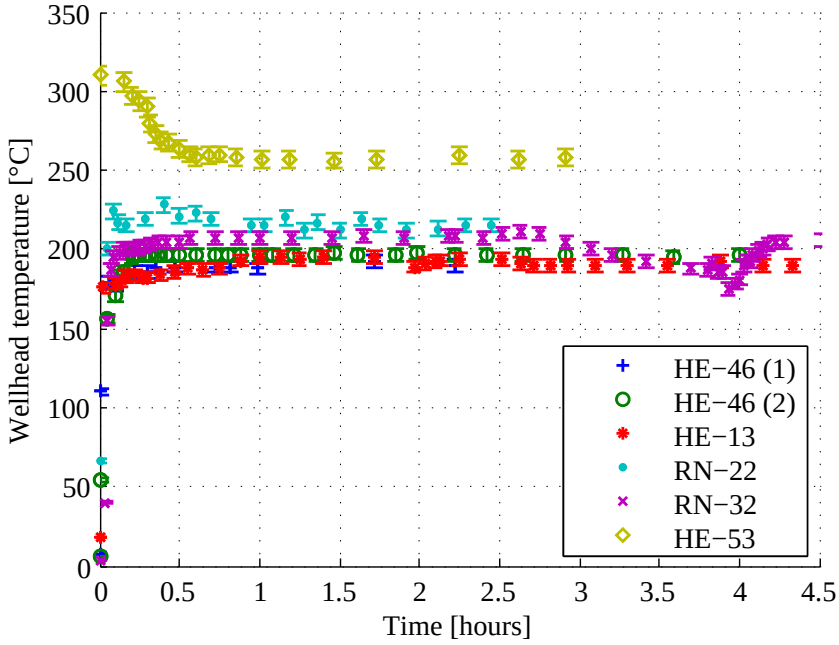

Figure 6.22: *Wellhead temperature during discharge of the monitored wells.*

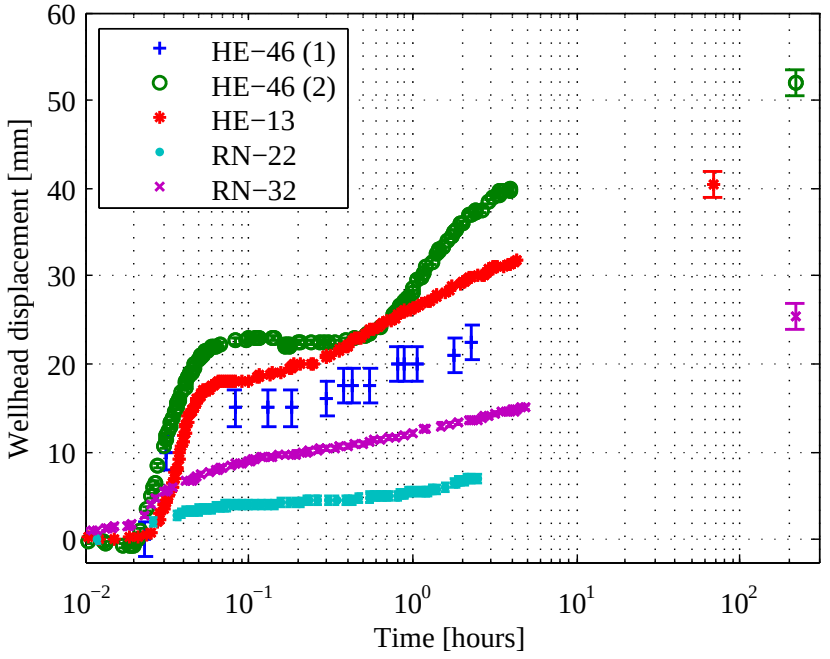

Figure 6.23: *Wellhead displacement data of the monitored wells during discharge.*

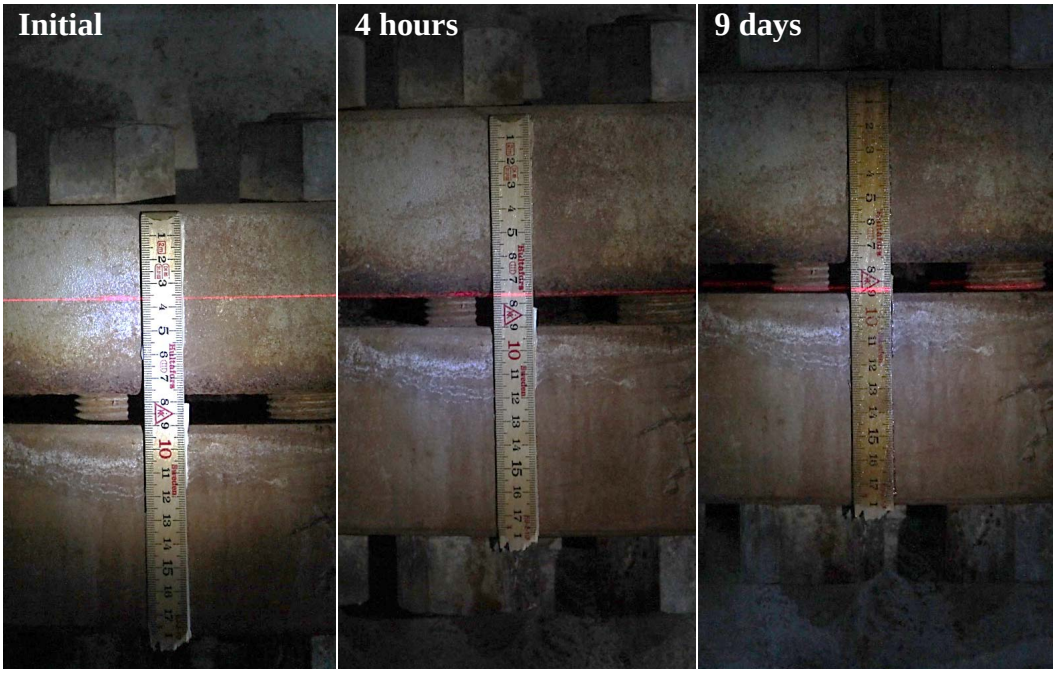

Figure 6.24: *Photographs of the wellhead displacement of well HE-46 during discharge. After 4 hours of discharge the displacement was 40 mm and after 9 days it was 52 mm.*

Table 6.6: *Monitored wellhead displacement and wellhead temperature change, ΔT, before discharge T_i and after discharge T_f. Well numbers marked with HE are located in the Hengill geothermal area and wells marked with RN are located in the Reykjanes geothermal area. Well HE-46 was monitored during two separate discharges marked (1) and (2).*

Well number	T_i (°C)	T_f (°C)	ΔT_{wh} (°C)	u_{wh} (mm)	Monitoring period
HE-46 (2)	6	197	191	52.0	9 days
HE-46 (1)	8	193	185	22.5	2.5 hours
HE-13	18	197	179	40.5	3 days
RN-22	66	215	149	7.0	2.5 hours
RN-32	3	207	204	15.0	9 days
HE-53	310	260	-50	-0.5	3 hours

A discharge attempt of HE-46 that failed, as pressurized air was released without initiating discharge, indicates that the wellhead displacement is governed by thermal expansion rather than wellhead pressure. A downward wellhead displacement of 1.5 mm was observed while the wellhead pressure decreased from 45 to 0 bar-g as shown in Fig. 6.25. Compared to the wellhead displacement during discharge, where the maximum observed upward displacement was 52 mm, the downward displacement due to pressure release is small.

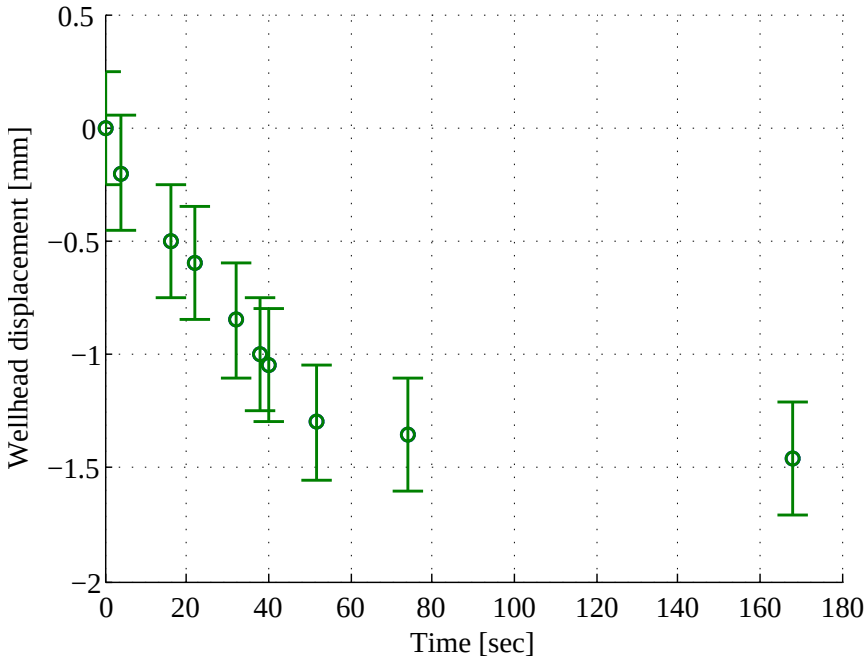

Figure 6.25: *Wellhead displacement from 45 to 0 bar-g during a failed discharge attempt of well HE-46.*

Photographs of the wellhead displacement of HE-46 is displayed in Fig. 6.24. Two photographs merged into one show the initial elevation of the wellhead of RN-32 and the displacment 9 days after discharge initiation.

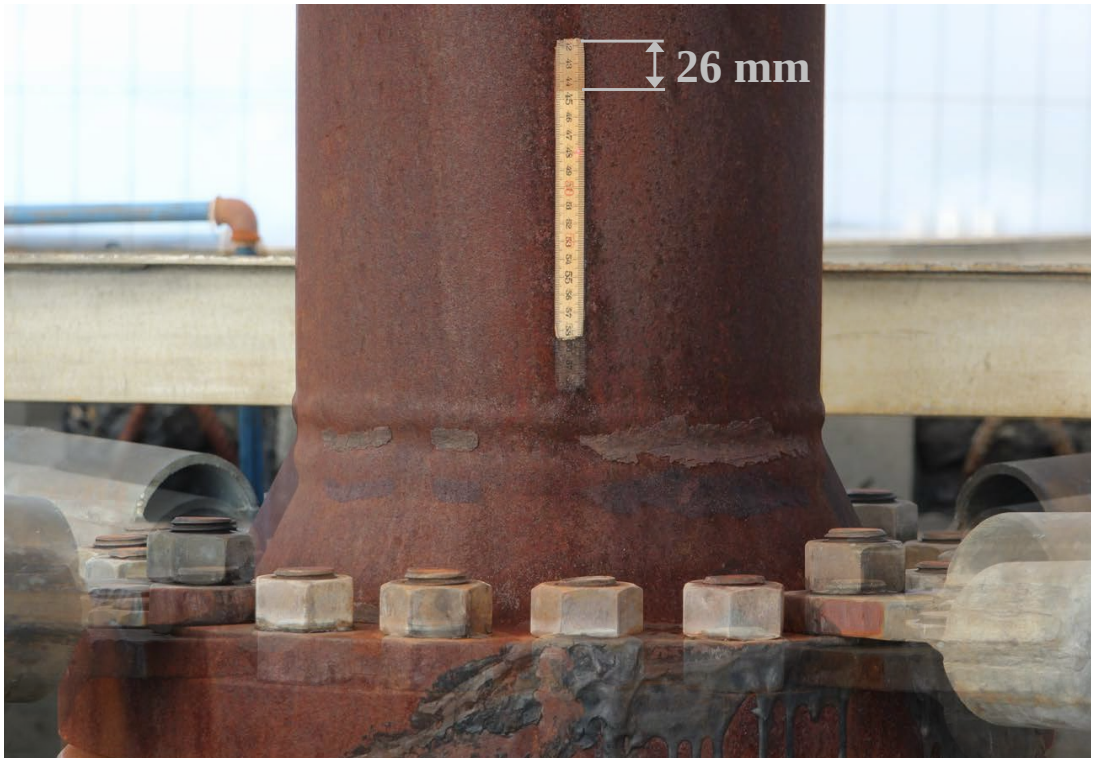

Figure 6.26: *Merged photographs of the initial elevation of the wellhead on RN-32 at 3°C and 35 bar-g and the displacement 9 days after discharge initiation at 207°C and 17 bar-g.*

Fig. 6.27 shows the locations where temperature measurements were taken on the wellhead of HE-46. The two discharges of the well, with two years in between, show nearly identical temperature changes. Figs. 6.28 and 6.29 show the measurement locations and temperature measurements on the wellhead of RN-22 and HE-13, respectively. Fig. 6.30, shows wellhead temperature, pressure and wellhead displacement of the initial flow-test of RN-32. The temperature measurements indicate that the wellheads and therefore also the wellbore have reached steady temperatures about one hour after discharge initiation. However, the wellheads keep rising which is explained by gradual temperature increase in the anchor and surface casings.

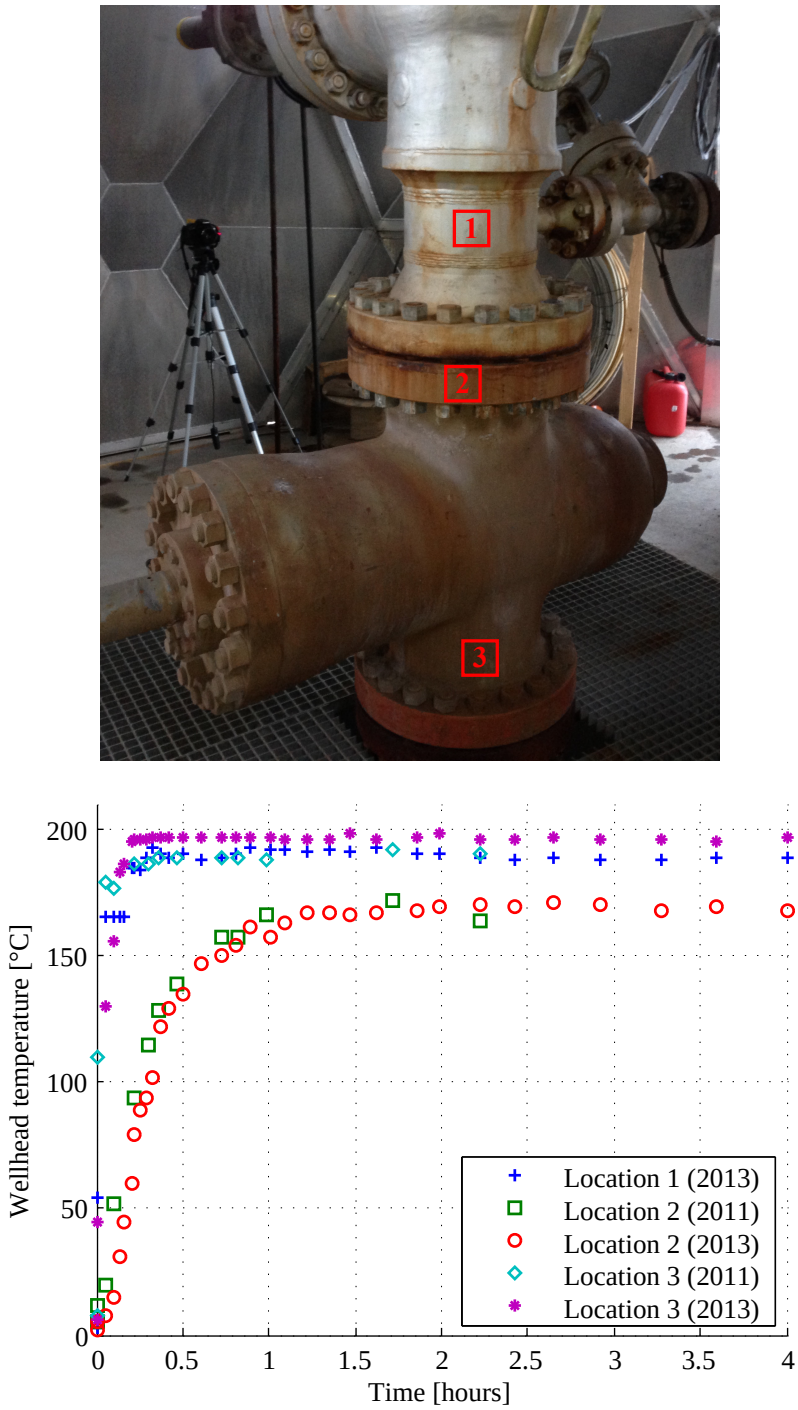

Figure 6.27: *Wellhead temparature measurement locations on HE-46 (2) and temperature data during two discharges of HE-46, 2011 (1) and 2013 (2).*

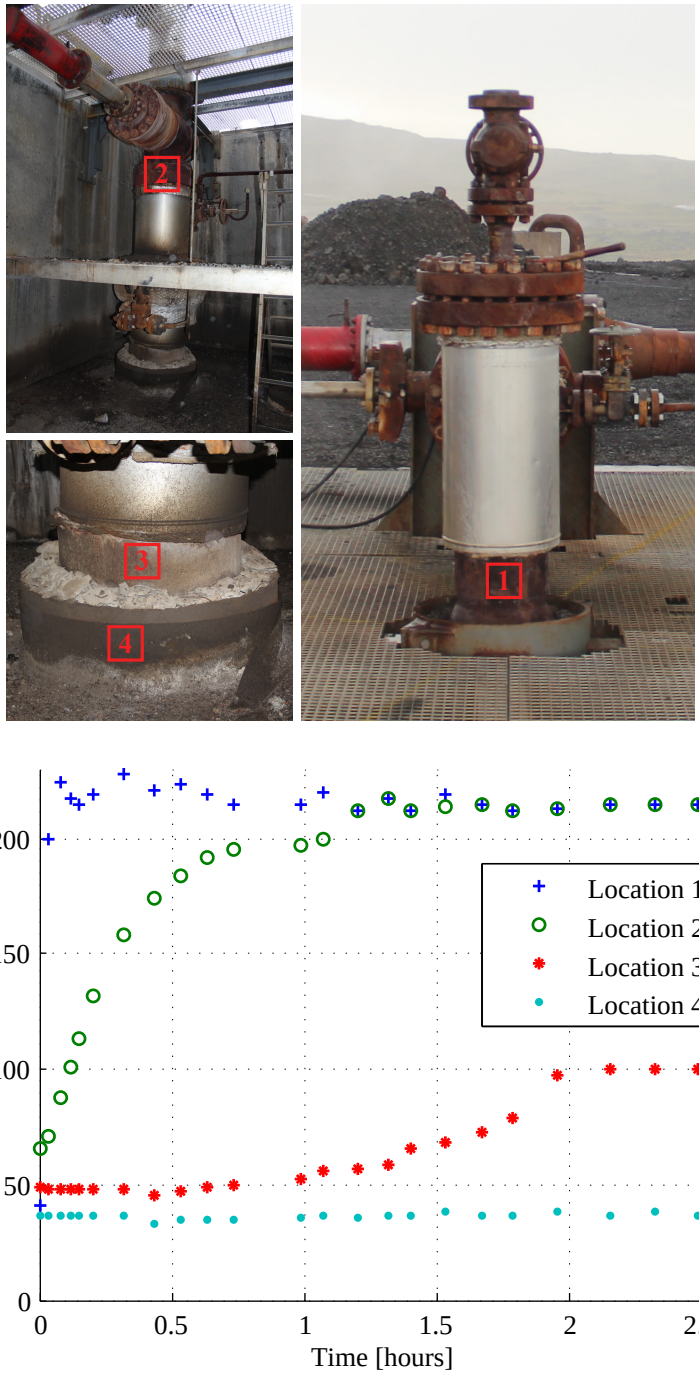

Figure 6.28: *Wellhead temperature measurement locations and temperature data during discharge of RN-22.*

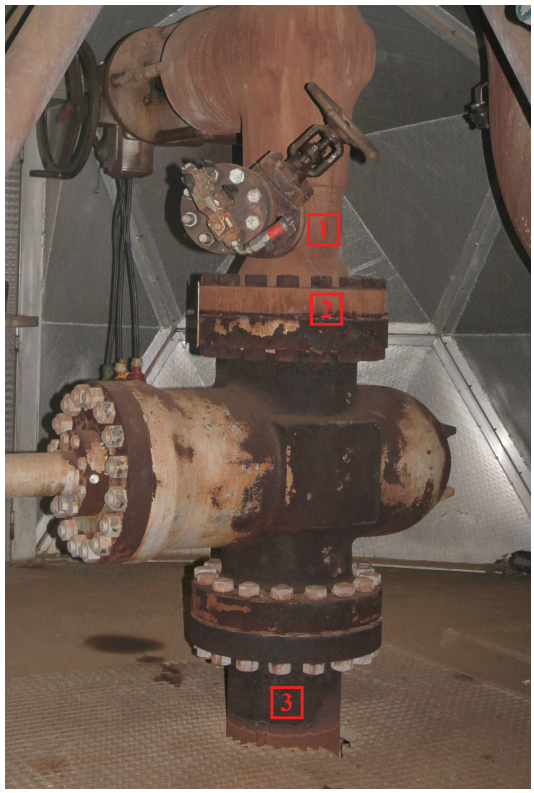

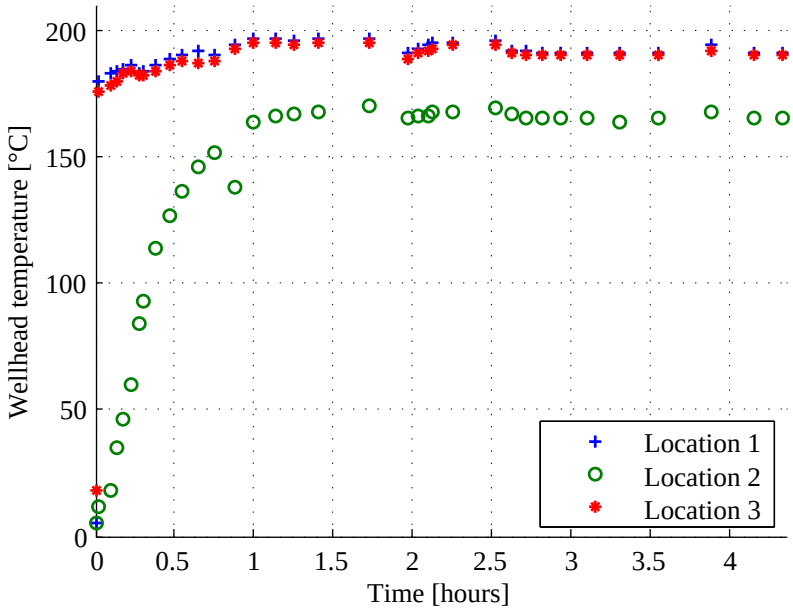

Figure 6.29: *Wellhead temperature measurement locations and temperature data during discharge of HE-13.*

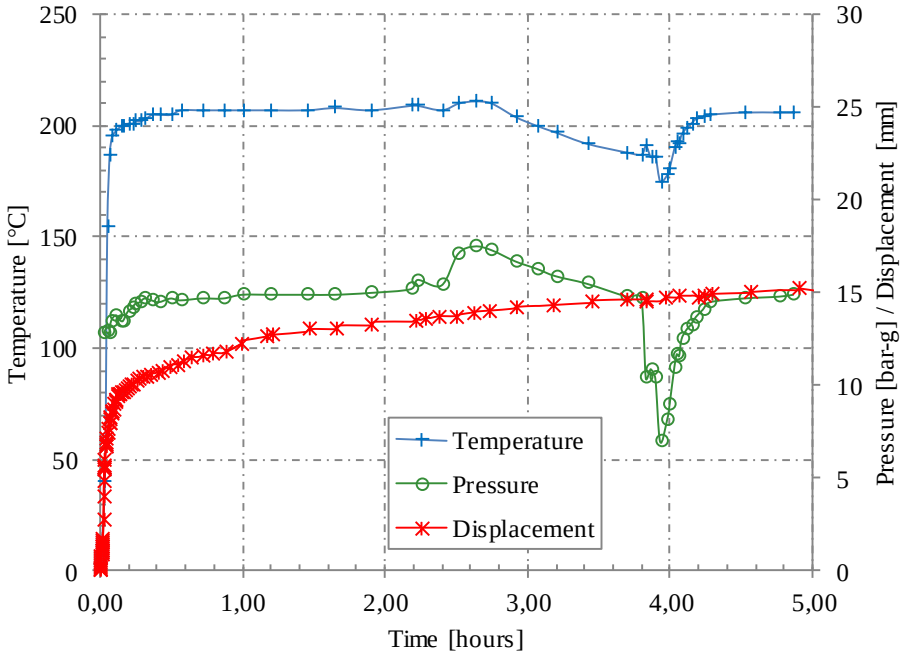

Figure 6.30: *Temperature, pressure and wellhead displacement data during initial flow-testing of RN-32.*

6.3.2 FEM analysis

The casing programs of wells HE-46, HE-13, RN-22, RN-32 and HE-53 are modeled with the 2D axi-symmetric model described in section 5.1, where the whole cased section is modeled. Numerical results, from the model are compared to the wellhead displacement measurements that are described in section 6.3.1. The transient temperature distribution of the wells is calculated from each assumed load history which is based on temperature and pressure logs and wellhead data. The load case for well HE-46 is shown in Fig. 6.31.The estimated formation temperature used as load to the whole model in the thermal analysis. Then assumed wellbore cooling from drilling, warm-up and lastly discharge is modeled with transient analysis. The thermal results are then used as load in the structural analysis along with defined wellbore pressure. Similar load input is prepared for each well with site specific formation temperatures and wellbore temperature and pressure loads.

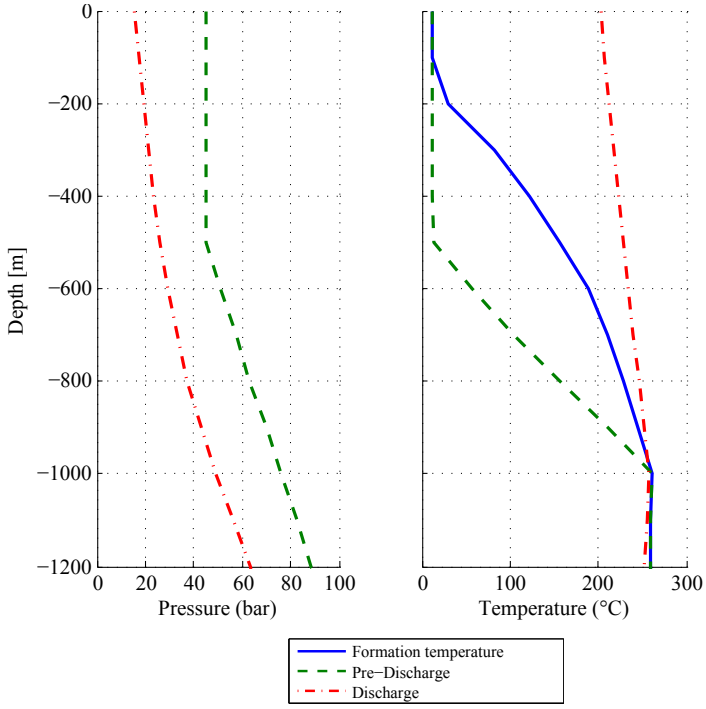

Figure 6.31: *Temperature and pressure profiles used as load cases for well HE-46.*

Fig. 6.32 is used for transition of the wellbore temperature load between the pre-discharge and discharge load cases, illustrating how the wellhead temperature of well HE-46 increases after flow-testing is initiated.

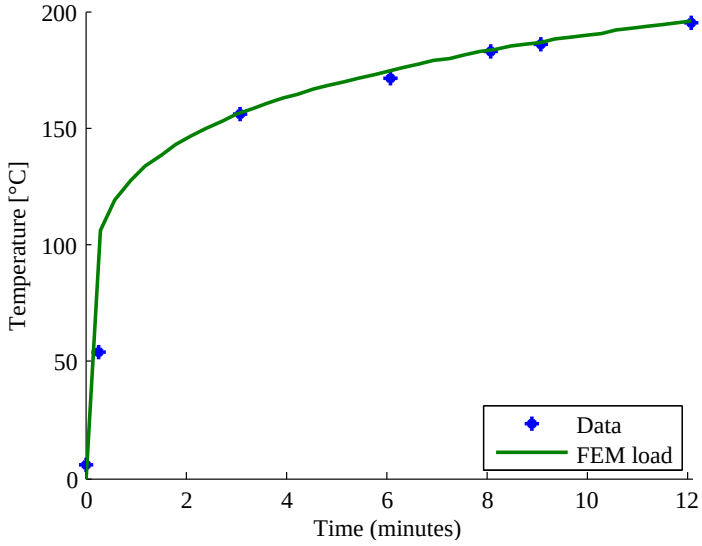

Figure 6.32: *Measured wellhead temperature during initiation of flow which is used as transition between the pre-discharge and discharge load cases of well HE-46.*

The modeled temperature distribution and displacement of the wellhead of HE-46 after 9 days of discharge are displayed in Fig. 6.33, respectively. The results show slight sliding of the production casing inside the wellhead. The modeled wellhead displacements are compared to the measured displacement for the 5 wells that were measured in Figs. 6.34 to 6.37. There is a good agreement between the model and the measurements.

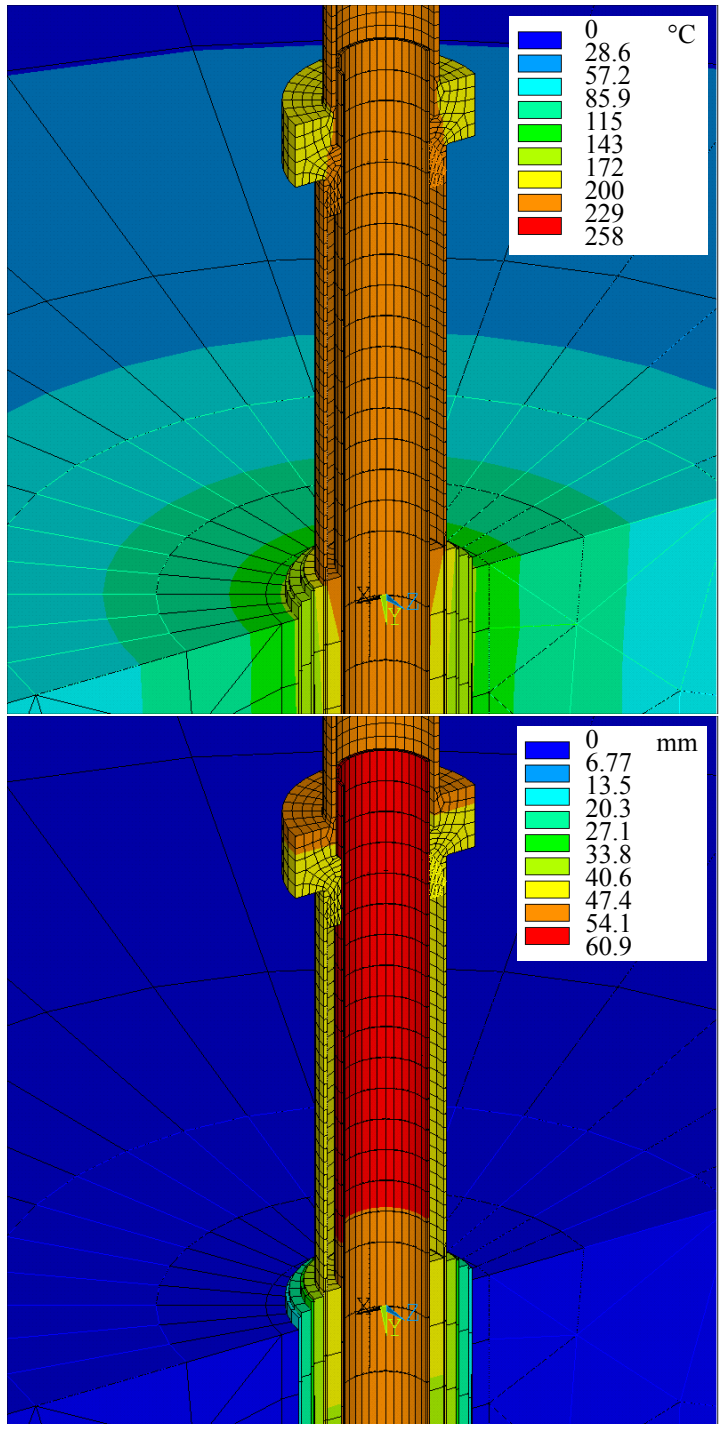

Figure 6.33: *Modeled wellhead temperature (top) and wellhead displacement (bottom) 9 days after discharge of well HE-46 (180° symmetry expansion).*

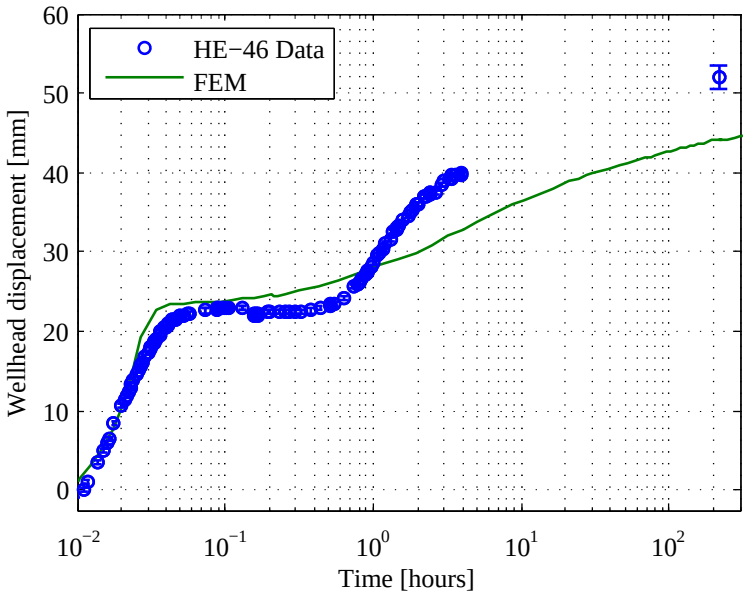

Figure 6.34: *Measured wellhead displacement for well HE-46 and FEM model results (default model parameters).*

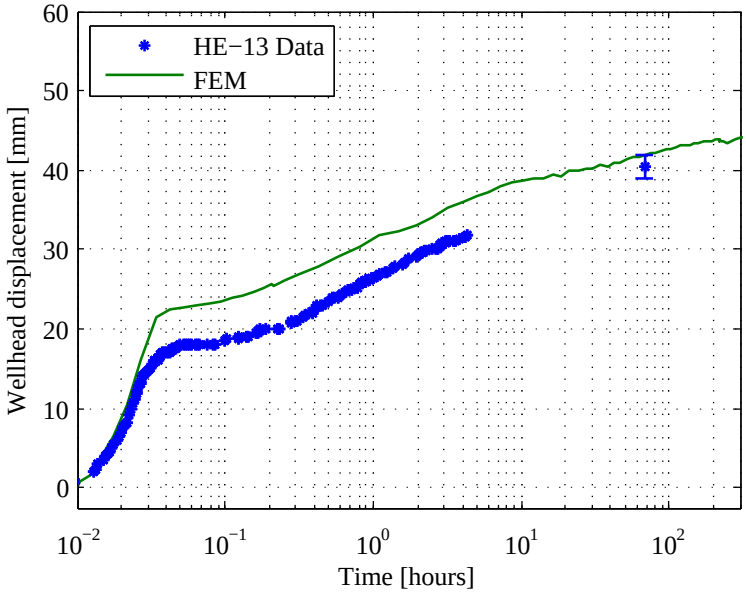

Figure 6.35: *Measured wellhead displacement for well HE-13 and FEM model results (default model parameters).*

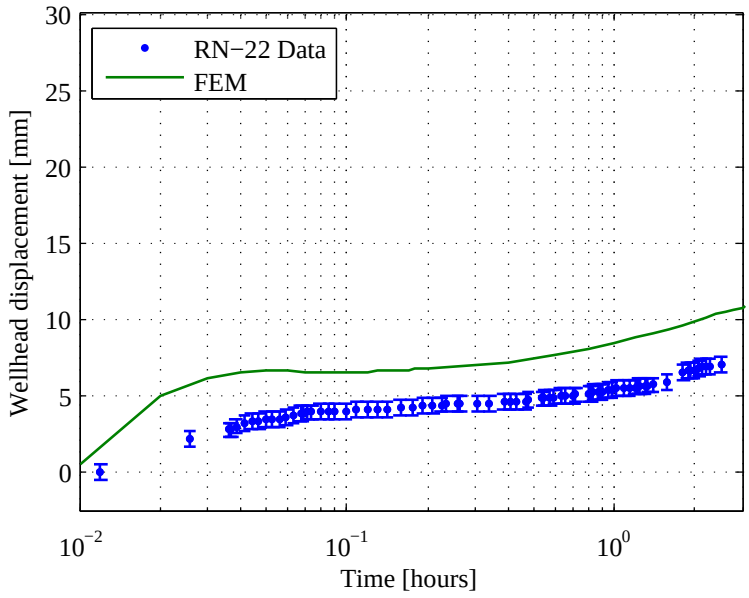

Figure 6.36: *Measured wellhead displacement for well RN-22 and FEM model results (default model parameters).*

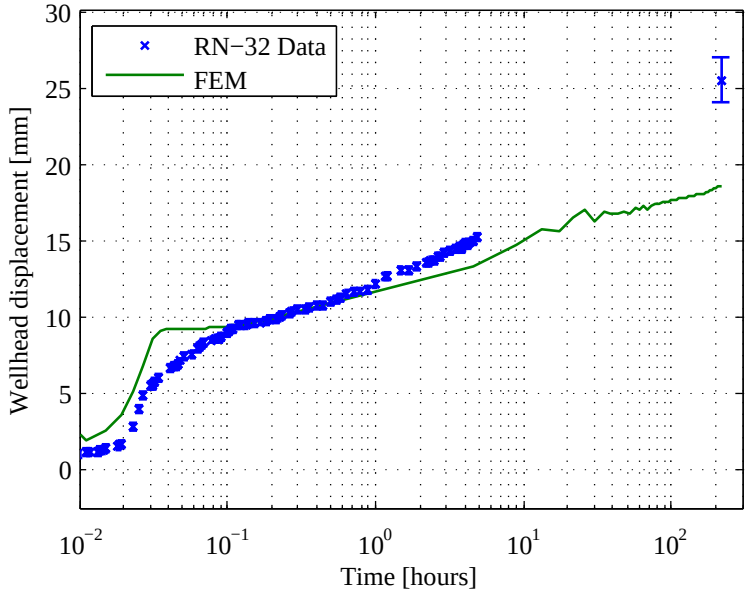

Figure 6.37: *Measured wellhead displacement for well RN-32 and FEM model results (default model parameters).*

6.4 Case study - Structural analysis of IDDP-1

6.4.1 Operation history and casing failures

The Iceland Deep Drilling Project (IDDP) consortium was established in the year 2000 to investigate the feasibility and economics of deep, high-enthalpy geothermal resources, and supercritical hydrothermal fluids, as possible future energy sources (Friðleifsson et al., 2014). The first well IDDP-1 was drilled in the Krafla geothermal field in north-east Iceland in years 2008-2009 with the aim of drilling to a total depth of 4500 m and reaching superheated or supercritical heat source. Due to the depth of the well, it was designed with five casings. But after unexpectedly drilling into magma the final depth became ∼2100 m (Hauksson et al., 2014; Hólmgeirsson et al., 2010; Pálsson et al., 2014). The production casing and the anchor casing were thus both ∼1950 m deep, but casings in conventional high temperature geothermal wells are typically about 700-1000 m deep. The casing program of the well is listed in Table 6.7.

Table 6.7: *The casing program of IDDP-1 (as built) (Thórhallsson et al., 2014; Pálsson et al., 2014).*

	D [in]	t [mm]	Length [m]	Steel grade	Connections
Surface casing	32 1/2	13.0	87	X56	Welded
Intermediate casing 1	24 1/2	13.0	254	K55	Welded
Intermediate casing 2	18 5/8	13.0	785	K55	BC
Anchor casing (Top 290 m)	13 5/8	15.9	290	T95	Hydril 563
Anchor casing (290-1949 m)	13 3/8	13.1	290-1949	K55	Hydril 563
Production casing	9 5/8	13.8	1935	K55	Hydril 563
Slotted liner	9 5/8	12.0	1935-2072	K55	BC

During cementing of the production casing it was evident that cementing was poor at around 620 m depth and as the well was flow tested the casing collapsed at that location. According to Cement Bond Logs (CBL) from ÍSOR (Iceland GeoSurvey) there was little evidence of a cement bond with the production casing at depth intervals 615-635 m and 725-785 m. The casing appears to have collapsed during the initial flow testing, near the suspected intersection between the two cementing operations (Pálsson et al., 2014). This inhibited further logging of the well below the casing failure, but a video log conducted by ÍSOR (Iceland GeoSurvey) later revealed the severe collapse, Fig 6.40.

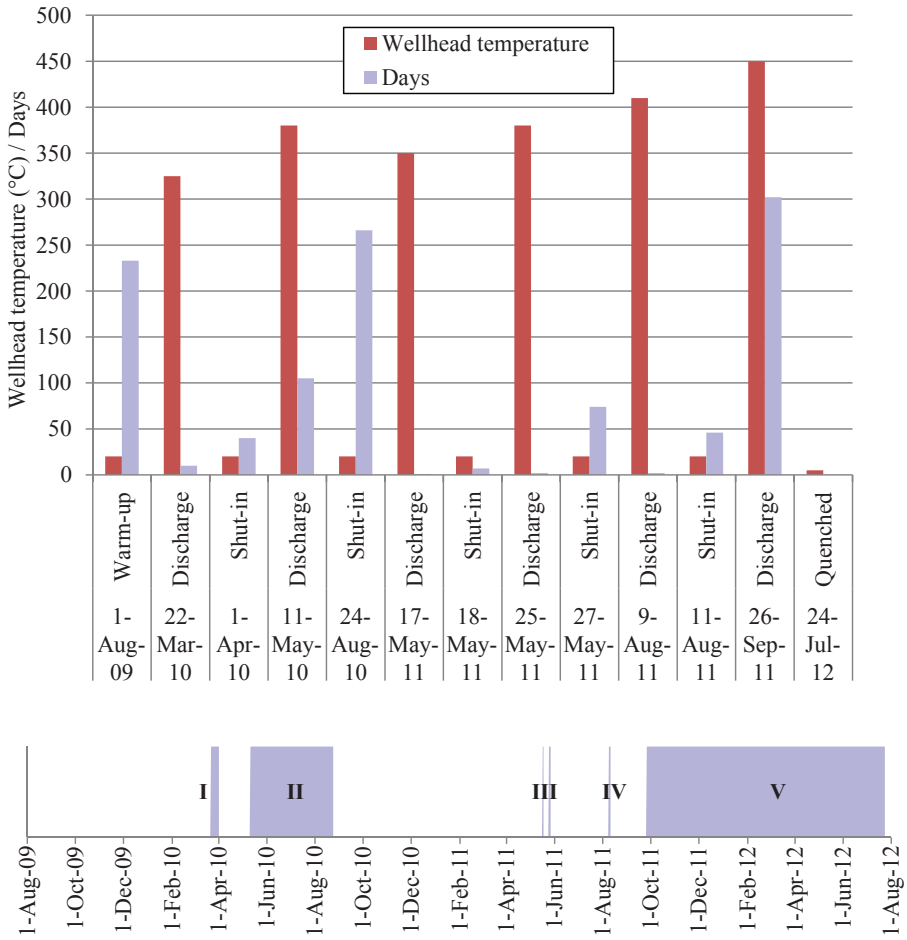

Figure 6.38: *Operation history and maximum wellhead temperature of each discharge phase of IDDP-1.*

The well was flow-tested several times with intermittent stops as surface equipment had to be redesigned. Ingason et al. (2014) presented the operation history data of the wellhead pressure (P) and temperature (T) of IDDP-1 during five discharge phases. The operation history, discharge phases and wellhead temperatures are shown in Fig. 6.38. During phase I, saturated steam was produced but in the succeeding phases the fluid became superheated, with wellhead conditions at 450°C and 140 bar-g (Hauksson et al., 2014; Ingason et al., 2014), as shown in Fig. 6.39. Since the load history is important for analyzing built-up plastic strain in the casings, the flow-test phases of the discharge system are used to reconstruct the load history for the structural analysis.

Due to a critical situation of steam leakage followed by a master valve malfunction after successfully flow-testing at superheated conditions for 10 months, the well was quenched by injecting water into it in July 2012 (Ingason et al., 2014). The video log of the well from the year 2014 revealed four failures in the production casing. Three connection failures were found at depths of 300 m, 356 m and 505 m. In all cases the casing had been pulled down from the coupling leaving the outer casing and cement exposed, see Figs. 6.41 to 6.43. The gap formed was approximately 0.4 m for the ruptures at 300 m and 356 m and 0.25 m at 505 m.

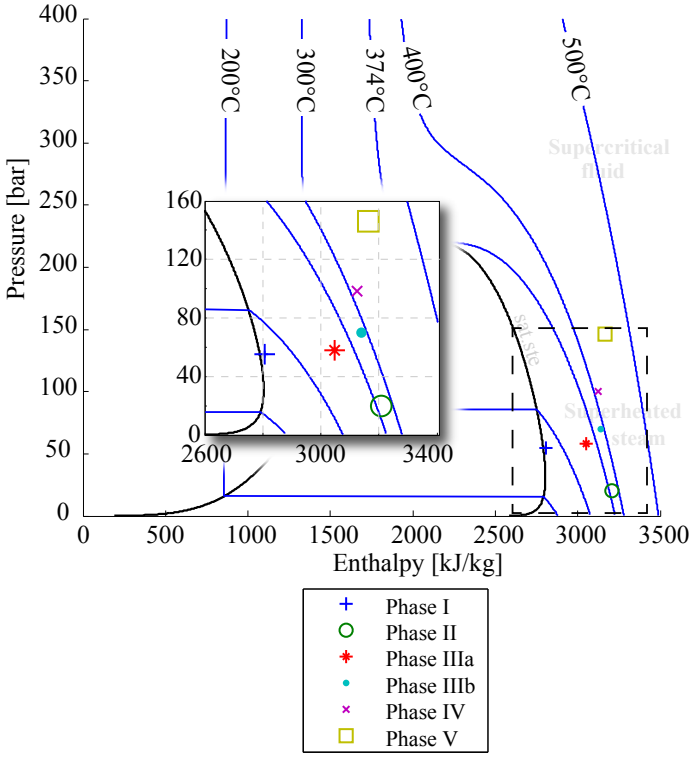

Figure 6.39: *Enthalpy estimation of the fluid in the different discharge phases of the IDDP-1 well. Saturated steam was produced from the well in phase I and in later phases the steam became superheated.*

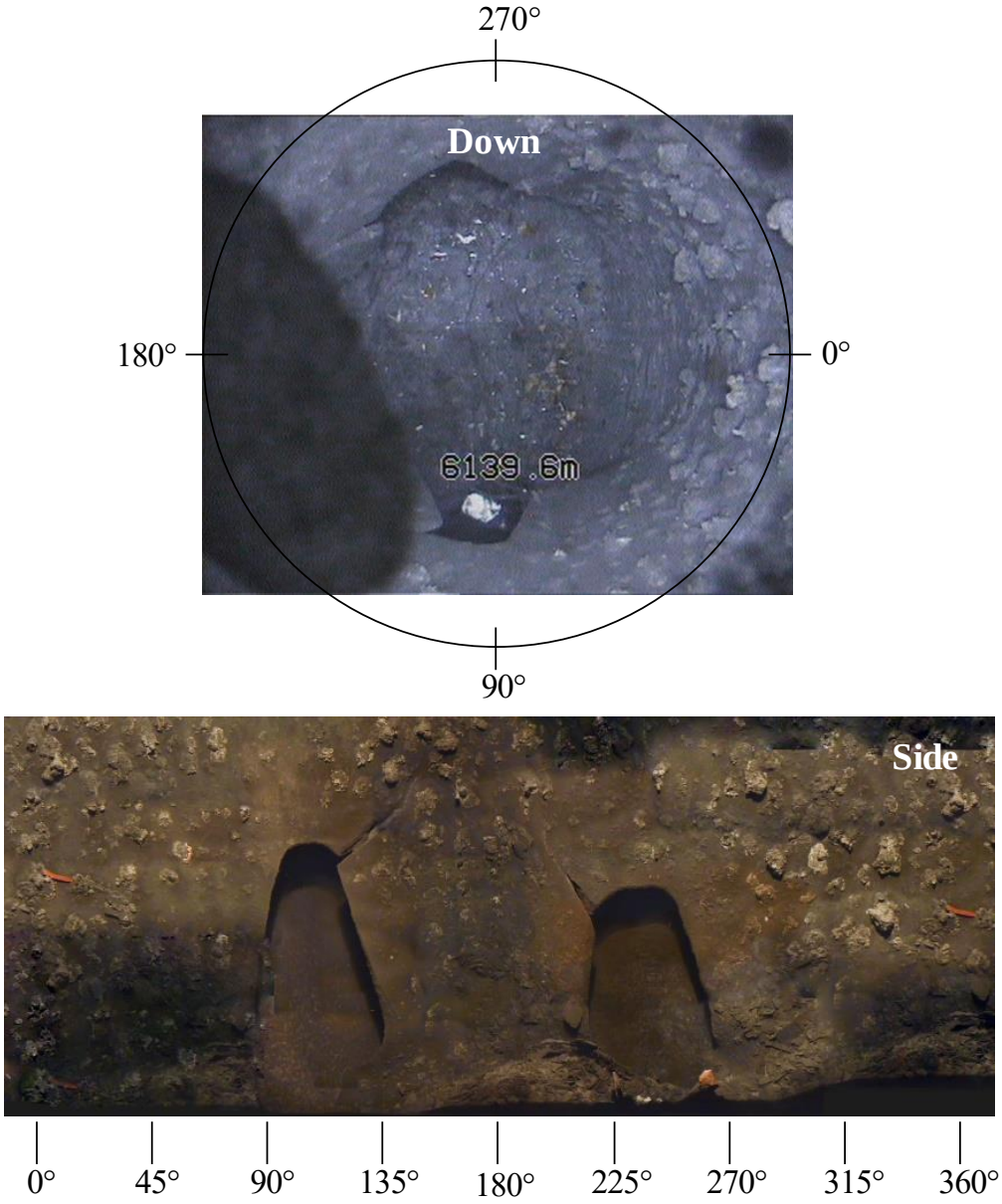

Figure 6.40: *Severe casing collapse at about 620 m depth in IDDP-1 (by courtesy of Landsvirkjun).*

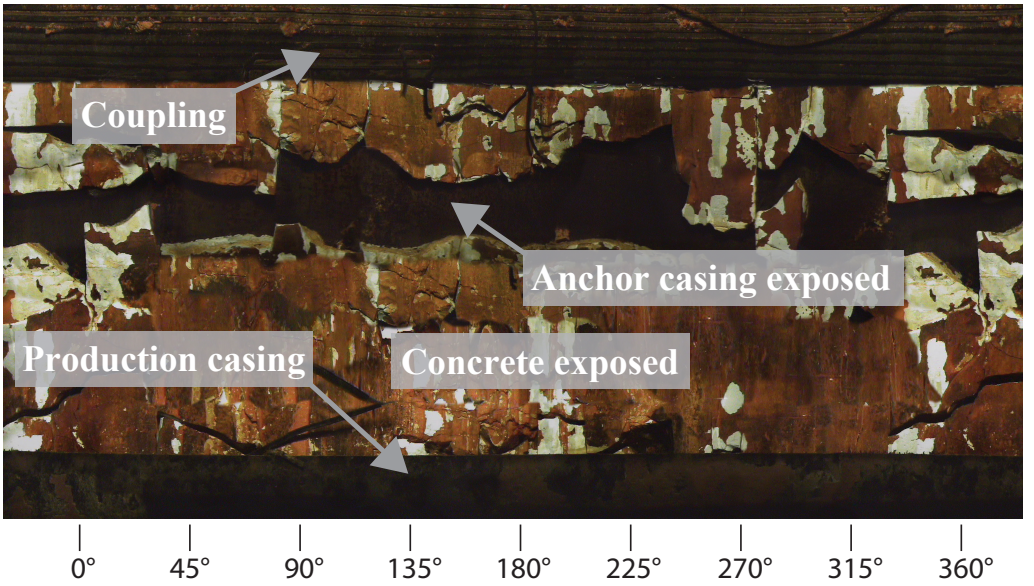

Figure 6.41: *Combined image from a video log of a coupling rupture at approximately 300 m depth in the IDDP-1 well. After the failure occurred the cement and the outer casing were exposed (by courtesy of Landsvirkjun).*

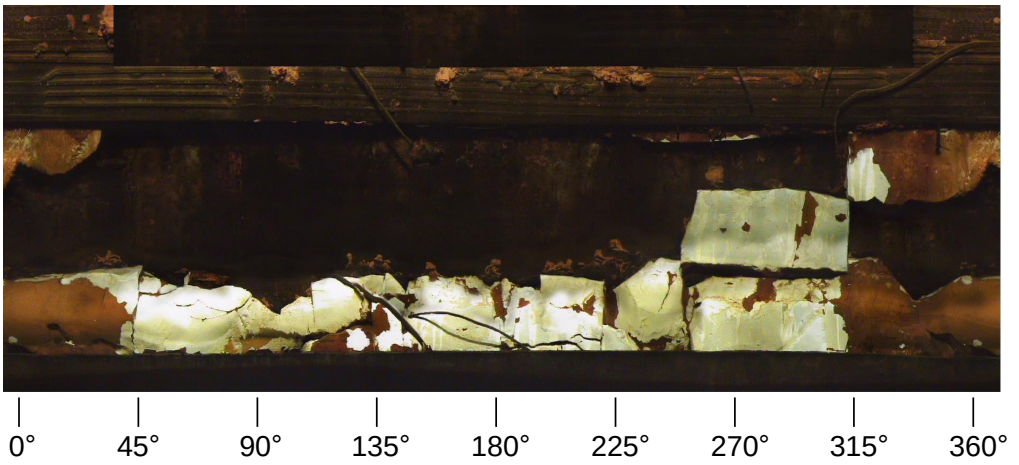

Figure 6.42: *A combined image of the coupling rupture at 356 m depth in IDDP-1 (black areas are regions that were not documented in the video). Much of the cement has fallen into the well and external casing is exposed (by courtesy of Landsvirkjun).*

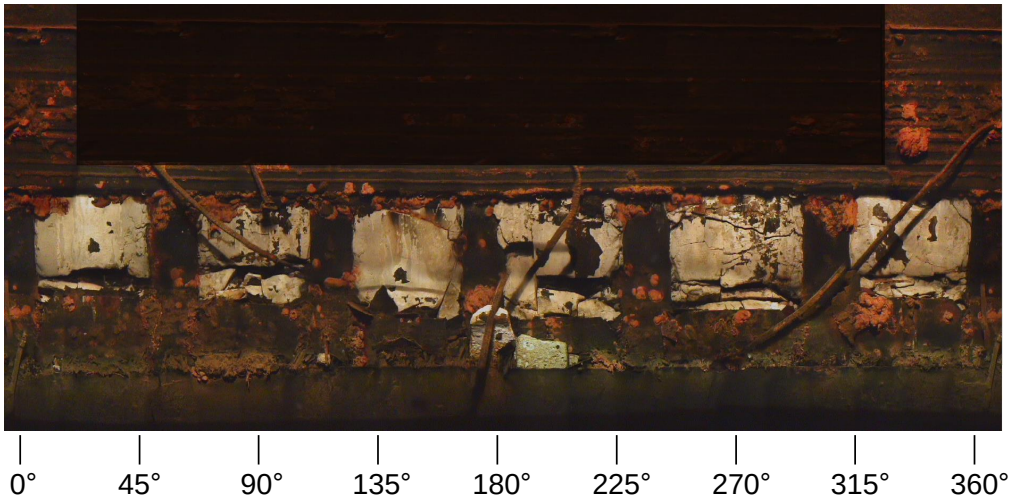

Figure 6.43: *A combined image of the coupling rupture at 505 m depth in IDDP-1 (black areas are regions that were not documented in the video). A casing bow-centralizer that is placed around the coupling is visible, holding the cement in place (by courtesy of Landsvirkjun).*

6.4.2 FEM analysis

The axisymmetric model of the IDDP-1 well is shown in Fig. 6.44. Due to the deep casings, the anchoring effect of couplings was included by using bonded contact at the connection locations instead of using simplified couplings as shown before (e.g. in Fig. 6.8).

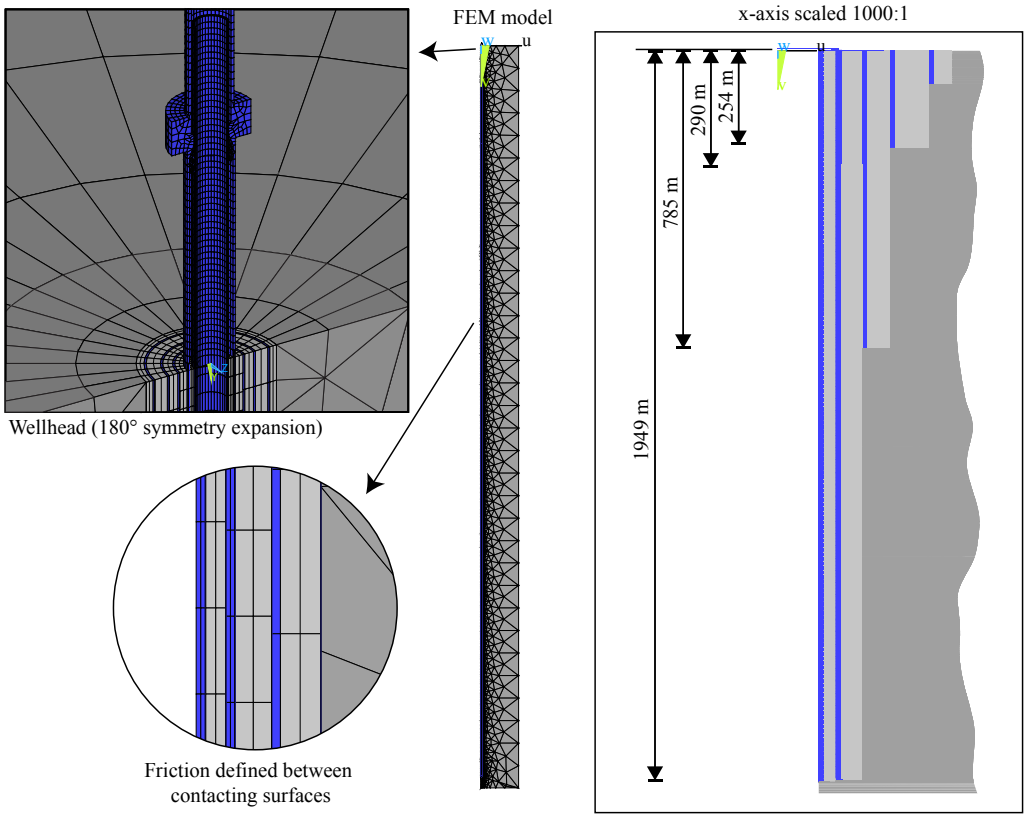

Figure 6.44: *Axisymmetric nonlinear FEM model of the IDDP-1 well. The anchoring effect of the couplings in the cement is included in the model by using bonded contact at the coupling locations. A simplified wellhead is also included to account for wellhead pressure and the interaction between the production casing and the wellhead. The casing depths are shown to the right by scaling the x-axis by 1000 to 1.*

Convergence studies of the axisymmetric model of the cased section of the well with respect to mesh density in the axial direction is shown in Fig. 6.45. The mesh configurations are listed in Table 6.8. In order to simplify the mesh sensitivity evaluation, the model is cut from the bottom. The convergence study shows similar results for all four meshes. Mesh IV is therefore chosen for the analysis and the casings are analyzed down to 1700 m depth. Furthermore, the convergence studies show that cutting the model from the bottom does not change the results since load premises are not changed. The element density is on the limit of being too coarse, but using coarser mesh would violate element shape checks. Therefore, small local stresses and strains can not be expected, only the global picture.

Table 6.8: *Considered mesh densities in radial (elements/thickness) and longitudinal (elements/m) directions.*

Mesh	Model depth (m)	Mesh density	Production casing	Production cement	Anchor casing	Anchor cement
I	390	Radial	4	3	2	2
		Longitudinal	15.6	15.6	7.6	7.6
II	774	Radial	2	2	2	2
		Longitudinal	7.6	7.6	7.6	7.6
III	1209	Radial	1	2	1	2
		Longitudinal	7.6	7.6	4.0	4.0
IV	1722	Radial	1	2	1	2
		Longitudinal	4.0	4.0	4.0	4.0

Residual stresses from installing the casings is accounted for by defining initial stress conditions. They consists of (i) tensile stress from a casing hanging free from the top in a well filled with cold water and (ii) thermal stress from the temperature difference between the cement as it sets and the drilling fluid. The cementing temperature of the four innermost casings displayed in Fig. 6.46 is estimated form temperature measurements taken before cement bond logging (CBL).

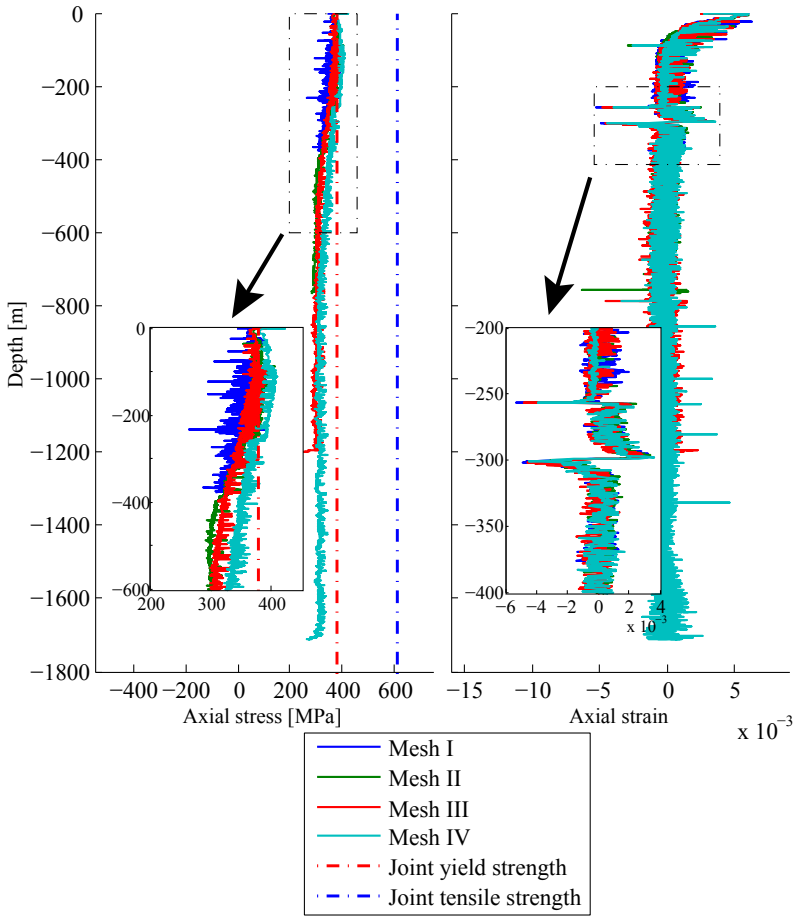

Figure 6.45: *Mesh convergence studies. Results taken after 30 seconds of cooling. The different mesh densities are listed in Table 6.8.*

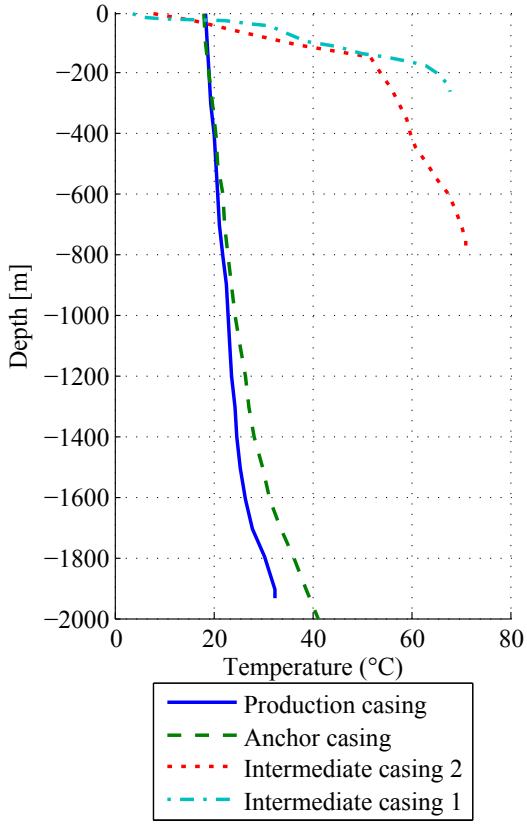

Figure 6.46: *Assumed cementing temperature of the four innermost casings, based on data from Landsvirkjun. This is used as a reference temperature for initial thermal stress calculations in the model.*

Fig. 6.47 shows estimated formation temperature from neighboring well KG-25 located ∼100 m from IDDP-1, used as initial temperature condition of the formation. Wellbore temperature and pressure loads for discharge phase I and V are also shown. The pressure in phase I shows two-phase fluid and for phase V superheated steam is produced.

The temperature distribution in and around the well after 7 months of thermal recovery from drilling is shown in Fig. 6.48. Fig. 6.49 and Fig. 6.50 show the temperature distribution in discharge phase V after 2 days and 11 months of discharge, respectively, and Fig. 6.51 shows the distribution after 8 hours of cooling while killing the well with cold water.

Axial stress and strain distribution down the production casing and anchor casing during discharge phase V and while quenching the well is shown in Figs. 6.52 and 6.53, respectively. During phase V, both casings develop high axial compressive stresses that reach above yield and plastic strains are formed. Near to the surface in the top ∼50 m the stresses are high initially in the production casing, but are relived as the outer casings heat up and expand as well. The material and thickness change from T95 to K55 at 300 m depth in the anchor casing is clearly visible. Stress in the production casing is affected by this material change. Stress concentrations are also seen in the production casing at external casing shoe locations, namely at 87 m, 254 m and 785 m depth. These points are of particular interest and might contribute to casing failures.

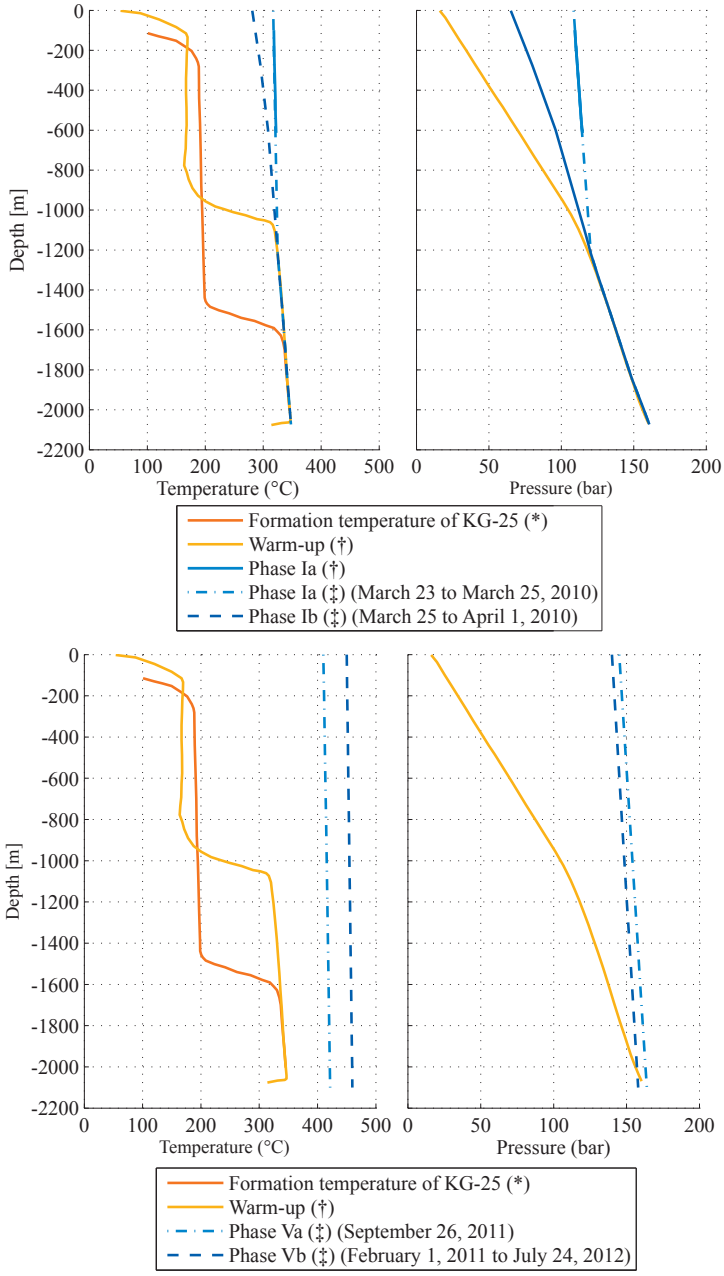

Figure 6.47: *Temperature and pressure loads for the modeling of phase I (top) and phase V (bottom). ∗ Formation temperature of KG-25 (Björnsson et al., 1990), † 8 months warm-up (Axelsson et al., 2014), ‡ Based on monitored well-head temperature and pressure (Ingason et al., 2014).*

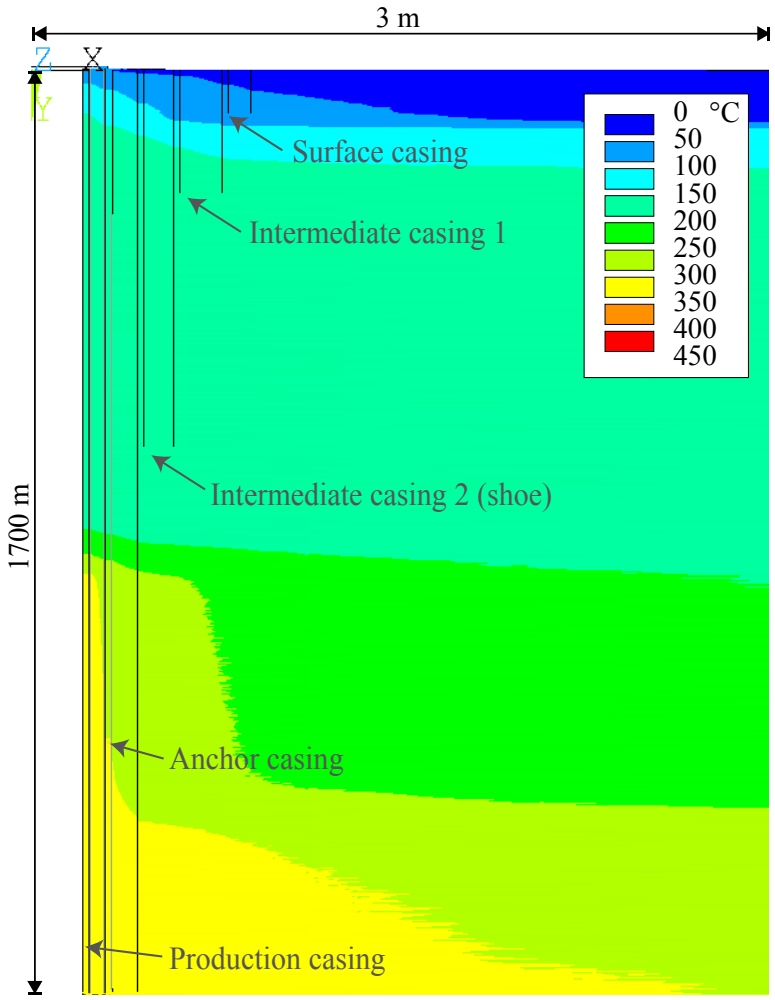

Figure 6.48: *Modeled temperature distribution (°C) of the well after 7 months of warm-up after drilling. The x-axis is scaled by 1000 to 1.*

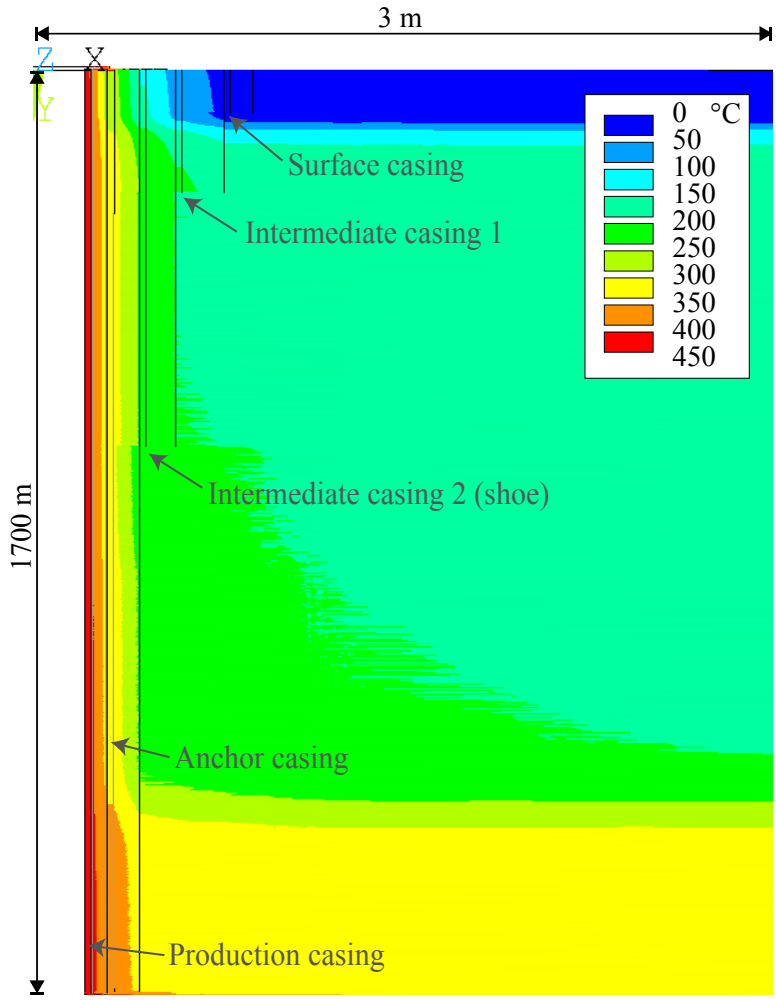

Figure 6.49: *Modeled temperature distribution (°C) of the well after 2 days of discharge in phase V. The x-axis is scaled by 1000 to 1.*

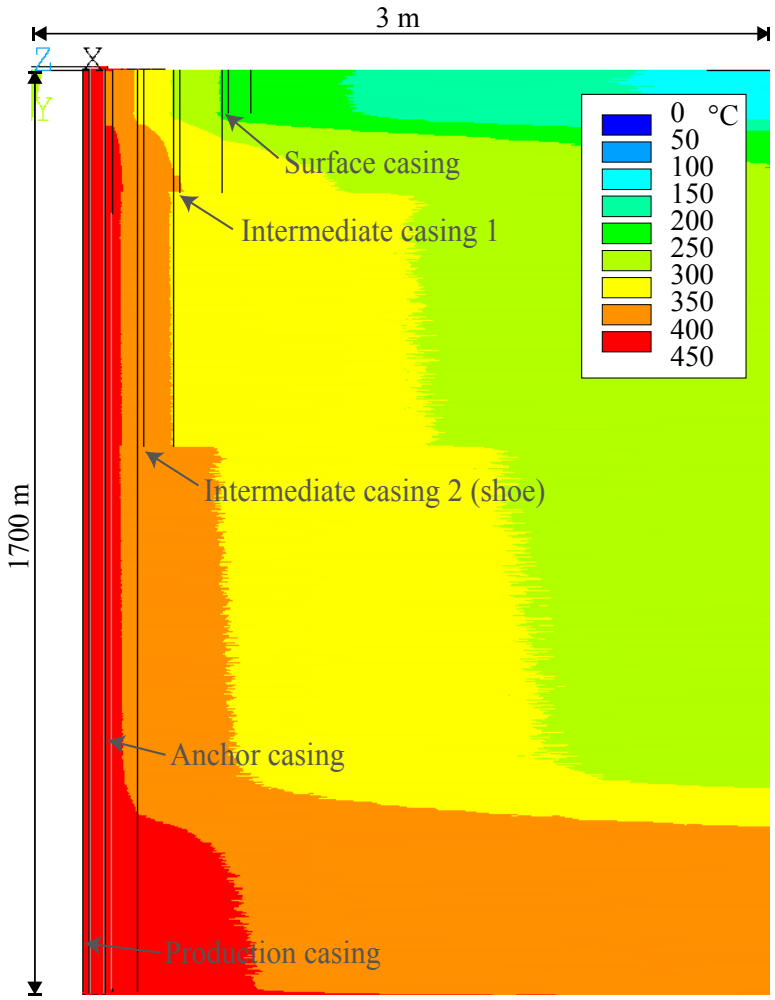

Figure 6.50: *Modeled temperature distribution (°C) of the well after 11 months of discharge in phase V. The x-axis is scaled by 1000 to 1.*

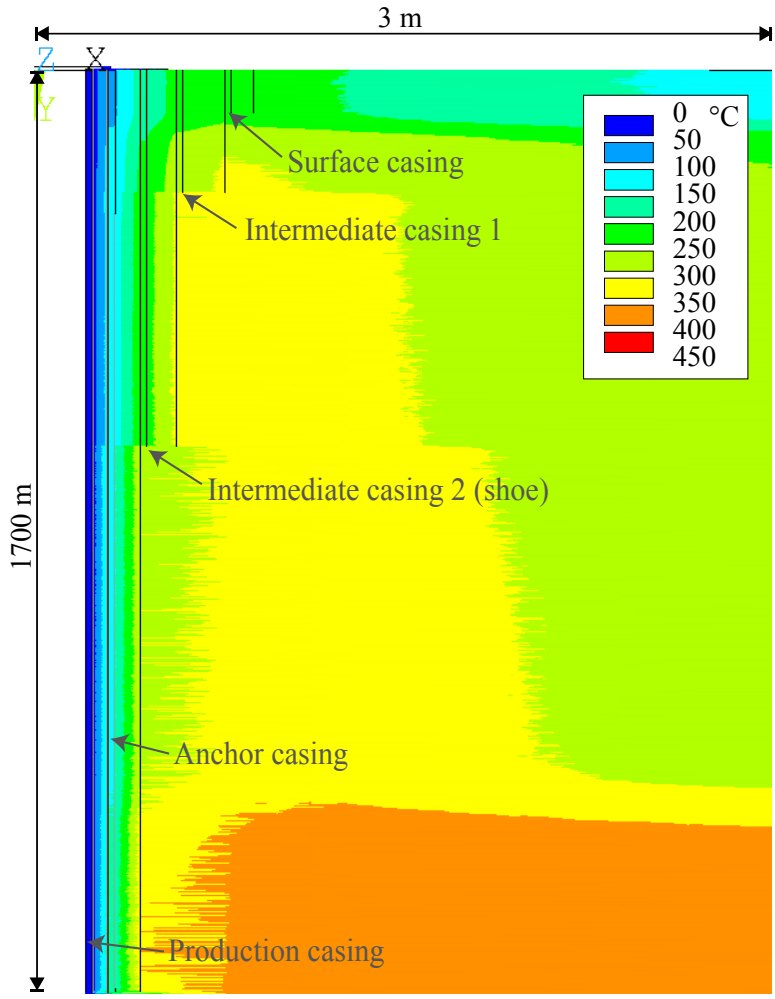

Figure 6.51: *Modeled temperature distribution (°C) of the well after 8 hours of quenching with cold water. The x-axis is scaled by 1000 to 1.*

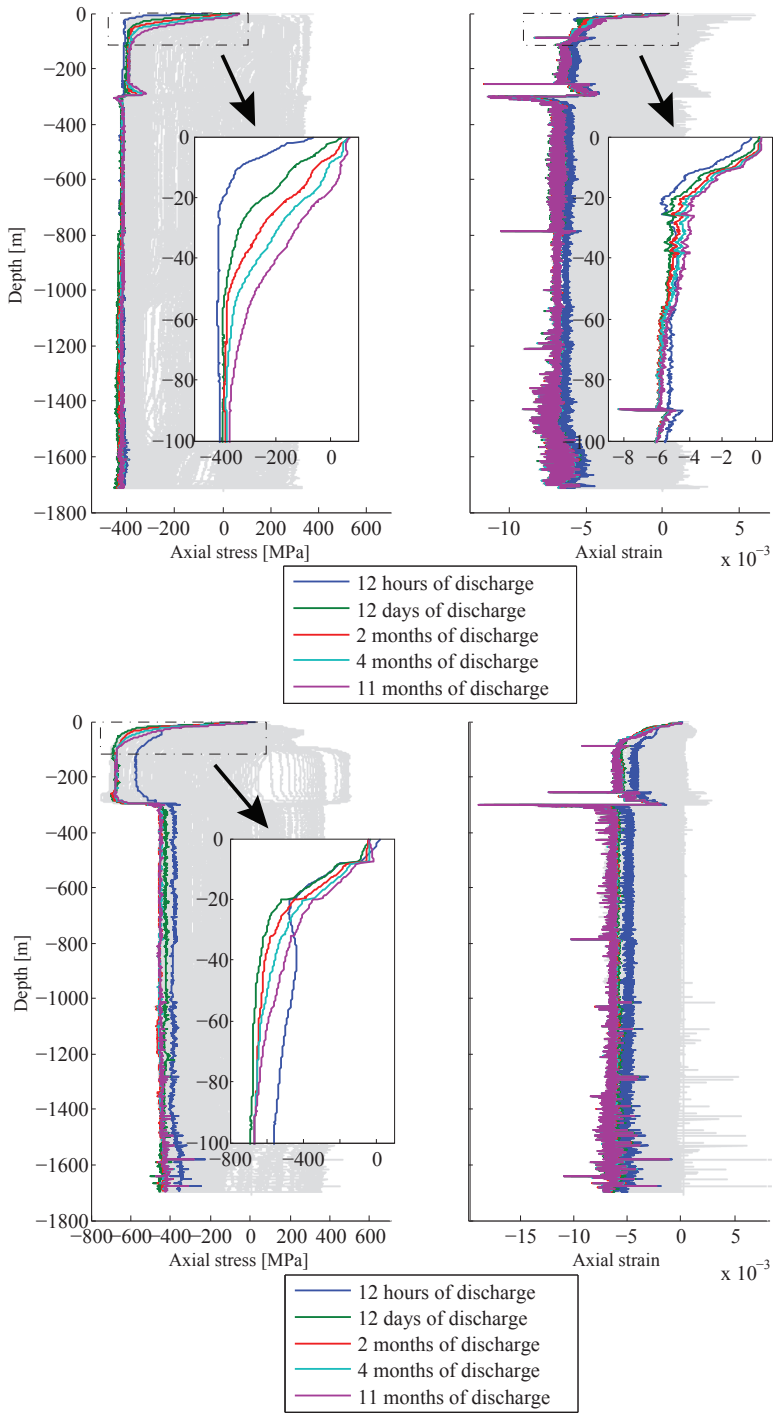

Figure 6.52: *Axial stress and total axial strain of the production casing (top) and anchor casing (bottom) in discharge phase V.*

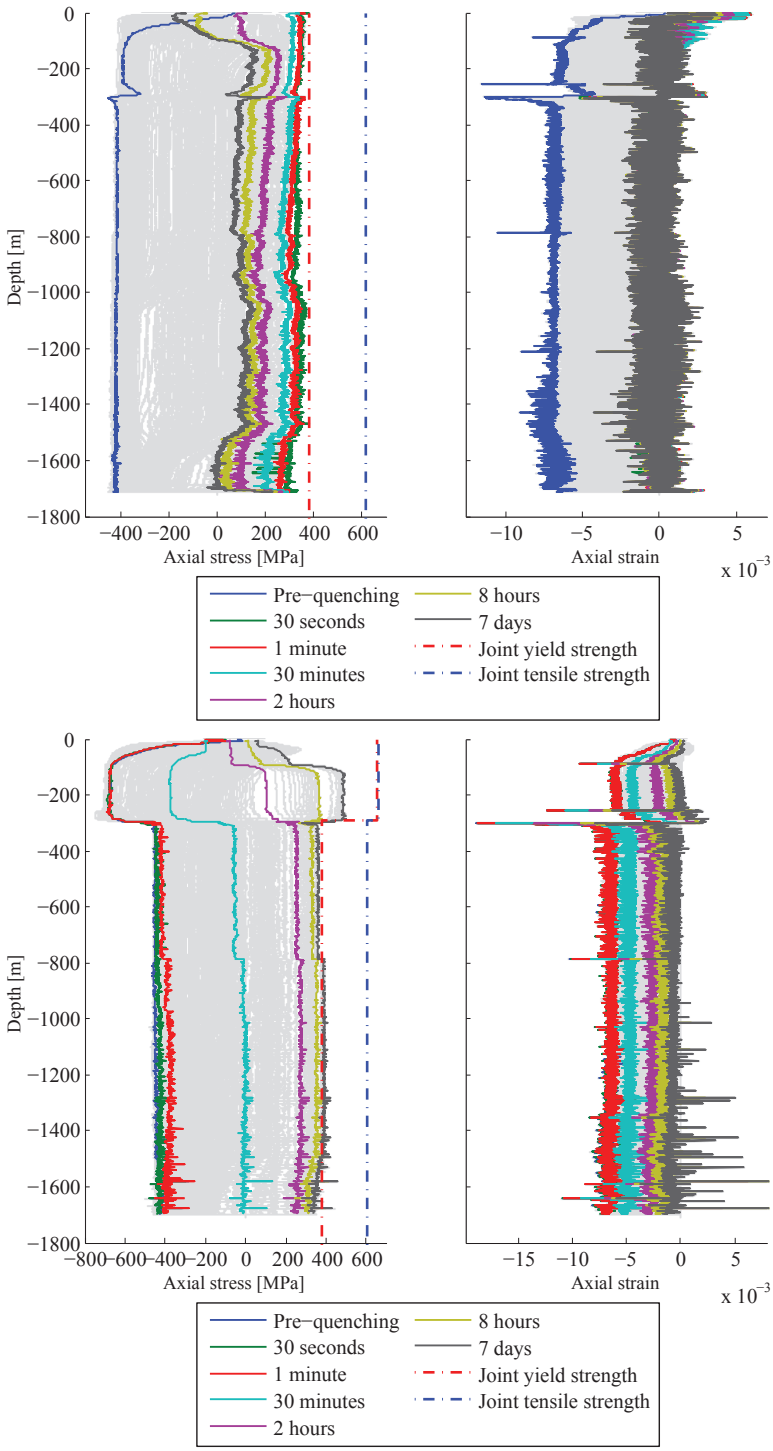

Figure 6.53: *Quenching. Axial stress and total axial strain of the production casing (top) and anchor casing (bottom) during quenching of the well.*

Fig. 6.54 shows the measured and modeled vertical displacement of the wellhead of IDDP-1 from warm-up, through multiple discharge phases and in the end killing of the well with water. The height of the wellhead was measured by Landsvirkjun's personnel at the lower flange of the master valve and the reference point for the measurements was the drilling platform which is grounded approximately 3.0 m outward from the center of the well.

The measured wellhead displacement is not recovered to its initial position during shut-ins, but interestingly the downward displacement during quenching of the well goes below the initial position of the wellhead, suggesting large tensile forces due to thermal contraction of the casings subsequent to being permanently strained in compression. This phenomenon is explained in Fig. 3.6. The modeled wellhead displacement shows similar trend as the measured elevation but does not capture accurately the displacement magnitude where for discharge phase V the final modeled displacement is 345 mm but the measured one is 440 mm.

The evolution of the maximum von Mises strain (total strain) of the production casing and the anchor casing over the operation history of the well is displayed in Fig. 6.55. Cyclic stress and strain results for the production casing at 50 m depth is displayed in Fig. 6.56 to illustrate the buildup of plastic strain in each thermal cycle. This differs depending on location selected in the casing. Following the load history, the first few thermal cycles show no signs of the tensile stress reaching yield, but in the last thermal cycle when the well is quenched, high tensile stress and plastic tensile strain forms. Table 6.9 lists a summary of the structural results.

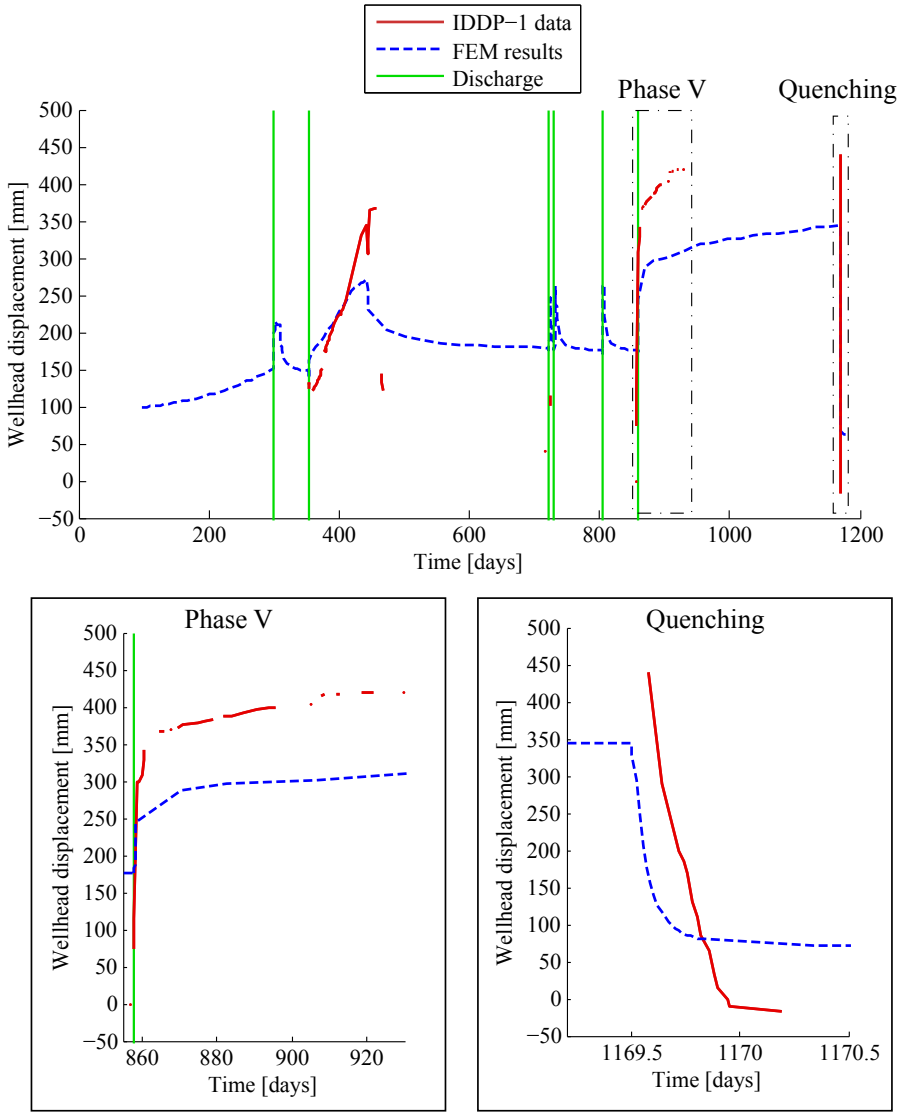

Figure 6.54: *Modeled and measured vertical height of the wellhead of IDDP-1. Wellhead height data is shown by courtesy of Landsvirkjun. The green lines indicate the start of each discharge phase.*

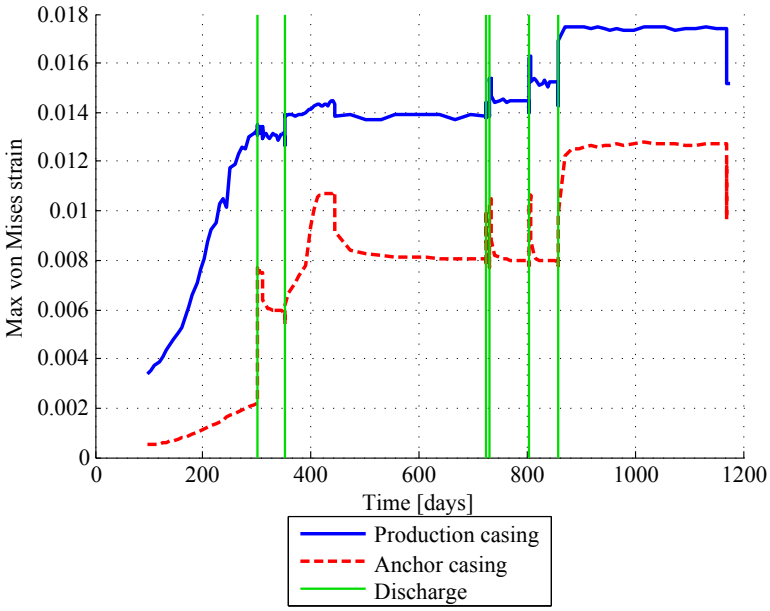

Figure 6.55: *Maximum von Mises strain (total strain) in the two innermost casings through the load history of the well. The green lines indicate the start of each discharge phase.*

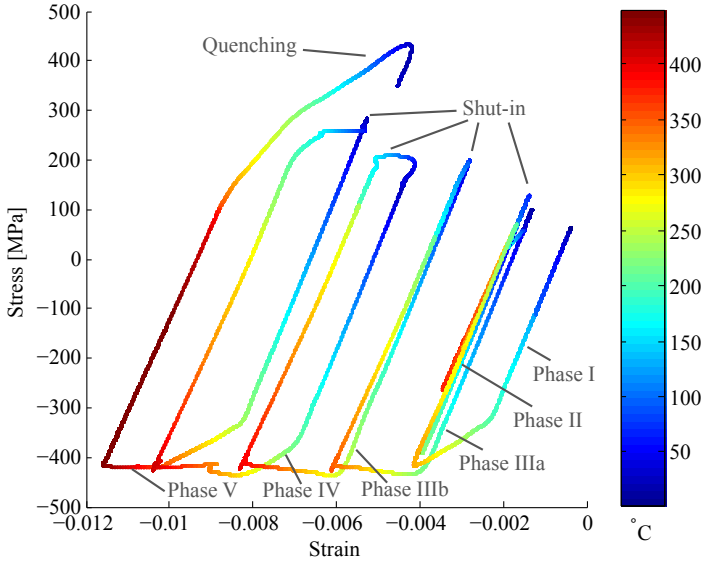

Figure 6.56: *Cyclic stress-strain and temperature of the production casing at 50 m depth. The load history is followed through warm-up and multiple thermal cycles.*

Table 6.9: *Summary of structural results. Maximum wellhead pressure (P_{wh}) and temperature (T_{wh}), maximum displacement of the wellhead (d_{wh}) and maximum von Mises stress and strain results for the production casing and anchor casing during different phases of the load history.*

				Production casing		Anchor casing	
	Max P_{wh} (bar)	Max T_{wh} (°C)	Max d_{wh} (mm) model (data)	Max von Mises stress [MPa]	Max von Mises strain	Max von Mises stress [MPa]	Max von Mises strain
Thermal recovery	0	30	150 (-)	382	0.0133	449	0.0022
Phase I	120	325	216 (368)	378	0.0135	665	0.0078
Phase II	20	380	272 (-)	382	0.0145	660	0.0107
Phase IIIa	105	350	246 (-)	359	0.0144	542	0.0100
Phase IIIb	70	390	262 (-)	374	0.0154	633	0.0105
Phase IV	112	410	265 (-)	403	0.0163	636	0.0106
Phase V	145	450	345 (440)	414	0.0175	627	0.0128
Quenching	0	≈10	63 (-17)	384	0.0156	607	0.0127

7

Discussion

In this study, the focus has been on analyzing structural response of high-temperature geothermal wells to operational loads, i.e. temperature and pressure changes. Quantification on the known number of casing failures occurring in geothermal wells does not exist as such data is in general rare and systematical survey is not practical. This is due to the fact that wells can be in production or shut-in for long periods and such failures are primarily found if restrictions are observed during downhole logging. However, qualification of the types of casing failures can be made from failures that have been recorded. This information indicates that the main casing failures that are found in wells are casing collapses and connection failures (discussed in section 3.5).

Connecting casing failures to specific load cases is thus of great value in order to improve design and operation of high-temperature geothermal wells. Procedures of drilling, running casing, cementing and well operations after completion all affect the structural integrity of the casing. The results from the multiple FEM analyses in this study show that the main factor contributing to the identified casing failures is thermal expansion in materials, both for structural materials as well as in annular fluids. The results also show the importance of the overall construction and geometry of wells, e.g. casing roundness and quality of cementing, for the well integrity.

During this PhD study, the effect of collapse on well integrity was seen in its most critical form, where the collapse of the production casing in the IDDP-1 well is considered to have lead to failures of two external casings, most likely due to high-velocity erosion in the annulus between casings after the production casing collapsed. Quenching the well later lead to multiple tensile connection failures demonstrating that killing wells with cold water should be an absolute last resort in such critical situations.

The findings of this study clearly indicate that cooling of casings that have reached beyond the yield point due to thermal (compressive) straining leads to high tensile stresses that can cause such failures. The temperature limit of non-recoverable compressive straining that subsequently results in failure if the well cools again depends on a number of factors. The main ones are: the yield strength and stress-strain relationship of the particular casing material (at elevated temperatures) and the temperature difference from the cementing setting temperature to the maximum temperature at operation conditions of a particular casing.

Additionally, the FEM analysis results of the load history of the IDDP-1 well using a two-dimensional axisymmetric model indicate that location of casing shoes and casing thickness changes affect how stresses and strains form in neighboring casings. The structural analysis indicate that the proximity to such casing changes could have contributed to failures where a connection failure was found in the production casing of IDDP-1 at the depth where the next outer casing changes both in thickness and material.

The time factor of wellbore temperature changes is also shown to be important. During discharges, the production casing is subjected to an abrupt temperature change while the anchor casing is somewhat protected by the thermal insulation of cement in between, where the warm-up is gradual. However, off-centered casing at various locations could complicate the thermal flow between casings, as one side is less insulated due to less cement and heats up faster than the other, which has greater thermal insulation due to increased cement thickness. The FEM results also illustrate that after 8 hours of quenching, large thermal differences still exist between casings. Therefore, it can be concluded that the stress and strain distribution in each casing is governed by several factors, e.g. cementing temperatures, material properties, thickness changes, locations of casing shoes of adjacent casings, surface friction and change in temperature/pressure distribution down the well with time.

In multiple collapse analyses, the positive effect of uniform cement support around casings is shown, where collapse resistance of cemented casing versus un-cemented casing is considerably higher. The results demonstrate how the collapse resistance is significantly reduced with small perturbations or geometric irregularities, e.g. ovality, defect or trapped annular water pockets or high residual water content in the cement. In all cases, the initial circular geometry of casings is shown to be tremendously important to reduce probability of casing collapse. Various

model setups indicate that couplings are anchored in the cement and between casing connections the constraint of the casing are governed by friction between the steel and cement surfaces.

In the study, various methods have been used to validate the results of the FEM analyses. Parameter uncertainty in the model is quantified by using sensitivity analysis and probabilistic design analysis which both help to understand the model and the structure. By using the method, parameter significance to specific results are revealed. Material properties are chosen according to literature and available data, using actual multilinear stress-strain curves from tensile testing of the steel materials used and design curves of strength reduction at elevated temperatures. However, material properties of cement are approximated with a bi-linear stress-strain curves defining a tangent modulus after its compressive strength is reached, simulating residual strength after occurrence of cement failure. This is necessary in order to achieve convergence while modeling load histories of wells where large displacements are modeled and loads reversed. Push-out test results of cemented casings at ambient temperatures are used as a baseline for frictional characteristics of casing-cement surfaces.

Downhole logging data is crucial to define realistic temperature and pressure loads with depth and time in the model. Similarly, access to continuous temperature and pressure data at the wellhead is important to understand changes with time. Time series data during warm-up in cement on the external surface of the anchor casing is used to validate the thermal model of the cased well. Wellhead temperature, pressure and elevation data is gathered for several wells and used to validate displacements in the model. Lastly, casing failures provide essetnial insights into the structural response to loads.

8

Conclusions

Previous studies have shown the importance of analyzing structural systems of multiple casings, cement and formation with models that involve plasticity, sliding surface contact and transient response to loads. This has been the aim of the PhD study, where several models were developed to understand the structural system. A global model that can solve local problems, e.g. multiple collapses in a production casing, is still not practical as such model would involve hundreds of millions of DOF due to the small diameter to depth ratio of wells. Instead the study was aimed at dividing the problem into smaller ones with the intention of analyzing different load cases using local models (3D collapse models) and global models (2D axisymmetric models).

The objective of the study was to gather information and gain knowledge of how the structure of a high-temperature geothermal well reacts as it goes through various load cases over its lifetime and by that increasing understanding of reasons for casing failures. The tool that was used to achieve this was the nonlinear finite-element method. The models that were developed were used to analyze near well temperature changes as a result of wellbore temperature changes during operation history of wells. This includes, temperature conditions of the formation (initial conditions), cooling from drilling, warm-up after drilling, flow-testing, production, production stops and killing by pumping in water. The structural impact of transient thermal loading was found by analyzing load histories of wells.

The main conclusion that can be taken from the field study are that wellhead displacement is primarily governed by temperature changes rather than by wellhead pressure. The main practical conclusions from the FEM analyses can be summarized as:

- In high-temperature wells, the temperature difference from cementing to production causes permanent plastic strains in the casings, because thermal stresses

reach beyond the yield strength of the constrained casings.

- Large residual tensile stresses are found in the casing if wells are cooled after being subjected to operational temperatures.

- Casings are primarily constrained (anchored) by cement at couplings, and between couplings the constraints are determined by friction between the steel and cement surfaces.

- The probability of casing collapse can be lowered significantly by selecting casings with proper circular geometry for the production casing, that has less collapse resistance if the casing is initially oval or eccentric.

- Proper lateral and radial support of cement greatly improves resistance of casings against collapse.

9

Further work

The feasibility of utilizing high enthalpy fluids from deep geothermal sources where temperatures and pressures are higher than seen in conventional high-temperature wells is a questions that could in part be answered by FEM analysis. The focus of this study has been to understand current design of high-temperature geothermal wells, but it is clear that further studies are needed in order to advance the evolution and development of geothermal or other thermal application well designs.

The FEM results demonstrate that time of warm-up of casings from the cooled conditions during drilling to operation temperatures plays an integral role in stress and strain development in layered steel casings and cement sheaths. Developing methods for controlled warm-up of wells where the cased portion of the well is allowed to warm-up to near production temperatures over a period of weeks or even months could reduce probability of casing failure occurring over the lifetime of the well. Engineering such method is not trivial since individual wells are different depending on reservoir conditions. The uppermost multi-cased section of wells can be difficult to warm-up slowly from the source deeper in the well. A possibility of initial warm-up of newly drilled wells from other heat sources, e.g. from another well or by separation water, followed by slow bleeding at the wellhead could reduce the effect of thermal expansion on the structure.

The core design of high-temperature geothermal wells has not changed much in the past three decades. New ideas for increased structural integrity are needed as it seems that a design limit has been reached, due to structural strength limitations at elevated temperatures, thermal expansion and material limitations due to harsh geothermal environments. Research and development for new emerging technologies and material selection for casings and cement are needed to push

this unclear boundary further. FEM analysis still provides a powerful tool for further research and development in this field.

A number of new studies and international collaboration projects touch the subject, including: Europe Union's Horizon 2020 projects GeoWell, DEEPEGS and Descramble. Objectives include introducing new technology for high-enthalpy wells, improving material selection and cement formulations of casings and cement for geothermal operations. The results from this study have already been implemented in development of flexible couplings, a patented solution that is designed to mitigate thermal straining by allowing displacements of casing segments and have been developed at ÍSOR (Iceland GeoSurvey) from year 2015 within projects GeoWell and DEEPEGS (Kaldal and Thorbjornsson, 2016; Thorbjornsson et al., 2017). The new technology could allow high-enthalpy wells to be utilized with increased change of success by reducing thermal strains in the casing.

Bibliography

Agustsson, K., Flovenz, O., 2005. The thickness of the seismogenic crust in iceland and its implications for geothermal systems. Proceedings World Geothermal Congress 2005 .

Allan, M., Philippacopoulos, A., 1998. Literature survey on cements for remediation of deformed casing in geothermal wells. Department of Applied Science, Brookhaven National Laboratory .

Ansys, Inc., 2012. Release 14.5 documentation for ANSYS.

ASM, 1992a. ASM Handbook: Volume 1: Properties and Selection: Irons Steels and High Performance Alloys. American Society for Metals.

ASM, 1992b. ASM Handbook: Volume 18: Friction, Lubrication, and Wear Technology. American Society for Metals.

Assanelli, A.P., Toscano, R.G., Dvorkin, E.N., 1998. Analysis of the collapse of steel tubes under external pressure.

Axelsson, G., Egilson, T., Gylfadóttir, S.S., 2014. Modelling of temperature conditions near the bottom of well iddp-1 in krafla, northeast iceland. Geothermics 49, 49 – 57.

Axelsson, G., Thórhallsson, S., Björnsson, G., 2006. Stimulation of geothermal wells in basaltic rock in Iceland. ENGINE - ENhanced Geothermal Innovative Network for Europe, Workshop 3, "Stimulation of reservoir and microseismicity" .

Bathe, K.J., 1996. Finite Element Procedures. Prentice-Hall.

Berger, A., Fleckenstein, W.W., Eustes, A.W., Thonhauser, G., 2004. Effect of eccentricity, cement channels, and pore pressure decline on collapse resistance of casing. SPE Annual Technical Conference and Exhibition, Houston, Texas, U.S.A., 26-29 September 2004 .

Bertani, R., 2015. Geothermal power generation in the world 2010-2014 update report. Proceedings World Geothermal Congress 2015 .

Birkisson, S.F., Hole, H., 2007. Aerated fluids for drilling of geothermal wells. Proceedings European Geothermal Congress .

Björnsson, G., Ragnars, K., Sigfússon, S., Þorbjörn Karlsson, 1978. Styrkleiki fóðurröra í háhitaborholum (Translation: Casing Strength in High Temperature Wells). Orkustofnun, Virkir hf. and VST HF. In Icelandic.

Björnsson, G., Steingrímsson, B., Ásgrímur Guðmundsson, 1990. Krafla - Hola KG-25 - Upphitun og upphafsástand (in Icelandic). Technical Report OS90052/JHD-30 B. Orkustofnun (National Energy Authority.

Bulson, P.S., 1982. The Stability of Underground Cylindrical Shells. volume 1. Applied Science Publishers, Ripple Road, Barking, Essex, England.

Böðvarsson, G., 1961. Physical characteristics of natural heat resources in iceland. Jökull 11, 29–38.

Chiotis, E., Vrellis, G., 1995. Analysis of casing failures of deep geothermal wells in Greece. Geothermics 24, 695–705.

Dall'Acqua, D., Hodder, M., Kaiser, T.M.V., 2012. Burst and collaspse responses of production casing in thermal applications. IADC/SPE Drilling Conference and Exhibition held in San Diego, California, USA, 6-8 March 2012 .

Dvorkin, E.N., Toscano, R.G., 2003. Finite element models in the steel industry: Part ii: Analyses of tubular products performance. Computers and Structures 81, 575 – 594. K.J Bathe 60th Anniversary Issue.

Elders, W.A., Fridleifsson, G.., Bignall, G., 2012. Saga report no 9. IDDP-ICDP Workshop .

Fairbairn, W., 1858. On the resistance of tubes to collapse. Journal of the Franklin Institute 66, 145 – 151.

Ferla, A., Lavrov, A., Fjær, E., 2009. Finite-element analysis of thermal-induced stresses around a cased injection well. Journal of Physics: Conference Series 181, 012051.

Friðleifsson, G., Sigurdsson, ., Þorbjörnsson, D., Karlsdóttir, R., Gíslason, ., Albertsson, A., Elders, W., 2014. Preparation for drilling well IDDP-2 at Reykjanes. Geothermics 49, 119 – 126.

Gretarsdottir, S., 2007. Mechanical and thermal properties of well cement. Master's thesis. University of Iceland.

Hauksson, T., Markusson, S., Einarsson, K., Karlsdóttir, S.N., Ásbjörn Einarsson, Möller, A., Þorsteinn Sigmarsson, 2014. Pilot testing of handling the fluids from the iddp-1 exploratory geothermal well, krafla, n.e. iceland. Geothermics 49, 76 – 82.

Hernandez, R., Bour, D., 2010. Reverse-circulation method and durable cements provide effective well construction: A proven technology. Proceedings Stanford Geothermal Workshop .

Hidayat, M.I.P., Irawan, S., Abdullah, M.Z., 2016. Casing strength degradation in thermal environment of steam injection wells. Journal of Physics: Conference Series 710, 012017.

Hilbert, L.B., Kalil, I.A., 1992. Evaluation of premium threaded connections using finite-element analysis and full-scale testing. SPE/IADC Drilling Conference, 18-21 February, New Orleans, Louisiana .

Hólmgeirsson, S., Ásgrímur Guðmundsson, Pálsson, B., Árni Bóasson, H., Ingason, K., Þórhallsson, S., 2010. Drilling operations of the first iceland deep drilling well (iddp). Proceedings World Geothermal Congress 2010, Bali, Indonesia, 25-29 April 2010 .

Hole, H., 2008. Geothermal well cementing. Petroleum Engineering Summer School Workshop 26.

Ingason, K., Arnason, A., Boasson, H.A., Sverrisson, H., Sigurjonsson, K., Gislason, T., 2015. Iddp-2, well design. Proceedings World Geothermal Congress 2015 .

Ingason, K., Kristjánsson, V., Einarsson, K., 2014. Design and development of the discharge system of IDDP-1. Geothermics 49, 58 – 65.

ISO/PAS 12835:2013, 2013. ISO/PAS 12835:2013 Qualification of casing connections for thermal wells. ISO (The International Organization for Standardization), CH-1211 Geneva 20.

ISO/TR 10400:2007(E), 2007. ISO/TR 10400:2007(E) Petroleum and natural gas industries - Equations and calculations for the properties of casing, tubing, drill pipe and line pipe used as casing or tubing. ISO (The International Organization for Standardization), CH-1211 Geneva 20.

Johnson, F.W., 1984. Microcomputer finite-element analysis of tubular connections. SPE Annual Technical Conference and Exhibition, 16-19 September, Houston, Texas .

Kaldal, G.S., Thorbjornsson, I., 2016. Thermal expansion of casings in geothermal wells and possible mitigation of resultant axial strain. European Geothermal Congress, Strasbourg, France, 19-24 Sept 2016 .

Kalil, I.A., McSpadden, A.R., 2011. Casing burst stresses in particulate-filled annuli: Where is the cement? SPE .

Karlsdottir, S., Ragnarsdottir, K., Thorbjornsson, I., Einarsson, A., 2015. Corrosion testing in superheated geothermal steam in iceland. Geothermics 53, 281 – 290.

Karlsdottir, S.N., 2013. Corrosion Testing Down-Hole in Sour High Temperature Geothermal Well in Iceland, in: NACE International Corrosion Conference & Expo 2013, pp. paper 51313–02550–SG.

Karlsdottir, S.N., Thorbjornsson, I.O., 2009. High Temperature Geothermal Wells - Center of Excellence in Iceland - Phase I: Corrosion Testing of Steel in High Temperature Geothermal Wells in Iceland. Technical Report for RANNIS (The Icelandic Centre for Research), in Icelandic.

Karlsdottir, S.N., Thorbjornsson, I.O., 2012. Hydrogen Embrittlement and Corrosion in High Temperature Geothermal Well, in: NACE International Corrosion Conference & Expo.

Landsvirkjun, 2016. Landsvirkjun annual report 2016 .

d. Leaver, J., 1982. Failure mode analysis for casing and liners in geothermal production wells. GProceedings of The New Zealand Geothermal Workshop 4, 217–221.

Lund, J.W., Boyd, T.L., 2015. Direct utilization of geothermal energy 2015 worldwide review. Proceedings World Geothermal Congress 2015 .

Magneschi, P., Bagnoli, C., Lazzarotto, A., Ricciardulli, R., 1995. Structural models for the analysis of stresses in the casings of geothermal wells , 1421–1426.

Magnusdottir, L., 2009. Nonlinear Finite Element Model of a Geothermal Well. Master's thesis. University of Iceland.

Maharaj, G., 1996. Thermal well casing failure analysis. SPE Latin America/Caribbean Petroleum Engineering Conference, Port-of-Spain, Trinidad and Tobago, 23-26 April 1996 .

Maruyama, K., Tsuru, E., Ogasawara, M., Inoue, Y., Peters, E.J., 1990. An experimental study of casing performance under thermal cycling conditions. SPE Drilling Engineering 5, 156–164.

Mortensen, A.K., Guðmundsson, ., Steingrímsson, B., Sigmundsson, F., Axelsson, G., Ármannsson, H., Björnsson, H., Ágústsson, K., Sæmundsson, K., Ólafsson, M., Karlsdóttir, R., Halldórsdóttir, S., 2009. Jarðhitakerfið í Kröflu. ÍSOR/Landsvirkjun, Reykjavik, Iceland.

Netto, T., 2009. On the effect of narrow and long corrosion defects on the collapse pressure of pipelines. Applied Ocean Research 31, 75 – 81.

Norsok D-010, 2004. Norsok D-010, Well integrity in drilling and well operations, Rev. 3. Standards Norway, Strandveien 18, P.O. Box 242, N-1326 Lysaker, Norway.

Norsok M-001, 2002. Norsok M-001, Materials selection, Rev. 3. Standards Norway, Strandveien 18, P.O. Box 242, N-1326 Lysaker, Norway.

Nowinka, J., Dall'Acqua, D., 2011. New standard for evaluating casing connections for thermal-well applications. SPE Drilling and Completion 26, 419–431.

NZS 2403:2015, 2015. NZS 2403:2015 Code of practice for deep geothermal wells. Standards New Zealand, Private Bag 2439, Wellington 6140.

Orkustofnun, 2014. Energy Statistics in Iceland 2014. The National Energy Authority of Iceland (Orkustofnun), Grensásvegi 9, 108 Reykjavík.

Palmason, G., 1980. Jarðhitinn sem orkulind (in Icelandic). volume 50. Reykjavik, Iceland.

Palmason, G., 2005. Jarðhitabók (in Icelandic). ISOR, Iceland GeoSurvey, Grensasvegi 9, 108 Reykjavik, Iceland.

Pattillo, P.D., Last, N.C., Asbill, W.T., 2004. Effect of nonuniform loading on conventional casing collapse resistance. SPE Drilling and Completion 19.

Phan, L.T., Carino, N.J., 2000. Fire performance of high strength concrete: Research needs. Proceedings of ASCE/SEI Structures Congress 2000, Philadelphia, USA .

Philippacopoulos, A., Berndt, M., 2000. Characterization and modeling of cements for geothermal well casing remediation. San Francisco, California: Geothermal Resources Council, 2000. .

Philippacopoulos, A.J., Berndt, M.L., 2002. Structural analysis of geothermal well cements. Geothermics 31, 657 – 676.

Pálsson, B., Hólmgeirsson, S., Guðmundsson, A., Bóasson, H., Ingason, K., Sverrisson, H., Thórhallsson, S., 2014. Drilling of the well IDDP-1. Geothermics 49, 23 – 30.

Ragnarsson, A., 2003. Utilization of Geothermal Energy in Iceland. International Geothermal Conference, Reykjavik, Iceland , 39–45.

Ragnarsson, A., 2015. Geothermal development in iceland 2010-2014. Proceedings World Geothermal Congress 2015 .

Rahman, S.S., Chilingarian, G.V., 1995. Casing design, theory and practice. Elsevier Science B. V., P.O. Box 211, 1000 AE Amsterdam, The Netherlands.

Rechard, R.P., Schuler, K.W., 1983. Euler Buckling of Geothermal Well Casing .

Reinsch, T., 2012. Structural integrity monitoring in a hot geothermal well using fibre optic distributed temperature sensing.

Sakakibara, N., Kyriakides, S., Corona, E., 2008. Collapse of partially corroded or worn pipe under external pressure. International Journal of Mechanical Sciences 50, 1586 – 1597.

Schwind, B.E., Payne, M.L., Otten, G.K., Pattillo, P.D., 2001. Development of leak resistance in industry standard octg connections using finite element analysis and full scale testing. Offshore Technology Conference (OTC), Houston, Texas, 30 April-3 May 2001 .

da Silva, F.V., Debande, G.G., Pereira, C.A., Plischke, B., 1990. Casing collapse analysis associated with reservoir compaction and overburden subsidence. European Petroleum Conference, 21-24 October, The Hague, Netherlands .

Snyder, R.E., 1979. Casing Failure Modes in Geothermal Wells. Geothermal Resources Council , 667–670.

Southon, J.N.A., 2005. Geothermal well design, construction and failures. Proceedings World Geothermal Congress .

Steingrimsson, B., 2013. Geothermal well logging, temperature and pressure logs, in: Presented at "Short Course V on Conceptual Modelling of Geothermal Systems", organized by UNU-GTP and LaGeo, in Santa Tecla, El Salvador, February 24 - March 2, 2013., UNU-GTP and LaGeo.

Sveinbjornsson, B.M., Thorhallsson, S., 2014. Drilling performance, injectivity and productivity of geothermal wells. Geothermics 50, 76 – 84.

Teodoriu, C., 2015. Why and when does casing fail in geothermal wells: a surprising question? Proceedings World Geothermal Congress 2015 .

Teodoriu, C., Falcone, G., 2009. Comparing completion design in hydrocarbon and geothermal wells: The need to evaluate the integrity of casing connections subject to thermal stresses. Geothermics 38, 238 – 246.

Thorbjornsson, I., Kaldal, G.S., Gunnarsson, B.S., Árni Ragnarsson, 2017. A new approach to mitigate casing failures in high-temperature geothermal wells. GRC Transactions, Vol. 41, 2017 .

Thorbjornsson, I.O., Karlsdottir, S.N., Einarsson, Á., Ragnarsdottir, K.R., 2015. Materials for Geothermal Steam Utilization at Higher Temperatures and Pressure, in: World Geothermal Congress 2015, Melbourne. p. 7.

Thorhallson, S., 2016. Viðhald á borholum - nokkur dæmi. Vorfundur Jarðhitafélags Íslands .

Thorhallsson, S., 2008. Geothermal drilling and well pumps, in: Workshop for Decision Makers on Direct Heating Use of Geothermal Resources, UNU-GTB, TBLRREM and TBGMED, Tianjin, China.

Thorhallsson, S., Palsson, B., Holmgeirsson, S., Ingason, K., Matthiasson, M., Boasson, H.A., Sverrisson, H., 2010. Well design and drilling plans of the Iceland Deep Drilling Project (IDDP), in: Proceedings World Geothermal Congress 2010, Bali, Indonesia, 25-29 April 2010, WGC 2010.

Thórhallsson, S., Pálsson, B., Hólmgeirsson, S., Ingason, K., Matthíasson, M., Bóasson, H., Sverrisson, H., 2014. Well design for the Iceland Deep Drilling Project (IDDP). Geothermics 49, 16 – 22.

Torres, A., 2014. Challenges of casing design in geothermal wells. IADC/SPE Asia Pacific Drilling Technology Conference, 25-27 August, Bangkok, Thailand .

Vogel, J.V., 1966. Thermal Oil Recovery. United States Patent Office.

W. J. Rodriguez, W. W. Fleckenstein, A.W.E., 2003. Simulation of collapse loads on cemented casing using finite element analysis. SPE Annual Technical Conference and Exhibition, 5-8 October, Denver, Colorado .

Wallevik, S.., Hjartarson, B., Alexandersson, K.F., Kubens, S., Oesterheld, S., Ólafur H. Wallevik, Ásgeirsdóttir, M.D., 2009. High Temperature Geothermal Wells - Center of Excellence in Iceland - Final report: Concrete Suited for High Temperature Geothermal Wells. Technical Report for RANNIS (The Icelandic Centre for Research), in Icelandic.

Watkins, R., Anderson, L., 1999. Structural Mechanics of Buried Pipes. Taylor & Francis.

Wu, J., Knauss, M.E., Kritzler, T., 2008. Casing failures in cyclic steam injection wells. IADC/SPE Asia Pacific Drilling Technology Conference, Jakarta, Indonesia, 25-27 August 2008 .

Yuan, Z., Schubert, J., Teodoriu, C., Gardoni, P., 2012. HPHT gas well cementing complications and its effect on casing collapse resistance. SPE Oil and Gas India Conference and Exhibition held in Mumbai, India, 28-30 March 2012 .

Paper I

PROCEEDINGS, Thirty-Sixth Workshop on Geothermal Reservoir Engineering
Stanford University, Stanford, California, January 31 - February 2, 2011
SGP-TR-191

LOAD HISTORY AND BUCKLING OF THE PRODUCTION CASING IN A HIGH TEMPERATURE GEOTHERMAL WELL

Gunnar Skúlason Kaldal[1]*, Magnús Þ. Jónsson[1], Halldór Pálsson[1], Sigrún N. Karlsdóttir[2], Ingólfur Ö. Þorbjörnsson[2,3]

[1]Faculty of Industrial Engineering, Mechanical Engineering and Computer Science, University of Iceland, Hjarðarhagi 2-6, Reykjavik, 107, Iceland
[2] Innovation Center Iceland, Department of Materials, Biotechnology and Energy, Keldnaholt, Reykjavik, 112, Iceland
[3]Reykjavik University, Menntavegur 1, Reykjavik, 101, Iceland
*e-mail: gunnarsk@hi.is

ABSTRACT

The production casing of a high temperature geothermal well is subjected to multiple thermo-mechanical loads in the period from installation to production. Temperature and pressure fluctuations are large in high temperature geothermal wells, for example during the first discharge the temperature difference from a non-flowing to a flowing well can be on the range of hundreds of degrees centigrade. During installation, stimulation and production, problems can arise due to these loads and due to a possible corrosive geothermal environment. Plastic buckling of the production casing is a problem that can occur. It results in a bulge in the wall of the casing and is detrimental to the geothermal energy production and the lifetime of the well. The cost of each well is very high. Therefore, it is important to analyze the structural environment of high temperature geothermal wells in effort to avoid repeated problems in the design and installment phases of the casing.
A finite-element model has been developed to evaluate the temperature distribution, deformation and stresses in a high temperature geothermal well and to evaluate the reasons for buckling in the production casing. The load history of the casing is followed from the beginning of the installment phase to the production phase.
The results show that the load history and also the sequence of loading is important in order to understand the true structural behavior of wells.

INTRODUCTION

Geothermal wells consist of several concentric steel casings and concrete sealant that is in contact with the surrounding rock formation. Plastic buckling of the production casing is a problem that can occur. The innermost casing, the production casing, buckles and forms a bulge on the inside of the casing wall. This deformation of the casing can lead to reduced energy output and in worst cases render the well inoperative.
A number of interesting cases of casing impairments have occurred in Iceland. There exist however some difficulties in tracking the history of the wells. For example the load history of wells is not always fully known, as down hole P-T measurements are often sparse and cannot be performed constantly. Icelandic well drilling, operation and completion reports, from the National Energy Authority and Iceland Geosurvey, were used to gather information and data on the load history and well completion processes.
Casing failure as a result of trapped fluid in the casing to casing annulus have been discussed as a suspected cause of casing collapse by for example Björnsson (1978), Magneschi (1995) and Southon (2005). Southon lists casing failure modes in geothermal wells and discusses the importance of ensuring that construction and design techniques are sound and carefully implemented. He also discusses that pre-tension loads need to be determined to avoid compression yielding when using buttress threaded couplings. Euler buckling and helical buckling are addressed by Leaver (1982) where analyses are performed and equations developed for buckling of an uncemented length of casing. Euler buckling is also addressed by Rechard and Schuler (1983) where buckling models are produced.
Chiotis and Vrellis (1995) list casing failures observed in Greek wells where wellhead movement, casing joint decoupling, buckling of a 9 5/8 in casing in 6 different places, tieback casing collapse and serious wellhead leakages associated with casing corrosion are discussed. They conclude that the major casing failures observed are caused by thermal stress

and that burst and collapse strengths are severely reduced by axial thermal stress.
Kane (1996) evaluates corrosion problems involving in-service failures of geothermal well production casings where high thermally induced tensile stress in combination with the presence of hydrogen sulfide results in sulfide stress cracking.
Few finite-element models of wells have been created. A 2D finite element model of the cross section of a double cased geothermal well was created for representing the behavior of the cement/sealant by Philippacopoulos and Berndt (2002) where the results showed the inadequacy of geothermal well design based solely on compressive strength. A plane strain finite element model for well failure due to formation movement and a three dimensional model to analyse the local behavior of the casing-cement-formation interaction in geothermal wells were developed also by Philippacopoulos and Berndt (2000) where the part of the results revealed the importance of the cement properties on the response of the casing patch cement included in the three dimensional model.
Peng, Fu and Zhang (2007) created a finite-element model to represent oil-field casing failure in unconsolidated formations where the results showed non-uniform and multi-directional casing deformation.
The buckling/bulging of the wall of the casing is presumably a local phenomenon, although the whole well should be considered since forces are transmitted throughout its whole length. A finite-element model has been developed where a section of a high temperature geothermal well is modeled. Boundary conditions are defined to represent the considered outer interaction. The well section is 24 m long and includes three casings, the production casing, the security casing and the outermost surface casing, as well as concrete and the rock formation. Two simplified couplings are included in the production casing in order to observe the effect of increased stress in the concrete near the couplings as well as the inverse effect on the casing.
The objective of the analysis is to evaluate the highest risk of production casing wall buckling/bulging with the use of the model.
The load history of the casing is tracked from the beginning of the installation of the casing, where the casing is hanging from the top of the well, to the production phase, where the casing has been subjected to high temperature change (possibly cyclic) due to operation on site and stimulation procedures. Tracking the load history is important because the casing can be damaged at various steps, such as in the installment phase, the stimulation process, warming-up periods, discharging of the well and even in the production phase. In addition stress builds up in the casing and plastic deformation occurs, constantly increasing the risk of instability and casing impairment.
In this article, the focus is on wall buckling and collapse of the production casing. Production casing impairment modes and load history are discussed. A finite-element model and a case study is represented and discussed. Finally the results from the model are presented and discussed.

PRODUCTION CASING IMPAIRMENT

Casing failure modes can be classified into (a) buckling failures, (b) coupling failures, (c) tear failures and (d) corrosion failures. Casing failure modes and possible load cases are listed in Table 1.
Indications of casing failures are often in limited numbers and casing failure can go unnoticed for a long period, if noticed at all. Casing failures can cause a serious hazard of leakage and blow out risk. For instance in one known example from the 70s, the production casing of a well in northern Iceland was in poor shape due to a highly corrosive environment, eventually causing an immense explosion, leaving a crater where the wellhead once stood (Pálmason 2005). Large wellhead movement and buckling/bulging of the casing suggests compressive forces in the casing due to thermal expansion, whereas body tear and coupling rupture indicate tensional forces that form during casing installment and when the completed well is cooled.

Table 1: Casing failure modes and possible load.

Casing failure mode		**Load**
(a) Buckling	Euler buckling	$+\Delta T$, axial compression
	Wall buckling	$+\Delta T$, ΔP, flow problem
(b) Coupling	Tensional tear	$-\Delta T$, gravity
	Compression thread slip	$+\Delta T$, axial compression
(c) Tear	Casing body	$-\Delta T$, gravity

After the casing string has been cemented, Euler buckling can occur, where the casing acts as a column, if there is a large enough un-cemented gap in the surrounding annulus allowing a large deflection (Rechard 1983). This can occur if the casing is subjected to compressive axial force for instance during temperature increase.
Buckling of the casing wall, where a bulge forms on one side, is a different scenario from Euler buckling. The absolute reason for the bulge deformation is unclear, but possible cause is a combination of various loads and imperfections. Possible imperfections could be a reduced casing wall thickness and the existence of enclosed water or un-cemented gap in the casing to casing annulus due to a

faulty cementing job. Complete collapse of the casing can occur if the pressure difference between the outer and inner wall exceeds the collapse resistance of the casing, for example during cementing.
High axial tension forces, for instance when negative temperature change occurs, can lead to coupling failures and in some instances casing body tear. When the casing depth is large and imperfections are present, the weight of an uncemented casing can cause a casing body tear or coupling failure in worst case scenario. Axial compression, for example due to increase in temperature, can cause a thread slip in the coupling area.
Corrosion can cause serious production casing failures. It can be very different between geothermal regions and even different within a geothermal region, for example from well to well or varying with depth. For H_2S rich environments sulfide stress cracking (SSC) and hydrogen embrittlement can cause problems depending on the material selection for the steel casing (Kane 1996). Other forms of corrosion, for example uniform corrosion, erosion, and cavitation can exist in geothermal wells. No general solution for corrosion in geothermal wells exists and each case should be treated separately.

PRODUCTION CASING LOAD HISTORY

Here the load history of the production casing is tracked from the installment phase to the production phase. The possible load cases considered occur at various phases, i.e. the (i) installation of the production casing, (ii) stimulation of the well, (iii) discharge of the well, and (iv) production.

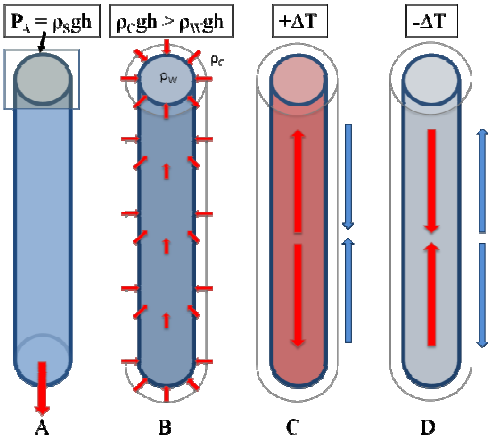

Figure 1: Production casing loads.

(i) Installation of the production casing

The discussed load cases are summarized in Table 2. During the installation of the production casing, casing components are screwed together and lowered down into the well one by one. The first load on the casing, load case 1, is tensional force due to gravity, see diagram A in Figure 1. The tension increases with increased depth, putting the highest strain on the last installed casing component that supports the whole casing before the concrete sets. While the casing is being installed, the well is kept full of cold water, which provides a buoyant force.

Table 2: Considered load cases.

Load case	*Description*	*Load*
(i) Installation of the production casing		
1	Casing hanging from the top of the well.	Gravity.
2	Cement slurry in place.	Outer pressure from cement slurry + pumping pressure.
3	Concrete setting.	Temperature increase due to heat of hydration and well surroundings.
4	Production section of the well drilled with cooling fluid.	Temperature decrease due to cooling fluid.
(ii) Stimulation of the well		
5a-i	Warm-up period.	Temperature increases.
5a-ii	Cooling, water is pumped into the well.	Temperature decreases due to cold water.
5b	Rock fractured with pressurized water.	Temperature decreases, pressure inside the well.
5c	Fracture cleaning with acid.	Can cause corrosion if it comes in contact with the casing.
5d	Rock fractured locally by burning rocket-fuel.	No load subjected on production casing.
(iii) Discharge of the well		
6a	Water column lifted with air bubbles through drill-string.	Temperature increase, small pressure de-crease,
6b	Water column pushed down and released quickly	Rapid depressurization and temperature increase
(iv) Production		
7	Harmful flow regimes.	Local dynamic pressure change.

If centralizers are taken into account as a weight relieving force, the relieving force has to be roughly estimated. This is due to friction between the centralizers and the outer steel casing wall and the formation below the outer casing shoe.

According to API SPEC 10D, *Specification for Bow-Spring Casing Centralizers*, the measured starting and running force of a previously run casing should be less than the weight of 40 feet (12.2 m) of medium weight casing (Mechanical Cementing Products 2009). If one centralizer is placed on each three casing components, then the maximum reduction of the load on the top of the casing should be less than 1/3 of the casing weight. The pressure at the top of the casing cross section then becomes,

$$P = -(\rho_s C - \rho_W)\, g\, L_{pr}$$

where ρ_s and ρ_w is the density of steel and water, g is gravity, L_{pr} is the length of the casing and C is the weight reduction due to the friction between the centralizers and the outer casing/formation. With this approach C has to be estimated but in all cases C should be larger than 2/3.

The second load case occurs when the cement slurry is being pumped in place. The concrete is pumped through the drill string, the casing collar and shoe, and up the annulus. The casing is full of water so the static pressure difference between the outer and inner wall of the casing is determined by the difference in density between concrete and water, normally about 1.6, see diagram B in Figure 1.

When the slurry is pumped in place the outer pressure on the casing must not exceed the collapse resistance of the casing. Pressure can build up for example because of a blockage in the annulus which can lead to a casing collapse.

The third load case deals with the reference temperature conditions inside the well when the concrete is setting. Heat of hydration, is released when cement comes in contact with water because of the exothermic chemical reaction in the cement (Portland Cement Association 1997). Temperature increases slightly as the concrete cures, a temperature increase of 12°C of a 300 mm thick curing concrete have been recorded (Portland Cement Association 1997). The annulus gap between casing and formation is much thinner so this temperature change can be considered small compared to the temperature conditions in a non-flowing geothermal well. In addition, when the cement has been placed and the cooling of the well is stopped, the well heats up slowly due to the hot surroundings. When the concrete bonds with the steel and solidifies the reference "zero" temperature of the casing-concrete is reached. After the bond between the casing and concrete is made, the well could heat up slowly due to the surroundings, but this depends on the rock formation, for example if there are hot fissures present.

In the fourth load case the production section of the well is drilled with cooling fluid or mud. This is the first major cooling of the casing resulting in its contraction. This leads to tensional forces in the casing as the concrete reactional forces are compressive, see diagram D in Figure 1.

(ii) Stimulation of the well

If wells do not perform properly the relationship between the well and the geothermal reservoir needs to be improved with stimulation methods.

In load case 5, several stimulation methods are reviewed with regards to load on the production casing. Method 5a, where intermittent cold water injection is used with periods of thermal recovery, is one of the most common ones used for high temperature wells in Iceland (Axelsson 2006). In this method cracking is caused in the rock with thermal shocking. Cyclic thermal loading and large temperature changes can cause damage in the production casing and the surrounding concrete due to thermal expansion/contraction of the steel, see diagram C and D in Figure 1.

In method 5b pressurized water is used to clean out and fracture already present fissures. This cools down the well causing contraction of the steel, see diagram D in Figure 1. This can be avoided by using inflatable packers, where the stimulation can be focused on specific intervals in the well rather than the whole open section (Axelsson 2006).

Method 5c involves cleaning out fissures with acid. The acid must not come into direct contact with the steel because of a possible corrosion risk.

Method 5d was used recently in Iceland, where rocket fuel was burned at specified location a high temperature geothermal well to create a shock wave which caused cracking in the rock(Sigurðsson 2010). This method separates the stimulation process from the well section above, minimizing the load on the casing.

(iii) Discharge of the well

Discharge methods are used if the flow in the well does not start automatically when the well is opened.

In load case 6, two discharge methods are described. In method 6a, flow is initiated with air that is pumped through the drill-string creating air bubbles that reduce the density of the water column above. In this method, increased temperature is the main load on the casing as well as the pressure changes from hydrostatic to flow conditions.

In method 6b, air pressure at the wellhead is used to push the water column down into the reservoir. Then after some time the pressure is released and the well discharges quickly. This causes a rapid depressurization and temperature increase.

(iv) Production

When the well is in production, harmful flow regimes could result in casing impairment. For example, plug flow can occur when the geothermal fluid boils, which could cause local dynamic pressure changes and cavitation.

FINITE-ELEMENT MODEL

The FE-model is a 3D thermal and structural model. The thermal model calculates the temperature distribution, or rather the temperature change from the reference cementing conditions. The reference conditions (or zero condition) for the model is where the concrete sets and forms a connection to the steel casings. The temperature distribution is first calculated through all casings, concrete and the surrounding rock formation. The solution from the thermal model is then used as a load for the structural model.

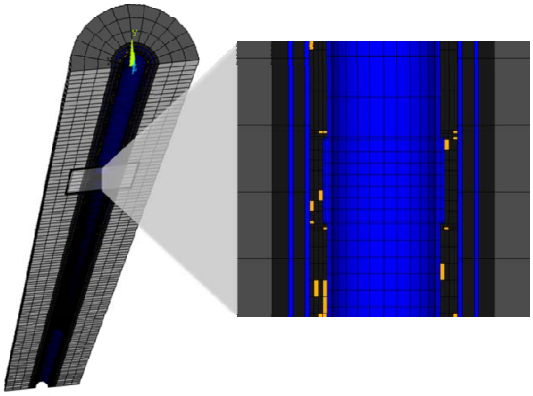

Figure 2: Element model geometry.

As mentioned before two couplings are included in the production casing. For simplification, the couplings are modeled as a solid body with no threads included. The couplings are included to see the steel-concrete interaction assuming no thread-slip in the coupling. For better efficiency half of the well is modeled, which is possible because of symmetry. Three casings are included, a 13 3/8 in (outer diameter) and 12.2 mm (0.48 in) thick production casing, 18 5/8 in and 13 mm (0.51 in) thick security casing and a 22 1/2 in also 13 mm (0.51 in) thick surface casing.
Figure 2 shows the model geometry and the included coupling. Imperfections are included in the concrete as a small variation in material properties. These variations are shown as yellow elements.

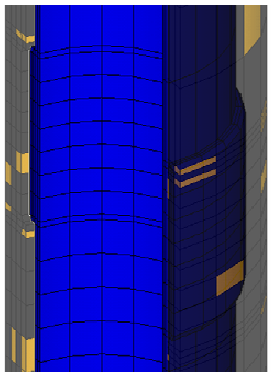

Figure 3: The coupling of the production casing and the surrounding concrete (transparent).

Material properties are defined separately for the steel, the concrete and the ground, see *Table 3*. The reference value for the compressive strength of the concrete is 27.6 MPa. Stress-strain behavior of K55 is used in the model for all three casings. In the model four different stress-strain curves can be used for the steel. Defined steel grades for K55, X56, L80 and T95 were obtained from tensile strength tests by Karlsdottir (Karlsdóttir 2009).

Table 3: Reference values, material properties used in the FE-analysis.

	Steel	*Concrete*	*Rock*
Young's modulus (E)	210 GPa	2,8 GPa	100 GPa
Poisson's ratio (γ)	0.3	0.15	0.31
Density (ρ)	7850 kg/m^3	1666 kg/m^3	2650 kg/m^3
Thermal conductivity (K)	46 W/(m°C)	0.81 W/(m°C)	2 W/(m°C)
Thermal expansion (α)	12e-6 /°C	9e-6 /°C	5.4e-6 /°C

The bonding characteristics between steel and concrete are one of the reasons for the numerical complexity of the model. During the solution process, the contact between the casing and the concrete is constantly changing from bonded to sliding to sticking to debonding. This makes the problem extremely complicated and computation time becomes considerably large.
Maximum surface shear strength (Wallevik 2009) between the steel casing and the concrete, before debonding occurs, is used in the analysis. When the friction stress reaches the maximum shear strength, the bond is broken and sliding begins.
Furthermore, a maximum normal contact stress is used to control the debonding characteristics.

CASE STUDIES

A load history case of the production casing is extracted from the load cases presented in the "Production casing Load history" section. The load history is put together with load cases *1-4*, *5a-i*, *5a-ii* and *6a* from Table 2. This particular case is supposed to represent a general load history of a typical well, although the load history for each high temperature geothermal well is unique. K55 steel in used in all casings and the material properties seen in Table 3 are used.

In another case, high positive temperature difference is applied on the casing to see at what temperature the casing buckles. To see the effect of enclosed water in the concrete, two cases are performed, one where a small water pocket is included in the analysis and one without it. A temperature change of 750°C and inside pressure of -5 MPa is applied on the casing in both cases. A small water pocket is included in the analysis, 1,6 m long, filling up half of the annulus circumference. Imperfections are randomly dispersed in the domain, consisting of 80% water and 20% concrete.

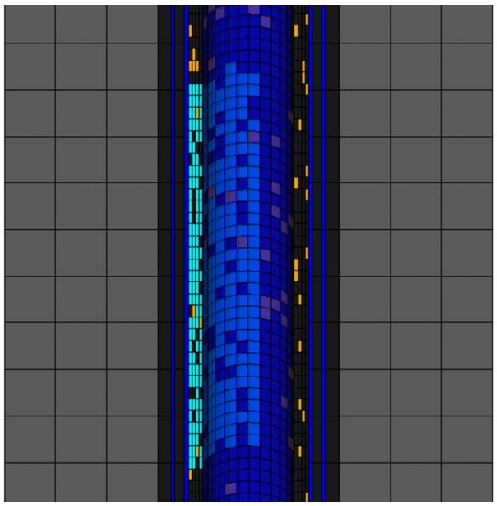

Figure 4: Water pocket in concrete (cyan colored), (production casing is transparent).

RESULTS

Load history results

In the following load cases, assumed temperature changes and pressure are used in the model, based on typical conditions that should be expected in reality.

In load cases 1 and 2, only the production casing is modeled. In load case 1, 600m of casing is assumed to be hanging freely below the modeled section. In load case 2, a cement slurry pressure of 0.6 MPa is subjected on the casing assuming 100 m of concrete above. In load case 3, all casings, concrete and the rock formation are added to the analysis, where the slurry is assumed to solidify at 50°C which is the reference temperature for the analysis. After bounding of the concrete with the steel, the temperature change is assumed to increase by 50°C because of the heat of hydration and the surroundings. At load case 4, the casing is cooled with cooling fluid, assuming that it reaches temperatures as low as 5°C. In load case 5a-i the casing heats up to 300°C as the well is allowed to heat up during stimulation procedures. In load case 5a-ii the well is cooled down to 5°C again during stimulation procedures. In the last load case the well heats up to production conditions, 350°C, as it is discharged.

Table 4 lists the load, temperature change, ΔT, and pressure difference, $P_{i\text{-}o}$, between the inner and outer wall of the casing, for each load case in the analysis.

Table 4: Load for the analysis.

Load Case	*ΔT [°C] (well temp.)*	*$P_{i\text{-}o}$ [MPa]*	*Comment*
1	-	-	Gravity of a 600 m casing hanging free.
2	-	-0.58	Cement slurry outer pressure on casing.
3	+50 (100)	-	Heat of hydration and surroundings.
4	-95 (5)	-	Production section of the well drilled with cooling fluid.
5a-i	+295 (300)	-	Stimulation, heating period
5a-ii	-295 (5)	-	Stimulation, cooling period
6a	+345 (350)	-	Discharge of the well

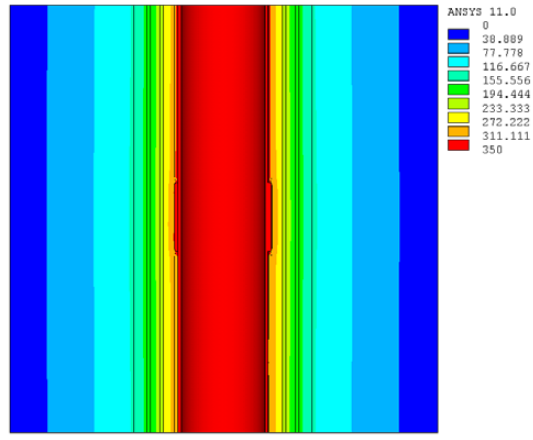

Figure 5: The temperature distribution (temperature difference) of load case 6a.

The temperature distribution solution from the thermal model for load case 6a can be seen in Figure 5. The temperature distribution is then used as a temperature difference load on the structural model.
In Table 5 the maximum von Mises stress is listed for the production casing and surrounding concrete for all load cases. The maximum radial displacement of the casing is displayed in Table 6 and the maximum axial displacement of the casing is displayed in Table 7.

Table 5: Maximum von Mises stress (MPa).

Load Case	Steel Casing		Concrete	
	Value	*Location*	*Value*	*Location*
1	31.2	Coupling border	-	-
2	97.0	Near coupling	-	-
3	160	Coupling border	2.87	Coupling border
4	284	Coupling border	4.96	Coupling border
5a-i	329	Coupling border	30.2	Coupling border
5a-ii	433	Between couplings	15.7	Coupling border
6a	374	Near coupling	34.5	Coupling border

Table 6: Maximum radial displacement of the casing (mm).

Load Case	Steel Casing	
	Value	*Location*
1	-0.00757	Near coupling
2	-0.0638	Near coupling
3	0.136	Near coupling
4	-0.567	Casing body
5a-i	0.726	Near coupling
5a-ii	-1.740	Between couplings
6a	0.897	Outer radius

Table 7: Maximum axial displacement of the casing (mm).

Load Case	Steel Casing	
	Value	*Location*
1	2.834	At lower end
2	2.798	At lower end
3	-0.0938	Coupling border (inner)
4	0.0583	Coupling border (outer)
5a-i	-0.689	Coupling border (inner)
5a-ii	-7.77	Between couplings
6a	-7.814	Between couplings

From these results it can be seen that the casing suffers the highest strain when it is cooled down during the supposed stimulation process in load case 5a-ii. The highest stress in the concrete occurs in warm-up periods at the coupling borders.
It is interesting to see that the highest inward radial displacement of the casing occurs during this cooling period.

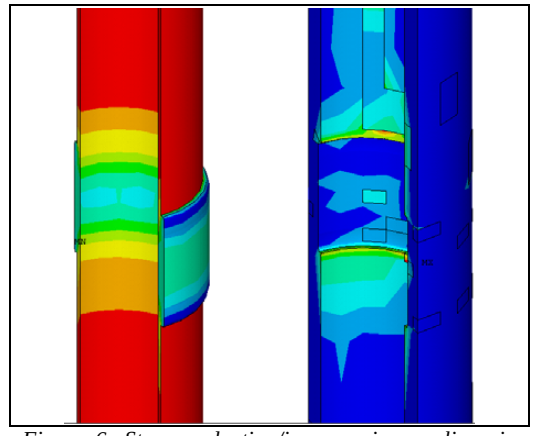

Figure 6: Stress reduction/increase in couplings in load case 6a.

Near the couplings, the stress increases in the concrete and reduces in the steel couplings, see Figure 6. Since there are no threads included in the couplings in the analysis the coupling failures can not be predicted precisely with this model, but this gives an indication of how the steel and concrete react.
Figure 7 shows that debonding of the production casing and concrete is progressing and a small gap is beginning to form, increasing the risk of buckling next time the well is heated up.

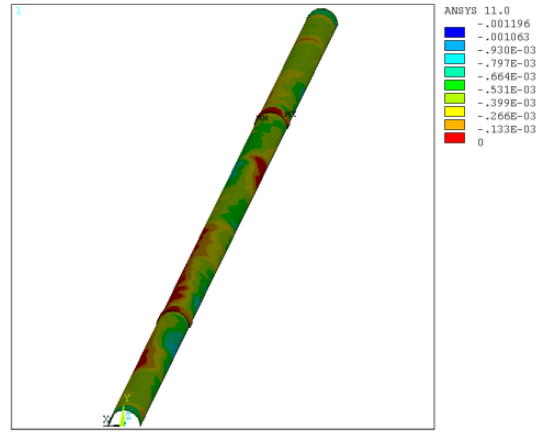

Figure 7: Contact gap between casing and concrete in load case 5a-ii.

The stimulation method where the rock is fractured with cyclic thermal shocking can cause damage to the casing if the difference in temperature is high and if this is done repeatedly.

Buckling

Since buckling did not occur in the load history analysis above, a load of a high temperature is subjected on the casing to see at what temperature buckling occurs.

Table 8: Maximum stress and displacements - case without water pocket.

	Steel casing	
Maximum	*Value*	*Location*
Von Mises stress [MPa]	358	Casing body
Radial displacement [mm]	2.20	Near coupling
Axial displacement [mm]	1.09	Near coupling

Table 9: Maximum stress and displacements at the buckling point - case with water pocket.

	Steel casing	
Maximum	*Value*	*Location*
Von Mises stress [MPa]	440	At water pocket
Radial displacement [mm]	-106	At water pocket
Axial displacement [mm]	63.7	At water pocket

In the case without the water pocket buckling does not occur despite the high temperature change. The results show that the casing expands radially pushing up against the concrete and causing no debonding from the concrete. The maximum von Mises stress in the concrete is 35.7 MPa at the coupling boundary.

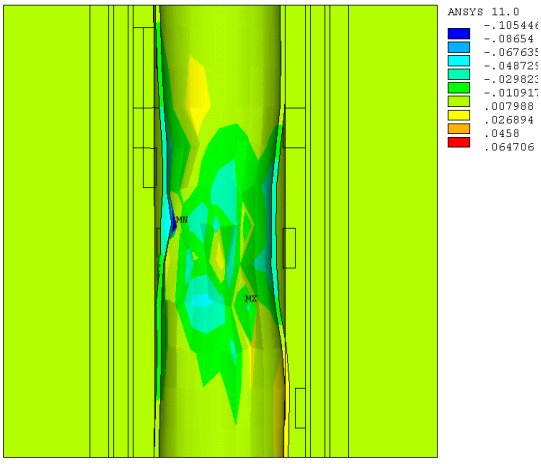

Figure 8: Buckling, radial displacement (meters).

In the case including the water pocket, buckling occurs at 40% of the load, i.e. at about 300°C and -2 MPa inside pressure. The maximum stress of the casing reaches the yield strength of the steel at the buckling point and the maximum von Mises stress in the concrete reaches 44 MPa at the boundary of the water pocket. The radial displacement and the buckling shape can be seen in Figure 8.

CONCLUSION

A finite-element model was developed to calculate the stresses in a casing that is subjected to thermo-mechanical loads.

The results show that the production casing experiences a peak in stress when the casing is cooled during a supposed stimulation process, whereas the concrete suffers the highest stress during heating periods. The stress in the concrete is increased near the couplings, whereas the inverse occurs in the steel couplings.

During cooling periods the casing contracts axially and it is interesting to see how much it contracts radially resulting in debonding between the steel and concrete. This leads to higher risk of buckling when the well heats up again because of reduced support from the concrete, which shows that the load history and the sequence of load cases is important. In addition the load history is important because of cumulative stresses and plastic strains that occur in the casing.

The results show buckling when a water pocket is included in the concrete surrounding the production casing, whereas a case without the water pocket shows radial expansion of the casing and no buckling. This shows that a water pocket that is enclosed in the casing-to-casing annulus clearly has an effect on the buckling phenomenon.

It is clear that further work needs to be done to gain a better knowledge of how the production casing behaves as a whole in a high temperature geothermal well and to gain a better insight into the failure modes that cause problems. In addition, values for a complete load history of a real failure case would be preferred to use as an input in the model. There are many uncertainties regarding what leads to casing impairment. It is apparent that a combination of factors are causing casing failures, which could include; imperfections and production flaws in casings, casing thickness deviation, ovality of the casing, casing centralization, concrete mix properties, quality of the cementing job, and various loading scenarios. In further work it would also be interesting to compare different casing sizes, the effect of concrete gap or water pocket size on the types of buckling, as well as different stimulation and discharge procedures and methods.

ACKNOWLEDGMENT

This work was supported by the Technology Development Fund at RANNIS - The Icelandic Centre for Research, GEORG - Geothermal Research Group and the Innovation Center Iceland. Their support is much appreciated.

REFERENCES

Axelsson, G., Thórhallsson, S., Björnsson, G. „Stimulation of geothermal wells in basaltic rock in Iceland.“ Kartause Ittingen, Zurich: ENGINE – ENhanced Geothermal Innovative Network for Europe, Workshop 3, Switzerland, 2006.

Björnsson, G., Ragnars, K., Sigfússon, S., Karlsson, Þ. *Styrkleiki fóðurröra í háhitaborholum (OS JHD 7805) (in Icelandic).* Reykjavík: Orkustofnun, 1978.

Kane, R. D. „Evaluation of Geothermal Production for Sulfide Stress Cracking and Stress Corrosion Cracking.“ Denver, Colorado: InterCorr/96, 1996.

Karlsdóttir, S. N., Thorbjornsson, I. O. „High Temperature Geothermal Wells – Center of Excellence in Iceland - Phase I: Corrosion testing of steel in high temperature geothermal wells in Iceland.“ Technical Report for RANNIS (The Icelandic Centre for Research), Reykjavik, Oct., 2009.

Leaver, J. D. „Failure Mode Analysis for Casing and Liners in Geothermal Production Wells.“ 1982.

Magneschi, P., Bagnoli, C. , Lazzarotto, A. , Ricciardulli, R. „Structural Models for the Analysis of Stresses in the Casings of Geothermal Wells.“ World Geothermal Congress, 1995.

Mechanical Cementing Products. Products manual, Houston, Texas: Weatherford International Ltd., 2009.

Pálmason, G. *Jarðhitabók (in Icelandic).* Reykjavík: Íslenskar orkurannsóknir og Orkustofnun, 2005.

Peng, S., Fu, J., Zhang, J. „Borehole casing failure analysis in unconsolidated formations: A case study.“ *Journal of Petroleum Science and Engineering 59*, 2007: 226-238.

Philippacopoulos, A. J., Berndt, M. L. „Characterization and Modeling of Cements for Geothermal Well Casing Remediation.“ San Francisco, California: Geothermal Resources Council, 2000.

Philippacopoulos, A. J., Berndt, M. L. „Structual analysis of geothermal well cements.“ *Elsevier Science Ltd.*, 2002.

„Portland Cement, Concrete, and Heat of Hydration.“ *Concrete Technology Today (Portland Cement Association)*, nr. Volume 18/Number 2 (July 1997).

Rechard, R. P., Schuler, K. W. *Euler Buckling of Geothermal Well Casing.* Albuquerque, New Mexico: Sandia National Laboratories, 1983.

Release 11.0 documentation for ANSYS. SAS IP, Inc., 2007.

Sigurðsson, Ó. „Nýjung við örvun borholna á Íslandi.“ *Fréttaveitan, HS-orka newsletter (in Icelandic)*, 2010: 10-11.

Southon, J. N. A. „Geothermal Well Design, Construction and Failures.“ Auckland, New Zealand: Proceedings World Geothermal Congress 2005, 2005.

Vrellis, G., Chiotis, E. „Analysis of Casing Failures of Deep Geothermal Wells in Greece.“ *Geothermics, Elsevier Science Ltd.*, 1995: 695-707.

Wallevik, S. O. „High Temperature Geothermal Wells – Center of Excellence in Iceland - Phase III: Rheological behavior and mechanical properties of cement paste for high temperature geothermal wells.“ Technical Report for RANNIS (The Icelandic Centre for Research), Reykjavik, Oct., 2009.

Paper II

PROCEEDINGS, Thirty-Seventh Workshop on Geothermal Reservoir Engineering
Stanford University, Stanford, California, January 30 - February 1, 2012
SGP-TR-194

Thermal and Structural Analysis of the Casing in a High Temperature Geothermal Well During Discharge

Gunnar Skúlason Kaldal[1]*, Magnús Þ. Jónsson[1], Halldór Pálsson[1], Sigrún N. Karlsdóttir[2]

[1]Faculty of Industrial Engineering, Mechanical Engineering and Computer Science, University of Iceland, Hjarðarhagi 2-6,
Reykjavik, 107, Iceland
[2] Innovation Center Iceland, Department of Materials, Biotechnology and Energy, Keldnaholt, Reykjavik, 112, Iceland
*e-mail: gunnarsk@hi.is

ABSTRACT

During the discharge of high temperature geothermal wells, the temperature difference in the well from non-flowing to flowing conditions is in the range of couple of hundreds of degrees centigrade and the pressure fluctuation is also large. The wellhead rises due to thermal expansion of the casing and the wellbore pressure, in some cases excessively because of concrete damage or poor cementing job.
Measurements of a particular high temperature well were performed during discharge. Temperature and pressure changes were measured at the wellhead as well as the wellhead rise. A model was constructed using the finite element method (FEM) and computational results from the model were compared to the measurements.
The results from the transient thermal FEM analysis show a rapid temperature response in the concrete layers of the well. In the concrete surrounding the production casing the temperature rises to roughly 95% of thermal equilibrium in only few hours. The coupling-concrete interactions in the FEM model indicate that the concrete has a weak spot and is most likely to get damaged at the coupling ends. The results show that the rise of the wellhead is exclusive to the uppermost 500 meters of the well but displacements are negligible beneath.

INTRODUCTION

At the start of the discharge of high temperature geothermal wells the geothermal fluid is abruptly sucked out of the reservoir by the low pressure conditions on the surface. This causes large pressure fluctuations inside the wellbore as well as local flow conditions, such as plug or slug flow, that causes vibration that can easily be felt on the surface by an observer and could be harmful for the casing. The large temperature change in the well causes thermal expansion of the casing, which in turn causes the wellhead to rise.
Relatively few studies have been published on structural finite-element (FEM) models of the casing in geothermal wells. A 2D FEM model of the cross section of a double cased geothermal well was created by Philippacopoulos and Berndt (2002) in order to represent the behavior of the cement/sealant, where the results showed the inadequacy of geothermal well design based solely on compressive strength. A plane strain finite element model for well failure due to formation movement and a three dimensional model to analyze the local behavior of the casing-cement-formation interaction in geothermal wells were developed also by Philippacopoulos and Berndt (2000) where the results revealed the importance of the cement properties on the response of the casing patch cement included in the three dimensional model.
Peng, Fu and Zhang (2007) created a FEM model to represent oil-field casing failure in unconsolidated formations where the results showed non-uniform and multi-directional casing deformation. Theodorio and Falcone (2008) presented a finite-element model and experimental work to evaluate the low-cycle fatigue (LCF) resistance of an 18-5/8 in diameter casing with Buttress threaded connections. Their results showed that under extreme loads the LCF resistance of the connection could be as low as 10 cycles.
In a M.Sc. thesis by Magnúsdóttir (2009) a two dimensional FEM model (as well as a three dimensional buckling model) of a geothermal well was constructed, where the upward displacement of the wellhead was analyzed with regards to the bonding characteristics between the production casing and concrete. The results for full, partial and no bonding between the surfaces, were compared and showed how the defined connection behavior greatly affected the results. Another M.Sc. thesis by Ólafsson (2011) covers a structural analysis of a wellhead on a

high temperature geothermal well using a FEM model where several load cases are analyzed with regard to pressure and temperature loads. The load history and buckling of the production casing was covered by Kaldal (2011) where a section of a well was analyzed with regards to local collapse of the casing. The results showed increased stress in the concrete around couplings indicating a potential risk of local damage.

Wellhead movement can be an indicator of failures in wells. Large wellhead movement for example could indicate that the concrete between casings is defective or damaged and could lead to serious casing damage. The wellhead movement of a "healthy" well can be a great contributor for the calibration of structural models dealing with the frictional interaction between steel casings and concrete. Measurements of the wellhead movement during discharge are therefore an excellent contribution to structural modeling of geothermal wells. Large wellhead movement can also be an indicator of a potential risk of casing damage in the well. Casing failures can cause a serious hazard of leakage and blow out risk. For instance in an extreme example from the 70s, the production casing of a well in northern Iceland was in poor shape due to a highly corrosive environment, eventually causing an immense explosion that created a crater at the wellhead location (Pálmason 2005).

In this article the rise of the wellhead, during discharge of high temperature geothermal wells, is examined. A case study is presented of well HE-46 in the Hellisheiði high temperature geothermal area located in south-west Iceland, where temperature, pressure and wellhead movement measurements were conducted during discharge. A transient axially symmetric two dimensional thermal and structural model of a geothermal well is presented.

FINITE-ELEMENT MODEL

The finite-element method (FEM) is used to construct thermal and structural models of a high temperature geothermal well from the wellhead to the bottom of the production casing. It is a two-dimensional axially symmetric model which includes nonlinearities in (i) material properties, (ii) geometrical displacements and (iii) connectivity between contacting surfaces (contact elements).

The main nonlinear material properties that are used are the stress-strain curves for K55, L80, T95 and X56 steel at room temperature, obtained from tensile strength tests by Karlsdottir (Karlsdóttir 2009). Strength reduction at elevated temperatures is included for the steel in the model. For the concrete, an approximation is made where a maximum compressive strength is defined before it is assumed to yield plastically. Defining a concrete material model that behaves differently in compression and tension for a model of this scale has proved to be unpractical but could be a subject for revisal in future studies. Other material properties are defined linearly.

The bonding characteristics between steel and concrete are one of the reasons for the nonlinear behavior of the model. In the model, all contacting surfaces are defined using contact elements. Coulomb friction is used to describe the bonding characteristics, where a coefficient of friction and maximum friction stress are defined. The maximum friction stress controls when bonded contact changes to sliding contact and relative sliding between surfaces initiates.

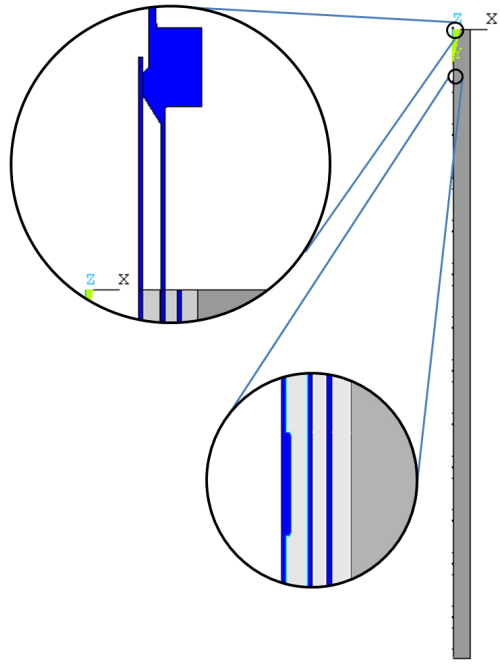

Figure 1: The geometry of the two dimensional axial-symmetric finite-element model. Upper magnification: simplified wellhead based on the actual design. Lower magnification: simplified coupling without threads.

The geometry of the model is shown in Figure 1. It is a two dimensional model, axially symmetric around the center of the well. It includes three casings at the top; the production casing, the security casing and the surface casing. The model reaches from the wellhead to the shoe of the production casing, where it sits on the rock formation which goes 20 meters deeper until it reaches the lower boundary of the model. The radial boundary of the rock formation goes 20 meters outward, which showed to be sufficient for both the thermal and the structural parts of the model. Modeling wells that are drilled in sedimentary basins or soft ground would probably require the outer

boundary to be larger, but in this model the formation is assumed to be solid rock.
As can be seen from the geometry of the model, it's diameter-to-depth ratio is very small, which requires a large number of elements because the elements must have proper width-to-length ratio to function correctly. Although the geometry of the well can be regarded as being simple in shape, the problem becomes computationally complex due to; the large number of elements and the numerous nonlinearities, such as material nonlinearities, large displacement nonlinearities, and the interaction between surfaces.
In the model the production casing has an outer diameter of 13 3/8 in, thickness of 12.2 mm and is 700 m in length. Simplified couplings with no threads are included in the model as can be seen on the lower magnification in Figure 1. A simplified wellhead based on an actual design is also included to see how the casing and the wellhead interact. The wellhead is welded to the security (anchor) casing as shown in the upper magnification in Figure 1. The first flange of the wellhead and the casing guidance gasket are simplified into a solid piece which are included in the model to see how the production casing slides inside the wellhead. The model is further described in the results chapter in connection with the results.

LOADS IN GEOTHERMAL WELLS

Casing design is generally based on axial tension and compression, burst pressure and collapse pressure, where axial tension is a measure of how much load can lead to pipe body failures and coupling failures, see diagram A in Figure 2. The internal yield pressure (burst pressure) is the minimum internal pressure that will cause a ductile rupture of the pipe body and the collapse resistance of casings is the minimum external pressure that will cause a collapse of the casing, see B in Figure 2. Standards provide equations and calculations for the properties of casings for the oil and gas industry. They are however lacking in calculations of high thermal loads.
To understand what loads act on the casing it is necessary to go through the load history of the casing. During the installation of the production casing, casing components are screwed together and lowered down into the well one by one. If residual stresses from the production of the casing are neglected, the first load on the casing is tensional force due to gravity, see diagram A in Figure 2. While the casing is being installed, the well is kept full of cold water, which provides a buoyant force. The tensional force increases with increased depth, putting the highest strain on the last installed casing component that supports the whole casing before the concrete sets. This load is however dependent on how many centralizers are used and the diameter of the hole.

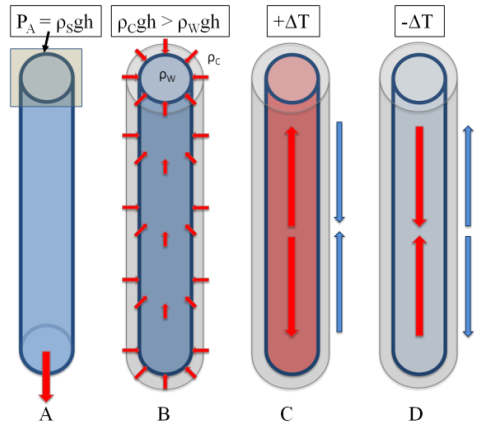

Figure 2: Production casing loads.

During cementing, the casing experiences both burst and collapse loads, i.e. the difference in internal and/or external pressure. The concrete is pumped through the drill string, the casing collar and shoe, and up the annulus. The casing is full of water so the pressure difference between the outer and inner wall of the casing is determined by the difference in density between concrete and water, normally about 1.6, see diagram B in Figure 2. When the slurry is pumped in place the outer pressure on the casing must not exceed the collapse resistance of the casing. Pressure can build up for example because of a blockage in the annulus which can lead to a casing collapse. When the concrete is setting, heat of hydration is released when cement comes in contact with water because of the exothermic chemical reaction in the cement (Portland Cement Association 1997). Temperature increases slightly as the concrete cures, a temperature increase of 12°C of a 300 mm thick curing concrete have been recorded (Portland Cement Association 1997). The annulus gap between casing and formation is much thinner so this temperature change can be considered small compared to the temperature conditions in a non-flowing geothermal well. In addition, when the cement has been placed and the cooling of the well is stopped, the well heats up slowly due to the hot surroundings.
When the concrete bonds with the steel and solidifies the reference "zero" temperature of the casing-concrete is reached. After the bond between the casing and concrete is made, the well heats up slowly due to the surroundings, but this depends on the rock formation, for example if there are hot fissures present. When the production section of the well is drilled cooling fluid or mud is used to cool the well and provide circulation for transporting cuttings to the surface. This is the first major cooling of the casing resulting in its contraction. This leads to tensional forces in the casing as the concrete

reactional forces are compressive, see diagram D in Figure 2.

If wells do not perform properly the relationship between the well and the geothermal reservoir needs to be improved with stimulation methods. Most of the methods involve injection of cold pressurized water. A method where intermittent cold water injection is used with periods of thermal recovery, is one of the most common ones used for high temperature wells in Iceland (Axelsson 2006). In this method cracking is caused in the rock with thermal shocking. Cyclic thermal loading and large temperature changes can cause damage to the production casing and the surrounding concrete due to thermal expansion/contraction, see diagram C and D in Figure 2. In a related method, pressurized water is used to clean out and fracture already present fissures. This cools down the well causing contraction of the steel, see diagram D in Figure 2.

Damage to the casing can be avoided by using inflatable packers, where the stimulation can be focused on specific intervals in the well rather than the whole open section (Axelsson 2006). In another method acid is used to clean out fissures. The acid must not come into direct contact with the steel because of a possible corrosion risk. Recently, rocket fuel was burned at a specified depth in a high temperature geothermal well in Iceland to create a shock wave which caused cracking in the rock (Sigurðsson 2010). This method separates the stimulation process from the well section above, minimizing the load on the casing.

In order for a well to flow unassisted, the pressure in the well needs to be higher than the atmospheric pressure. The wellhead is usually kept closed for a period of time in order to increase the pressure on the wellhead.

Discharge methods are used if the flow in the well does not start automatically when the well is opened. In one method an air pump is used to build pressure at the wellhead that pushes the water column down. After a period of time the pressure is released and the well discharges quickly. This causes a rapid depressurization and temperature increase.

Three conceptual load cases, pre and post discharge can be seen in Figure 3. In the figure to the left, a schematic is shown of a non-flowing well with no top pressure. The pressure (black line) is hydrostatic below the water table which lies somewhere in the well and the temperature (blue line) is low above the water table.

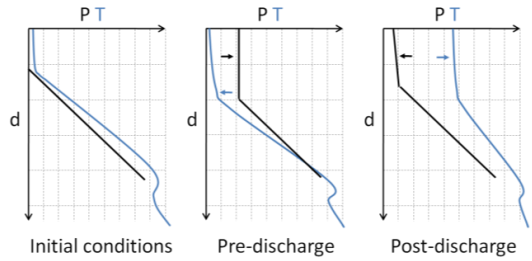

Figure 3: Conceptual load cases before and after discharge.

On the figure in the middle the well has either been closed to gain pressure of non-condensable gases or a pump is being used to increase the wellhead pressure. In both cases the water table is pushed down in the well, causing the temperature where the water table was before to decrease. This state is held until the wellhead pressure is enough for the well to be discharged. On the last figure to the right, the pressure and temperature conditions after discharge can be seen. In the discharge the pressure uppermost in the well decreases and the temperature increases abruptly.

Another more advanced discharge method requires a drill rig on site, where the flow is initiated with air that is pumped through the drill-string creating air bubbles that reduce the density of the water column above, thus creating momentum. In this method, increased temperature is the main load on the casing and the pressure changes slowly from hydrostatic to flow conditions. This method, however, is rarely used due to increased cost.

After the well is discharged harmful dynamic flow conditions, such as plug and slug flow, could result in casing impairment. At the phase change where the geothermal fluid boils, the flow becomes turbulent and could cause local dynamic pressure changes and cavitation, which can erode the casing.

CASE STUDY - MEASUREMENTS OF WELL HE-46 IN HELLIHEIÐI, ICELAND

Temperature, pressure and the rise of the wellhead during discharge were measured at the wellhead on well HE-46 which is located on the Hellisheiði high temperature geothermal area in south-west Iceland. The well, drilled in the year of 2008, has a total depth of 2444 meters with a production casing that reaches down to 1032 meters. The wellhead of HE-46 can be seen in Figure 4.

Air pump was used to build up pressure inside the well for few weeks before discharge. On the day of discharge the pump had built up a pressure of 37.5 bar-g (the discharge of the well was delayed for few days due to a rare Icelandic thunderstorm). The well was opened quickly, causing an abrupt discharge of the steam rich geothermal media which was then directed out to the silencer. A large pressure

fluctuation occurred at the beginning of the discharge, the first 10 minutes of the discharge can be seen in Figure 6. The pressure decreased rapidly to 7.0 bar-g and then rose to steady 19.5 bar-g. This fluctuation and its influence on the casing could be interesting to investigate further. The outer temperature of the expansion spool rose steadily from 8°C to 193°C in 5 minutes, see Figure 5. The temperature had reached 197°C one day later.

Figure 4: The expansion spool and master valve of the wellhead of well HE-46 (figure: Heimir Hjartarson).

The rise of the wellhead basement and the flange above the expansion spool on the wellhead was measured with an optical elevation meter and a laser. Temperature was measured at several locations on the wellhead; at the upper and lower flange of the expansion spool and on the outer surface of the expansion spool. Pressure was measured with a pressure gauge located above the master valve.
The wellhead is restrained by three main features; the concrete layers of the casings (the wellhead is an extension of the second casing outward, the security casing), a "spider" support which consists of four bars in tension on top of the wellhead and four centralizing bars in the wellhead basement. The total rise of the wellhead during the observation can be seen in Figure 7. Unfortunately, the measurement period was to short to observe the final wellhead rise but the wellhead was still rising at the end of the measurement period. The sharp rise at the beginning stages of the discharge is however interesting and illustrates the substantial force due to the thermal expansion of the casing.

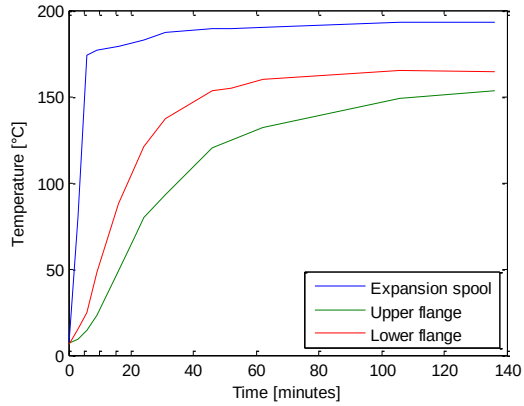

Figure 5: Measured wellhead temperature during discharge (outer temperature of the expansion spool).

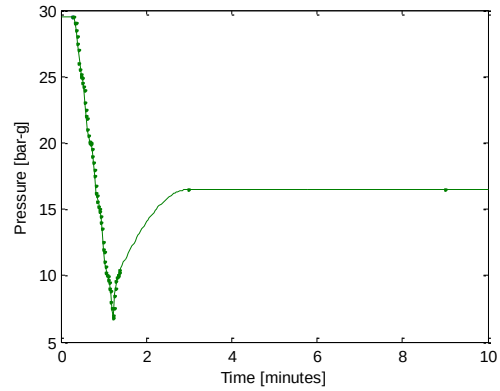

Figure 6: Wellhead pressure during the first ten minutes of discharge.

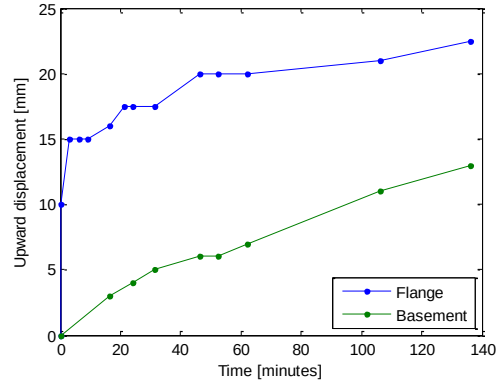

Figure 7: Wellhead rise; upper flange of the expansion spool, wellhead basement.

RESULTS

Thermal calculations

One dimensional casing-concrete layer model

A one dimensional thermal model of the upper layers of a high temperature geothermal well with a top temperature of 200°C, was constructed and time-dependent analysis were performed to obtain information on how fast the system reaches thermal equilibrium. The well is assumed to have three casings that are all cemented. The boundary conditions at the outer boundary of the ground, which is selected as 50 m from the center of the well, is set to T_{gr} = 0°C and at the inner wall of the production casing is set to T_{pr} = 200°C, assuming production conditions uppermost in the well. The analysis is time-dependant where the load is changed in a step to simulate a well discharge.

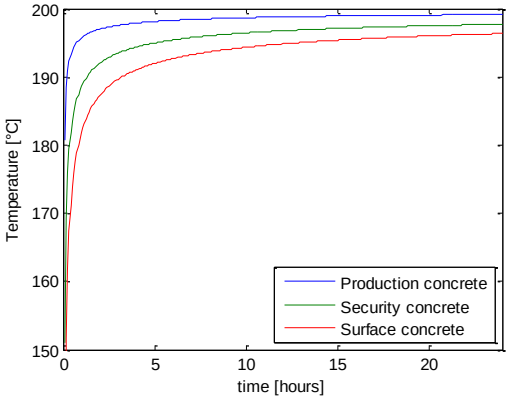

Figure 8: Thermal response in the concrete layers of the well.

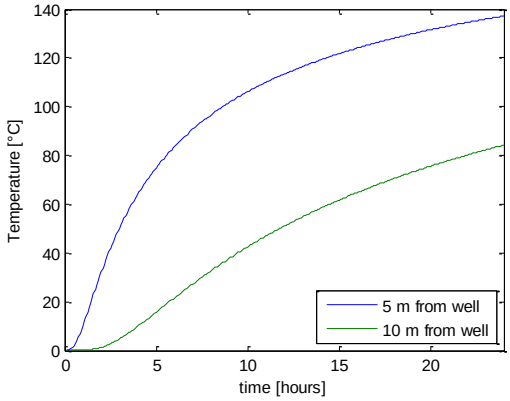

Figure 9: Thermal response in the surrounding rock, 5 and 10 meters from the well.

The thermal response is calculated through a period of 30 days. A steady-state analysis is performed in comparison to the transient analysis to see when thermal equilibrium is reached in the well casings and in the surrounding ground, assuming constant temperature conditions inside the well.
The results show that the thermal response in the casings of the well is relatively fast, taking only few hours to reach thermal equilibrium. But the thermal gradient from the center of the well to outer layers is still rather high, as can be seen by the temperature difference in the concrete layers, i.e. the concrete around the production casing, the security casing and the surface casing, as well as the surrounding rock in Figure 8 and Figure 9.

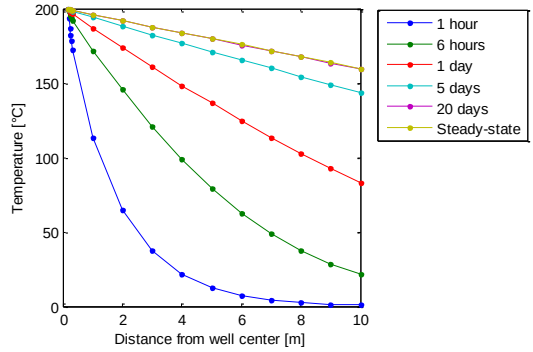

Figure 10: Temperature distribution in the vicinity of the well.

The temperature distribution in the vicinity of the well at various points in time can be seen in Figure 10. The thermal gradient is still very steep 1 hour after the beginning of the discharge and continually drops over time until a thermal equilibrium is reached, after 20 days of constant production.

Two dimensional well model

The temperature change of a well and its surroundings during a discharge of the well is presented here. These results are later used as a thermal load in the structural analysis. The rock temperature remains unchanged at the outer boundary of the model, therefore the boundary conditions at the outer boundary of the ground, which is 20 m from the center of the well, is T_{gr} = 0°C. At the inner wall of the production casing, the temperature change is based on pre and post discharge temperature data from the Iceland Geosurvey.

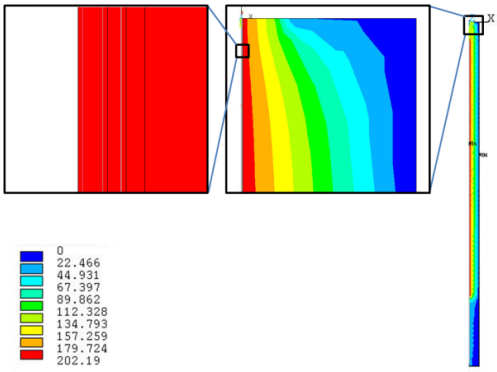

Figure 11: Steady-state thermal results, temperature change before and after discharge.

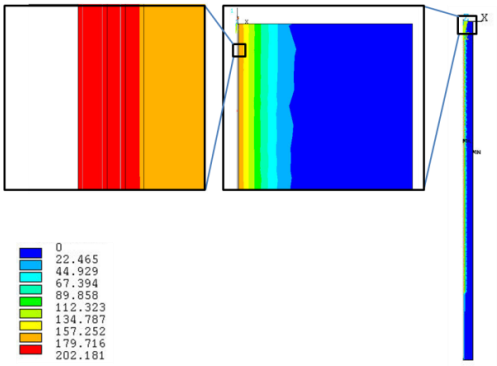

Figure 12: Transient thermal results, temperature change two hours and twenty minutes after the beginning of discharge.

The steady state thermal results in Figure 11 show the total temperature change in the well after the discharge has started. The transient thermal results in Figure 12 show the temperature change two hours and twenty minutes after initiating the discharge, which is the same time interval as the measurement period of well HE-46. The transient thermal results show how the temperature increases through time into the outer layers of the well.

Structural calculations

Two dimensional well model

The load for the structural model consists of the temperature and pressure change from pre- to post-discharge. The temperature change results, obtained from the transient thermal model, are used as load on a geometrically identical structural model. The pressure change is also applied as a load on the inside of the production casing and the wellhead. Both a nonlinear static analysis and a nonlinear transient analysis are performed.

To understand better how the load changes, a schematic of the conceptual load cases is shown in Figure 13, focusing on the location uppermost in the well above the water table. In phase I-II shown in the figure the pressure is built up until it reaches a steady target pressure value which is then kept constant for a period of time until the well is discharged in phase III. The discharge phase takes shorter time compared to the other phases, i.e. minutes vs. weeks. In phase IV, pressure and temperature remain steady in the production phase. The pressure and temperature change in phase III is of primal concern in this analysis.

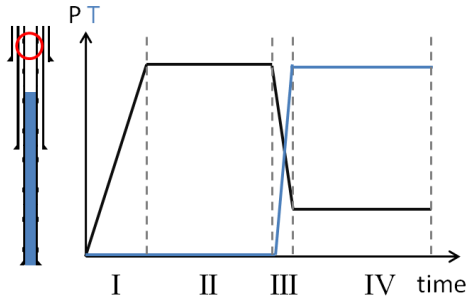

Figure 13: Conceptual load case phases uppermost in the well (red circle) above the water table; I.-II. Pressure buildup, III. Discharge and IV. Production.

The pressure change before and after the discharge can be seen in Figure 14. The pressure difference (from the blue to the green curve) is based on measurements at well HE-46 and is used as a load in the analysis.

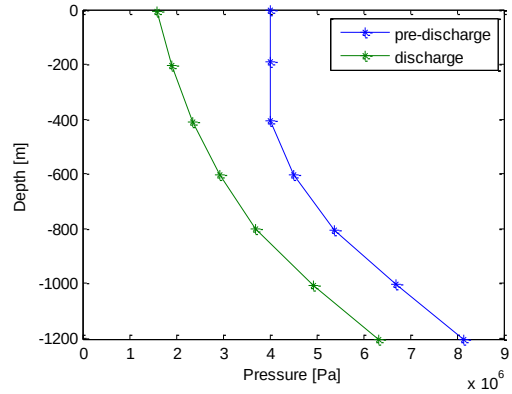

Figure 14: Pressure load on the structural model. The difference between the pre-discharge and the discharge pressure profile.

The static structural analysis is solved using a nonlinear static solution method, where the numerous nonlinearities, i.e. contact elements, nonlinear material properties and large deformation effects, are accounted for. The transient structural analysis is

solved using a nonlinear transient solution method with time-dependent loading.
The results from both solution methods, i.e. static and transient, show that the production casing moves almost freely inside the wellhead. The casing, with the help of the external couplings, overcomes the friction with the concrete in connection with the outer casing and pulls it up, as can be seen in Figure 18. This occurs because of the thermal expansion of the casing and the concrete. The ratio of damaged concrete, i.e. the concrete that has surpassed the compressive and tensional strength of the concrete used in the well, can also be seen in Figure 15. The high ratio above 150°C is mainly concrete in tension at the top of the well as well as concrete near the couplings of the production casing. Figure 16 shows how the concrete is more likely to get damaged around the couplings. This is consistent with the results from a three dimensional collapse model by Kaldal (2011).

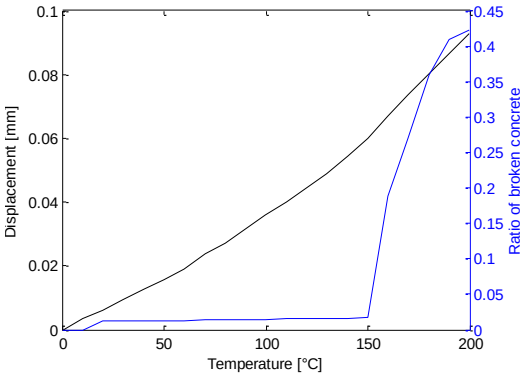

Figure 15: Steady-state results of the wellhead rise at various temperatures and the ratio of broken concrete around the production casing.

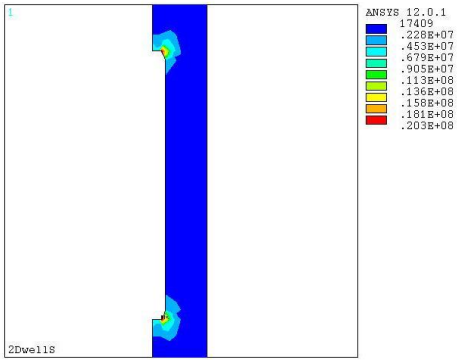

Figure 16: Stress (Von Mises, MPa) in the concrete surrounding one of the coupling on the production casing (only the concrete is visible).

In Figure 17 the steady state discharge results show a wellhead rise of 92.3 mm and a maximum displacement of 665 mm of the production casing inside the wellhead.

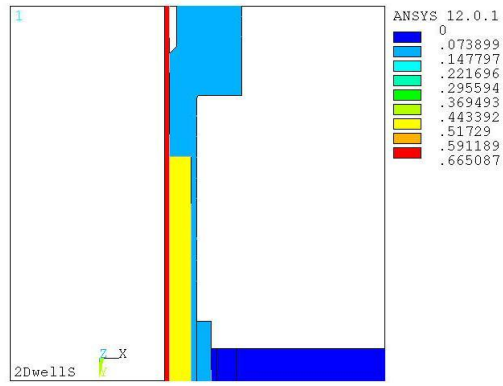

Figure 17: The steady-state results of the wellhead rise at 200°C at the top. Total wellhead rise of 92.3 mm and maximum displacement of the production casing inside the wellhead of 0.665 m.

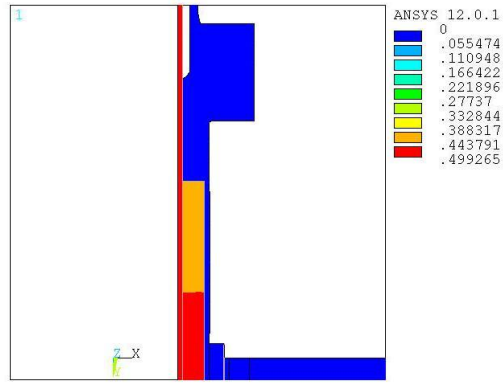

Figure 18: The wellhead rise 48 seconds after initiating discharge. Wellhead rise of 37 mm.

The transient wellhead rise in Figure 18, 48 seconds after discharge, shows that the production casing rises faster than the wellhead, because the temperature of the production casing is much higher in the beginning than the temperature of the security casing connected to the wellhead.
If the transient results from the model are compared to the measured wellhead rise of well HE-46, in Figure 19, it can be observed that the measured wellhead rise is fast at the beginning and then slows down. The FEM results also show a fast wellhead movement in the beginning but the rise is about four times larger then the measured values. This could be explained by additional constraints on the actual wellhead compared to the modeled wellhead. The measured wellhead includes additional "spider" constraint, that consists of four tension bars, as well as a bulky concrete cellar which provides additional constraints. This is not included in the model. The

FEM results can be regarded as the unconstrained wellhead results, but it should be noted that further analysis and measurements are needed to validate the model.

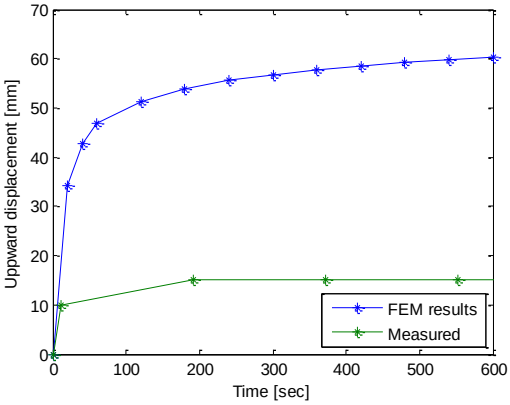

Figure 19: Wellhead displacements of the first ten minutes of the discharge.

CONCLUSION

Measurements of pressure, temperature and wellhead movement during discharge of well HE-46 in the Hellisheiði high temperature geothermal area, south-west Iceland, have been presented in this study. The measured outer temperature of the expansion spool showed that the temperature increases quickly in the first few minutes as expected. The pressure measurements showed fluctuations during the discharge, where the pressure decreased rapidly initially and then increased again up to a steady value. The monitoring of the wellhead movement showed a rise of 15 mm in one minute and then the wellhead continued to rise up to 22 mm in the next two hours.

An axially symmetric two dimensional nonlinear transient thermal and structural finite element model of a high temperature geothermal well was presented and used to simulate the discharge of well HE-46. The results were then compared to the measurements performed on the well during discharge. The results from a one dimensional transient thermal model showed the thermal response of the uppermost layers of a well with three casings. These results showed that the thermal response of the well is fast and the temperature increased to roughly 95% of the final temperature in only few hours. Thermal equilibrium is reached after 20 days according to the one dimensional model. The two dimensional thermal results showed the temperature change during a discharge of a high temperature geothermal well based on the measurements of well HE-46. The results were used as an input load for a transient structural model used to calculate the structural response due to thermal and pressure loads.

Results from the steady state structural analysis showed a wellhead rise of 92.3 mm and a rise of 665 mm of the production casing inside the wellhead. Results from the transient structural analysis showed a wellhead rise of 48 mm during the first minute of discharge while the measured wellhead rise during the first minute was 12 mm. This indicates that the modeled wellhead is not as well constrained as the actual wellhead. It should be noted that the friction between contacting surfaces is probably the main uncertainty in the analysis. The additional constraint of the actual wellhead could also be explained by the "spider" support which consists of four bars in tension on top of the wellhead and holds the wellhead in place as well as by the additional weight of the wellhead and the concrete cellar around it.

A structural model of an underground structure is hard to validate with actual displacement or strain measurements below the surface. The validation must therefore mostly rely on measurements above the surface, such as of the rise of the wellhead during discharge as well as strain measurements on the pipe walls at the wellhead. Other measurements, such as tensile tests of the steel used in the casings and push-out tests to valuate the steel-concrete interaction, are also important for the model. It is clear that additional measurements during discharge must be performed in order to be able to validate the model adequately. Once the model has been validated, it can provide a variety of information regarding displacements and stress of the well in its entirety. Future work will involve analysis of the breakage of the concrete near the couplings in more detail. Another interesting topic is a comparison of different wellhead designs in order to find the optimal design in discharge situations of high temperature geothermal wells.

ACKNOWLEDGMENT

This work was supported by the University of Iceland research fund, the Technology Development Fund at RANNIS - The Icelandic Centre for Research, the Innovation Center Iceland and GEORG - Geothermal Research Group. Their support is much appreciated.

REFERENCES

Axelsson, G., Thórhallsson, S., Björnsson, G. „Stimulation of geothermal wells in basaltic rock in Iceland.“ Kartause Ittingen, Zurich: ENGINE – ENhanced Geothermal Innovative Network for Europe, Workshop 3, Switzerland, 2006.

Kaldal, G. S., „ Load History and Buckling of the Production Casing in a High Temperature Geothermal Well.“ *Proceedings, Thirty-Sixth*

Workshop on Geothermal Reservoir Engineering Stanford University, 2011.

Karlsdóttir, S. N., Thorbjornsson, I. O. „High Temperature Geothermal Wells – Center of Excellence in Iceland - Phase I: Corrosion testing of steel in high temperature geothermal wells in Iceland.“ Technical Report for RANNIS (The Icelandic Centre for Research), Reykjavik, Oct., 2009.

Magnúsdóttir, L. „Nonlinear Finite Element Model of a Geothermal Well.“ *Master thesis at the University of Iceland*, 2009.

Ólafsson, Á. „Structural and Stress Analysis of a High Temperature Geothermal Wellhead.“ *Master thesis at the University of Iceland*, 2011.

Pálmason, G. *Jarðhitabók (in Icelandic).* Reykjavík: Íslenskar orkurannsóknir og Orkustofnun, 2005.

Peng, S., Fu, J., Zhang, J. „Borehole casing failure analysis in unconsolidated formations: A case study.“ *Journal of Petroleum Science and Engineering 59*, 2007: 226-238.

Philippacopoulos, A. J., Berndt, M. L. „Characterization and Modeling of Cements for Geothermal Well Casing Remediation.“ San Francisco, California: Geothermal Resources Council, 2000.

Philippacopoulos, A. J., Berndt, M. L. „Structual analysis of geothermal well cements.“ *Elsevier Science Ltd.*, 2002.

„Portland Cement, Concrete, and Heat of Hydration.“ *Concrete Technology Today (Portland Cement Association)*, nr. Volume 18/Number 2 (July 1997).

Sigurðsson, Ó. „Nýjung við örvun borholna á Íslandi.“ *Fréttaveitan, HS-orka newsletter (in Icelandic)*, 2010: 10-11.

Teodoriu, C., Falcone, G. „Fatigue Life Prediction of a Buttress Casing Connection Exposed to
Large Temperature Variations“ *Proceedings, Thirty-Third Workshop on Geothermal Reservoir Engineering Stanford University*, 2008.

Paper III

PROCEEDINGS, Thirty-Eighth Workshop on Geothermal Reservoir Engineering
Stanford University, Stanford, California, February 11-13, 2013
SGP-TR-198

COLLAPSE ANALYSIS OF THE CASING IN HIGH TEMPERATURE GEOTHERMAL WELLS

Gunnar Skúlason Kaldal[1]*, Magnús Þ. Jónsson[1], Halldór Pálsson[1], Sigrún N. Karlsdóttir[1,2]

[1] Faculty of Industrial Engineering, Mechanical Engineering and Computer Science, University of Iceland, Hjarðarhagi 2-6, 107 Reykjavík, Iceland
[2] Innovation Center Iceland, Department of Materials, Biotechnology and Energy, Keldnaholt, Reykjavik, 112, Iceland
*e-mail: gunnarsk@hi.is

ABSTRACT

Casing failures such as collapse is the suspected result of combined loads and impurities in the casing and/or the surrounding concrete. In this paper a simple case of collapse caused by a geometric defect in the casing is analyzed using the finite-element method (FEM). The collapse of an impaired casing and its resulting shape is investigated with respect to the external supporting concrete. A specific load history for the production casing is used in the analysis. The first load consists of the external pressure of the cement slurry during well cementing, followed by subsequent cyclic thermal loads. The load history represents the fundamental loads which occur during the lifetime of a typical well. The magnitude of the external pressure and its stimulus for later collapse is also analyzed. The collapse shape obtained in the FEM analysis is similar to collapse shapes that have been observed in geothermal wells.

INTRODUCTION

High temperature geothermal wells are constructed of several concentric steel casings with cement in between the casing walls. The structural integrity of such well casings is essential for the utilization of high temperature geothermal wells. Casing failures can lead to a reduced energy output from the well, render the well inoperative and in worst cases cause unsafe conditions above the surface.

Casing failures such as collapse are the result of combined loads and impurities in the casing and/or surrounding concrete. Collapse or bulging of geothermal well casings is an example of a serious casing failure. Bulging is referred to as the buckling shape where the collapse occurs on one side of the cross section of the casing. This bulging collapse shape is related to the external support of the concrete and it only occurs when this support is present.

A well with a decreased cross sectional area, due to a collapsed production casing, produces less than an intact well, since the output of the well is proportional to the cross sectional area of the casing (Thorhallsson 2006). If the casing gets damaged, for example by tearing or collapse, the risk of well blow-out or more catastrophic well failures increases. Therefore, it's important to understand fully the structural system and its response to various loads during well operations. Accordingly, it is important to recognize the expected load history of the structure so that the deformation and stress fields that form during the lifetime of the well can be anticipated.

Analysis of the bulging collapse shape is the motivation for this paper. A simple case of collapse caused by a geometric defect in the casing is analyzed using the finite-element method (FEM). The collapse of the impaired casing and its collapse shape is investigated with respect to the presence of external supporting concrete.

The collapse of pipes in general has been profusely studied, often in connection to specific topics. Such analysis has been performed for the necessity of economical design and safety dating back to the end of the industrial revolution where the resistance of tubes to collapse was studied extensively and empirical equations were derived from numerous experiments (Fairbairn 1858). Since then many studies have been performed on the subject to improve empirical equations of pipe collapse. Casing collapse is highly dependant on geometrical imperfections of the casing. In collapse experiments, imperfections like the average outside diameter, average wall thickness, eccentricity and ovality have been measured and predicted with (empirical) equations (C. R. Kennedy et al. 1962, ISO/TR 10400:2007(E)). Collapse of well casings is an example of a specific case of pipe collapse. Collapse due to external pressure, e.g. during cementing, is similar to other cases of pipe collapse such as in deepwater sea-floor pipelines due to ambient external pressure. Effects of defects on the collapse pressure of pipes have been studied with experiments and finite element models (Assanelli et al. 1998,

Sakakibara et al. 2008, Netto 2009). The bulging collapse of well casings, that takes place during well operations after well completion, is a different case because of the lateral/radial support of the external concrete. This is to some extent comparable to horizontal soil supported pipes that have greater capacity to withstand net external pressures than pipes without support (Watkins and Anderson 2000). In well-compacted soil the cross section remains sensibly circular until failure by wall-buckling takes place (Bulson 1983). Likewise for burst design, the support of the external cement sheath increases the burst resistance of casings (Kalil et al. 2011). Collapse of pipes is caused by excessive net external pressure as well as instability due to various impurities. For concrete supported casings, instability in the casing to casing annulus is introduced, e.g. due to off centered casing and trapped fluid. Casing failure as a result of the expansion of trapped fluid in the annulus between casings has been discussed to a certain extent as a suspected cause of casing bulge collapse (Björnsson et al. 1978, Magneschi et al. 1995, Southon 2005).

In the remaining sections casing impurities and collapse loads are discussed, a three dimensional finite element model of a casing with a small geometrical defect is described, and finally collapse analysis results are presented and discussed.

CASING IMPURITIES AND COLLAPSE LOADS

A complete collapse of casings is a buckling shape that is governed by uniform external to internal differential pressure. The empirical equations used in standards for collapse resistance of casings is based on combined theoretical, numerical and statistical tools (ISO/TR 10400:2007(E)). These empirical equations do however not account for external supporting concrete and non-uniform loads and are also considered to be rather conservative.

In general, the ratio of outer diameter to thickness (*D/t*) determines whether collapse occurs in the elastic-, plastic- or intermediate range of the wall compressive stresses. For high values of the *D/t* ratio, elastic collapse is a governing factor. For lower values, the buckling occurs in the plastic range and for the lowest values the buckling is governed by the yield strength of the material (10400:2007(E) 2007). The critical elastic buckling pressure for long tubes under uniform radial pressure is

$$p_{cr} = \frac{E}{4(1-\nu^2)}\left(\frac{t}{R}\right)^3$$

(Timoshenko 1961, Bulson 1983, Chater and Hutchinson 1984) where ν is Poisson's ratio, E is Young's modulus, t is the tube thickness and R is the tube radius. This equation does however not account for collapse as a result of plastic deformation in the material which occurs in thicker casings. For thicker casings a tangent modulus, E_t is used in place of E, to find the critical buckling pressure beyond the proportional limit.

After completion of geothermal wells the concrete surrounding the production casing provides a structural support for the casing. When the well warms up, the concrete restrains the thermally expanding casing and limits both axial and radial movement to some extent. The bulging collapse shape, seen in Figure 1, only occurs in completed wells. The concrete support restricts the radial movement which results in a different collapse shape from that seen in casings without external support. Furthermore, the buckling shape suggests instability that is caused by non-uniform conditions on the outer surface of the casing.

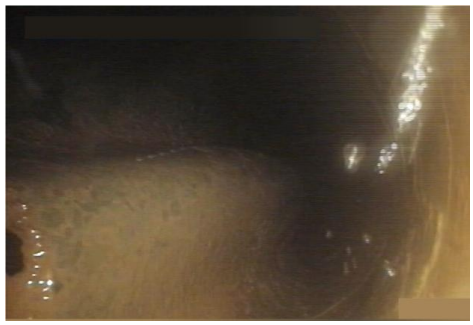

Figure 1: The buckling shape of a collapsed casing with external concrete support[1].

The collapse of casings in completed wells is the result of combined loads, e.g. pressure and temperature, and impurities in the casing and/or surrounding concrete.

It is well documented that geometric imperfections, e.g. average outside diameter, average wall thickness, eccentricity, and ovality, reduce the collapse resistance of casings. Defects, such as pitting due to external corrosion, external casing damage or other asymmetric conditions, also cause instability that can result in premature casing collapses.

Although the concrete should act as a pressure seal, concrete damage and impurities could lead to non-uniform conditions around the circumference of the casing. Instability can be caused by an off-center casing which can cause water/mud accumulation at the narrower side of the annulus due to lower flow rate during cementing. This could lead to fluid entrapment at one side of the annulus.

[1] Courtesy of HS Orka hf.

Material impurities and manufacturing residual stress result in decreased collapse resistance as well. Furthermore, corrosion can cause serious production casing failures. It can be very different between geothermal regions and even different within a geothermal region, for example from well to well or even varying with depth. For H_2S rich environments sulfide stress cracking (SSC) and hydrogen embrittlement can cause problems depending on the material selection for the steel casing (Kane 1996). No general solution of corrosion problems in geothermal wells exists and each case needs to be treated separately.

External to internal differential pressure is the main cause for the collapse of pipes. External casing pressure can be the result of thermally expanding fluids in the annulus during discharge. Wellbore pressure fluctuations due to cavitation and slug flow could also cause local casing collapse.

The maximum pumping pressure at the top of the well is described with

$$P_{pump} = P_{CR} - P(z)$$

where P_{CR} is the API rated collapse resistance of the casing, z is the casing depth and $P(z)$ is the hydrostatic differential pressure of external concrete and internal water at the bottom of the casing. While the casing is being cemented on the outside, the inside is filled with cold water. If however this is neglected and in addition the external concrete pumping pressure gets too high, the casing can collapse due to excessive external pressure. Excessive pumping pressure could also merely create a deformation in the casing which could end in collapse due to subsequent wellbore loads, e.g. cyclic thermal loading.

Cracked or otherwise damaged concrete can also cause external pressure load on the casing, for example if small steam channels form or if water is present in the annulus when the well is discharged.

The effect of temperature is twofold since it produces thermal stresses in the casing and lowers the strength of the material. The latter occurs at high temperatures, around 300°C and above. Collapse of pipes as a result of temperature loading is not as well documented as collapse from external pressure, but cyclic temperature loading could ultimately lead to collapse or tearing of the casing.

A combination of geometric imperfections, material impurities and dynamic loading, such as local cavitation or rapid temperature change during discharge (or cooling), are likely causes of casing collapse.

MODELING

The finite element method (FEM) is used to construct a three dimensional model of the casing. The model is divided into two parts, thermal and structural. If thermal loads are to be included in the structural analysis, the change in temperature is first calculated in the thermal part of the model and the temperature distribution results are then used as load for the structural part. Eigenvalue buckling analysis is used to predict the theoretical collapse strength and the collapse mode shapes of the casing. The eigenvalue analysis is a linear solution method in which nonlinear properties, e.g. interaction of contacting surfaces, are not taken into account. Nonlinear buckling analysis is then used to account for nonlinearities which are found in the (i) material properties, (ii) large geometrical displacements and (iii) connectivity between contacting surfaces (contact elements). The limit load of the casing is obtained and stabilization is used to track the post-buckling shape of the casing.

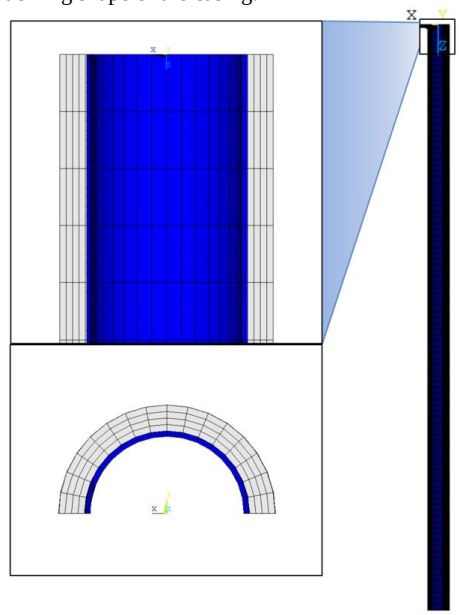

Figure 2: The geometry of the finite element model.

Available data on the stress-strain behavior of K55 casing steel and compressive strength of the concrete is used in the model. The stress-strain curves for the casing steel were obtained from standardized tensile tests (Karlsdottir 2009). The maximum compressive strength of concrete is defined as 27.6 MPa in the analysis. When the maximum compressive strength is reached the concrete is assumed to yield plastically. The material properties used in the FE analysis are listed in Table 1.

Table 1: Material properties used in the FE analysis (non-linear MP are discussed in the text).

	Steel	Concrete
Young's modulus (E) [GPa]	205	2,79
Poisson's ratio (γ)	0.3	0.15
Density (ρ) [kg/m^3]	7850	1666
Th.conductivity (K) [W/(m°C)]	46	0.81
Specific heat (c) [kJ/kg°C]	0.49	0.88
Thermal expansion (α) [1/°C]	12e-6	9e-6
Compressive strength (f_c) [MPa]	-	27.6
Coefficient of friction (μ)	0.5	
Max shear stress (τ_{max}) [MPa]	0.72	

The finite-element program Ansys is used to construct the model. Contact element pairs are used between contacting surfaces. Their main purpose is to prevent surfaces to intersect each other, while still allowing gap formation and tangential movement between casing and concrete. The Coulomb friction model is used to describe friction between contacting surfaces, where they can withstand shear stresses up to a certain magnitude across their interface before they start sliding relative to each other(Release 11.0 documentation for ANSYS 2007). Once the equivalent shear stress exceeds τ_{max} relative sliding begins. The friction model is defined as:

$$\tau_{lim} = \mu P + b$$
$$|\tau| \leq \tau_{lim}$$

where τ is the equivalent shear stress, τ_{lim} is the limit shear stress, μ is the isotropic coefficient of friction, b is the contact cohesion and P is the contact normal pressure, see Figure 3 for the graphical interpretation of the Coulomb friction model.

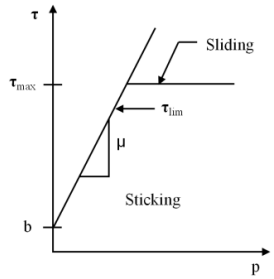

Figure 3: The Coulomb friction model in Ansys (Release 11.0 documentation for ANSYS 2007).

The geometry of the casing model is shown in Figure 2. A 12 meter section of the production casing is modeled in three dimensions. The concrete around the production casing is also included and for simplification external casings are not included. No radial displacement is allowed at the outer radial boundary of the concrete and axial displacements are constrained at both ends. The geometrical parameters that are used in the analysis are shown in Table 2. Half of the casing is modeled, which is possible due to the symmetry of the casing and its collapse shape. The thickness of the pipe wall is scaled with the manufacturing tolerance which is assumed to be −12,5% in the analysis.

Table 2: Geometrical parameters for the FE analysis.

	in	mm
Outer diameter of casing (*D*)	13 3/8	339.7
Thickness of casing (*t*)	0.48	12.2
Thickness of concrete (t_c)	2.10	53.4

Due to the perfect geometry of the model some imperfections or perturbations need to be introduced to create instability in the structure. Instead of applying a small radial force, which is a common practice, instability is created with randomly distributed material imperfections in the steel casing. These imperfections are included in the casing as small variations in material properties. Overview of the diminished casing used in the analysis can be seen in Table 3.

Table 3: Diminished casing overview

	%
Manufacturing tolerance	-12.5
Random material imperfections	20
Local external defect	10-50 of thickness

The effect of a small local defect, located on the outside of the production, casing is also analyzed. The size and shape of the defect is controlled by three parameters; thickness, angle size and length, see Figure 4. The defect can be interpreted as pit corrosion, defect or damage for example from scratching while running down the casing.

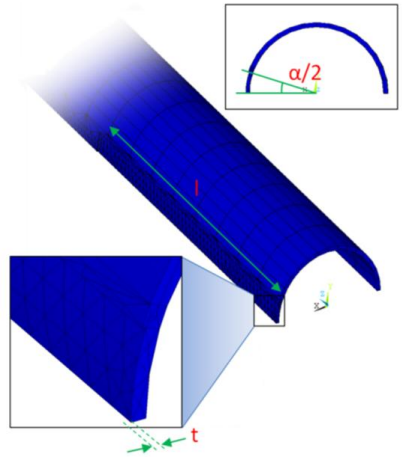

Figure 4: Size and shape of the external defect of the casing.

RESULTS

Eigenvalue buckling analysis is used to predict the theoretical collapse strength or the bifurcation point of a perfectly round casing subjected to uniform external pressure. Manufacturing tolerance of −12,5% is used to scale the wall thickness of the casing. Theoretical collapse strength values for mode shapes 1-8 are listed in Table 4 and the obtained collapse mode shapes can be seen in Figure 5.

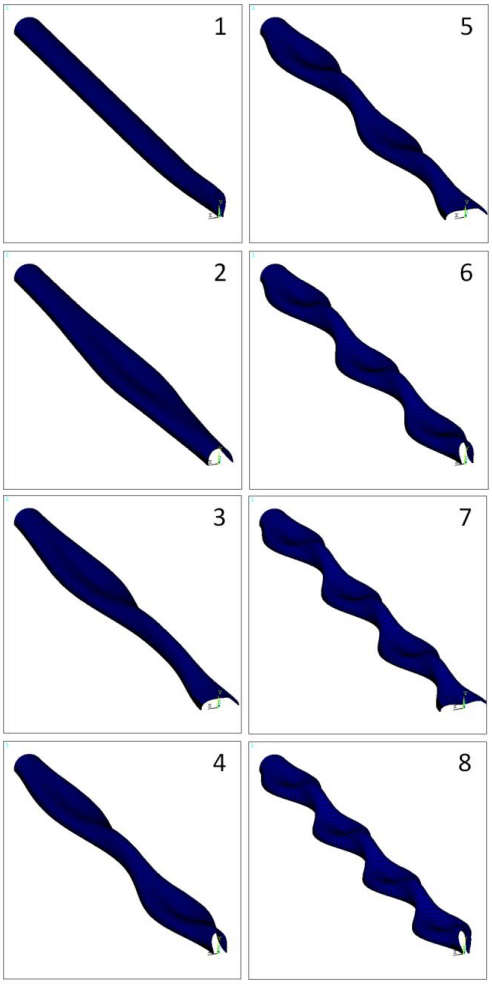

Figure 5: Collapse mode shapes 1-8 of the production casing (eigenvalue buckling analysis).

The theoretical collapse strength values obtained from the eigenvalue buckling analysis are slightly higher than the calculated API collapse resistance which is calculated as 13.4 MPa. There are no imperfections in the casing and the standard is known to provide rather conservative values for the collapse resistance. This implies that the eigenvalue buckling analysis underestimates the actual limit load of the casing although the results give a close match to the API collapse resistance.

Table 4: Theoretical collapse strength of the modeled casing using eigenvalue buckling analysis. API collapse resistance of this casing is calculated as 13.4 MPa.

Mode shape nr.	Theoretical collapse strength [MPa]	% of API collapse resistance
1	14.4	107.1
2	14.5	107.9
3	14.5	108.4
4	14.7	109.6
5	15.1	112.4
6	15.7	117.1
7	16.7	124.9
8	18.1	135.3

Nonlinear buckling analysis is used to predict the actual collapse limit load. Nonlinearities are now accounted for the casing. Additionally, the first mode shape from the eigenvalue buckling analysis is scaled down and used as perturbation to the initial geometry for the nonlinear buckling analysis. The limit load for the collapse is determined as 21.6 MPa, see Figure 6, which is higher than the theoretical collapse strength (bifurcation point) obtained in the eigenvalue buckling analysis. This is in agreement with the statement above that the linear eigenvalue buckling analysis probably underestimates the collapse strength of the casing.

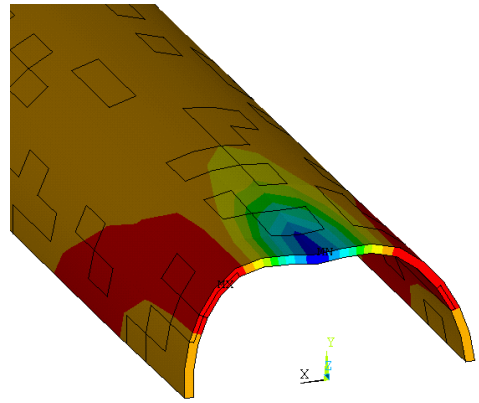

Figure 6: Initiation of collapse of a casing without geometrical defect. A nonlinear buckling analysis with the first mode shape scaled and used as perturbation. Collapse occurs at 21.6 MPa.

In Figure 7, load-displacement collapse curves are plotted for a perfectly round casing as well as a casing mode shape perturbation. The collapse limit load of a perfectly round casing is 38.4 MPa. For first mode shape perturbation the collapse occurs at 26.4 MPa and 21.6 MPa for scaling constants of 0.0005 and 0.001, respectively.

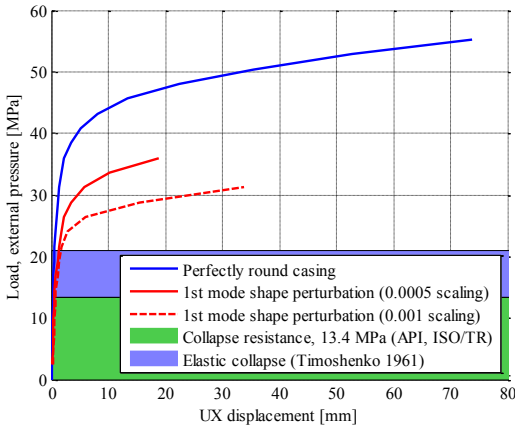

Figure 7: Effect of initial geometry on collapse. Perfectly round casing and mode shape perturbation. Results from a nonlinear buckling analysis.

The effect of ovality on collapse strength of the casing is analyzed. Ovality of pipes is defined as

$$\text{Ovality} = \frac{D_{max} - D_{min}}{D}$$

where D_{max} is the maximum outer diameter, D_{min} is the minimum outer diameter and D is the mean outer diameter.

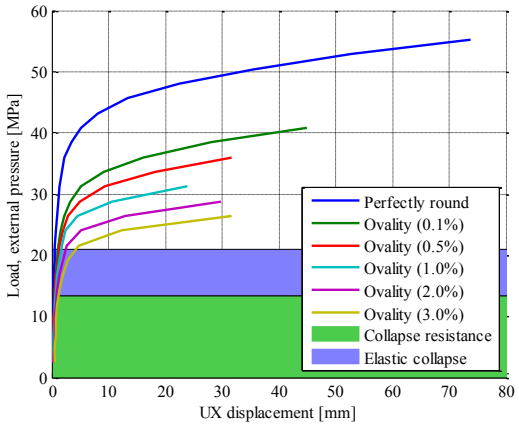

Figure 8: Effect of casing ovality on collapse. Results from a nonlinear buckling analysis.

Collapse curves of casings with ovality of 0.1% - 3.0% can be seen in Figure 8 and the collapse limit loads are listed in Table 5.

The effect of a geometric defect on the external surface of the casing is analyzed. First, the extreme case is analyzed where the defect depth is 0.5 times the casing thickness, 20° in circumference and one meter long. The collapse resistance of a casing with and without the structural support of the external concrete is analyzed as well, see Figure 9.

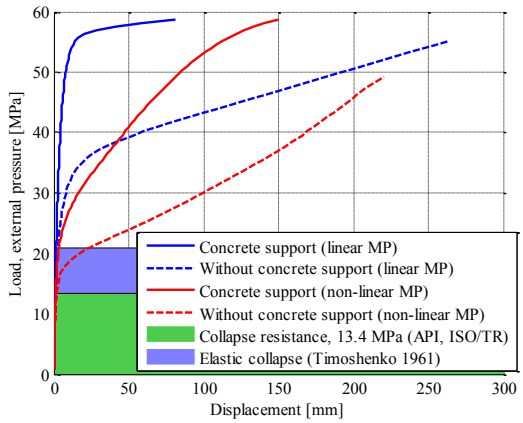

Figure 9: The effect of concrete structural support to the casing. Load-displacement collapse and post-collapse curves of an extreme defect case where the defect depth is 50% of the casing thickness.

The effect of nonlinear material properties, i.e. nonlinear stress-strain curves for K55 steel, are also compared and can be seen in Figure 9. The collapse limit load of the casing without concrete support is 14.4 MPa and with concrete support it increases to 18.1 MPa. Using linear material properties, the collapse limit load for same cases is 37.2 MPa and 56.4 MPa. When nonlinear material properties are used, plastic deformations take place which creates instability and leads to collapse. Conversely, when linear material properties are used, the casing remains stable until it collapses elastically. Why the elastic collapse does not match the theoretical elastic collapse, seen in blue box on the graphs, can be explained by the *D/t* ratio of the analyzed casing which collapse is determined by the transition between plastic and elastic collapse. The collapse and post-collapse shape with and without concrete structural support can be seen on the section diagrams in Figure 10.

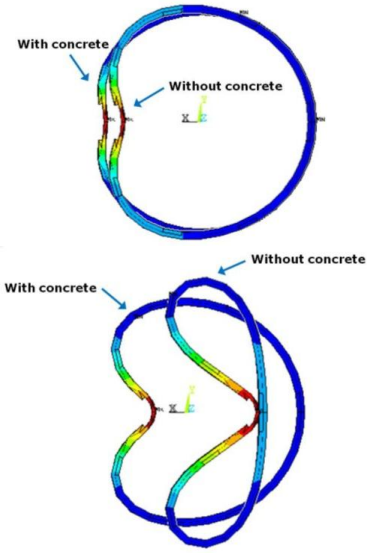

Figure 10: Collapse shapes of a casing with external defect depth of 50% the casing thickness, with and without concrete support (concrete not shown). Initiation of collapse (above) and post-collapse (below).

The effect of defect dept on the collapse shape of a casing supported by external concrete is analyzed as well. Defect depths of 10% to extreme 80% of the casing thickness can be seen in Figure 12. At 10% the defect merely makes the casing unstable but the location of the defect does not dominate the location of the collapse. At 20-30% the collapse is located at the defect but the deformation is relatively small.

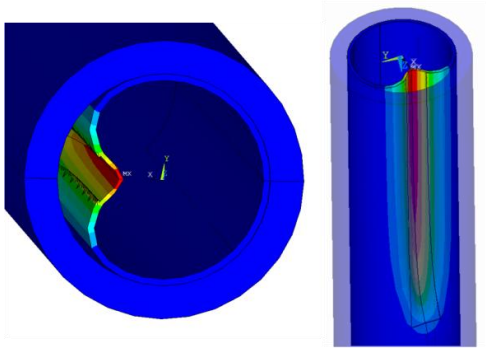

Figure 11: A collapsed casing with external defect depth of 40% of the thickness of the casing. Collapse load of 15.3 MPa.

At 40% defect depth, also seen in Figure 11, the deformation of the collapse becomes substantial, both inward and along the length. The radial displacement is 85mm and the length of the deformation is approximately 2 meters, twice as long as the defect length. For the cases of 50% to 60%, which are extreme cases unlikely to exist in reality, the deformation is similar to the 40% case, but cases above 70% the collapse becomes local to the defect and begins to resemble plate buckling. Collapse curves of various defect depths can be seen in Figure 13 and corresponding limit loads are listed in Table 5.

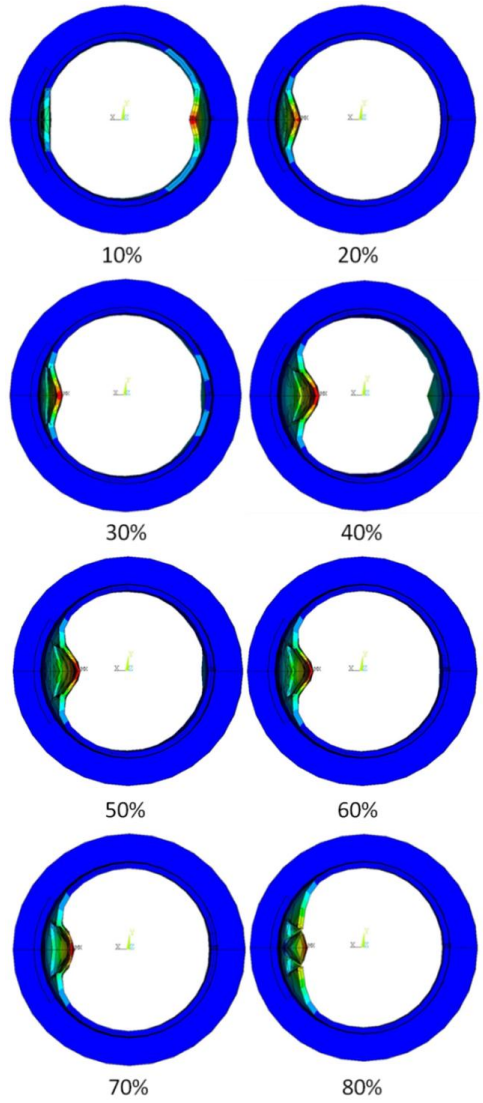

Figure 12: Effect of external defect depth on the collapse shape (percentage of casing thickness). End view of the casing and external concrete.

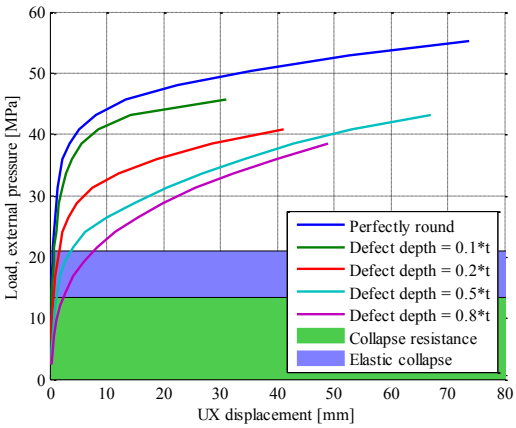

Figure 13: Effect of external defect depth on collapse.

A summary of the effect of initial geometry on collapse limit load can be seen in Table 5.

Table 5: Summary; effect of initial geometry on collapse. Mode shape perturbation, ovality and external defect. API collapse resistance of this casing is calculated as 13.4 MPa.

Initial geometry	Collapse limit load [MPa]	% of API collapse resistance
Without external concrete:		
Perfectly round	38.4	287
1st mode shape (0.0005)	26.4	197
1st mode shape (0.001)	21.6	161
Ovality (0.1%)	26.4	197
Ovality (0.5%)	24.0	179
Ovality (1.0%)	22.8	170
Ovality (2.0%)	21.0	157
Ovality (3.0%)	19.8	148
External defect (0.5*t)	14.4	107
With external concrete:		
External defect (0.1*t)	33.6	251
External defect (0.2*t)	25.2	188
External defect (0.5*t)	15.6	116
External defect (0.8*t)	12.0	89.6

The effect of a small deformation due to external pressure and its stimulus on subsequent collapse due to cyclic thermal loads is analyzed. A casing with external defect depth of 40% of the casing thickness is used in the analysis. The external pressure, which can be looked at as an excessive concrete pumping pressure, generates a small permanent deformation in the casing. Pressure is excluded from the analysis after the first load step to observe the thermal effect.

The thermal distribution for the cyclic thermal analysis can be seen in Figure 14.

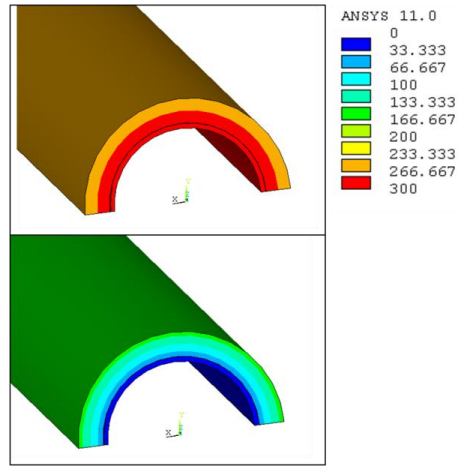

Figure 14: Thermal load used in the analysis; warm-up (above) and cooling (below).

The load history used in the analysis consists of external pressure which is then removed to see the resulting plastic deformation, following is cyclic thermal load which consists of a temperature difference of 300°C. This is a steady-state analysis so transient effects, such as rapid cooling, are not included. Pressure, reaching from 10 MPa to excessive 20 MPa, is subjected on the external surface of the casing which for pressure above 10 MPa results in plastic deformation.

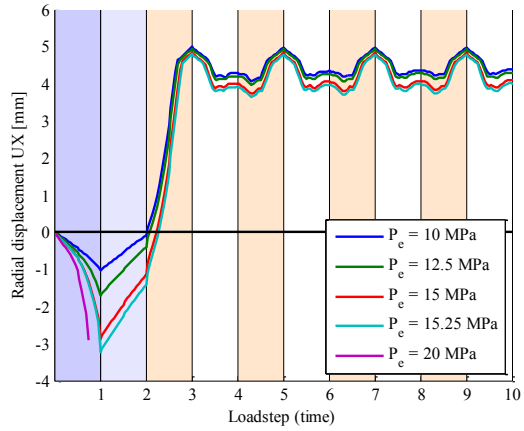

Figure 15: Initial external pressure and its effect on subsequent deformations. Blue: external pressure load, light blue: pressure removed, red: warm-up to 300°C, white: cooling.

Pressure above 15.3 MPa collapses the casing before temperature load is applied. Radial displacement curves can be seen in Figure 15. During cooling, stress relaxation is followed by tensile stress buildup in the casing, which goes beyond the proportional limit of the stress-strain curve of the steel. Because the radial displacement is still positive, this reverses the displacement of the defect, initially moving inward, forcing the displacement outwards again. By using linear material properties, see Figure 16, this does not occur. As the load history shows, subsequent collapse due to excessive initial pressure does not occur.

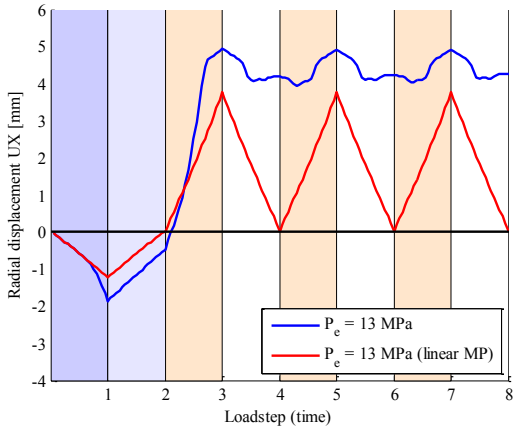

Figure 16: Nonlinear material properties and linear material properties compared.

CONCLUSION

In this study collapse limit loads of casings were analyzed with respect to pressure and temperature loads combined with casing imperfections with and without external concrete support. Eigenvalue buckling analysis was used to find the collapse mode shapes of a geometrically perfect casing. Nonlinear buckling analysis showed that the limit load for the casing was higher than the theoretical collapse strength (bifurcation point) of the eigenvalue buckling analysis, indicating that the eigenvalue buckling analysis underestimated the collapse strength of the casing.

The effect of initial geometry on collapse was analyzed. The collapse limit load of a perfectly round casing was compared to casings with geometry perturbation of the first mode shape from the eigenvalue buckling analysis. The casings with the mode shape perturbation showed reduced collapse strength of approximately 30-50%, using two scaling factors for the first mode shape. The reduction in collapse strength due to ovality was also analyzed. It showed that slight ovality reduces the collapse strength of the casing substantially. The effect of external defect and the defect depth on the collapse strength and collapse shape was analyzed. Modeled collapse shapes of a casing subjected to external pressure with and without the support of concrete were obtained. The latter resembled bulge collapse shapes documented in high temperature wells.

A load history was used consisting of external pressure followed by cyclic temperature difference of 300°C. The results showed that the initial pressure did not result in subsequent collapse. This is partly due to the nonlinear behavior of stress-strain curves of steel when reaching beyond the proportional limit.

It is apparent that a combination of factors cause casing failures. The load, consisting of temperature and pressure changes, and the load history is probably the main contributor. When subjected to load, imperfections in casings and surrounding concrete have also proved to play a big role in the generation of casing failures such as casing collapse.

Future work will involve analyzing more load histories and including transient loads, such as wellbore pressure fluctuations due to cavitation and slug flow, as well as further studying casing and concrete imperfections.

ACKNOWLEDGMENT

This work was supported by the University of Iceland research fund, the Technology Development Fund at RANNIS - The Icelandic Center for Research, the Innovation Center Iceland and GEORG - Geothermal Research Group. Their support is much appreciated.

REFERENCES

10400:2007(E), ISO/TR. *ISO/TR 10400, Petroleum and natural gas industries - equations and calculations for the properties of casing, tubing, drill pipe and line pipe used as casing or tubing.* Geneva: ISO copyright office, 2007.

Andrea P. Assanelli, Rita G. Toscano, Eduardo N. Dvorkin. „Analysis of the Collapse of Steel Tubes Under External Pressure.“ *Computational Mechanics*, 1998.

Björnsson, G., Ragnars, K., Sigfússon, S., Karlsson, Þ. *Styrkleiki fóðurröra í háhitaborholum (OS JHD 7805) (in Icelandic).* Reykjavík: Orkustofnun, 1978.

Bulson, P. S. „The Stability of Underground Cylindrical Shells.“ Í *Developments in Thin-Walled Structures - 1*, by J Rhodes og A. C. Walker, 53-80. Essex, England: Applied Science Publishers, 1983.

C. R. Kennedy, J. T. Venard. *Collapse of Tubes by External Pressure.* U. S. Atomic Energy Commision, 1962.

Chater, E., og J. W. Hutchinson. „On the Propagation of Bulges and Buckles.“ *Journal of Applied Mechanics*, 1984.

Fairbairn, William. „On the Resistance of Tubes to Collapse.“ *Philosophical Transactions of the Royal Society of London*, 1858: 389-413.

Kalil, Issa A., McSpadden, Albert R. „Casing Burst Stresses in Particulate-filled Annuli: Where's the Cement?“ *SPE/IADC Drilling Conference and Exhibition, 1-3 March 2011*. Amsterdam, The Netherlands: 2011. SPE/IADC Drilling Conference and Exhibition, 2011.

Karlsdottir, S. N., Thorbjornsson, I. O. „High Temperature Geothermal Wells – Center of Excellence in Iceland - Phase I: Corrosion testing of steel in high temperature geothermal wells in Iceland.“ Technical Report for RANNIS (The Icelandic Centre for Research), Reykjavik, Oct., 2009.

Magneschi, P., Bagnoli, C. , Lazzarotto, A. , Ricciardulli, R. „Structural Models for the Analysis of Stresses in the Casings of Geothermal Wells.“ World Geothermal Congress, 1995.

Naoto Sakakibara, Stelios Kyriakides, Edmundo Corona. „Collapse of Partially Corroded or Worn Pipe Under External Pressure.“ *International Journal of Mechanical Sciences*, 2008: 1586-1597.

Netto, T.A. „On the effect of narrow and long corrosion defects on the collapse pressure of pipelines.“ *Applied Ocean Research*, 2009: 75-80.

Release 11.0 documentation for ANSYS. SAS IP, Inc., 2007.

Southon, J. N. A. „Geothermal Well Design, Construction and Failures.“ Auckland, New Zealand: Proceedings World Geothermal Congress 2005, 2005.

Thorhallsson, Sverrir. „New Developments in Geothermal Drilling.“ *Workshop for Decision Makers on Geothermal Projects in Central America*. El Salvador: UNU-GTP and LaGeo, 2006.

Timoshenko, S. P., og Gere J. M. *Theory of Elastic Stability*. New York: McGraw-Hill, 1961.

Watkins, Reynold King, and Loren Runar Anderson. *Structural mechanics of buried pipes.* CRC Press LLC, 2000.

Paper IV

Using Probabilistic Analysis with Finite Element Modeling of High Temperature Geothermal Well Casings

Gunnar Skúlason Kaldal *, Magnús Þór Jónsson, Halldór Pálsson, and Sigrún Nanna Karlsdóttir

Faculty of Industrial Engineering, Mechanical Engineering and Computer Science, University of Iceland, Hjarðarhagi 2-6, 107 Reykjavík, Iceland

Abstract

High temperature geothermal wells which are drilled in geothermal areas are constructed of several concentric steel casings that are cemented together. The structural integrity of such well casings is essential for the utilization of high temperature geothermal wells. The temperature change in high temperature geothermal wells is large and much larger than commonly seen in oil wells. This large temperature change can cause problems in the casing due to thermal expansion of materials. The wellhead rises during discharge due to thermal expansion of the steel in the casing and the large temperature change can also lead to casing collapse due to expanding annular fluids. With recent increasing interest in drilling deeper geothermal wells the strength of the casing becomes one of the most limiting factor. A nonlinear structural finite element model of the cased well is presented and discussed here. The purpose of the model is to evaluate the structural integrity of the casing when it is subjected to thermo-mechanical loads. The outcome of the model depends highly on the accuracy of the input parameters, i.e. geometrical sizes and material properties. The accuracy of the results are evaluated with the use of probabilistic design analysis where selected input parameters of the model are assumed to contain a reasonable amount of scatter. The uncertainties of the model can thus be quantified.

1. Introduction

Geothermal wells are constructed of several concentric steel casings which are fully cemented together and cemented to the rock formation. Usually, three casings are used; the production casing, anchor casing and surface casing. The wellhead consists of a casing head flange, expansion spool and a master valve. The wellhead is attached to the top of the anchor casing and the production casing movements relative to the anchor casing is accommodated below the master valve inside the expansion spool [5].

During the discharge of high temperature geothermal wells, the temperature difference in the well from non-flowing to flowing conditions is large. To take an example, reservoir temperatures in the Krafla high temperature geothermal area in Iceland typically range from $210\,^{\circ}\mathrm{C}$ to $350\,^{\circ}\mathrm{C}$ [11]. The large temperature change generates thermal stress in the casing which is partially constrained by the concrete. While the well warms up the wellhead rises as a result of thermal expansion of the casings and concrete. Casing failures can lead to a reduced energy output from the well, render it inoperative and in worst cases cause unsafe conditions above the surface. Thus the structural integrity of well casings is essential for the utilization of high temperature geothermal wells.

The casings and the wellhead form a structural system which is unpractical to solve analytically mainly due to the nonlinear behavior of the contacting surfaces. Therefore, the structural system is analyzed numerically with the use of the nonlinear finite element method (FEM). A thermal and nonlinear structural model of the cased well is constructed where nonlinearities, e.g. friction, plasticity and large non-uniform deformations are accounted for. The nonlinear axi-symmetric model described here is a continuation of the work described by Kaldal [7]. Other models of geothermal wells have been created, e.g. an elastic 2D FEM model presented by Gretarsdottir [4] and a nonlinear FEM model by Magnusdottir where the bonding characteristics between the production casing and its outer concrete were analyzed [10]. The collapse of

*gunnarsk@hi.is

the production casing is a non-symmetrical phenomenon which cannot be analyzed with this model but has been modeled with nonlinear 3D FEM models by Kaldal [6][8].

As opposed to deterministic analysis, where input parameters are treated as constants which results in a one possible solution, a probabilistic approach is used, where the input parameters are assumed to contain a reasonable amount of scatter, which then gives an estimate of the model uncertainties. Here, selected results from the FEM model are used as outputs for the probabilistic analysis. Scatter plots of the input parameters versus the output results reveal which input parameters are significant to the results of the FEM model. A cumulative distribution function of the wellhead movement and the maximum von Mises stress in the casings and surrounding concrete is obtained here and are used to review the uncertainty of the model. In this paper, probabilistic analysis of the FEM model is presented where several input parameters are evaluated.

2. Probabilistic design

Probabilistic design is an analysis technique for assessing the effect of uncertain input parameters and model assumptions [1]. Using this method the uncertainties of the model can be quantified by acknowledging that the input parameters are not constants but rather parameters that follow statistical distribution functions such as Gaussian or normal distribution. By this assumption the limited outcome of deterministic results is avoided and the uncertainties in the model and probability distribution of the results are analyzed. Of course, the modeling error which refers to the difference between the physical system and its mathematical model [2] can be larger due to numerous approximations made to the geometry, material properties, load, etc. But all in all this method gives a map of the results rather than one point.

Intertwined in the method is the determination of the sensitivity of individual parameters to the results. For the model described below, each input parameter is assumed to follow normal distribution given by assumed mean and standard deviation. The probabilistic analysis employs the Monte Carlo Simulation method with Latin Hypercube Sampling, which avoids repeated samples [1]. A given number of simulation loops are performed and before each loop, individual input parameter is randomly given a value within its normal distribution domain. When the simulation loops are finished the sensitivity of the input parameters to the results can be visualized with scatter plots.

For the probabilistic analysis used on the FEM model described below, 400 simulation loops were used. The selected input parameters that were used for the probabilistic analysis are listed in Table 1. Their assumed means and standard deviation are listed as well. The standard deviation σ provides the sample range for the parameter and 99.7% of the samples should fall within 3σ from the mean provided that the number of simulation loops is sufficient.

Table 1: Probabilistic design input parameters (mean and assumed standard deviation).

Parameter	Units	Mean	Std
μ	-	0.45	0.15
τ_{max}	MPa	0.46	0.13
E_{co}	GPa	2.4	0.6
E_{gr}	GPa	80	20
f_c	MPa	30	7.5
ρ_{st}	$^{\mathrm{kg}}/_{\mathrm{m}^3}$	6125	150
ρ_{co}	$^{\mathrm{kg}}/_{\mathrm{m}^3}$	1600	200
α_{st}	$^{1}/_{^{\circ}\mathrm{C}}$	12e-6	1e-6
α_{co}	$^{1}/_{^{\circ}\mathrm{C}}$	10e-6	1.5e-6
σ-ϵ_{sc}	-	1	0.1

3. FEM model description

A nonlinear thermal and structural model of a high temperature geothermal well which reaches from the wellhead to the bottom of the production casing is constructed with the use of the finite-element method (FEM). The focus is to analyze the structural system which consists of a wellhead and several concentric casings connected together and to the formation with concrete. The model is two dimensional and axisymmetric around the center of the well. It includes nonlinearities which are found in large geometrical displacements, in material properties and in connectivity between contacting surfaces.

The model, shown in Figure 1, is parametrically designed so geometrical sizes and material properties are adjustable by the user. Simplified couplings with no threads are included in the production casing to account for the anchoring effect of the couplings in the concrete. A simplified wellhead based on an actual design is also included to account for pressure loads and the interaction between the casing and the wellhead. Material properties and reference values that are used in the model are listed in Table 2. Additionally, the reference value for the coefficient of friction between steel and concrete is $\mu = 0.5$ and

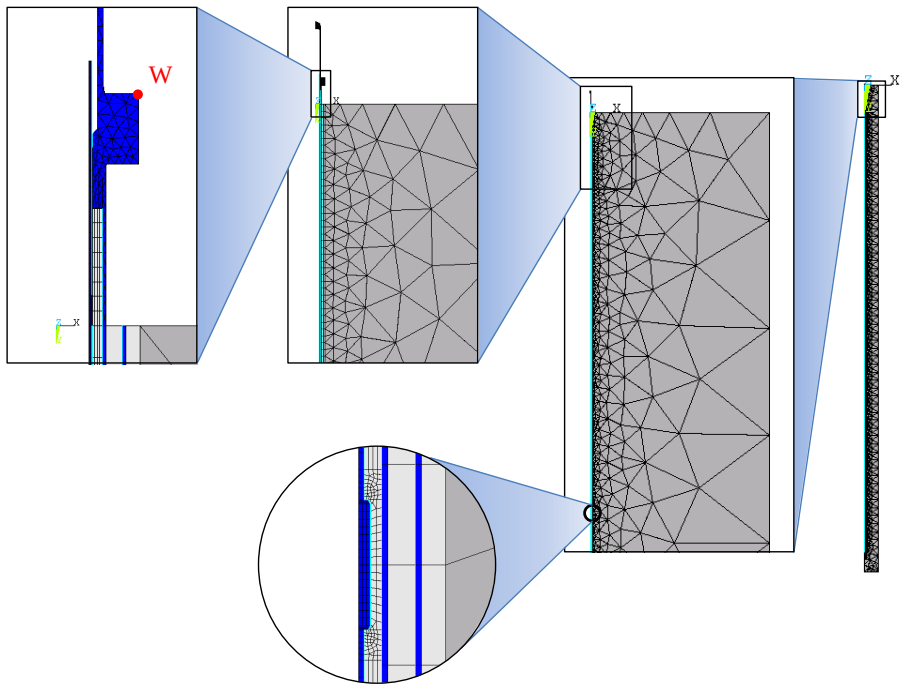

Figure 1: The geometry of the model.

the maximum shear stress when sliding initiates is $\tau_{max} = 0.46\,\text{MPa}$. Nonlinear material properties of steel grades K55, L80, T95 and X56 are implemented in the model with the use of stress-strain curves which were obtained from tensile tests [9]. The concrete is assumed to yield plastically above its maximum compressive strength and the formation is assumed to be solid basaltic rock.

Table 2: Material properties and numerical values used in the model.

Material property	Units	Steel	Concrete
Young's modulus (E)	GPa	210	2.4
Poisson's ratio (ν)	-	0.3	0.15
Density (ρ)	$^{kg}/_{m^3}$	7850	1600
Th. conductivity (K)	$^{W}/_{m^\circ C}$	50	0.81
Specific heat (c)	$^{J}/_{kg^\circ C}$	400	880
Th. expansion (α)	$^{1}/_{^\circ C}$	12e-6	10e-6
Compressive strength (f_C)	MPa	-	25e6

The frictional connection between surfaces in particular makes the model computationally complex. Contact element pairs are used between contacting surfaces. Their main purpose is to prevent surfaces to intersect each other, while still allowing gap formation and tangential movement between casings and concrete. The Coulomb friction model is used to describe friction between contacting surfaces, where it can withstand shear stresses up to a certain magnitude across its interface before they start sliding relative to each other [1]. Once the equivalent shear stress exceeds τ_{max} relative sliding begins. The Coulomb friction model is defined as:

$$\tau = \begin{cases} \mu P + b & \text{if } \tau < \tau_{max} \\ \tau_{max} & \text{if } \tau \geq \tau_{max} \end{cases} \tag{1}$$

where τ is the equivalent shear stress, τ_{max} is the maximum shear stress, μ is the isotropic coefficient of friction, b is the contact cohesion and P is the contact normal pressure, see Figure 2 for the graphical interpretation of the Coulomb friction model.

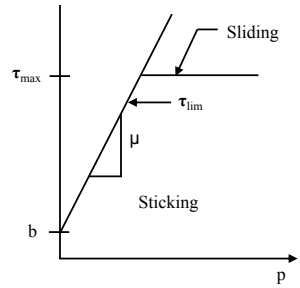

Figure 2: The Coulomb friction model in Ansys [1].

The boundary conditions of the model are defined such that no displacements are allowed in the lower and outer boundary of the model. The lower boundary is located 20 m deeper than the production casing shoe and the outer (radial) boundary of the rock formation is 20 m outward from the well, which is sufficient for both the thermal and the structural parts of the model. The wellhead movement is observed at the nodal point denoted with W on Figure 1.

4. Results

4.1. *FEM results from a single simulation run*

FEM results from a single simulation run, with the material properties values listed in Table 2, are presented here.

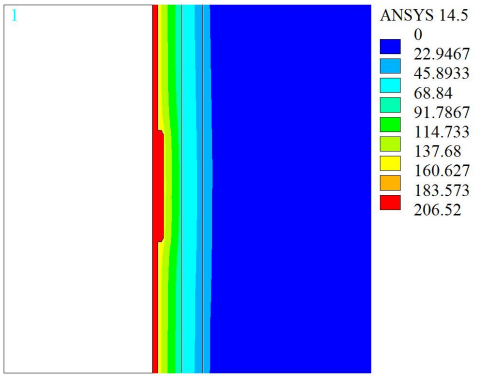

Figure 3: Temperature distribution 2.5 hours after discharge (°C).

The calculated temperature distribution at the top of the well 2.5 hours after discharge, which will be the reference time of the subsequent results, is displayed in Figure 3. A temperature change of 200 °C is assumed. The displacement at the top of the well is displayed in Figure 4. In this run the displacement of the production casing is 35.8 mm and the wellhead displacement is 11.7 mm. Stress concentration near the couplings of the casing is illustrated in Figure 5 where the maximum stress in the steel is produced near the couplings and in Figure 6 where the maximum stress in the concrete forms at the top of the couplings. In this case the maximum stress for both the concrete and the casing is formed at the second highest coupling.

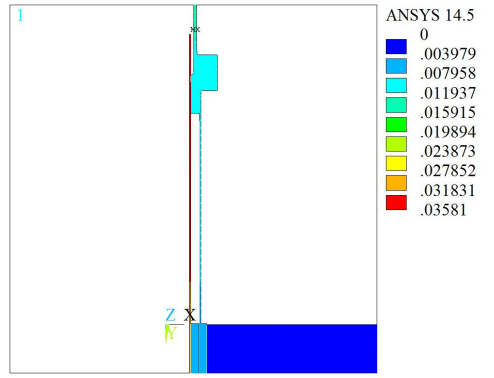

Figure 4: Displacement of the wellhead 2.5 hours after discharge (m). The displacement of the production casing is 35.8 mm and the wellhead displacement is 11.7 mm.

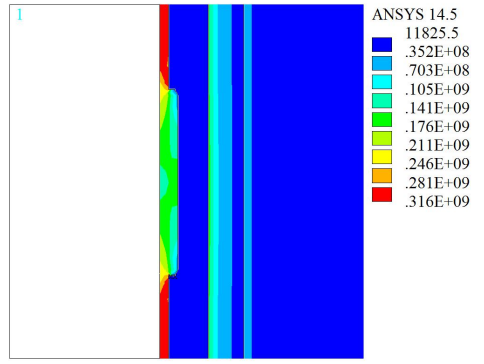

Figure 5: Von Mises stress at the second highest coupling (Pa).

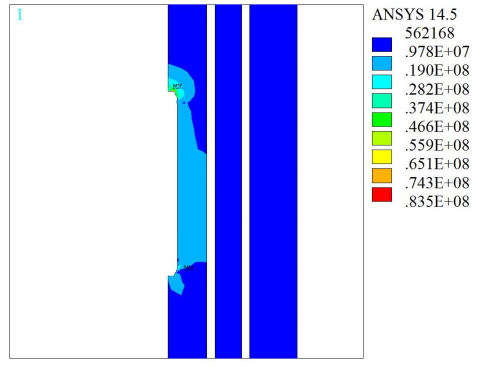

Figure 6: Von Mises stress of concrete at the second highest coupling (Pa).

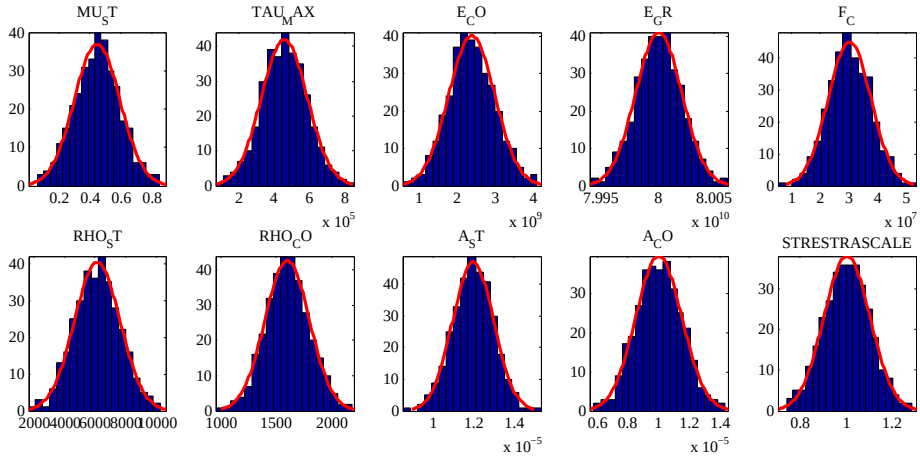

Figure 7: Histograms of normally distributed input parameters.

4.2. *Distribution of inputs and outputs*

The material properties for the FEM model that were selected as input parameters for the probabilistic analysis are listed in Table 1. Histograms of the input parameters which were assumed to follow normal distribution are seen in Figure 7. The samples of the input parameters follow normal distribution which confirms that for the probabilistic analysis, 400 Monte Carlo simulation loops are sufficient.

The results from the FEM model that were selected as outputs for the probabilistic analysis, i.e. wellhead displacement and maximum von Mises stress in the production casing, the anchor casing and the surrounding concrete for each casing, are displayed in the histograms in Figure 8 and discussed in the discussion section below.

4.3. *Correlation between inputs and outputs*

Scatter plots showing the correlation between the selected input parameters and the selected outputs of the model are illustrated in Figure 14. A significance level of the correlation between input and outputs is chosen to be 2.5%, so that $R^2 < 0.025$ is dismissed as insignificant.
For the first column, the wellhead displacement, the significant parameters are; μ_{st}, τ_{max} and α_{st} with correlations of $R^2 = 0.02528$, $R^2 = 0.32987$ and $R^2 = 0.35066$. All other input parameters are of no significance to the wellhead movement. Summary of the significant parameters and correlations is listed in Table 3.

Table 3: Significant input parameters and correlation with the results.

Output	Input	R^2
Wellhead displacement	μ_{st}	0.02528
	τ_{max}	0.32987
	α_{st}	0.35066
Max. von Mises stress of the production casing	α_{st}	0.36826
	σ-ϵ_{sc}	0.73963
Max. von Mises stress of the production concrete	τ_{max}	0.62363
	E_{co}	0.15270
	f_c	0.03274
	α_{st}	0.09283
	σ-ϵ_{sc}	0.02940
Max. von Mises stress of the anchor casing	ρ_{st}	0.02701
	ρ_{co}	0.21588
	α_{st}	0.73663
Max. von Mises stress of the anchor concrete	E_{co}	0.83435
	α_{st}	0.11622

4.4. *Cumulative distribution function*

If the results from all the Monte Carlo simulations are sorted and plotted against the proportion of the result values an empirical cumulative distribution function (CDF) of the results is obtained. These plotted curves can then be used to visualize the results. From the wellhead displacement results for example, seen in Figure 9, it can be stated with 90% certainty that the wellhead displacement is less than or equal to

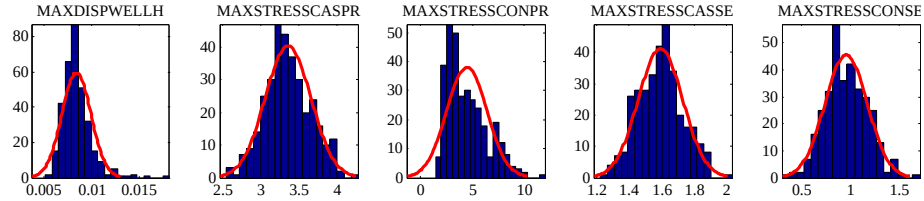

Figure 8: Histograms of the selected output results from the probabilistic analysis.

10 mm, with 95% certainty that the displacement is below 11 mm and with 99% certainty that the maximum rise of the wellhead during discharge will be 15 mm. This of course depends on the premises of all the input parameters, the model assumptions and limitations, and the assumed load the well is subjected to.

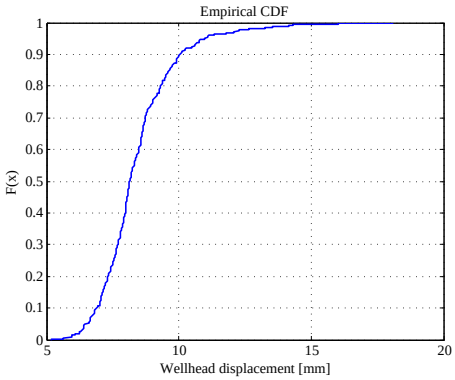

Figure 9: Empirical cumulative distribution function (CDF) plot of the wellhead displacement

Similar statements, as were made to the wellhead movement, can be made to the cumulative distribution function plot of the maximum von Mises stress for the production casing, its surrounding concrete, the anchor casing and its surrounding concrete which are displayed in Figures 10-13. Statistical summary of the output results from the probabilistic analysis is listed in table 4.

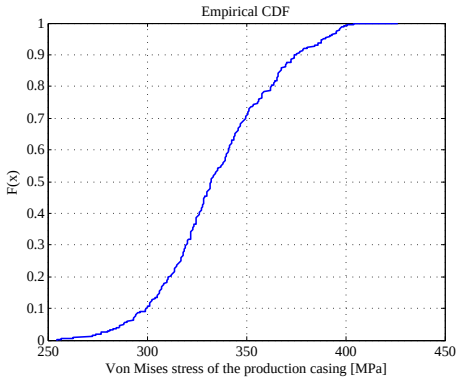

Figure 10: Empirical CDF plot of the maximum von Mises stress in the production casing

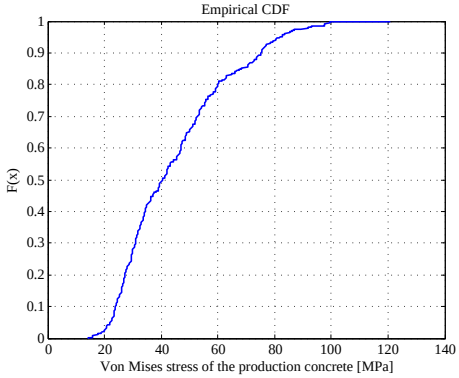

Figure 11: Empirical CDF plot of the maximum von Mises stress in the production concrete

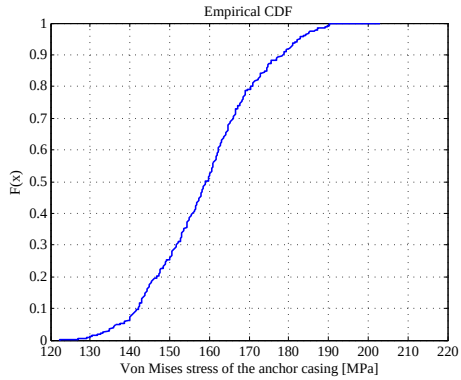

Figure 12: Empirical CDF plot of the maximum von Mises stress in the anchor casing

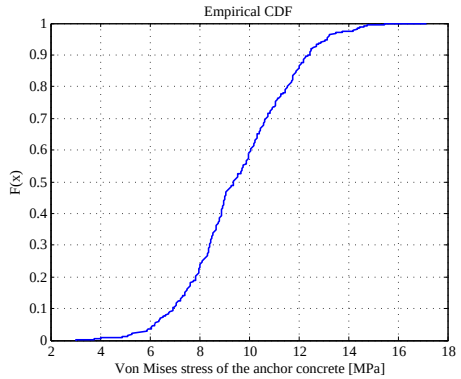

Figure 13: Empirical CDF plot of the maximum von Mises stress in the anchor concrete

Table 4: Statistical summary of the output results from the probabilistic analysis.

	Mean	Std	Min	Max
i.	8.43	1.52	5.19	18.1
ii.	335.6	29.73	254.6	426.5
iii.	44.86	19.55	14.11	120.6
iv.	159.2	13.69	122.3	203.1
v.	9.589	2.163	3.010	17.16

i: Wellhead displacement.

ii: Max. von Mises stress of the production casing.

iii: Max. von Mises stress of the production concrete.

iv: Max. von Mises stress of the anchor casing.

v: Max. von Mises stress of the anchor concrete.

5. Discussion

In the single run of the FEM model it was illustrated how the results appear after 2.5 hours which was the reference time for the probabilistic analysis. The temperature distribution shown in Figure 3 illustrates how shallow the temperature front has reached during this time. Figure 4 illustrates the wellhead displacement and how the production casing slides inside the wellhead. The stress concentration region which is located at the couplings is illustrated in Figures 5 and 6.

The selected outputs of the FEM model for the probabilistic analysis are not as distinctively normally distributed as the input parameters which were randomly given a value within the normal distribution domain. The histograms of the results seen in Figure 8 do however reveal that, apart from the maximum von Mises stress in the concrete surrounding the production casing, the results follow normal distribution nevertheless. The standard deviation given for the input parameters in the probabilistic analysis are intentionally large but might be a bit too spacious. Excluding the insignificant input parameters and narrowing the standard deviation of the significant input parameters should remove some of the noise and improve the results from the probabilistic analysis.

The correlations between input and output parameters reveal which input parameters are significant for each of the output results, see Table 3. Thermal expansion of the casings α_{st} and the parameters for friction, μ_{st} and τ_{max}, proved to be significant to the wellhead displacement, μ_{st} the least significant of the three with a correlation of $R^2 = 0.02528$. Thermal expansion of steel α_{st} is significant for all the selected output results. Specially for the maximum von Mises stress of the production casing and the anchor casing. Scaling the stress-strain curve for steel appears only to be significant for the maximum stress in the production casing and its surrounding concrete sliding freely inside the anchor casing and the wellhead. The anchor casing on the other hand is connected to the wellhead which results in less degree of freedom.

The maximum von Mises stress might not be a good output from the probabilistic analysis since it is a local peak stress which does not resemble the whole casing. Instead or rather additionally, because the maximum is surely of interest, mean stress with standard deviation could be a better option of outputs for comparison.

The cumulative distribution functions (CDF) of the output results, Figures 9 to 13, illustrate the uncertainties of the model. For ex-

ample it can be stated with 95% certainty and with these premises that the wellhead displacement is below 11 mm, the maximum von Mises stress in the production casing will be lower than 390 MPa, its surrounding concrete 82 MPa, the anchor casing 182 MPa and its surrounding concrete 13 MPa. This means that the production casing has reached beyond the proportional limit of the stress-strain curve for K55 steel which has a minimum yield strength of 379 MPa[3], its surrounding concrete is partially broken, but the security casing and its surrounding concrete are still intact, again with 95% certainty.

6. Conclusion

In this paper, probabilistic analysis of a structural FEM model of a high temperature geothermal well was presented. Using probabilistic methods on FEM models provide a broader understanding of the problem and the model itself and produce a topography of the results as well as enabling the uncertainties of the model to be quantified.

7. Acknowledgment

This work was supported by the University of Iceland research fund, the Technology Development Fund at RANNIS - The Icelandic Center for Research, the Innovation Center Iceland, Landsvirkjun Energy Research Fund, and GEORG - Geothermal Research Group. Their support is much appreciated.

Nomenclature

E	Young's modulus
E_{st}	Young's modulus of steel
E_{co}	Young's modulus of concrete
E_{gr}	Young's modulus of formation
ν	Possion's ratio
ρ	Density
ρ_{st}	Density of steel
ρ_{co}	Density of concrete
fc	Compressive strenght of concrete
K	Thermal conductivity
c	Specific heat
α	Thermal expansion
α_{st}	Thermal expansion of steel
α_{co}	Thermal expansion of concrete
μ	Coefficient of friction
τ_{max}	Maximum shear stress
τ_{lim}	Limit shear stress
τ	Equivalent shear stress
P	Contact normal pressure
b	Contact cohesion
R^2	Coefficient of determination
σ	Standard deviation
σ-ϵ_{sc}	Stress-strain curve scaling factor

References

[1] *Release 14.5 documentation for ANSYS*, 2012.

[2] Robert D. Cook, David S. Malkus, Michael E. Plesha, and Robert J. Witt. *Concepts and Applications of Finite Element Analysis*. John Wiley & Sons, Inc, 111 River Street, Hoboken, NJ 07030, 2002.

[3] Gilles Gabolde and Jean-Paul Nguyen. *Drilling Data Handbook*. IFP publications, Éditions Technip, 27 rue Ginoux, 75737 Paris Cedex 15, France, 2006.

[4] S. Gretarsdottir. Mechanical and thermal properties of well cement. Master's thesis, University of Iceland, 2007.

[5] Hagen Hole. Geothermal well design - casing and wellhead. *Petroleum Engineering Summer School*, June 2008. Workshop 26.

[6] Gunnar Skúlason Kaldal. Load history and buckling of the production casing in a high temperature geothermal well. *Thirty-Sixth Workshop on Geothermal Reservoir Engineering, Stanford University, Stanford, California*, february 2011.

[7] Gunnar Skúlason Kaldal. Thermal and structural analysis of the casing in a high temperature geothermal well during discharge. *Thirty-Seventh Workshop on Geothermal Reservoir Engineering, Stanford University, Stanford, California*, february 2012.

[8] Gunnar Skúlason Kaldal. Collapse analysis of the casing in high temperature geothermal wells. *Thirty-Eighth Workshop on Geothermal Reservoir Engineering, Stanford University, Stanford, California*, february 2013.

[9] S. N. Karlsdottir and I. O. Thorbjornsson. High Temperature Geothermal Wells - Center of Excellence in Iceland - Phase I: Corrosion Testing of Steel in High Temperature Geothermal Wells in Iceland. Technical Report for RANNIS (The Icelandic Centre for Research), October 2009.

[10] L. Magnusdottir. Nonlinear finite element model of a geothermal well. Master's thesis, University of Iceland, 2009.

[11] A. Ragnarsson. Utilization of Geothermal Energy in Iceland. *International Geothermal Conference, Reykjavik, Iceland*, pages 39–45, September 2003.

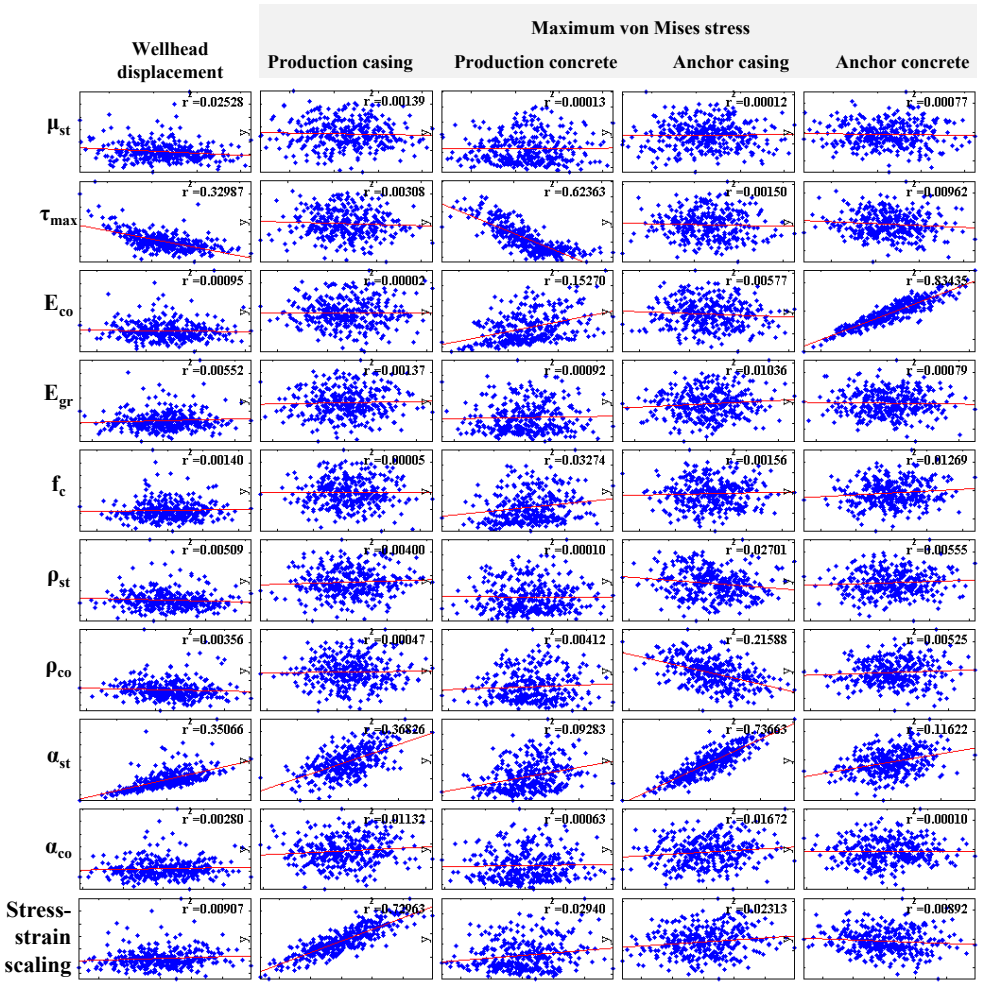

Figure 14: Correlation between selected input parameters and results.

Paper V

Geothermics 55 (2015) 126–137

Contents lists available at ScienceDirect

Geothermics

journal homepage: www.elsevier.com/locate/geothermics

Structural modeling of the casings in high temperature geothermal wells

Gunnar Skulason Kaldal*, Magnus T. Jonsson, Halldor Palsson, Sigrun N. Karlsdottir

Faculty of Industrial Engineering, Mechanical Engineering and Computer Science, University of Iceland, Hjardarhagi 2-6, IS-107 Reykjavik, Iceland

ARTICLE INFO

Article history:
Received 12 September 2014
Accepted 11 February 2015

Keywords:
Structural analysis
Steel casing
High temperature geothermal well
Wellhead displacement
Finite-element analysis

ABSTRACT

High temperature geothermal wells are constructed of several concentric steel casings that are fully cemented up to the surface. The structural integrity of such casings is essential for the utilization of wells. The casing is subjected to multiple thermo-mechanical loads that can cause casing failures. Thermal expansion generates thermal stresses in the casings and causes the wellhead to rise slightly during discharge. In this paper, a nonlinear structural finite-element model of the cased section of a geothermal well is presented and validated. The numerical results show good agreement with wellhead displacement measurements of 5 different wells in Iceland.

1. Introduction

Large temperature changes pose many design challenges in a diverse range of structures. This applies to high temperature geothermal wells which are subjected to large wellbore temperature and pressure changes. The wells are constructed of several concentric steel casings that are fully cemented together as well as to the surrounding rock formation. The structural integrity of the casings is essential for the utilization of geothermal wells.

During its lifetime, casings are subjected to multiple thermo-mechanical loads that can increase the risk of casing failures. With recent increasing interest in drilling deeper geothermal wells the strength of the casing is one of the limiting factors because of increased casing depths, higher pressures and temperatures and more difficult corrosive environment, when compared to conventional wells.

When high temperature geothermal wells, which are located in high temperature geothermal areas where temperatures at 1000 m depth reach beyond 200 °C (Böðvarsson, 1961; Palmason, 2005; Axelsson et al., 2006), are discharged the geothermal fluid flows abruptly from the reservoir because of the lowered pressure on the surface. This decrease in wellbore pressure causes boiling in the geothermal fluid. For most high temperature geothermal wells a mixture of hot water and steam is present at the wellhead (Palmason, 1980; Garcia-Gutierrez et al., 2002; Sveinbjornsson and Thorhallsson, 2014).

The flowing mixture causes pressure fluctuations with demanding wellbore flow conditions. The resulting vibration can sometimes be felt on the surface and can cause local casing problems, but the most powerful mechanical force in the structure is driven by large temperature changes which generate large thermal stresses and causes the wellhead to rise during discharge. The thermal stress caused by thermal expansion of the casings is mainly attributed to the thermal gradient between the alternating casing and concrete layers.

In high temperature geothermal wells, 2–5 casings are used; conductor casing, surface casing, intermediate casing which is sometimes omitted, anchor casing and production casing (Thorhallsson, 2008). The concrete in between the casings provides axial constraints for the casings as well as providing radial and lateral support which lowers the risk of buckling and collapse of the casings. In most Icelandic wells, the wellhead is connected to the anchor casing and the production casing is allowed to slide inside an expansion spool below the master valve of the wellhead. Fig. 1 shows a diagram of a typical casing program for high temperature geothermal wells in Iceland.

Wellbore temperature changes can lead to casing failures, especially when the stress reaches the yield point and beyond. The thermal tensile stresses that form during the cooling of wells may also be large enough to exceed the coupling joint strength of the casing, resulting in casing failure (Maruyama et al., 1990).

The expected temperatures in wells that are located in high temperature areas are determined by their position within the

* Corresponding author. Tel.: +354 525 4700; fax: +354 525 4632.
E-mail address: gunnarsk@hi.is (G.S. Kaldal).

http://dx.doi.org/10.1016/j.geothermics.2015.02.003
0375-6505/

P_A	tensile stress due to casing weight (MPa)
g	acceleration of gravity (m/s^2)
h	height (m)
t	thickness (mm)
D	outer diameter (in)
E	Young's modulus (GPa)
ν	Poisson's ratio
ρ	density (kg/m^3)
ρ_w	density of water (kg/m^3)
k	thermal conductivity (W/m° C)
c	specific heat (J/kg° C)
α	thermal expansion (1/° C)
f_c	compressive strength of concrete (MPa)
μ	coefficient of friction
μ_{wh}	coefficient of friction between the production casing and the wellhead
τ_{max}	maximum shear stress (MPa)
τ_{lim}	limit shear stress (MPa)
τ	equivalent shear stress (MPa)
P	contact normal pressure (MPa)
b	contact cohesion (MPa)
T_i	initial wellhead temperature (° C)
T_f	final wellhead temperature (° C)
ΔT	wellbore temperature change (° C)
ΔT_{wh}	wellhead temperature change (° C)
T_{wh}	wellhead temperature (° C)
P_{wh}	wellhead pressure (MPa)
u_{wh}	wellhead displacement (mm)
$_{st}$	subscript for steel
$_{co}$	subscript for concrete
$_{ro}$	subscript for rock formation

geothermal reservoir, the location of inflow fissures and the temperature of the reservoir. For example, in the Krafla high temperature geothermal field in Iceland, the reservoir temperatures typically range from 210 °C to 350 °C (Ragnarsson, 2003). Recently, wellhead temperatures as high as 440 °C (Axelsson et al., 2014; Armannsson et al., 2014; Hauksson et al., 2014; Ingason et al., 2014) were seen in the first Iceland Deep Drilling Project (IDDP) well IDDP-1 located in the same reservoir but closer to the heat source. The well became the world's hottest producing geothermal well (Elders et al., 2012).

The nonlinear behavior of materials used in geothermal wells and the nonlinear frictional characteristics between contacting surfaces creates a problem that is unfeasible to solve analytically. Therefore, to get a wider understanding of the structural response of the system to temperature and pressure loads, a numerical model has been developed to simulate stresses, strains and large displacements in the cased section of high temperature geothermal wells. The nonlinear finite-element method (FEM) is used to construct a two-dimensional axis-symmetric structural model of the cased well which is presented and discussed here. Preliminary results of the model have been presented by Kaldal et al. (2012, 2013).

Few FEM models of wells have been published where the frictional characteristics between the surfaces in contact are taken into account. Philippacopoulos and Berndt (2002) presented a two-dimensional FEM model of a cross section of a double cased geothermal well with the objective of evaluating the stress field of the concrete, where the need for further general research to focus on the transient structural response of a geothermal well as a structural system was emphasized. Gretarsdottir (2007) presented an elastic two dimensional FEM model of a geothermal well where no separation between surfaces was accounted for. By using a

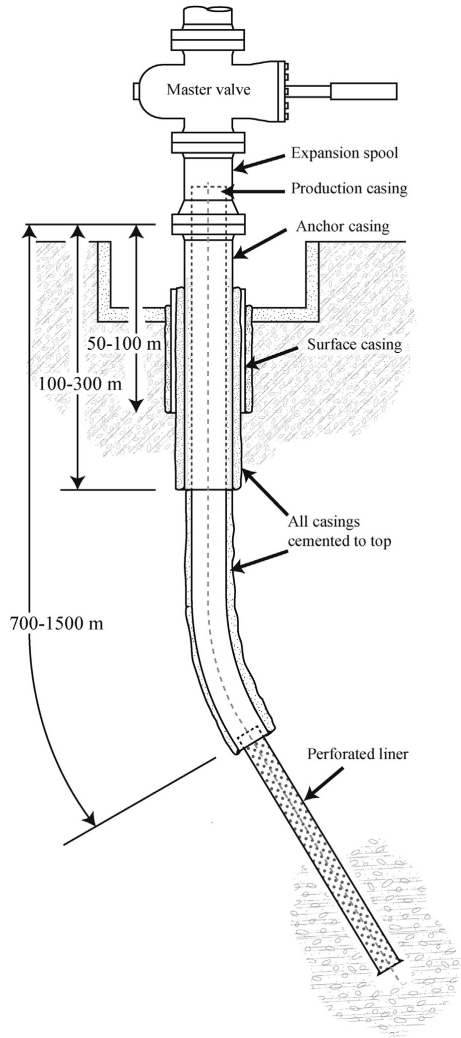

Fig. 1. A diagram of a typical casing program for high temperature geothermal wells in Iceland.

three-dimensional push-out model and push-out test results obtained in a laboratory along with the two dimensional model, the displacement of the production casing at the surface was estimated. Magnusdottir (2009) presented a nonlinear two-dimensional FEM model of a geothermal well, where the upward displacement of casings was analyzed with regards to the bonding characteristics between the production casing and concrete by using contact elements. The results for no-, partial- and full separation between the surfaces, were compared and showed how the defined contact behavior greatly affected the results. Ferla et al. (2009) proposed a linear axis-symmetrical model of a short section of a well with a casing surrounded by concrete and rock, where thermal-induced stresses around a cased injection well were modeled. The model included two types of rock which showed that interbedding

layers of relatively soft and relatively stiff rock types have a major effect on the thermal stress distribution along the casing. They also analyzed casing pre-tension and its effect on the reduction of the thermal compressive stress.

In the model presented here, friction is defined for all surfaces in contact. The model predicts temperature distribution, displacements, stresses and strains. Unsymmetrical phenomenons such as collapse, buckling and structural effects of directionally drilled wells, can however not be analyzed with the model due to its axial symmetry.

To get a greater insight into the structural response of high temperature geothermal wells to wellbore pressure and temperature changes, wellhead displacement data was gathered during discharge of 5 wells, located in the Hengill and Reykjanes geothermal areas in Iceland. In this paper the wellhead displacement data is presented and used to validate the proposed nonlinear FEM model. The model can then be further used to analyze the structural integrity and structural response of steel casings to thermo-mechanical loads.

2. Casing loads in geothermal wells

Numerous load cases arise during the lifetime of geothermal wells. The loads mainly consist of casing weight, temperature and pressure changes. In general, casing design is based on (i) axial tension, (ii) burst and (iii) collapse pressures. The casing must withstand the expected loads that are likely to occur during its lifetime. Standards, e.g. ISO/TR 10400:2007(E), which provide equations and calculation guidelines for the properties of casings, have been developed for the oil and gas industry. But well design and the definition of anticipated loads is currently outside the scope of standardization for the petroleum and natural gas industries (ISO/TR 10400, 2007).

In casing design for oil and gas wells, the most important parameters are fluid pressure, casing weight and tensile loading (Hole, 2008). In geothermal wells however, high temperature loading is generally the most severe (Hole, 2008). To understand what loads act on the casing it is useful to go through the load history of the casing. It can be different from well to well but the most critical load cases are similar and will be described to a certain extent.

The load cases considered here occur at various time periods, i.e. during installation, well operations (e.g. opening and closing of wellhead valves and cooling with cooling water), and during production of high enthalpy steam. After well completion the casing loads consist of wellbore temperature and pressure changes. For high temperature geothermal exploration, where reservoir temperatures are not well known, the inflow temperature and pressure of wells is assumed to follow the boiling point-depth curve (BPD) for water (Björnsson et al., 1978; Thórhallsson et al., 2014). If, however, wells have been drilled in the area and the reservoir temperatures are known, pressure and temperature conditions of prior wells can be used as basis for design.

During the installation of the production casing, casing components are joined and lowered down into the well. If residual stresses from the production of the casing are neglected, the first load case consists of axial tension due to gravity, see diagram A in Fig. 2. While the casing is installed, the well is kept full of cold water, which provides a counteracting buoyancy force. The tensile force on the top increases with increasing length of the casing, putting the highest strain on the last installed casing component that holds up the whole casing. The axial tensile load depends on several factors, e.g. thickness and diameter of the steel casing, how many centralizers are used, the diameter of the hole, cementing method, the deviation of the hole and the density of the mud/water/cement that provides the buoyancy force.

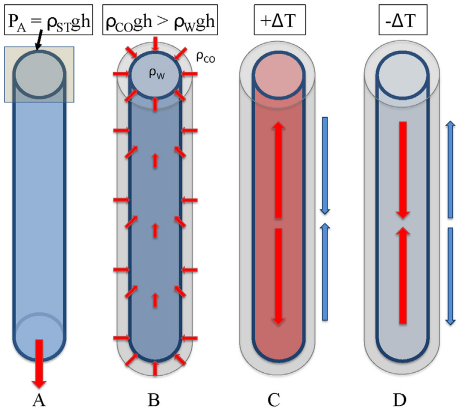

Fig. 2. Casing load cases.

Prior to cementing, the well is cooled with cooling fluid. During cementing, using the inner string method, the concrete slurry is pumped down through the drill string and up the annulus. Unlike oil and gas wells, geothermal well casings are usually run back to the surface and are fully cemented over the full length of the casing (Hole, 2008). The casing is kept full of cold water so the differential pressure between the outer and inner surface of the casing wall does not reach critical levels, i.e. exceeding the collapse resistance of the casing. The differential pressure is determined by the hydrostatic pressure difference between concrete and water, as well as the additional cement pumping pressure, see diagram B in Fig. 2.

The solidified concrete, which seals up the annulus between the casings and the formation, provides support to the casings. The temperature at which the concrete solidifies at is the reference temperature for subsequent thermal stresses in the casing. The temperature gradually increases with depth down the well and after the cement has been placed the temperature increases due to external warm-up of the well and due to the exothermic chemical reaction while the cement sets. The neutral thermal stress conditions of each casing is therefore determined by its temperature distribution when the cement sets.

While the well is allowed to warm-up during its thermal recovery from drilling, the initial tensile stress in the casing is relieved and compressive thermal stress slowly builds up, see diagram C in Fig. 2. The intensity depends on the temperature difference and how fast the well warms up. Drilling into permeable zones in geothermal areas, using water as circulation fluid, large volumes of cold water are lost to the reservoir and full thermal recovery takes from 2 weeks to 3 months (Birkisson and Hole, 2007). During this period the wellbore is normally full of water and wellhead pressure slowly builds up.

In some cases the water inside the wellbore prevents wellhead pressure to naturally build up. In those cases wellheads are sometimes shut completely to allow accumulation of non-condensable gases at the top. Pressure then builds up gradually and pushes the water column down into the reservoir making discharge possible when the well is opened. Air-pumps at the wellhead are also used for this purpose. The disadvantage of using air is that the well and the wellhead cools down while cold air is pumped into the well which then causes a greater thermal shock when the well is discharged.

When the well is discharged the wellhead pressure decreases rapidly and the temperature in the well increases sharply. The large temperature change causes thermal expansion of the casing which

Table 1
The casing sizes of the monitored wells.

HE-13	*D* (in)	*t* (mm)	Length (m)
Production casing	9 5/8	12.2	775
Anchor casing	13 3/8	12.2	255
Surface casing	18 5/8	11.0	78
HE-46	*D* (in)	*t* (mm)	Length (m)
Production casing	13 3/8	12.2	1032
Anchor casing	18 5/8	11.0	337
Surface casing	22 1/2	11.0	83
HE-53	*D* (in)	*t* (mm)	Length (m)
Tieback casing	7	12.6	607
Production casing	9 5/8	12.2	965
Anchor casing	13 3/8	12.2	306
Surface casing	18 5/8	11.0	70
RN-22	*D* (in)	*t* (mm)	Length (m)
Production casing	13 3/8	12.2	729
Anchor casing	18 5/8	12.3	292
Surface casing	22 1/2	12.5	74
RN-32	*D* (in)	*t* (mm)	Length (m)
Production casing	13 3/8	12.2	1077
Anchor casing	18 5/8	12.3	345
Surface casing	22 1/2	12.0	100

causes the wellhead to rise, as shown later. The sharp wellbore temperature change also generates thermal stress in the production casing which is in direct contact to the geothermal fluid. The temperature rise in the outer casings of the well is much slower and more gradual than the almost immediate temperature change of the production casing. Since the upper layers of the well warm up from within during discharge, thermal expansion generates thermal stress in all casings as they gradually warm up. The production casing is therefore much more affected by cyclic temperature change than the outer casings which warm up slower because of the thermal buffer the concrete in between the casings provides.

When wells need to be closed, for example for maintenance, thermal stress forms due to the cooling of the well. For a typical well, the wellhead temperature slowly decreases after the wellhead is closed and thermal stress due to cooling is not a problem. If however the well needs to be shut off with cold water the casing rapidly contracts, creating tensile forces due to the support of the outer casing and concrete layers, see diagram D in Fig. 2. If the stress in the casing reaches beyond the yield point during warm-up or discharge, cooling it down again generates tensile stress which could lead to a coupling rupture and/or rupture of the casing body.

Thermal stresses generate similar problems in oil wells where steam injection is used. Steam is used to heat the formation down at the pay-zone to a temperature sufficient to reduce the viscosity of the hydrocarbons which then flow back into the heat injection well (Vogel, 1966).

In essence, the largest casing stresses that are produced in high temperature geothermal wells are axial thermal stresses caused by thermal expansion that occurs due to large temperature changes.

3. Wellhead displacement survey

A change in wellhead elevation during changes in wellbore pressure and temperature provides information on the structural response of the well. Monitoring wellhead displacement during discharge can be used to study the rapid displacement during the sudden wellbore pressure and temperature changes.

Wellhead elevation displacement data was gathered for 5 high temperature geothermal wells in the Hengill and Reykjanes geothermal areas which are both located on an active volcanic ridge in SW Iceland. The wellhead displacement was monitored while the wells were discharged. The monitored wells HE-13, HE-46 and HE-53 are located in the Hengill geothermal field in Iceland and wells RN-22 and RN-32 are located in the Reykjanes geothermal field in Iceland. The geometrical sizes of the casings of the monitored wells are listed in Table 1.

Table 2
Examples of wellhead displacements during discharge of selected wells in Iceland. Mainly from discharge reports from the National Energy Authority (Orkustofnun) and Iceland Geosurvey (ISOR) in Icelandic.

Well	Year	Discharge method	u_{wh} (mm)	Time from discharge	
KJ-19	1982	Natural	20	5 h	[1]
			45	22 days	
KJ-21	1982	Natural	22	2 h	[2]
			33	1 day	
			68	52 days	
KJ-22	1983	Natural	27	Missing	[3]
NJ-12	1986	Wire-piston	41	11 days	[4]
NJ-13	1985	Natural	9	5 h	[5]
NJ-14	1986	Air-pump	20	1.5 h	[6]
NJ-16	1986	Natural	5	Missing	[7]
PG-1	2004	Air-pump	15	14 days	[8]
IDDP-1	2011	Natural	420	10 weeks	[9]

[1] Krafla, Hola KJ-19 (OS82099/JHD27), October 1982.
[2] Krafla, Hola KJ-21 (OS83013/JHD03), February 1983.
[3] Krafla, Hola KJ-22 (OS84008/JHD02), February 1984.
[4] Nesjavellir, Hola NJ-12 (OS85100/JHD56), November 1985.
[5] Nesjavellir, Hola NJ-13 (OS85101/JHD57), November 1985.
[6] Nesjavellir, Hola NJ-14 (OS86031/JHD09), April 1986.
[7] Nesjavellir, Hola NJ-16 (OS87007/JHD06), February 1987.
[8] Þeistareykir, Hola ÞG-01 (ISOR-2004/040), November 2004.
[9] Ingason et al. (2014).

Table 2 shows examples of typical wellhead displacements during discharge of selected wells in Iceland. Time-series data of wellhead displacement provides additional information on the structural response of the casings to large temperature changes. In this study, wellhead displacement data along with temperature and pressure data was gathered at the wellheads during the first few hours of discharge. A laser line was projected onto a ruler which was attached above the master valve of the wells, see Fig. 3. The reference point, where the laser tripod was located, was 2.5–3 m from the wellhead, depending on the setup. A digital single-lens reflex camera (Canon EOS 600D) was then used to take high-resolution snapshots of the ruler to minimize the measurement error, which with this method is estimated to be ±0.25 mm.

The temperature of the wellhead was measured using an infrared thermometer, with ±2% reading accuracy, at various locations on the wellheads. The wellhead pressure was observed with gauges located above the master valve.

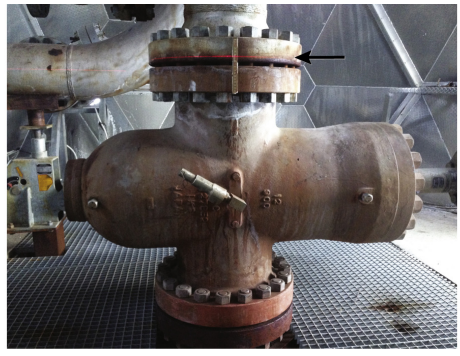

Fig. 3. The wellhead of well HE-46. Arrow showing the laser projected on a ruler on the top flange of the master valve.

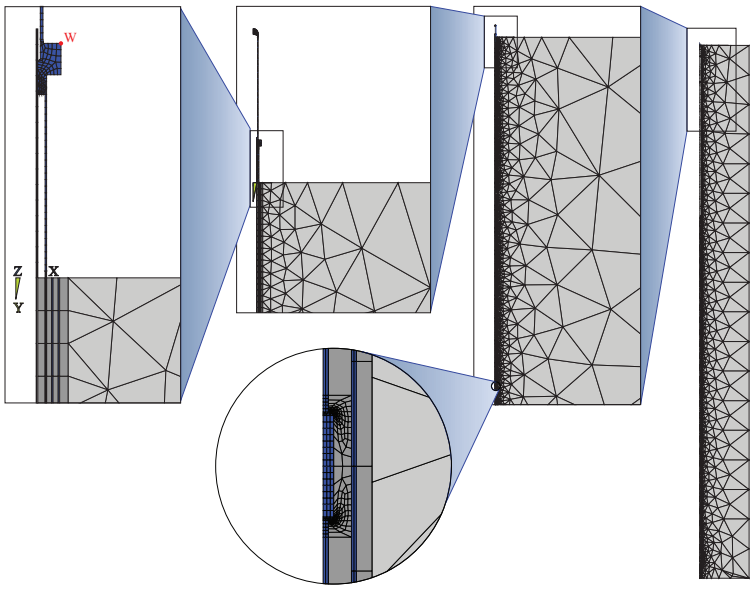

Fig. 4. The geometry of the model. The whole model is displayed on the right and the wellhead and a simplified coupling are shown in close-ups. The wellhead displacement is monitored at the node denoted with W.

4. Model description

The finite-element program Ansys is used to construct a nonlinear FEM model. It is divided into two parts, thermal and structural. Before the structural part is run, a transient thermal analysis is performed. The thermal results are then used as load in the structural model.

The model is two-dimensional and axially symmetric around the center of the well. Axial and radial deformations can therefore be analyzed but lateral and unsymmetrical deformations, e.g. bending, buckling and collapse can not. Although the angular displacements are zero, hoop strains and stresses can nevertheless be analyzed because of the revolving axial symmetry. Nonlinear behavior, i.e. (i) large geometrical displacements, (ii) nonlinear material properties and (iii) connection between contacting surfaces are solved with the modified Newton–Raphson method (Ansys Inc.).

The model, seen in Fig. 4, reaches from the wellhead down to the bottom of the production casing and 20 m further down where the lower boundary is located. The radial boundary of the model is located 100 m from the center of the well. The wellhead displacement is tracked at the node denoted with W in Fig. 4.

Simplified couplings with no threads are included to account for the anchoring effect of the couplings in the concrete. A simplified wellhead is also included to account for pressure loads and the interaction between the casings and the wellhead. The first flange of the wellhead and the casing guidance ring, which for simplification are joined into a solid piece, are included in the model to account for the sliding of the production casing inside the wellhead, see Fig. 5. The model is designed so that geometrical sizes and material properties are easily adjustable by the user.

The material properties and default values that are used in the model are listed in Table 3. Additionally, the value used for the coefficient of friction between steel and concrete is $\mu = 0.45$ and the maximum shear stress when sliding initiates is $\tau_{max} = 0.46$ MPa which is based on two separate shear strength studies of

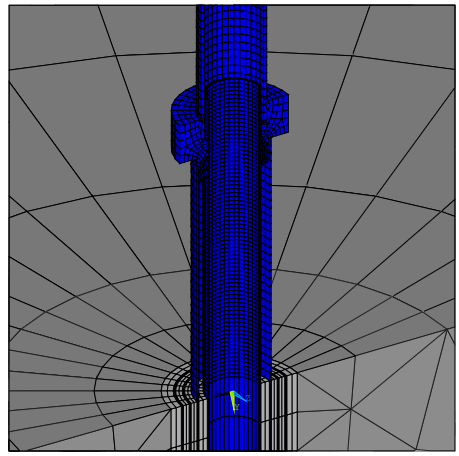

Fig. 5. Symmetry expansion (180°) of the simplified wellhead for the axis-symmetric model. The wellhead is fixed to the anchor casing and the production casing is allowed to slide inside the wellhead.

Table 3
Material properties and default numerical values used in the model.

Material property	Units	Steel	Concrete	Rock
Young's modulus (E)	GPa	205	2.40	80.0
Poisson's ratio (ν)	–	0.30	0.15	0.31
Density (ρ)	kg/m^3	7850	1600	2650
Th. conductivity (K)	W/m° C	50.0	0.81	2.00
Specific heat (c)	J/kg° C	490	880	840
Th. expansion (α)	1/° C	12e−6	10e−6	5.4e−6
Compressive strength (f_C)	MPa	–	25e6	

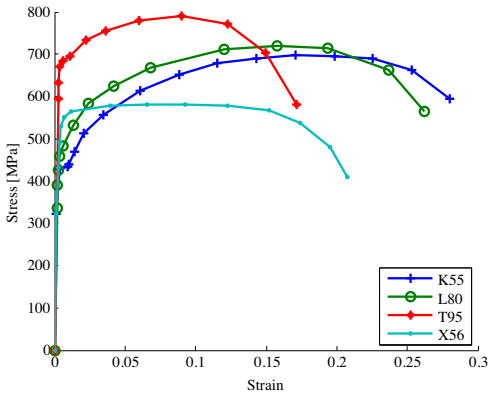

Fig. 6. Stress–strain curves used in the model for steel grades K55, X56, L80 and T95 (Karlsdottir and Thorbjornsson, 2009).

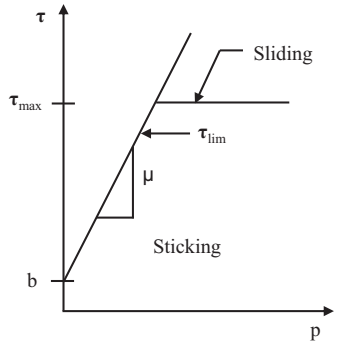

Fig. 7. The Coulomb friction model in Ansys (Ansys Inc.).

externally cemented casings. Shear strengths performed by Gretarsdottir (2007) showed maximum shear strength of 0.26 MPa and 0.64 MPa, for 1 day strength and 28 days strength, respectively. Similar results were obtained by Wallevik et al. (2009), where the maximum shear strength was 0.21 MPa and 0.72 MPa, for 1 day strength and 28 days strength, respectively. The steel–steel coefficient of friction between the production casing and the wellhead is not known but is chosen to be $\mu_{wh} = 0.7$, near the upper limit of the static coefficient of friction for steel–steel contact which is 0.6±0.11 according to ASM (1992).

Nonlinear material properties of steel grades K55, L80, T95 and X56 are implemented in the model by using stress–strain curves which were obtained from tensile tests by Karlsdottir and Thorbjornsson (2009), seen in Fig. 6. Due to lack of data for the stress–strain curves of casing steel at elevated temperatures, strength reduction is accounted for by scaling these curves according to Snyder (1979).

The steel is assumed to follow the kinematic hardening rule, which is observed in cyclic loading of metals and can be used to model behavior such as the Bauschinger effect (Thakur et al., 1996) and buildup of plastic strain during cyclic loading, known as plastic ratcheting (Ansys Inc.).

In the model, the concrete is assumed to yield plastically above its maximum compressive strength. It is however arguable how this should be defined due to the question of the post-failure compressibility of the concrete in tri-axial stress state. In the model, the Young's modulus of the concrete after it has reached the maximum compressive strength is reduced by 50%. A concrete material model that behaves differently in compression and tension is not defined in the model but could be implemented in future studies. Other material properties are defined linearly and the formation is assumed to have the properties of solid basaltic rock.

The influence of the material properties on the results have been analyzed by Kaldal et al. (2013) with probabilistic design analysis, where the significant parameters to the wellhead displacement were found to be the frictional parameters as well as the thermal expansion coefficient for steel.

Contact between surfaces is defined with contact elements and the frictional characteristics are solved using the Coulomb friction model for all contacting surfaces. Contact element pairs are used between contacting surfaces. Their main purpose is to prevent surfaces from intersecting each other while still allowing gap formation and tangential movement. Using the Coulomb friction model, friction is described with a friction coefficient, μ, and maximum shear stress, τ_{max}. The surfaces can withstand shear stresses up to a certain magnitude across its interface before relative sliding initiates (Ansys Inc.). Once the equivalent shear stress exceeds τ_{max}, relative sliding begins.

The Coulomb friction model is defined as:

$$\tau = \begin{cases} \mu P + b & \text{if } \tau < \tau_{\max} \\ \tau_{\max} & \text{if } \tau \geq \tau_{\max} \end{cases} \quad (1)$$

where τ is the equivalent shear stress, τ_{max} is the maximum shear stress, μ is the isotropic coefficient of friction, b is the contact cohesion and P is the contact normal pressure. Fig. 7 shows the graphical interpretation of the Coulomb friction model.

The boundary conditions are such that no displacements are allowed at the lower and radial boundary of the model. The load consists of wellbore temperature and pressure (T–P) profiles.

Tensile stress due to the installation of the casings is accounted for by including initial tensile stress in each casing. This initial stress corresponds to a casing hanging from the top in cold water. The thermal stress formed due to the temperature difference between the drilling fluid and the cementing temperature conditions is also included in the initial tensile stress for each casing with the assumption that the casing is fully constrained initially.

The casings and concrete are meshed with eight-node quadrilateral-shaped elements and the rock formation is meshed with six-node triangle-shaped elements. The diameter-to-depth ratio of the model is very small, as can be seen in Fig. 4. This requires a large number of elements because the elements must have proper width-to-length ratio to function correctly. Convergence studies of the model with respect to mesh density in the axial direction of the well can be seen in Fig. 8. When the axial element density of the casings is changed, the density of the external elements which represent the rock formation, change as well. Average element length of 0.25 m proved to be adequate. This is equivalent to 100.000 elements for a test model with a 285 m long production casing.

When simulating discharge, the initial wellbore conditions are important. The time period the pre-discharge conditions apply to are also important, because of the temperature distribution of the outer casing-, concrete- and rock layers. Therefore, the initial T–P profiles before discharge and the time the well has been in that state need to be included in the analysis. Same applies to wellbore conditions after discharge. The load history for well HE-46 that is used in the modeling is listed in Table 4. Similar load histories are used for all the wells, but with different T–P profiles, pre-discharge conditions and time periods.

Figs. 9–13 show the T–P profiles that are used for the modeling of the geothermal wells referred to as HE-46, HE-13, RN-22,

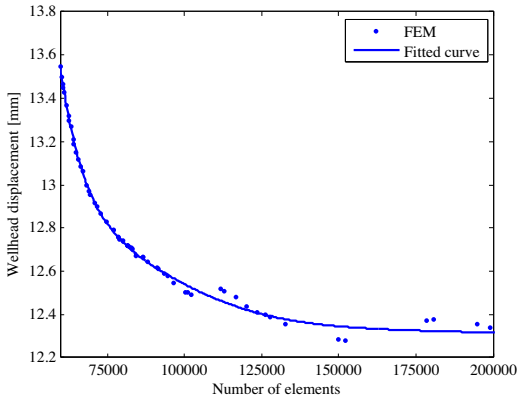

Fig. 8. Convergence studies of the element mesh density of the model.

Table 4
The load history for well HE-46.

Case	Description	Time period
1.	Rock temperature	Initial
2.	Cooling due to drilling	40 days
3.	Temperature recovery	8 months
4.	Pre-discharge (air-pump)	18 h
5.	Discharge (ΔP)	1 min
6.	Discharge (ΔT)	12 min
7.	Post-discharge 1	9 days
8.	Post-discharge 2	3 months

RN-32 and HE-53, respectively. Fig. 14 illustrates how the wellhead temperature of well HE-46 increases with time right after the wellhead valve is opened. This is used for transition between the pre-discharge and discharge load cases seen in Fig. 9.

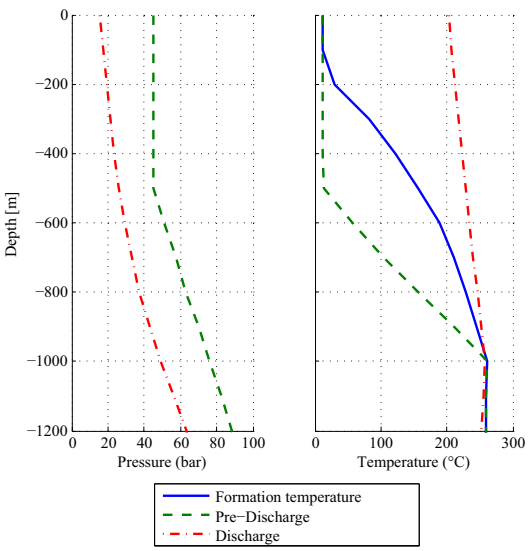

Fig. 9. Temperature and pressure profiles used as load cases for well HE-46.

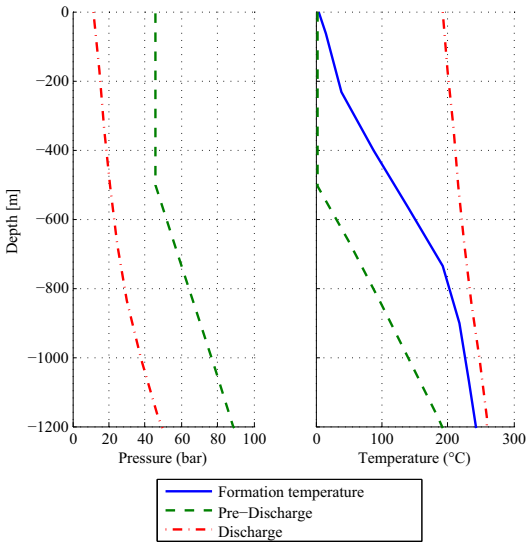

Fig. 10. Temperature and pressure profiles used as load cases for well HE-13.

5. Results

5.1. Wellhead displacement survey

A photographic series of the wellhead displacement during discharge of HE-46 can be seen in Fig. 15, where the elevation of the wellhead is seen for the initial state of the closed well, 4 h after discharge and 9 days after discharge.

The wellhead displacement during discharge of wells HE-13, HE-46, RN-22 and RN-32 is displayed in Fig. 16. All of the monitored

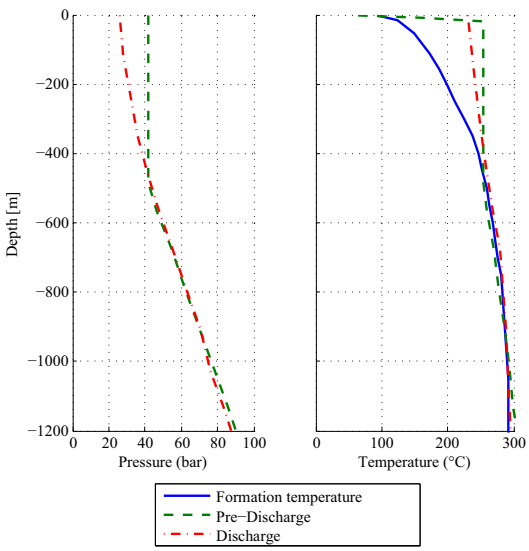

Fig. 11. Temperature and pressure profiles used as load cases for well RN-22.

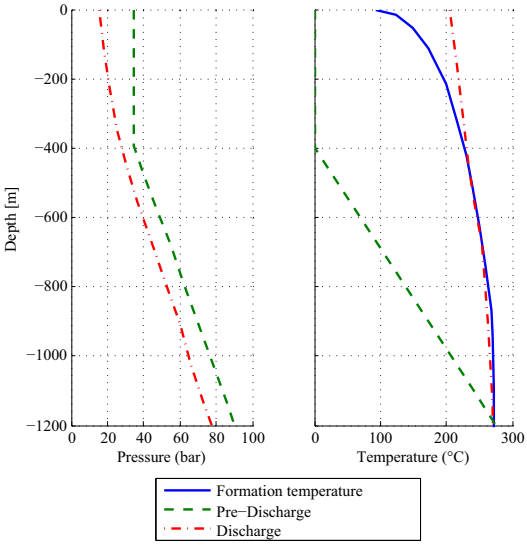

Fig. 12. Temperature and pressure profiles used as load cases for well RN-32.

wells, except HE-53, started to show upwards displacement of the wellhead shortly (<1 min) after discharge was initiated. Virtually no displacement (−0.5 mm) was seen for the wellhead of HE-53 during its observation period of 3 h. The corresponding wellhead temperature change during discharge is shown in Fig. 17 and Table 5 lists the wellhead temperature change before and after discharge, the monitored wellhead displacement and the observation period.

Some of the wells had already built up pressure naturally while others were full of water beforehand and needed discharge assistance. For wells HE-13, HE-46 and RN-32 air-compressor was used

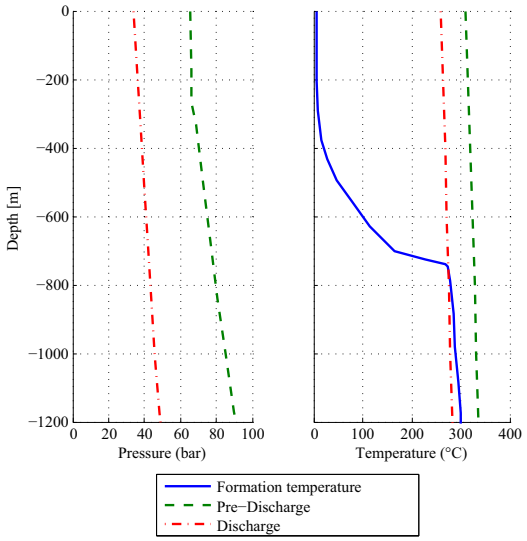

Fig. 13. Temperature and pressure profiles used as load cases for well HE-53.

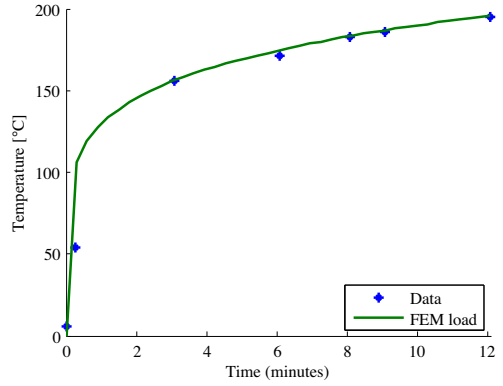

Fig. 14. Measured wellhead temperature which is used as transition between the pre-discharge and discharge load cases in the model at the start of discharge of well HE-46.

to build-up wellhead pressure before discharge, but wells RN-22 and HE-53 had developed wellhead pressure naturally. The wellhead temperature change, ΔT_{wh}, during discharge of the wells that needed air-pressure assistance was therefore much larger than that of wells RN-22 and HE-53.

Prior to discharge of HE-53 the wellhead temperature was 310 °C and the wellhead displacement was presumably near its maximum. During the discharge of the well the decrease in pressure resulted in temperature decline of 50 °C and the wellhead lowered by mere 0.5 mm in 3 h, which is barely within the measurement error. Prior to discharge of well RN-22, however, the wellhead temperature was 66 °C and a gradual wellhead rise of 7.0 mm was observed in 2.5 h as the temperature rose to 215 °C.

Two separate discharges of well HE-46 were monitored with two years in between, shown in Fig. 16, labeled (1) and (2) respectively. Pressure had been built up with a small air-compressor for discharge 1 for about two weeks and the pressure had reached 38 bar-g when the well was discharged. In discharge 2, a larger air-compressor was used and a pressure of 45 bar-g was built up in just under 2 h. When the well was then opened for discharge the pressure was released but without initiating flow. A downward wellhead displacement of 1.5 mm was observed while the wellhead pressure decreased from 45 to 0 bar-g, see Fig. 18. Pressure was built up again to 48 bar-g and held for a day before the well was discharged successfully maintaining, a pressure of 11.8 bar-g.

For well HE-13, the large air-compressor was used to build up wellhead pressure. The well was closed for 12 days with a pressure of 46 bar-g prior to discharge.

Well RN-32 had naturally built up wellhead pressure of 4 bar-g but a discharge trial failed. An air-compressor was used to build-up wellhead pressure three days prior to a successful discharge. The wellhead pressure was 34.8 bar-g prior to discharge.

Table 5
Monitored wellhead displacement and corresponding wellhead temperature difference, ΔT, before discharge T_i and after discharge T_f.

Well	T_i (°C)	T_f (°C)	ΔT_{wh} (°C)	u_{wh} (mm)	Monitoring period
HE-46 (2)	6	197	191	52.0	9 days
HE-46 (1)	8	193	185	22.5	2.5 h
HE-13	18	197	179	40.5	3 days
RN-22	66	215	149	7.0	2.5 h
RN-32	3	207	204	15.0	9 days
HE-53	310	260	−50	−0.5	3 h

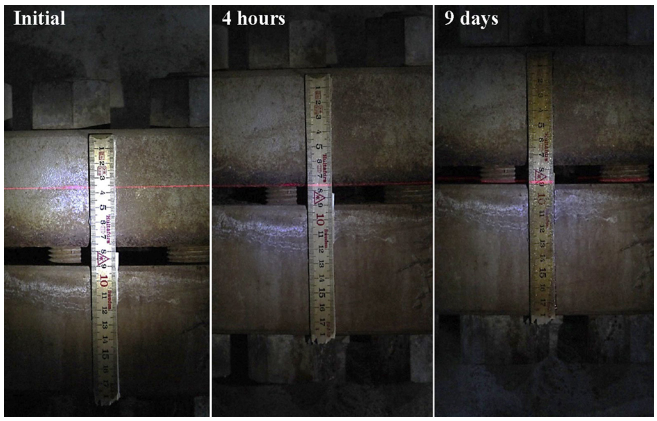

Fig. 15. Photographic series of the wellhead displacement of well HE-46 during discharge.

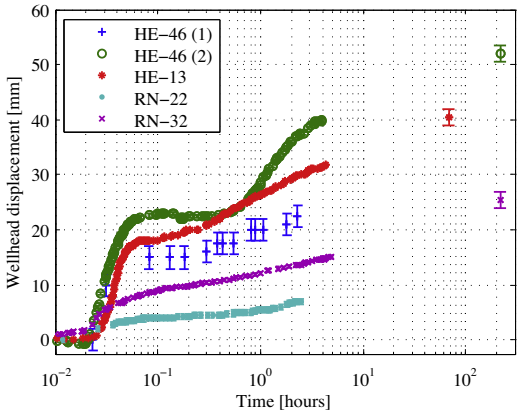

Fig. 16. Wellhead displacement data of the monitored wells during discharge.

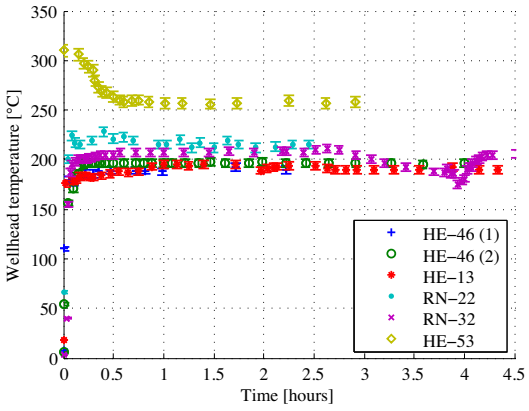

Fig. 17. Wellhead temperature during discharge of the monitored wells.

5.2. Numerical results

As an example, the modeled temperature distribution of the wellhead of well HE-46 and the wellhead displacement 9 days after discharge is displayed in Figs. 19 and 20, respectively. The results show how the production casing slides inside the wellhead, but the phenomenon has not been confirmed even though recent video logs indicate its existence.

The temperature distribution of the modeled wells and the surrounding rock is calculated according to the assumed load history and load cases for each well. The modeled wellhead displacement is compared to the measured wellhead displacement in Figs. 21–25 for wells HE-46 (2), HE-13, RN-22, RN-32 and HE-53 respectively.

By using the default model parameters and material properties, as outlined in the model description section, the results show similarities to the measured wellhead displacement for the majority of the wells.

The particular wellhead displacement of HE-46, seen in Fig. 21, differs from the other wells and the model tracks the 15 min break poorly. However, the initial sharp displacement is a good match with a modeling error of 1.0 mm or 4.2%. The modeling error of the final observed displacement is 8.0 mm or 15.4%.

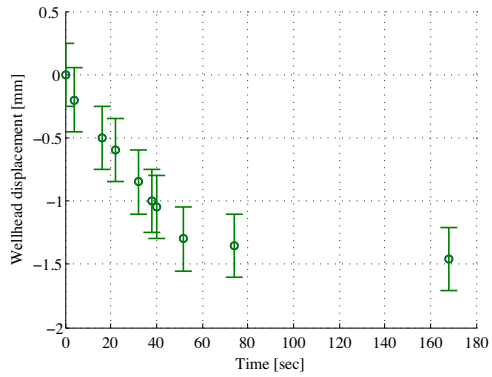

Fig. 18. Wellhead displacement from 45 to 0 bar-g during a failed discharge attempt of well HE-46.

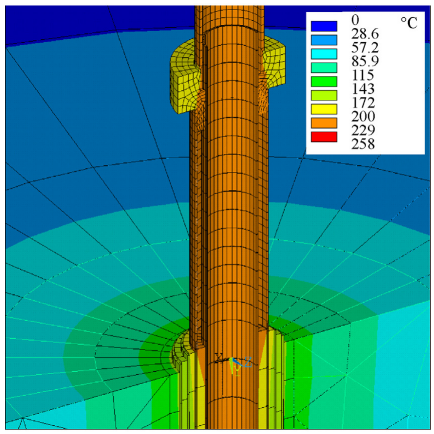

Fig. 19. Modeled wellhead temperature 9 days after discharge of well HE-46 (180° symmetry expansion).

The modeled wellhead displacement of HE-13, Fig. 22, shows a good match to the measured displacement in terms of slope and final displacement but it overshoots the initial displacement by 5 mm or about 25% and the final displacement observation by 3 mm or about 7%.

The model overshoots the initial displacement of well RN-22 by 3 mm and then tracks the slope of the displacement with good accuracy, see Fig. 23.

The FEM results for RN-32, Fig. 24, show a close match but the change in wellhead displacement with time is underestimated. The final measured point, 9 days after discharge, is underestimated by 6.9 mm or about 27%.

For well HE-53, where a total wellhead displacement of −0.5 mm was observed, the modeled downward wellhead displacement fluctuates with time and overshoots the downward displacement by 2.5 mm, see Fig. 25.

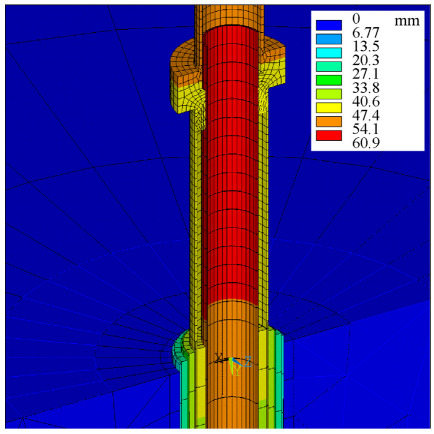

Fig. 20. Modeled wellhead displacement 9 days after discharge of well HE-46 (180° symmetry expansion).

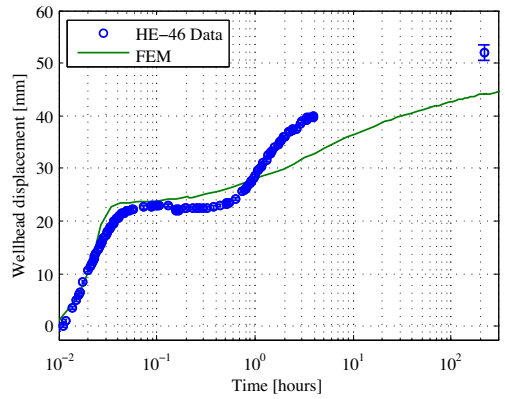

Fig. 21. Measured wellhead displacement for well HE-46 and FEM model results (default model parameters).

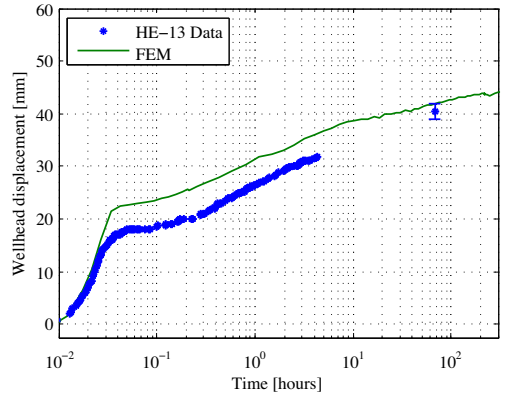

Fig. 22. Measured wellhead displacement for well HE-13 and FEM model results (default model parameters).

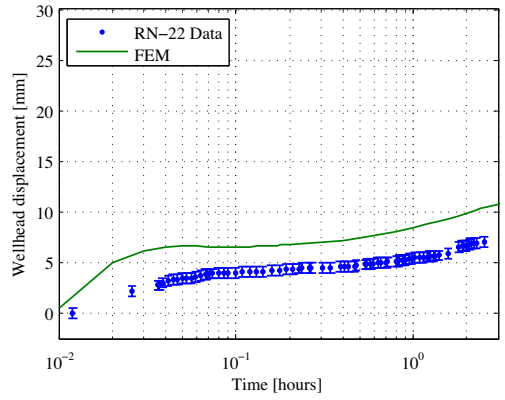

Fig. 23. Measured wellhead displacement for well RN-22 and FEM model results (default model parameters).

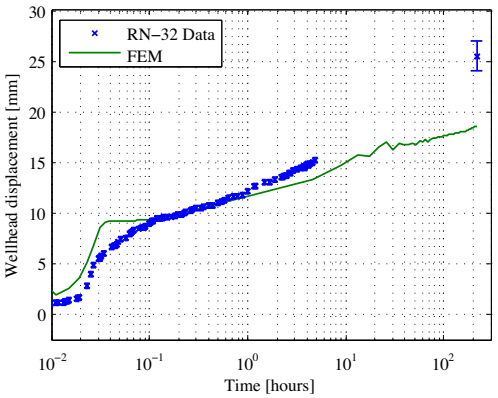

Fig. 24. Measured wellhead displacement for well RN-32 and FEM model results (default model parameters).

6. Discussion

In the wellhead displacement survey, two types of discharges were observed; (i) discharge from initially cold wells that needed air-pressure assistance and (ii) discharge from wells that developed wellhead pressure naturally. Although the data set is small, it is interesting to compare the wellhead displacement of the different types of discharges. For the initially cold wells HE-13, HE-46 and RN-32 the wellhead displacement was very fast in the first minutes after the wellhead valve was opened and then the displacement proceeded at a slower pace. For well HE-53, where the wellhead displacement was presumably at its maximum before discharge, almost no displacement (<0.5 mm) was observed after discharge. For well RN-22, which also had developed wellhead pressure naturally but was not as hot as well HE-53 before discharge, the fast initial displacement as was seen in the initially cold wells was missing. This indicates that thermal stresses and strains produced in the initially warm wells are less severe than that of the initially cold wells because of lower thermal gradient between casings resulting from a long warm-up period. The abrupt temperature change of the initially cold wells on the other hand produces a large thermal gradient between casings in the shallow region of the wells.

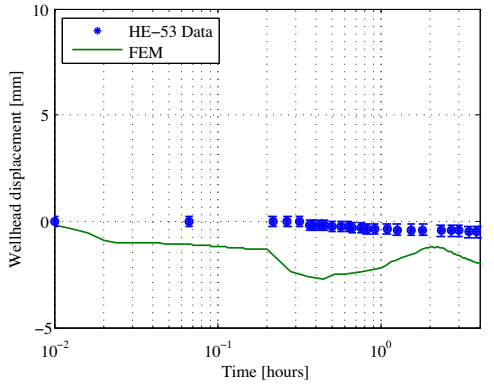

Fig. 25. FEM model results for well HE-53 (default model parameters).

Two separate discharges of well HE-46 show different wellhead displacement curves which shows that the wellhead displacement is not always the same for the same well. The different wellhead pressures before discharge might be the cause, since the water level in the well is pushed lower down the well with increasing pressure. The pre-discharge wellhead pressures were 38 bar-g and 48 bar-g, for discharges 1 and 2, respectively. The difference might also be associated with strain aging of the casings, since the casings repeatedly reach the yield point for repeated discharge-cooling cycles at such high temperatures. In discharge 2, the wellhead displacement was sharp in the beginning, stopped for about 15 min and then proceeded again. The wellhead displacement of HE-13 was similar to that of HE-46, since the displacement also came to a halt after the initial sharp rise, but only for about 3 min in this case. For all of the wells, except HE-53, the wellhead displacement slows down with time and shows signs of exponential decay.

The small wellhead displacement of the failed discharge attempt of HE-46, Fig. 18, suggests that the wellhead displacement of high temperature wells is primarily governed by temperature changes rather than wellhead pressure. The displacement due to the air-pressure release was roughly 2.5% of the final observed displacement when it was discharged successfully. It should however be noted that for saturated steam, pressure and temperature are dependent variables and high wellhead pressure results in increased wellhead temperature, as can be seen in the case of well HE-53.

A detailed probabilistic design analysis of the model, where scatter of the material properties is taken into account, is the next step in this study. By using a probabilistic design approach, effects of material properties, e.g. Young's modulus, thermal expansion coefficient and compressive strength of the concrete, can be determined. This has already been done with a subset of the material properties by Kaldal et al. (2013) but is outside the scope of this paper. As presented by Kaldal et al. (2013), the wellhead displacement changes significantly by changing the shear strength between the steel and concrete surfaces, and the shear strength is presumably quite irregular down the well. By using the default material properties of the model and shear strength data of cemented casings, the modeled wellhead displacement was similar to the measured wellhead displacement for the majority of the wells. The largest difference between the model and the measured displacement was 8 mm for well HE-46, where the final observed displacement 9 days after discharge was 52 mm but the results from the model showed 44 mm. Small wellhead displacement, as was seen in HE-53, was difficult to track as the results fluctuated with time. This is the result of contact element interactions and could be improved by increasing the element mesh density of the model. Additionally, the particular 15 min break in the displacement of HE-46 was not tracked well by the model. Greater resolution and time-series data of the wellbore T–P changes might resolve this, but no such data is available to the authors knowledge.

7. Summary and conclusions

In this paper, a survey of wellhead displacement of high temperature geothermal wells is presented and used to validate a nonlinear structural FEM model of a cased well. To understand the structural response of high temperature wells in greater detail, wellhead displacement data of 6 discharges from 5 wells, located in the Hengill and Reykjanes geothermal areas in Iceland, was gathered. A nonlinear structural FEM model of a cased well is presented and the wellhead displacement data is compared to the modeled results.

The results show good agreement between the model results and wellhead displacement measurements of the 5 different wells.

When modeling small displacements (<1 mm), the results fluctuate which can be resolved by increasing the element mesh density of the model.

Although the wellhead displacement was used here to validate the model, tracking the wellhead displacement is secondary to stress and strain analysis of the cased well. In future studies the model can be used to analyze the structural integrity of casings when subjected to various load cases and load histories. The model can be used to assist with the design process of geothermal well casing programs by predicting various things, e.g. wellhead displacement, stress and strain distribution in each casing and the location of potential joint failures. Additionally, potential load cases and various materials can be tested with the model.

Acknowledgments

This work was financially supported by the University of Iceland research fund, the Technology Development Fund at RANNIS – The Icelandic Centre for Research, the Innovation Center Iceland, Landsvirkjun Energy Research Fund, and GEORG – Geothermal Research Group. Their support is much appreciated. The author would like to thank Reykjavik Energy, HS Orka, Landsvirkjun, Iceland Drilling, Iceland Geosurvey (ISOR), Mannvit and the Innovation Center Iceland for providing data and useful information for the work presented here.

References

Ansys, Inc., 2012. Release 14.5 Documentation for ANSYS.

Ármannsson, H., Fridriksson, T., Guðfinnsson, G.H., Ólafsson, M., Óskarsson, F., Thorbjörnsson, D., 2014. IDDP-the chemistry of the IDDP-01 well fluids in relation to the geochemistry of the Krafla geothermal system. Geothermics 49, 66–75, Iceland Deep Drilling Project: The first well, IDDP-1, drilled into Magma.

ASM, 1992. ASM Handbook: Volume 18: Friction, Lubrication, and Wear Technology. American Society for Metals.

Axelsson, G., Thórhallsson, S., Björnsson, G., 2006. Stimulation of geothermal wells in basaltic rock in Iceland. In: ENGINE – ENhanced Geothermal Innovative Network for Europe, Workshop 3, "Stimulation of Reservoir and Microseismicity".

Axelsson, G., Egilson, T., Gylfadóttir, S.S., 2014. Modelling of temperature conditions near the bottom of well IDDP-1 in Krafla, Northeast Iceland. Geothermics 49, 49–57, Iceland Deep Drilling Project: The first well, IDDP-1, drilled into Magma.

Böðvarsson, G., 1961. Physical characteristics of natural heat resources in Iceland. Jökull 11, 29–38.

Birkisson, S.F., Hole, H., 2007. Aerated fluids for drilling of geothermal wells. In: Proceedings European Geothermal Congress.

Björnsson, G., Ragnars, K., Sigfússon, S., Þorbjörn, Karlsson, 1978. Styrkleiki fóðurröra í háhitaborholum[[nl]]Translation: Casing Strength in High Temperature Wells. Orkustofnun, Virkir hf. and VST HF, In Icelandic.

Elders, W.A., Fridleifsson, G., Bignall, G., 2012. Saga Report No 9. IDDP-ICDP Workshop.

Ferla, A., Lavrov, A., Fjær, E., 2009. Finite-element analysis of thermal-induced stresses around a cased injection well. J. Phys.: Conf. Ser. 181, 012051.

Garcia-Gutierrez, A., Espinosa-Paredes, G., Hernandez-Ramirez, I., 2002. Study on the flow production characteristics of deep geothermal wells. Geothermics 31, 141–167.

Gretarsdottir, S., 2007. Mechanical and Thermal Properties of Well Cement. University of Iceland, Master's thesis.

Hauksson, T., Markusson, S., Einarsson, K., Karlsdóttir, S.N., Ásbjörn Einarsson, Möller, A., Þorsteinn Sigmarsson, 2014. Pilot testing of handling the fluids from the IDDP-1 exploratory geothermal well, Krafla, N.E. Iceland. Geothermics 49, 76–82, Iceland Deep Drilling Project: The first well, IDDP-1, drilled into Magma.

Hole, H., 2008. Geothermal well cementing. In: Petroleum Engineering Summer School Workshop 26.

Ingason, K., Kristjánsson, V., Einarsson, K., 2014. Design and development of the discharge system of IDDP-1. Geothermics 49, 58–65, Iceland Deep Drilling Project: The first well, IDDP-1, drilled into Magma.

ISO/TR 10400, 2007. ISO/TR 10400:2007(E) Petroleum and Natural Gas Industries – Equations and Calculations for the Properties of Casing, Tubing, Drill Pipe and Line Pipe used as Casing or Tubing. ISO (The International Organization for Standardization), CH-1211 Geneva 20.

Kaldal, G.S., Jónsson, M., Pálsson,.H., Karlsdóttir, S.N.,2012. Thermal and structural analysis of the casing in a high temperature geothermal well during discharge. In: Thirty-Seventh Workshop on Geothermal Reservoir Engineering. Stanford University, Stanford, California.

Kaldal, G.S., Jónsson, M., Pálsson, H., Karlsdóttir, S.N., 2013. Using probabilistic analysis with finite element modeling of high temperature geothermal well casings. In: SIMS 54th Conference in Bergen, Norway, pp. 176–184.

Karlsdottir, S.N., Thorbjornsson, I.O.,2009. High Temperature Geothermal Wells – Center of Excellence in Iceland – Phase I: Corrosion Testing of Steel in High Temperature Geothermal Wells in Iceland. In: Technical Report for RANNIS. The Icelandic Centre for Research, in Icelandic.

Magnusdottir, L., 2009. Nonlinear Finite Element Model of a Geothermal Well. University of Iceland, Master's thesis.

Maruyama, K., Tsuru, E., Ogasawara, M., Inoue, Y., Peters, E.J., 1990. An experimental study of casing performance under thermal cycling conditions. SPE Drill. Eng. 5, 156–164.

Palmason, G., 1980. Jarðhitinn sem orkulind (in Icelandic). volume 50. Reykjavik, Iceland.

Palmason, G., 2005. Jarðhitabók (in Icelandic). ISOR, Iceland GeoSurvey, Grensasvegi 9, 108 Reykjavik, Iceland.

Philippacopoulos, A.J., Berndt, M.L., 2002. Structural analysis of geothermal well cements. Geothermics 31, 657–676.

Ragnarsson, A., 2003. Utilization of geothermal energy in Iceland. In: International Geothermal Conference, Reykjavik, Iceland, pp. 39–45.

Snyder, R.E., 1979. Casing Failure Modes in Geothermal Wells. In: Geothermal Resources Council., pp. 667–670.

Sveinbjornsson, B.M., Thorhallsson, S., 2014. Drilling performance, injectivity and productivity of geothermal wells. Geothermics 50, 76–84.

Thórhallsson, S., Pálsson, B., Hólmgeirsson, S., Ingason, K., Matthíasson, M., Bóasson, H., Sverrisson, H., 2014. Well design for the iceland deep drilling project (IDDP). Geothermics 49, 16–22, Iceland Deep Drilling Project: The first well, IDDP-1, drilled into Magma.

Thakur, A., Nemat-Nasser, S., Vecchio, K., 1996. Dynamic Bauschinger effect. Acta Mater. 44, 2797–2807.

Thorhallsson, S., 2008. Geothermal drilling and well pumps. In: Workshop for Decision Makers on Direct Heating Use of Geothermal Resources, UNU-GTB, TBLRREM and TBGMED, Tianjin, China.

Vogel, J.V., 1966. Thermal Oil Recovery. United States Patent Office.

Wallevik, S.Ó., Hjarrecrtarson, B., Alexandersson, K.F., Kubens, S., Oesterheld, S., Wallevik, Ó.H., Ásgeirsdóttir, M.D., 2009. High temperature geothermal wells – Center of Excellence in Iceland – Final report: Concrete suited for high temperature geothermal wells. In: Technical Report for RANNIS. The Icelandic Centre for Research, in Icelandic.

Paper VI

Proceedings World Geothermal Congress 2015
Melbourne, Australia, 19-25 April 2015

Structural Analysis of Casings in High Temperature Geothermal Wells in Iceland

Gunnar Skúlason Kaldal, Magnús Þ. Jónsson, Halldór Pálsson, Sigrún Nanna Karlsdóttir

Faculty of Industrial Engineering, Mechanical Engineering and Computer Science, University of Iceland, Hjardarhagi 2-6, 107 Reykjavík, Iceland

gunnarsk@hi.is

Keywords: Casing, structural analysis, concrete, finite element, thermal loading, thermal expansion

ABSTRACT

Large temperature changes are a central design concern in a diverse range of structures. Large and quick wellbore temperature changes in high temperature geothermal wells, e.g. during discharge and quenching of wells, produce large thermal stresses in the production casing which can cause casing failures. The wellbore temperature change during discharge causes the wellhead to rise due to thermal expansion of the casings, since the wells are constructed of several concentric steel casings which are fully cemented to the top. The structural integrity of such casings is essential for the utilization of high temperature geothermal wells. The casings in connection to the wellhead form a structural system which involves nonlinear interaction of the contacting surfaces. Therefore, the structural system is analyzed numerically with the use of the nonlinear finite element method (FEM). Three FEM models are presented here with the purpose of evaluating the structural integrity of high temperature geothermal well casings. A load history is used in the analysis, consisting of transient wellbore temperature and pressure changes.

1. INTRODUCTION

Energy of deep geothermal heat sources is extracted from geothermal reservoirs through geothermal wells. The energy rich water turns to steam as the pressure drops while it flows up the well. High temperature geothermal wells are often constructed of three concentric casings; a surface casing, an anchor casing and a production casing where the geothermal fluid flows. The casing components that form the casing are either connected with threaded couplings or welded together. Each casing is cemented externally all the way to the top for structural support and leakage prevention. The purpose of the casings is multifold; to prevent collapse of the borehole, to prevent flow from unwanted aquifers, for blow out prevention during drilling and to be a conductor for the geothermal fluid to flow up the well (Björnsson et al., 1978). The anchor casing is connected to an expansion spool below the master valve, allowing for axial displacement for the production casing inside the wellhead when it expands thermally. Numerous casing load cases arise during different stages of geothermal wells, see Figure 1, the main ones being; casing weight (A), differential pressure between outer and inner surface of the casing (B) and temperature changes (C and D).

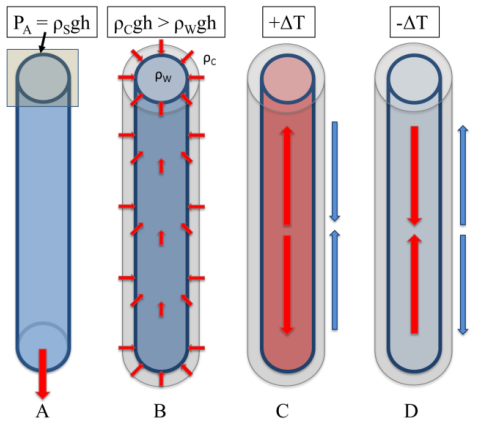

Figure 1: Main load cases of casings; (A) Self weight, (B) Differential pressure and (C and D) Temperature changes.

In general, casing strength is calculated in terms of axial tensile strength, collapse and burst pressures. The most important design loads for oil and gas are casing weight, tensile loading and fluid pressure, in geothermal wells however, high temperature loading is the most severe (Hole, 2008). The temperature change from the cementing temperature conditions to production temperature conditions is typically around 200-300°C uppermost in the well, but the temperature distribution of the casings during cementing provides the initial conditions for thermal stress calculations. Thermal expansion generates thermal stress in the casings and concrete because of the thermal gradient in between the layers. Assuming completely constrained casing, the thermal stress is about 2.5 MPa/°C, which means that a K55 steel casing reaches its yield point (f_{ym} = 379 MPa) at a temperature change of approximately 150°C. Fortunately, K55 casing steel is very ductile and can therefore generate large strain before problems occur. A well composed of concentric steel casings, concrete and surrounding rock formation forms a structural system which involves a number

of structural components, e.g. friction between contacting surfaces, tensile and compressive properties of materials and diminished material properties at elevated temperatures, all of which add nonlinear characteristics to the structure. The load subjected on the structure, the cased well, consists of transient wellbore pressure and temperature changes. The temperature rise while the well is initially discharged can lead to stresses reaching the yield strength of the casing which results in formation of plastic strain. The plastic strain is permanent so if the well cools down again, the plastic strain leads to tensile forces in the casing. These tensile stresses may be large enough to exceed the coupling joint strength of the casing which could result in casing failure (Maruyama et al., 1990). Because the well is composed of alternating layers of casings and concrete, the innermost casing, the production casing is most affected by temperature changes and the external casings are somewhat protected against thermal shocks by the insulation effect of the concrete in between. When initially cold wells are discharged, the thermal shock leads to sudden thermal expansion of the production casing which results in the production of large thermal stresses. Same applies when wells need to be quenched with cooling water, where instead of thermal expansion the cooling results in thermal contraction of the production casing. It's therefore favorable for the production casing that all the casings warm up as uniformly and with as little thermal gradient between them as possible. For that reason slow wellbore temperature changes are required, this can however be difficult to control. Recently, interests have developed in drilling deeper wells. With deeper wells the casing design becomes more challenging due to increased casing depths, higher pressures and temperatures and difficult corrosive environment. Therefore, it's important to know the structural risks involved.

A high temperature geothermal well consisting of a number of concentric cemented steel casings forms a nonlinear structural system where nonlinearities are found in material properties, large displacements and connection between contacting surfaces. The nonlinear finite element method (FEM) is used to construct three models of the cased well providing a tool which can be used to assess casing failure risks by modeling various possible load scenarios that could lead to casing problems. Such modeling also provides evaluation prospects of different materials that could be used in future wells. In this paper, three FEM models of high temperature geothermal well casings and numerical results are presented, some of which have previously been presented.

2. MODELING

2.1 Models

The analysis of the structural system of a high temperature geothermal well can be divided into categories depending on what is to be studied. A specific failure mode, such as a local casing failure, does not necessarily require a full 3D modeling of the whole well – a section of the well could be sufficient to explain the failure mode. In this paper, three models are essentially used to analyze different aspects of the structural system of the high temperature geothermal well; (i) a 2D axisymmetric model of the whole cased well used to model temperature, displacements, stress and strain distributions down the well, (ii) a 2D axisymmetric model of a detailed coupling surrounded by concrete used to further model coupling strength and concrete damage near couplings, and (iii) a 3D model of a section of the well which can be used to model non-symmetric phenomena such as collapse. Casing failure modes and the corresponding FEM models that are used to analyze them are listed in Table 1.

Table 1: Casing failure modes and corresponding FEM model used for analysis.

Failure mode	Description	FEM model
Axial tearing	Tearing at couplings due to high tensile stress.	(i) 2D axisymmetric model of the whole cased well. (ii) 2D axisymmetric model of a detailed coupling surrounded by concrete.
Collapse	Collapse due to pressure difference between the outer and inner pipe wall.	(iii) 3D model of a section of the well, includes impurities and geometrical defects, i.e. manufacturing tolerance, off center casing, external defect, eccentricity and ovality of the casing.
Burst	Rupture due to high internal pressure and low external pressure.	Not specifically modeled.
Concrete damage	Concrete braking because of stress reaching beyond the strength of the concrete.	(i) 2D axisymmetric model of the whole cased well. (ii) 2D axisymmetric model of a coupling surrounded by concrete. (iii) 3D model of a section of the well.
Wellhead displacement	Wellhead displacement due to wellhead pressure and wellbore temperature change.	(i) 2D axisymmetric model of the whole cased well.

Eight-node quadrilateral-shaped elements and six-node triangle-shaped elements are used in the 2D analyses, and 20-node structural solid elements are used in the 3D analysis. Contact element pairs are used between contacting surfaces with the main purpose of preventing intersection of surfaces, while still allowing gap formation and frictional displacement between casing and concrete surfaces. The Coulomb friction model is used to describe friction between contacting surfaces.

The largest of the three models, the (i) 2D axisymmetric model of the whole cased well is used to analyze the structural response of wells to wellbore temperature and pressure changes, see Figure 2. The geometrical sizes and material properties of a particular well and a load history of the well can be read into the model with specific input files. Temperature, displacements, stresses and strains of the casings and concrete at any depth is the output of the model. The structural response of geothermal wells to various load cases can therefore be analyzed. Wellhead displacement due to wellbore temperature changes and wellhead pressure can also be modeled with the model and the model shows correlation with measured wellhead displacement. The model is further described by Kaldal et al. (2013b, 2014).

The (ii) 2D axisymmetric model of a detailed coupling is used to analyze buttress couplings which have been cemented. The interaction between the casing, coupling and the concrete can therefore be modeled. The structural integrity of the concrete near the couplings can also be specially focused on, but all three models show signs of concrete damage near the couplings which are

essentially anchored in the concrete. Results from the two-dimensional model of the whole cased well can be superimposed on this model thus improving the resolution of the results. The geometry of the model can be seen in Figure 4. The boundaries of the model are located 3.5 meters up and down from the center of the coupling and 2 meters outwards from the center of the well.

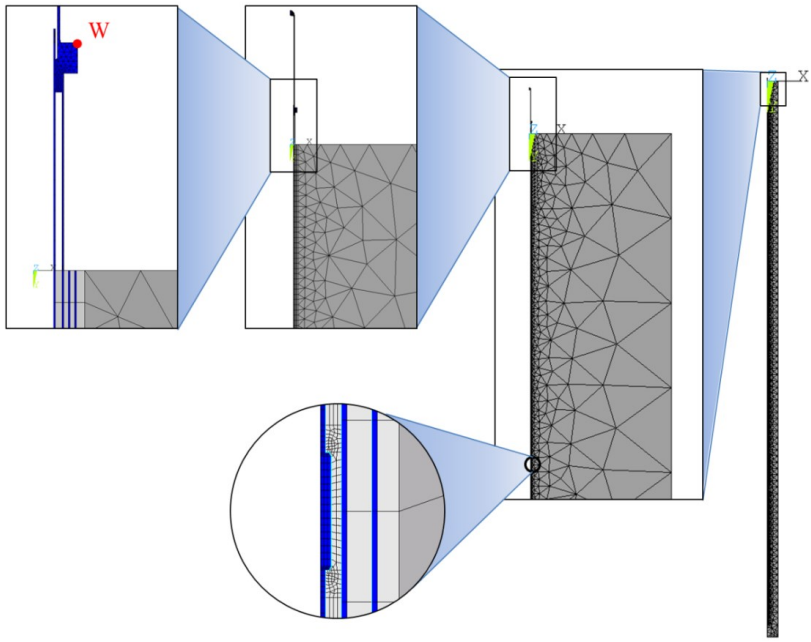

Figure 2: Model i, 2D axisymmetric model of the whole cased well used to model temperature, displacements, stress and strain distributions down the well. W denotes the node location where the wellhead displacement is followed, Kaldal (2013b, 2014).

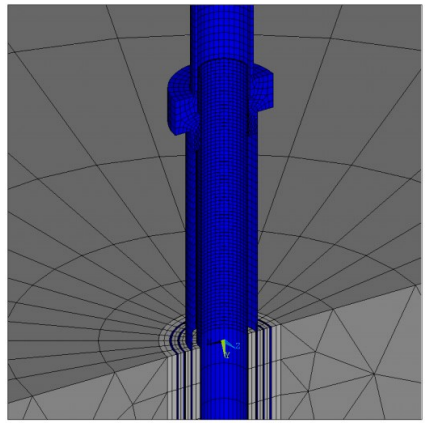

Figure 3: Symmetry expansion (180°) of the wellhead of model i.

The (iii) 3D model of a section of the well is used to model collapse of the production casing. A number of collapse analyses with various geometric imperfections, material impurities and combinations of loads have been modeled by Kaldal (2011, 2013a) where the model is further described.

2.2 Material properties

All models share the same material properties, the default material properties values are listed in Table 2. Tensile data by Karlsdottir and Thorbjornsson (2009) is used for the nonlinear stress-strain curves in the model. The strength reduction of casing steel at elevated temperatures has been tested and presented by Thomas (1967) and Snyder (1979), where reduction of the Young's modulus, yield strength and tensile strength are reported, but accurate stress-strain curves are not available. The stress-strain data in

model is therefore scaled according to the reduction in Young's modulus and yield strength with increased temperature. In the model the maximum compressive strength of concrete is defined as 27.6 MPa and when the maximum compressive strength is reached the concrete is assumed to yield plastically. The coefficient of friction between steel and concrete is defined as $\mu = 0.45$ and the maximum shear strength between the surfaces is defined as $\tau_{max} = 0.46$MPa, which is the mean value of two separate push-out shear strength tests of externally cemented casings performed by Gretarsdottir (2007) and Wallevik et al. (2009).

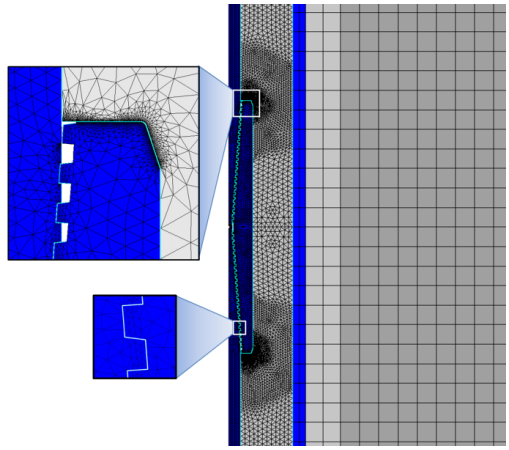

Figure 4: Model ii, 2D axisymmetric model of a detailed coupling.

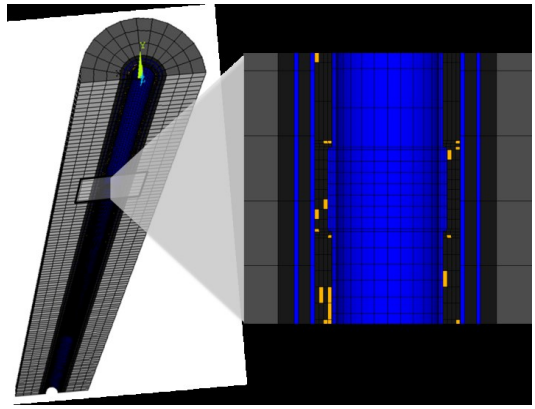

Figure 5: Model iii, a 3D model of a section of the well which is used to model non-symmetric phenomena such as collapse, Kaldal (2011).

Table 2: Default values of several material properties used in the FEM models. Other material properties are discussed in the text.

Item	Symbol	Unit	Steel	Concrete	Rock
Young's modulus	E	GPa	205	2,40	80.0
Poisson's ratio	γ	-	0.30	0.15	0.31
Density	ρ	kg/m3	7850	1600	2650
Thermal conductivity	K	W/(m°C)	50	0.81	2.00
Specific heat	c	kJ/(kg°C)	0.40	0.88	0.84
Thermal expansion	α	1/°C	12e-6	10e-6	5.4e-6

2.3 Loads

In all cases the models are divided into two parts, a thermal part and a structural part. The thermal analysis precedes the structural analysis and calculates the transient temperature distribution of the model. The resulting temperature distribution is then used as temperature load in the structural analysis. In model i, the 2D axisymmetric model of the whole cased well, the load is based on wellbore temperature and pressure data which is logged down the well. In models ii and iii, the load is uniform inside the well,

since only a small section of the well is modeled. A load history of the well, i.e. the wellbore temperature and pressure changes with time, are important to evaluate the stresses that form during the lifetime of the well. A short load history of a well is listed in Table 4. The initial stress of the casings is important to evaluate further stress formation. It consists of casing weight and tensile stress due to cooling of the casing, from cementing conditions to further drilling with cooling fluid. The temperature distribution when the cement sets provides the initial conditions for calculating subsequent thermal stresses in each casing.

3. RESULTS AND DISCUSSION

3.1 Structural analysis of the whole cased well and detailed coupling

The casing program of the modeled well is listed in Table 3 and the load history of the well is listed in Table 4. The initial condition of the surrounding rock formation is the assumed virgin temperature before the well is drilled. When installed, the casings are assumed to hang free from the top before they are cemented and the temperature distribution of the casings during cementing provides the initial temperature for thermal stress calculations. Therefore, the initial conditions of the casings are (a) tensile stress due to casing weight and (b) tensile stress due to cooling, from the cementing temperature distribution to the drilling fluid temperature from further drilling.

Table 3: The casing program of the modeled well.

Casing	Outer diameter [inches]	Thickness [mm]	Depth [m]	Steel grade
Production casing	13 3/8	12.2	700	K55
Anchor casing	18 5/8	11.0	300	K55
Surface casing	22 ½	11.0	75	X56

The load history of the well, listed in Table 4, consists of the initial conditions, cooling of the well due to drilling, temperature recovery, pre-discharge conditions where air-pressure is used for discharge assistance, discharge (ΔP and ΔT), and post-discharge where constant production conditions are assumed.

Table 4: A load history of the well for model i.

Nr.	Load case	Description	T_{wh} [°C]	$T_{@700m}$ [°C]	Time period
1.	Rock temperature	Assumed virgin temperature of rock formation.	11	210	Initial
2.	Cementing temperature	Initial temperature of casings when cemented.	4	107	Initial
3.	Cooling due to drilling	Cooling while drilling the total depth of the well.	5	10	40 days
4.	Temperature recovery	Well warm-up from cold conditions.	11	210	9 months
5.	Pre-discharge (air compressor)	T and P conditions prior to discharge assuming discharge assistance by pumping air into the well to increase wellhead pressure.	5	104	24 hours
6.	Discharge (ΔP)	Wellhead opened and pressure changes sharply.	5	104	1 minute
7.	Discharge (ΔT)	The wellbore temperature changes gradually.	203	240	12 minutes
8.	Post-discharge	Post discharge conditions followed assuming constant production.	203	240	9 days
9.	Post-discharge	Post discharge conditions further followed.	203	240	3 months

The temperature distribution of the well and the surrounding rock formation at different times in the load history are displayed in Figure 6. The geometry of the modeled wellhead and the displacement of the wellhead after going through the load history are displayed in Figure 7 and the modeled wellhead displacement during discharge can be seen in Figure 8. The wellhead displacement is fast during the first minute and then slows down.

Formation of stress during discharge near the topmost coupling of the production casing and the surrounding concrete is displayed in Figure 9. As the production casing expands due to thermal expansion, during the increasing wellbore temperature, the wellhead rises and large stress is produced in the surrounding concrete which warms up slower than the production casing. Similar production of stress is seen in the detailed coupling model (model ii), see Figure 12.

Axial stress in the production casing at various times in the load history of the well are plotted in Figure 10. The casing is initially in tension due to the casing weight and cooling from drilling, then when the well is allowed to warm up the tensile stress is decreased as the casings warm up from the outside. Since the well is warmer deeper in the well, compressive stress builds up as the casing expands thermally. In this case, air-compressor is assumed to be used to generate enough wellhead pressure in order for the well to be discharged. This cools down the casing and tensile stress is formed again. Now, the well is discharged and it warms up suddenly which generates high compressive thermal stress. Due to this, permanent strain is produced in the casing as the stress reaches above the yield strength of the material. As external casing layers slowly warm-up and the casings expand thermally, the stress is slowly reduced in the production casing.

When wells need to be quenched with cooling water in order to be shut down, large thermal stresses are produced. In Figure 11 the model is used to analyze the production of stress in the concrete near a production casing coupling during cooling. Cooling the well gradually over a longer period of time results in lower stress in the surrounding concrete due to lower thermal gradient between the casing and the concrete, this is shown in Figure 11.

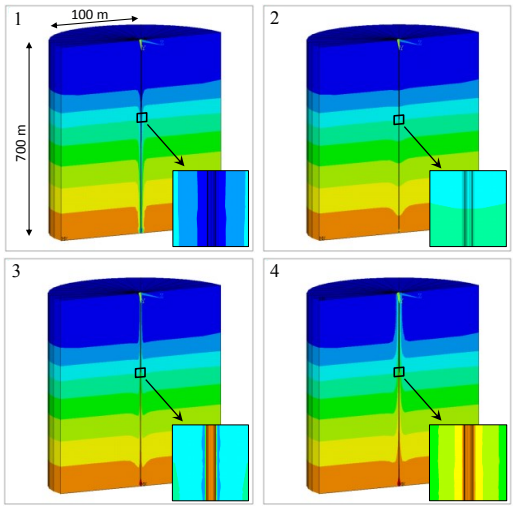

Figure 6: Temperature distribution of the well and formation at different times (180° symmetry expansion of model i). 1. Cooling due to drilling, 2. Warm-up, 3. Discharge (12 min), and 4. Discharge (3 months).

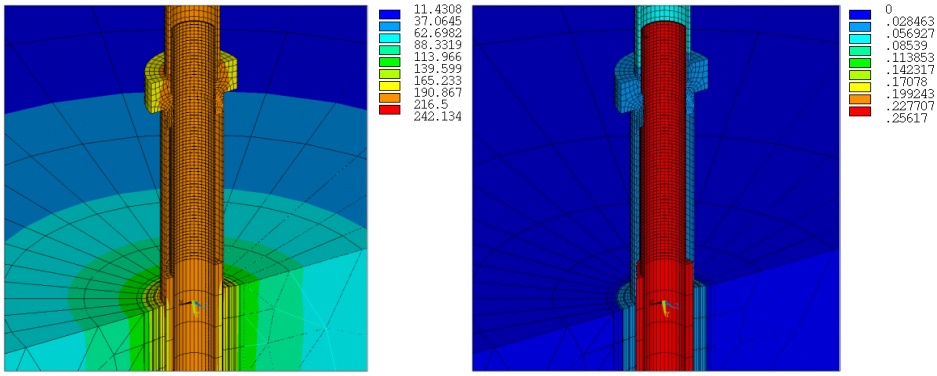

Figure 7: Left: temperature distribution of the wellhead three months after discharge (°C). Right: axial displacement of the wellhead (meters) after going through the load history that is listed in Table 4 (180° symmetry expansion of the wellhead of model i).

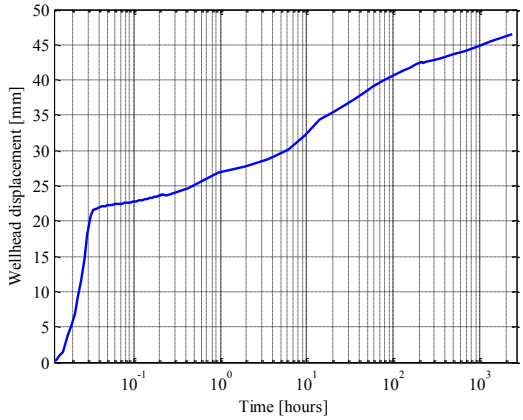

Figure 8: Modeled wellhead displacement of the well during discharge (model i).

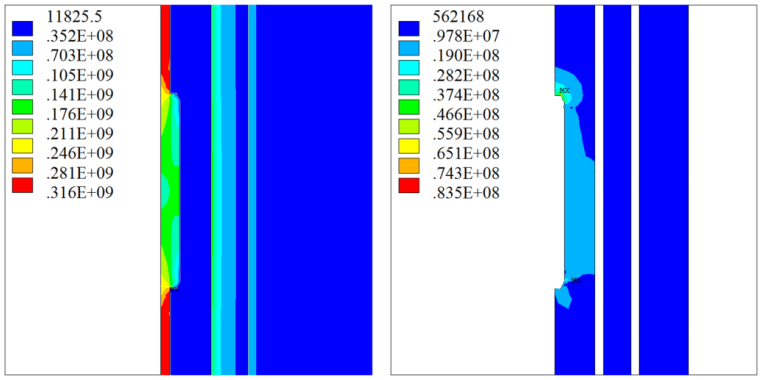

Figure 9: Stress (von Mises) in near the topmost coupling of the production casing during discharge (model i, concrete shown separately on the right), Kaldal 2014.

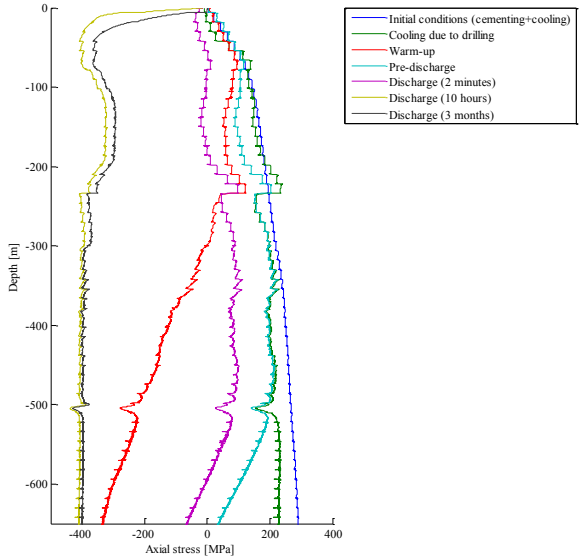

Figure 10: Axial stress in the production casing at different times in the load history analysis (model i).

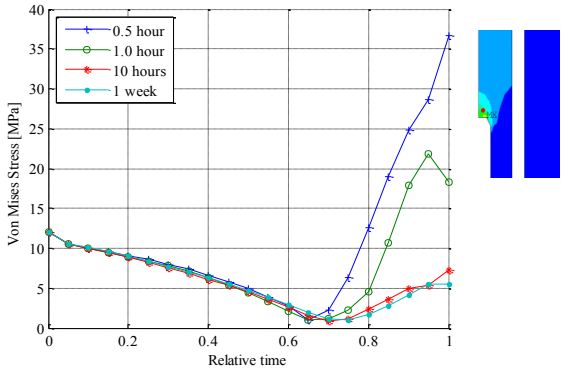

Figure 11: Comparison of stress in concrete near the topmost coupling of the production casing with different cooling times of a well (ΔT of ~200°C).

The detailed coupling model is here used to further model concrete damage near the topmost coupling of the production casing in the well. First, the top end of the production casing is subjected to a displacement of 5 mm. This could be interpreted as tension due to a sudden cooling of the casing, or if the focus is on the concrete only, a displacement due to sudden thermal expansion in the top of the well. The displacement leads to tensile stress in the topmost threads of the coupling as is seen in the top left corner in Figure 12.

In this case, the concrete is modeled elastically, thus the stress is linear according to the Young's modulus, and in each step the concrete elements are checked if they have exceeded the concrete compressive and tensile strength. The tensile strength is assumed to be 10% of the compressive strength. The elements that have exceeded the concrete strength are given diminished material properties to simulate concrete damage. These elements are colored red in the top right corner in Figure 12. Using this approach the large production casing displacement of 5 mm generates a concrete damage through the full thickness of the concrete.

Although this might be an overestimation, the analysis indicates that concrete damage could be substantial near the topmost couplings of the production casing where the casing displacement is not as restricted as it is deeper in the well.

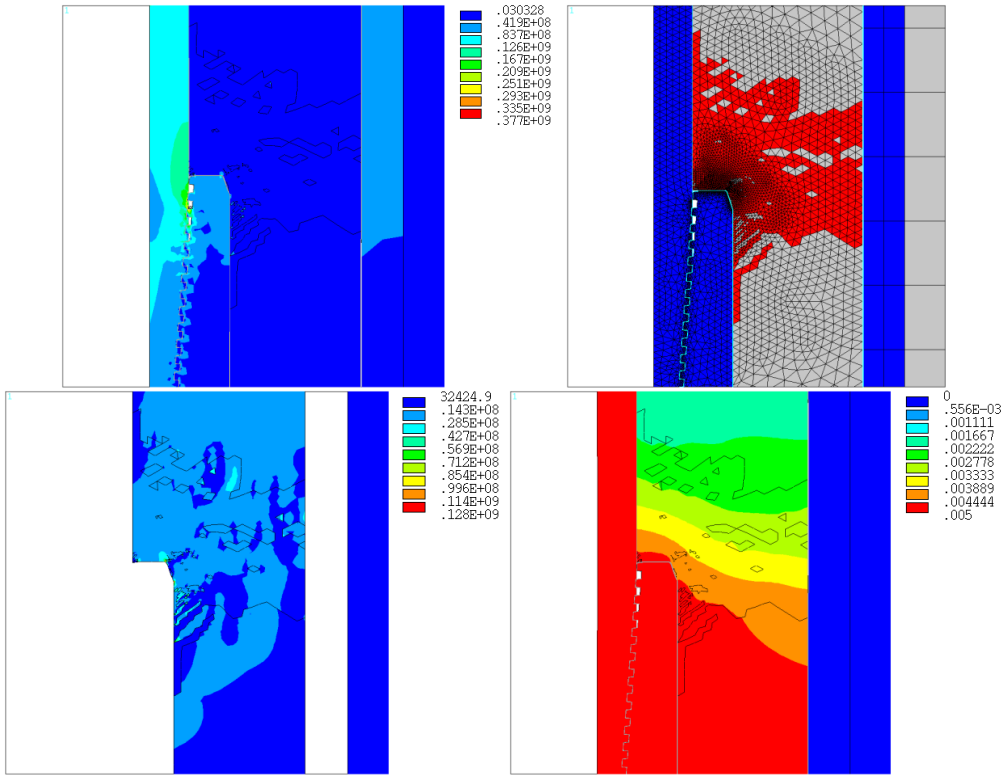

Figure 12: Model ii, analysis of the topmost coupling of the production casing, 5 mm upward displacement of the top end of the production casing. Top left corner: Stress (von Mises) in the casing and coupling due to displacement of the production casing. Bottom left corner: stress (von Mises) in concrete due to upwards displacement of the casing. Top right corner: concrete elements that have exceeded the compressive strength of the concrete are shown in red. Bottom right corner: displacement due to upwards casing displacement.

In the second analysis, the lower end of the production casing is subjected to the same displacement of 5 mm, see Figure 13. This could resemble sharp warm-up of the production casing. In this case, almost no stress is generated in the concrete near the top of the coupling, as the displacement fades out in the coupling. Instead, tensile stress is produced in the concrete near the bottom of the coupling.

In both these cases, concrete damage occurs near the coupling due to displacement of the production casing. If wells go through numerous discharge-cooling cycles, the top couplings in the production casing and the surrounding concrete might lose its sealing capacity and the topmost couplings of the casing might also become a weak point due to decreased support of the surrounding concrete.

3.2 Collapse analysis of the production casing of the well

Collapse analysis using the 3D model, were water is assumed to be trapped inside the annulus between the production casing and the external casing, is seen in Figure 14. The modeled casing has an outer diameter of 13 3/8 inch and wall thickness of 12.2 mm.

Imperfections, consisting of 80% water and 20% concrete, are randomly distributed in the area where the water is assumed to be trapped (Kaldal et al., 2011). In the analysis, the casing collapses at a load consisting of 300°C internal temperature and additional differential pressure between the outer and inner casing wall of 20 bars.

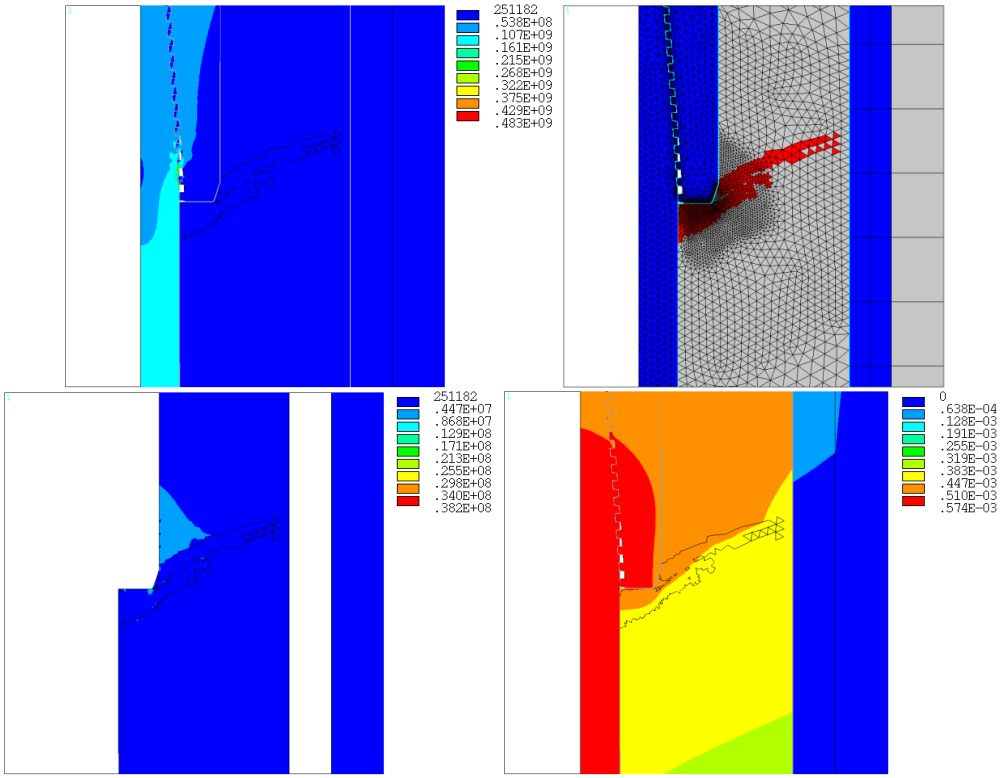

Figure 13: Model ii, analysis of the topmost coupling of the production casing, 5 mm upward displacement of the lower end of the production casing. Top left corner: Stress (von Mises) in the casing and coupling due to displacement of the production casing. Bottom left corner: stress (von Mises) in concrete due to upwards displacement of the casing. Top right corner: concrete elements that have exceeded the tensile strength of the concrete are shown in red. Bottom right corner: displacements due to upwards casing displacement.

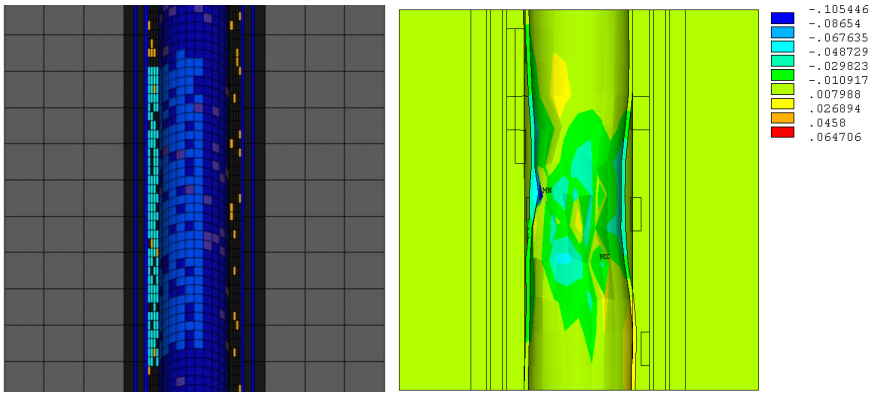

Figure 14: On the left: trapped water in concrete (water elements are cyan colored and production casing is transparent), Kaldal (2011). On the right: collapse at 300°C and 20 bar additional pressure difference between outer and inner casing wall (radial displacement in meters, 13 3/8 inch casing outer diameter with wall thickness of 12.2 mm, model iii), Kaldal (2011).

The effect of structural support of concrete and various defects have also been analyzed by Kaldal et al. (2013a). The results show how the collapse resistance of the modeled casing increases when support of concrete is added, see Figure 15 and Figure 16. The collapse shape of the casing that is structurally supported by concrete resembles collapse shapes that have been documented in high temperature geothermal wells. The results also show that defects and deformations, such as ovality and mode shape perturbation, results in reduction in collapse resistance of the casing of approximately 30-50% compared to a perfectly round casing, see Kaldal et al. (2013a).

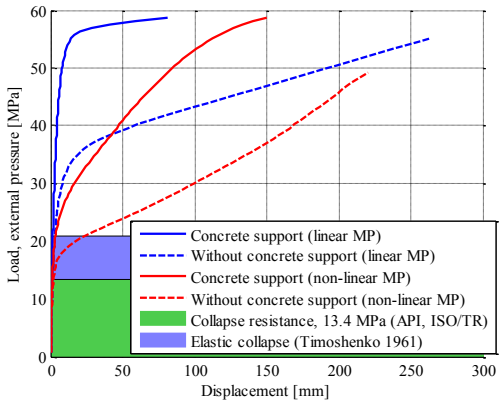

Figure 15: Load displacement curves comparing casing collapse with and without concrete support, external defect of 50% of the casing thickness is included, Kaldal (2013a).

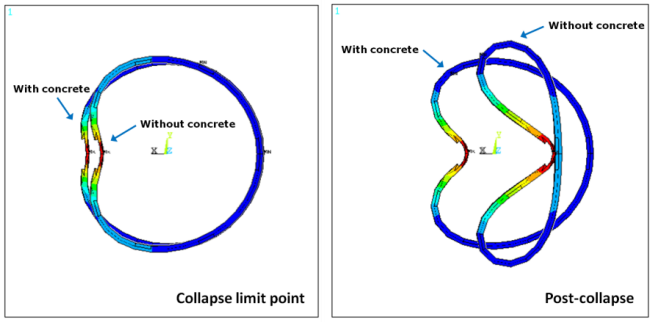

Figure 16: Collapse limit point and post-collapse with and without concrete support (cross-section view), Kaldal (2013a).

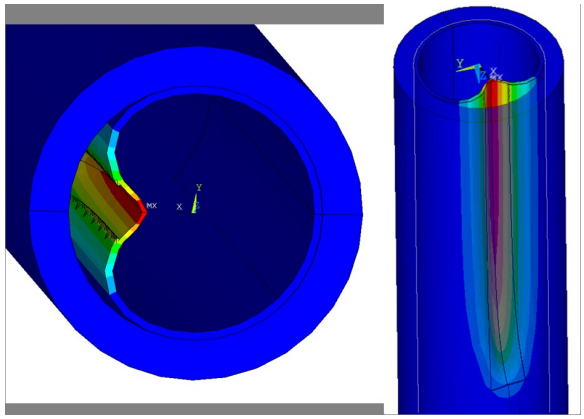

Figure 17: Collapsed casing with external defect with a depth of 40% of the wall thickness (13 3/8 inch casing outer diameter with wall thickness of 12.2 mm), Kaldal (2013a). Collapse occurs at external pressure of 13.3 MPa.

4. CONCLUSION

Analysis of a high temperature geothermal well using three FEM models was presented here. The results that were presented show how the models can be used to structurally evaluate the casing of the well. Possibilities of analysis by using these models are virtually unlimited in terms of load scenarios and material selection. By using the models, well design and well operations could be improved by analyzing material selection, casing sizes and various load scenarios during the lifetime of the well.

ACKNOWLEDGMENT

This work was financially supported by the University of Iceland research fund, the Technology Development Fund at RANNIS - The Icelandic Centre for Research, the Innovation Center Iceland, Landsvirkjun Energy Research Fund, and GEORG - Geothermal Research Group. Their support is much appreciated. The authors would like to thank Reykjavik Energy, HS Orka, Landsvirkjun, Iceland Drilling, Iceland Geosurvey, Mannvit and the Innovation Center Iceland for providing data and useful information for the work presented here.

REFERENCES

Björnsson, G., Ragnars, K., Sigfússon, S., Karlsson, Þ.: Styrkleiki fóðurröra í háhitaborholum (In Icelandic, translation: Casing Strength in High Temperature Wells). Orkustofnun, Virkir HF. and VST HF. Reykjavik (1978).

Gretarsdottir, S., 2007. Mechanical and thermal properties of well cement. Master's thesis. University of Iceland.

Hole, H.: Geothermal well cementing. Petroleum Engineering Summer School Workshop 26, (2008)

Kaldal, G. S., Jonsson, M. Þ., Palsson, H., Karlsdottir, S. N.: Load History and Buckling of the Production Casing in a High Temperature Geothermal Well. Proceedings, 36th Workshop on Geothermal Reservoir Engineering, Stanford University, Stanford, CA (2011).

Kaldal, G.S., Jonsson, M. Þ., Palsson, H., Karlsdottir, S. N.: Thermal and structural analysis of the casing in a high temperature geothermal well during discharge. 37th Workshop on Geothermal Reservoir Engineering, Stanford University, Stanford, CA (2012).

Kaldal, G. S., Jonsson, M. Þ., Palsson, H., Karlsdottir, S. N.: Collapse Analysis of the Casing in High Temperature Geothermal Wells. Proceedings, 38th Workshop on Geothermal Reservoir Engineering, Stanford University, Stanford, CA (2013a).

Kaldal, G. S., Jonsson, M. Þ., Palsson, H., Karlsdottir, S. N.: Using probabilistic Analysis with Finite Element Modeling of High Temperature Geothermal Well Casings. SIMS 54th conference in Bergen, Norway, October 16-18 (2013b).

Kaldal, G. S.: Structural Modeling of Casings in High Temperature Wells in Iceland (in Icelandic), Vélabrögð, **35**, (2014), 12-14

Karlsdottir, S.N., Thorbjornsson, I.O.: High Temperature Geothermal Wells - Center of Excellence in Iceland - Phase I: Corrosion Testing of Steel in High Temperature Geothermal Wells in Iceland (in Icelandic). Technical Report for RANNIS (The Icelandic Centre for Research), Innovation Center Iceland, Reykjavik (2009).

Maruyama, K., Tsuru, E., Ogasawara, M., Inoue, Y., Peters, E.J., 1990. An experimental study of casing performance under thermal cycling conditions. SPE Drilling Engineering 5, 156–164.

Snyder, R.E.: Casing Failure Modes in Geothermal Wells. Geothermal Resources Council, (1979), 667–670.

Thomas, P.D.: High temperature tensile properties of casing and tubing. API Division of Production 1967 Midyear Standardization Conference, San Francisco, CA (1967).

Wallevik, S.., Hjartarson, B., Alexandersson, K.F., Kubens, S., Oesterheld, S., Ólafur H. Wallevik, Ásgeirsdóttir, M.D., 2009. High Temperature Geothermal Wells - Center of Excellence in Iceland - Final report: Concrete Suited for High Temperature Geothermal Wells. Technical Report for RANNIS (The Icelandic Centre for Research), in Icelandic.

Paper VII

Geothermics 62 (2016) 1–11

Contents lists available at ScienceDirect

Geothermics

journal homepage: www.elsevier.com/locate/geothermics

Structural modeling of the casings in the IDDP-1 well: Load history analysis

Gunnar Skulason Kaldal*, Magnus T. Jonsson, Halldor Palsson, Sigrun N. Karlsdottir

Faculty of Industrial Engineering, Mechanical Engineering and Computer Science, University of Iceland, Hjardarhagi 2-6, IS-107 Reykjavik, Iceland

ARTICLE INFO

Article history:
Received 26 November 2015
Received in revised form 31 January 2016
Accepted 2 February 2016

Keywords:
Structural analysis
Steel casing
High temperature geothermal well
Wellhead displacement
Finite-element analysis
IDDP

ABSTRACT

Flow testing of IDDP-1, the first Icelandic Deep Drilling Project (IDDP) well drilled in the Krafla geothermal field in Iceland, demonstrated promising results by producing superheated steam. During an unavoidable quenching of the well the innermost casing failed presumably due to tensile stresses caused by thermal contraction. Since the structural integrity of casings is essential for utilization of high temperature geothermal wells, the well has not been discharged again. In this paper, the casings of the well are analyzed structurally with a nonlinear finite-element model. The load history of the casings is followed from installation and through several thermal cycles, but the well was discharged at least six times before it was quenched with cold water. The results show that changes in stiffness due to the presence of casing shoes and changes in casing thickness have an effect on the stress and strain formations in neighboring casings. The results illustrate that during each thermal cycle, the wellbore thermal load is more severe for the production casing than for the external casings that are somewhat protected, provided that cementing in between is adequate.

1. Introduction

Thermal expansion and degradation of materials at elevated temperatures pose challenges to the structural design of high temperature geothermal wells. With recent increasing interest in drilling deeper geothermal wells the strength of casings becomes one of the limiting factors, particularly due to effects caused by thermal expansion and material degradation. The thermal gradient that develops between multiple casings, e.g. early on in discharges and during quenching, causes thermal expansion mismatch that generates large stresses and commonly permanent (plastic) strains in the steel casings.

The Iceland Deep Drilling Project (IDDP) is a research and development project that is investigating the possibility of increasing the energy resources in Iceland by obtaining high-enthalpy, supercritical geothermal fluids (Elders et al., 2014). The first well, IDDP-1, was drilled at the Krafla geothermal field in the years 2008–2009. It was designed to reach supercritical conditions at 4500 m depth but the drilling came to an end at about 2100 m depth after drilling into magma (Hólmgeirsson et al., 2010; Pálsson et al., 2014). Despite this, the well was completed and flow testing demonstrated promising results, where the steam output eventually became superheated. The well became the world's hottest producing geothermal well (Elders et al., 2012). It was discharged several times with intermittent shut-in periods and the operation history shows that the casings have gone through several thermal cycles. Due to a critical situation of steam leakage followed by a master valve malfunction, the well was quenched by injecting water into it (Ingason et al., 2014). A video log of the well revealed three failures where the production casing had been teared apart, at approximate depths of 300 m, 356 m and 505 m. In all cases the failures developed at joints where the casing had been pulled down from the coupling, presumably due to tension from thermal contraction. Fig. 1 illustrates the rupture that occurred at 300 m depth. In all three cases the failures exposed the concrete and external casing to the geothermal fluid. The direct contact of the fluid to the anchor casing could cause potential corrosion problems and the thermal insulation provided by the concrete in between is lost. During the initial flow testing of the well, the production casing collapsed at about 620 m depth, near to a suspected intersection between two cementing operations, partially blocking the well (Pálsson et al., 2014).

A nonlinear finite-element model that is used to structurally analyze the cased section of the IDDP-1 well is presented here. The purpose of the model is to evaluate the structural integrity of the casings when subjected to temperature and pressure loads as were seen in the IDDP-1 well. The model has previously been tested against wellhead displacement data of 5 different wells during

* Corresponding author.
E-mail address: gunnarsk@hi.is (G.S. Kaldal).

http://dx.doi.org/10.1016/j.geothermics.2016.02.002
0375-6505/

Table 1
The casing program of IDDP-1 (as built) (Thórhallsson et al., 2014; Pálsson et al., 2014).

	D [in]	*t* [mm]	Length [m]	Steel grade	Connections
Surface casing	32 1/2	13.0	87	X56	Welded
Intermediate casing 1	24 1/2	13.0	254	K55	Welded
Intermediate casing 2	18 5/8	13.0	785	K55	BTC
Anchor casing (Top 290 m)	13 5/8	15.9	290	T95	Hydril 563
Anchor casing (290–1949 m)	13 3/8	13.1	290–1949	K55	Hydril 563
Production casing	9 5/8	13.8	1935	K55	Hydril 563
Slotted liner	9 5/8	12.0	1935–2072	K55	BTC

discharge and shows good agreement with the data (Kaldal et al., 2015), but is here adapted for transient stress and strain analysis of the cased section of the IDDP-1 well. The load history of the well is analyzed, in particular to assess the structural consequences of multiple discharges with intermediate shut-in stops and the structural impact of quenching the well with cold water. Since the load history is important for analyzing built-up plastic strain in the casings, the phases of the discharge system, given by Ingason et al. (2014), are used to reconstruct the load history for the structural analysis.

2. Modeling of IDDP-1

The casing program of IDDP-1 was designed to withstand severe pressure and temperature conditions and therefore has two additional intermediate casings (Pálsson et al., 2014). The casing program of the well as it was built is listed in Table 1. Hydril/Tenaris 563 connections were selected for the production casing and anchor casing and the top part of the anchor casing was designed for creep and rupture conditions (Thórhallsson et al., 2014). The anchor casing therefore consists of two different thicknesses and steel grades. The top 290 m, consist of 15.9 mm thick API grade T95 steel casing with a diameter of 13 5/8″ and the lower section, below 290 m, consist of 13.1 mm thick API grade K55 steel casing with a diameter of 13 3/8″.

A nonlinear finite-element model (FEM) created in Ansys was used to model the well. The model, see Fig. 2, is two-dimensional and axially symmetric around the center of the well. The stress–strain curves of the steel grades that are implemented in the model were obtained from tensile tests by Karlsdottir and Thorbjornsson (2009). The curves are converted to true stress–true strain before implementation. Strength reduction at elevated temperatures is accounted for by scaling the curves according to guidelines in the recently updated New Zealand standard NZS 2403:2015, "Code of Practice for Deep Geothermal Wells". Concrete strength reduction at elevated temperatures is based on strength reduction curves of the Young's modulus and compressive strength of concrete by Phan and Carino (2000). In the model the steel follows a kinematic hardening material model where the Bauschinger effect and buildup of plastic strain during thermal cycles is included. The Bauschinger effect is commonly observed in metals where the yield stress in one direction (e.g. in tension) is reduced if the preceding stress in the reverse direction (e.g. in compression) has reached beyond yield (Paul et al., 2016). Contact between surfaces is defined with contact elements and frictional characteristics are implemented with the Coulomb friction model for all contacting surfaces. Material properties and friction implementation of the model are further described by Kaldal et al. (2015).

The casings and concrete are meshed with eight-node quadrilateral-shaped elements and the rock formation is meshed with six-node triangle-shaped elements. Since the diameter-to-depth ratio of the model is very small, a large number of elements is required because the elements must have proper width-to-length ratio to function correctly. Modeling the IDDP-1 well is therefore computationally demanding because of deep multiple casings which have multiple contact surfaces and due to the long transient load history of the well. In order to model the cased section of the well, some simplifications are made. The anchoring effect of the couplings in the concrete is included by using bonded contact at the coupling locations. A simplified wellhead is also included to account for wellhead pressure and the interaction between the production casing and the wellhead.

Mesh sensitivity convergence studies were performed with the mesh configurations that are listed in Table 2. In order to evaluate the mesh sensitivity, the model needs to be cut from the bottom due to node limitations of the academic version of Ansys. The convergence study shows similar results for all four meshes, see Fig. 3. Mesh IV is therefore chosen for the analysis and the casings are analyzed down to 1700 m depth. Using coarser mesh would violate element shape checks. Furthermore, the convergence studies show that cutting the model from the bottom does not change the results since load premises are not changed.

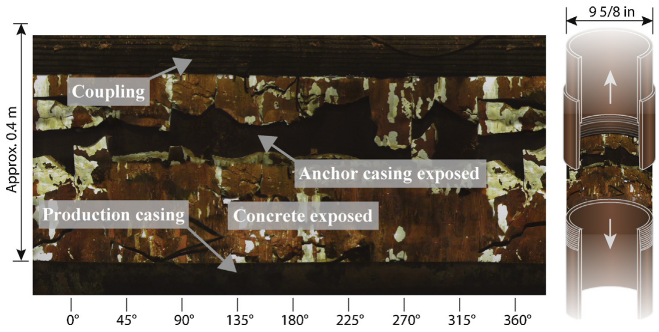

Fig. 1. Coupling rupture at approximately 300 m depth in the IDDP-1 well (by courtesy of Landsvirkjun). Combined image from a video log after the well was quenched. The failure generated a gap (approximately 0.4 m) and exposed external concrete and the anchor casing.

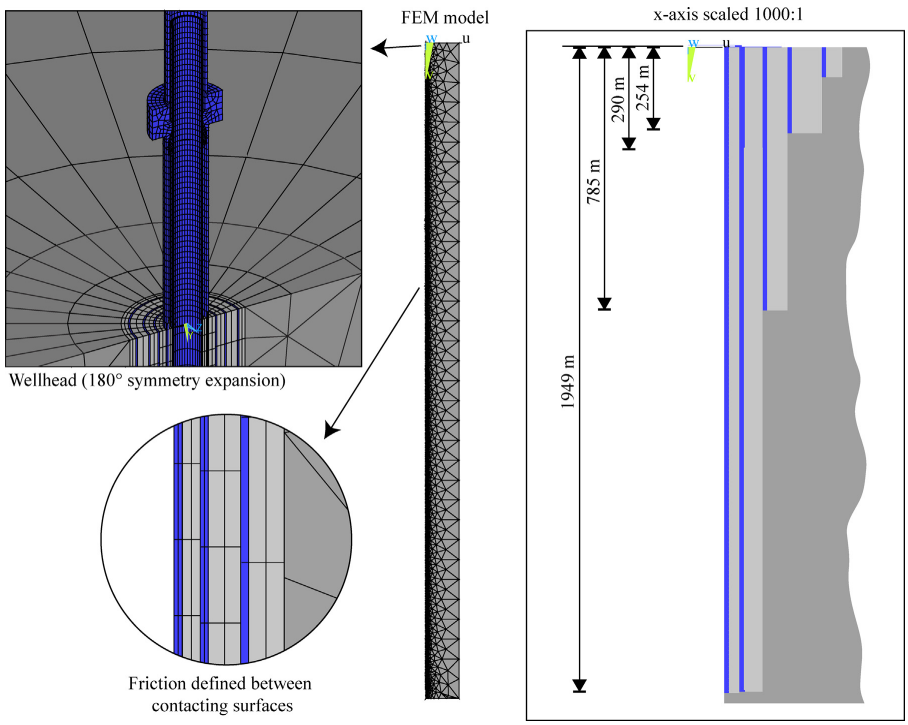

Fig. 2. Axisymmetric nonlinear FEM model of the IDDP-1 well. The anchoring effect of the couplings in the concrete is included in the model by using bonded contact at the coupling locations. A simplified wellhead is also included to account for wellhead pressure and the interaction between the production casing and the wellhead. The casing depths are shown to the right by scaling the x-axis by 1000 to 1.

Table 2
Considered mesh densities in radial (elements/thickness) and longitudinal (elements/m) directions.

Mesh	Model depth (m)	Mesh density	Production casing	Production concrete	Anchor casing	Anchor concrete
I	390	Radial	4	3	2	2
		Longitudinal	15.6	15.6	7.6	7.6
II	774	Radial	2	2	2	2
		Longitudinal	7.6	7.6	7.6	7.6
III	1209	Radial	1	2	1	2
		Longitudinal	7.6	7.6	4.0	4.0
IV	1722	Radial	1	2	1	2
		Longitudinal	4.0	4.0	4.0	4.0

The solution process of the model is divided into thermal and structural parts that use identical meshes and the transient results from the thermal model are used as load in the structural part of the model. The boundary conditions at the outer boundary of the model, located 100 m from the center of the well, are defined as the formation temperature in the thermal model and displacements are not allowed in the structural model. Likewise, no displacements are allowed at the bottom boundary of the formation which is located 20 m deeper than the scaled depth of the casing shoe. All casings are fully fixed to the formation at the casing shoe and are otherwise restrained by friction. The model represents the global structural system and local details, e.g. threads of couplings and centralizers, are excluded. The objective is to analyze the structural response of the well throughout its load history.

The effect of stress that formed during the installation of the casing is accounted for with initial stress conditions for each casing. It consists of (i) tensile stress from a casing hanging free from the top in a well filled with cold water and (ii) thermal stress from the temperature difference between the cement as it sets and the drilling fluid. The cementing temperature of the four innermost casings displayed in Fig. 4 is based on data from the operator of the well, the Icelandic power company Landsvirkjun.

The formation temperature is used as an initial condition and is based on the estimated formation temperature of a neighboring well KG-25 which is located about 100 m from IDDP-1. Ingason et al. (2014) presented the operation history data of the wellhead pressure (P) and temperature (T) of IDDP-1 during five discharge phases. The operation history, discharge phases and wellhead temperatures are shown in Fig. 5. During phase I, saturated steam was produced but in the succeeding phases the fluid became superheated as shown in Fig. 6. The load cases for each discharge phase is applied with temperature and pressure inside the well, shown in

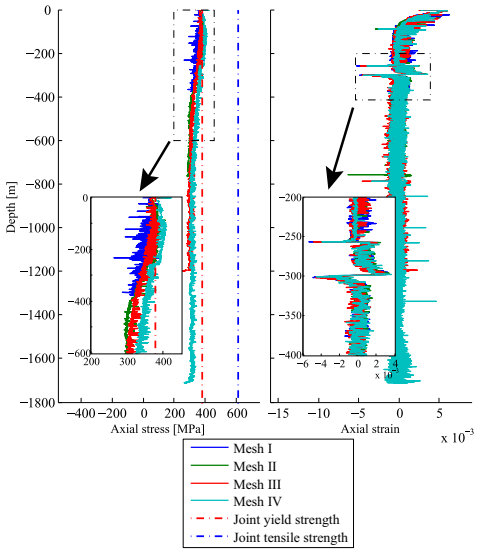

Fig. 3. Mesh convergence studies. Results taken after 30 s of cooling. The different mesh densities are listed in Table 2.

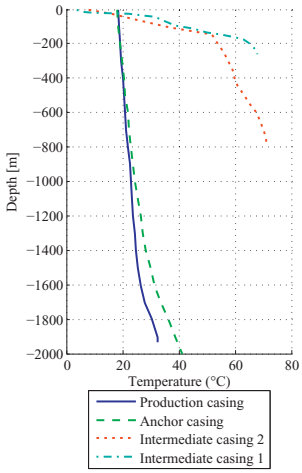

Fig. 4. Assumed cementing temperature of the four innermost casings, based on data from Landsvirkjun. This is used as a reference temperature for initial thermal stress calculations in the model.

Figs. 7–11 . The temperature load inside the well is released during shut-in periods, so the well cools radially from the outside, and the pressure is assumed to reach the same condition as in the initial warm-up period. During quenching, the cooling of the wellbore and the inner surface of the production casing is assumed to be almost instantaneous. The load is thus a step load except for the first 10 s which are ramped.

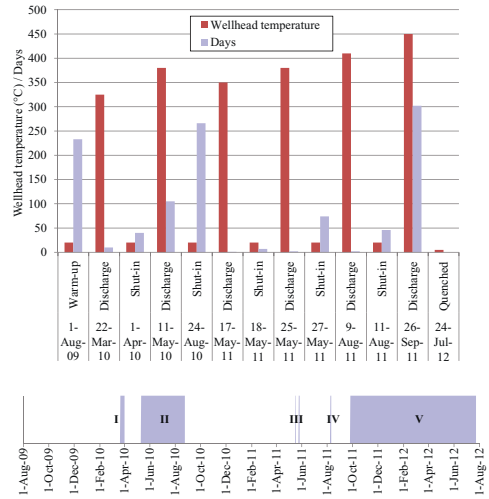

Fig. 5. Operation history and maximum wellhead temperature of each discharge phase of IDDP-1.

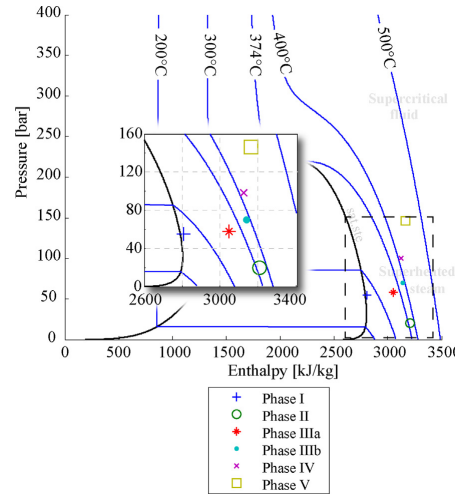

Fig. 6. Enthalpy estimation of the fluid in the different discharge phases of the IDDP-1 well.

3. Results

Fig. 12 shows the measured and modeled vertical displacement of the wellhead of IDDP-1 during warm-up, multiple discharge phases and quenching of the well. The height of the wellhead was measured (by Landsvirkjun personnel) at the lower flange of the master valve and the reference point for the measurements was the drilling platform which is grounded approximately 3.0 m outward from the center of the well. In the graph, the start of each discharge phase is indicated with green lines.

The evolution of the maximum von Mises strain (total strain) of the production casing and the anchor casing over the operation history of the well is displayed in Fig. 13. Cyclic stress and

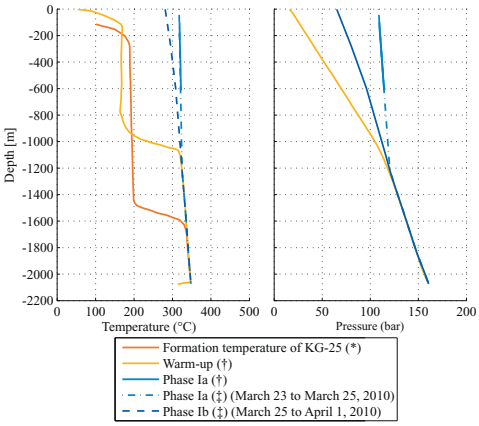

Fig. 7. Temperature and pressure loads for the modeling of phase I. * Formation temperature of KG-25 (Björnsson et al., 1990), † 8 months warm-up (Axelsson et al., 2014), ‡ Based on monitored wellhead temperature and pressure (Ingason et al., 2014).

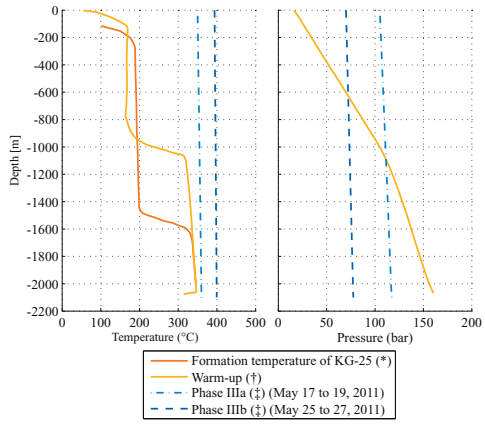

Fig. 9. Temperature and pressure loads for the modeling of phase III. * Formation temperature of KG-25 (Björnsson et al., 1990), † 8 months warm-up (Axelsson et al., 2014), ‡ Based on monitored wellhead temperature and pressure (Ingason et al., 2014).

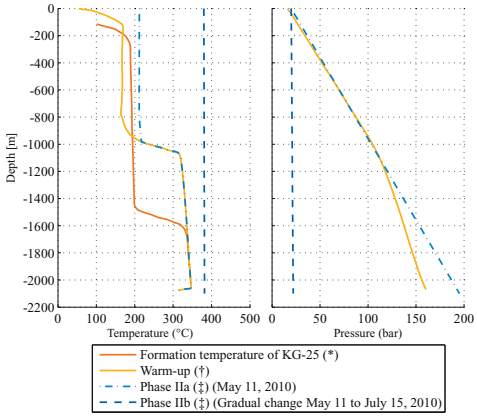

Fig. 8. Temperature and pressure loads for the modeling of phase II. * Formation temperature of KG-25 (Björnsson et al., 1990), † 8 months warm-up (Axelsson et al., 2014), ‡ Based on monitored wellhead temperature and pressure (Ingason et al., 2014).

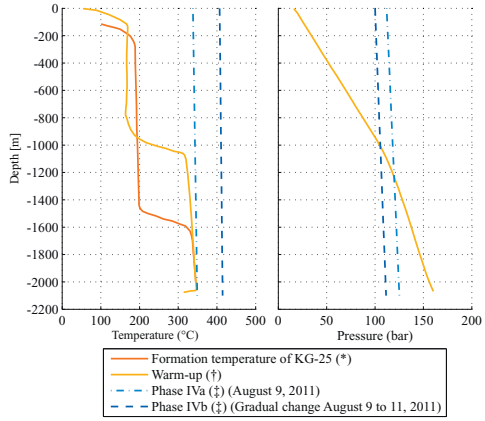

Fig. 10. Temperature and pressure loads for the modeling of phase IV. * Formation temperature of KG-25 (Björnsson et al., 1990), † 8 months warm-up (Axelsson et al., 2014), ‡ Based on monitored wellhead temperature and pressure (Ingason et al., 2014).

strain results for the production casing at 50 m depth is displayed in Fig. 14 to illustrate the buildup of plastic strain in each thermal cycle. Following the load history, the first few thermal cycles show no signs of the tensile stress reaching yield, but in all cases plastic compressive strain is produced. In the second last shut-in period of the well, the last period before quenching, plastic tensile strain is reached while the well slowly cools down. In the last thermal cycle the well is quenched and high tensile stress is formed. With further cooling of the well, the tensile stress is reduced because of contraction of the external casings.

Temperature distribution of the well during thermal recovery, discharge and quenching are shown in Figs. 15–18 . Fig. 15 shows the temperature distribution in and around the well after 7 months of thermal recovery from drilling, Figs. 16 and 17 show the temperature distribution in discharge phase V after 2 days and 11 months of discharge, respectively, and Fig. 18 shows the distribution after 8 h of quenching with cooling water. Fig. 17 also represents the hot well conditions just before quenching. Note that the *x*-axis, referring to the horizontal direction, is scaled by 1000 to 1 in order to see the casings.

Axial stress and strain results for the production casing and the anchor casing are shown in Figs. 19–30 and a summary of the results is listed in Table 3. In the figures, the results for the whole discharge history are shown in gray in the background. As the well slowly warms up during thermal recovery from drilling compressive axial stress is produced in the casings, see Figs. 19 and 20 for axial stress and strain distribution in the production casing and anchor casing, respectively. Figs. 21 and 22 show the distribution during discharge phase I. During this period the compressive stress reaches the yield point of the material both in the production casing and the anchor casing. Small strain is however produced but it is apparent that strain concentration is seen in both casings at

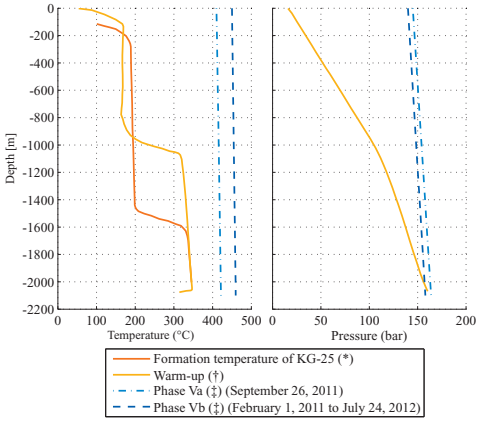

Fig. 11. Temperature and pressure loads for the modeling of phase V. * Formation temperature of KG-25 (Björnsson et al., 1990), † 8 months warm-up (Axelsson et al., 2014), ‡ Based on monitored wellhead temperature and pressure (Ingason et al., 2014).

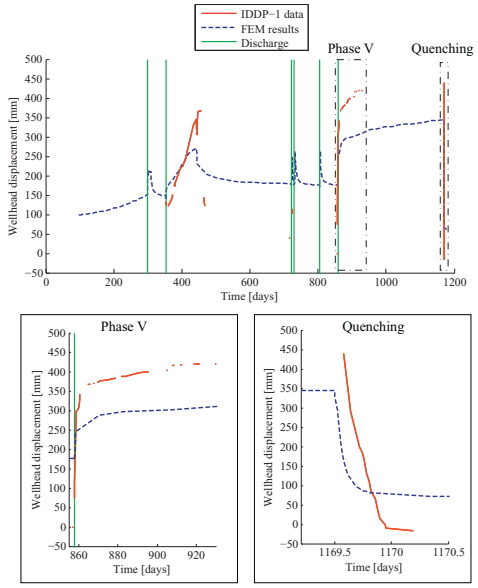

Fig. 12. Modeled and measured vertical height of the wellhead of IDDP-1. Wellhead height data is shown by courtesy of Landsvirkjun. The green lines indicate the start of each discharge phase. (For interpretation of the references to color in this figure legend, the reader is referred to the web version of the article.)

the depths of the shoe locations of the outer casings. Similarly, the thickness change of the anchor casing at 300 m depth is seen in the strain formation in the production casing. Figs. 23 and 24 show the axial stress and strain distribution after the fluid has become superheated during discharge phase II. The formation of strain continues as the casings experience high compressive forces in the succeeding phases which are shown in Figs. 25 and 26 for discharge phase IV and Figs. 27 and 28 for discharge phase V. Finally, the stress and strain results for the quenching of the well are displayed in

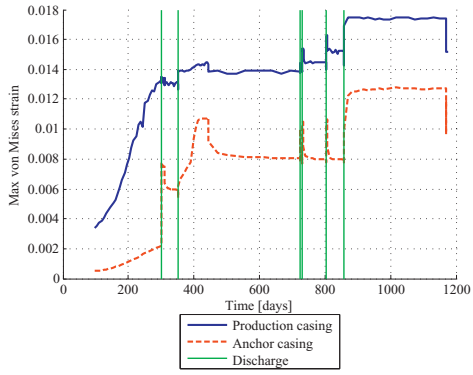

Fig. 13. Maximum von Mises strain (total strain) in the two innermost casings through the load history of the well. The green lines indicate the start of each discharge phase. (For interpretation of the references to color in this figure legend, the reader is referred to the web version of the article.)

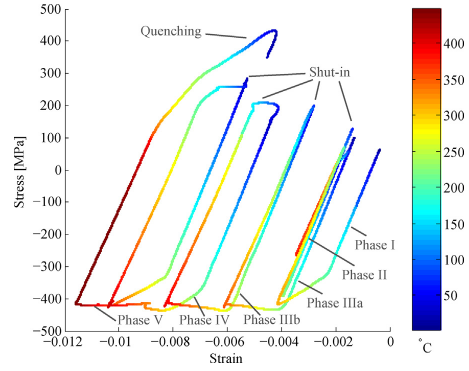

Fig. 14. Cyclic stress–strain and temperature of the production casing at 50 m depth. The load history is followed through warm-up and multiple thermal cycles.

Figs. 29 and 30 and the joint yield strength and tensile strength of the connections are plotted additionally for reference.

4. Discussion

The modeled wellhead displacement during the operation history of IDDP-1, shown in Fig. 12, shows similar trend as the measured elevation of the wellhead. The displacement is however sensitive to initial conditions, material properties, frictional properties and loads, and is therefore difficult to model with precision. The measured wellhead displacement is not recovered to its initial position during shut-ins, but interestingly the downward displacement during quenching of the well goes below the initial position of the wellhead suggesting large tensile forces due to thermal contraction of the casings.

After thermal recovery from drilling, see Fig. 15, the transient temperature distribution shows that after 7 months of warm-up, the radial thermal gradient through the casing and concrete layers is very small, with little temperature difference between casings in shallow regions of the well. Fig. 16 shows the modeled temperature distribution during discharge (phase V) where the radial thermal gradient is high after 2 days of discharge with approximately 100 °C temperature difference between the two innermost casings. The

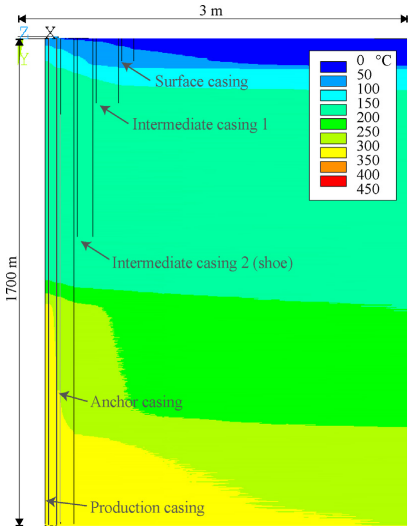

Fig. 15. Modeled temperature distribution (°C) of the well after 7 months of warm-up after drilling. The *x*-axis is scaled by 1000 to 1.

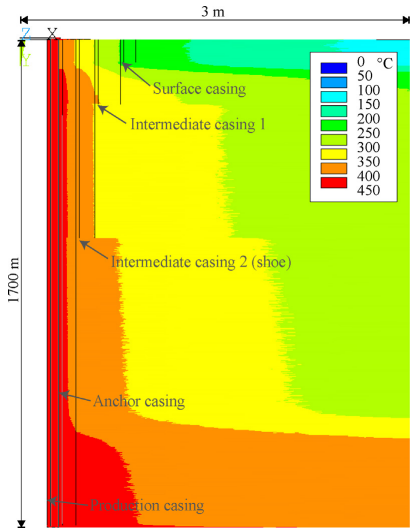

Fig. 17. Modeled temperature distribution (°C) of the well after 11 months of discharge in phase V. The *x*-axis is scaled by 1000 to 1.

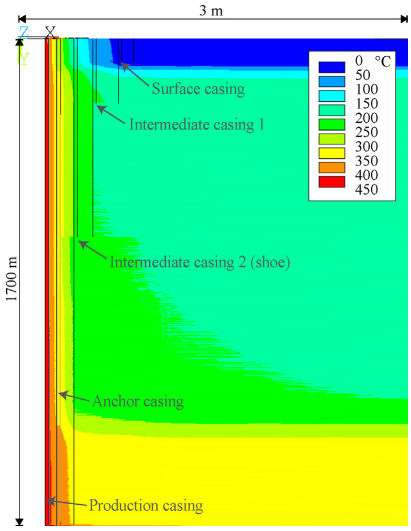

Fig. 16. Modeled temperature distribution (°C) of the well after 2 days of discharge in phase V. The *x*-axis is scaled by 1000 to 1.

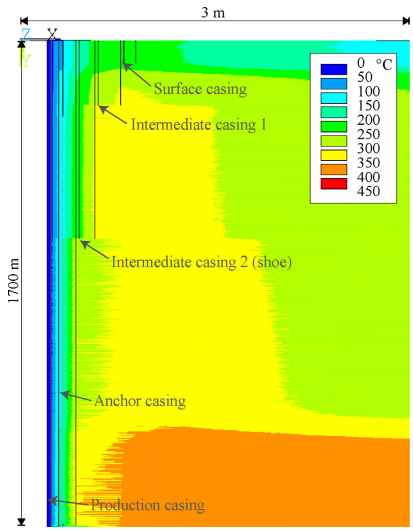

Fig. 18. Modeled temperature distribution (°C) of the well after 8 h of quenching with cold water. The *x*-axis is scaled by 1000 to 1.

thermal gradient is in contrast much lower after 11 months discharge as is shown in Fig. 17. This illustrates the demanding thermal load the production casing is subjected to during discharge. Similarly, the production casing sustains an abrupt temperature change during quenching of the well, as can be seen in Fig. 18. After 8 h of quenching, large thermal gradients still exist between casings which illustrates that for large axial strains to be less severe the quenching must be performed as slowly as possible.

The maximum von Mises strain (total strain) for the production casing and the anchor casing over the operation history of the well, see Fig. 13, illustrates how the anchor casing is protected against abrupt thermal loads but the production casing is not, assuming that the concrete in between casings is in good condition and perfectly cemented. In each thermal cycle the production casing reaches yield and forms plastic strain. Although plastic strain is also formed in the anchor casing, the effect is less pronounced due to the thermal insulation of the concrete in between casings.

The effect of neighboring casings on strain formation is clearly seen throughout the load history of the well, see Figs. 19–30. This materializes as sudden stress and strain changes with depth and

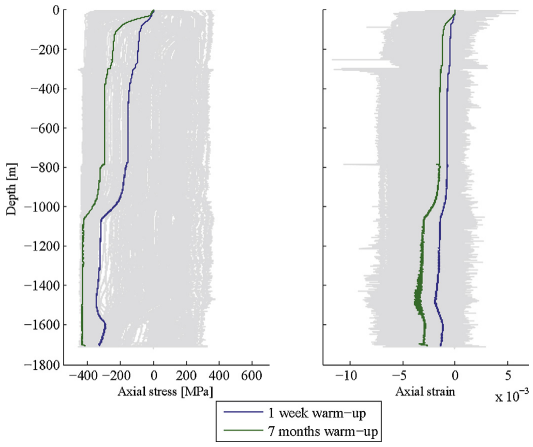

Fig. 19. Axial stress and total axial strain of the production casing, after 1 week and 7 months of warm-up.

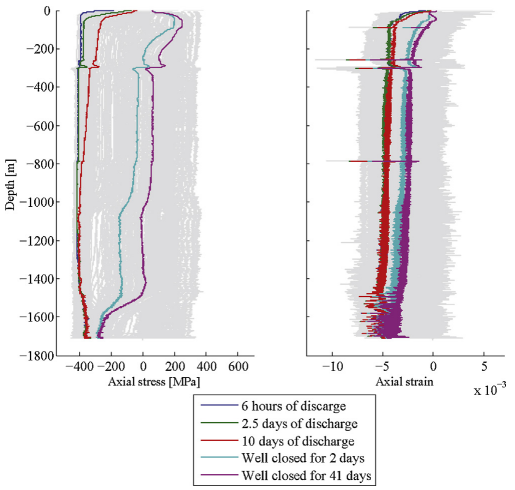

Fig. 21. Axial stress and total axial strain of the production casing in discharge phase I.

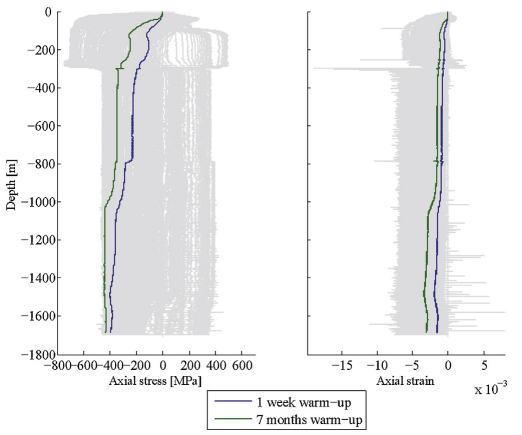

Fig. 20. Axial stress and total axial strain of the anchor casing, after 1 week and 7 months of warm-up.

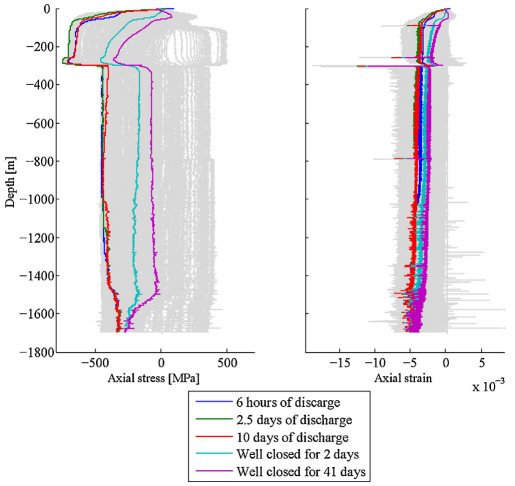

Fig. 22. Axial stress and total axial strain of the anchor casing in discharge phase I.

Table 3
Summary of structural results. Maximum wellhead pressure (P_{wh}) and temperature (T_{wh}), maximum displacement of the wellhead (d_{wh}) and maximum von Mises stress and strain results for the production casing and anchor casing during different phases of the load history.

				Production casing		Anchor casing	
	Max P_{wh} (bar)	Max T_{wh} (°C)	Max d_{wh} (mm) model (data)	Max von Mises stress [MPa]	Max von Mises strain	Max von Mises stress	Max von Mises strain
Thermal recovery	0	30	150(–)	382	0.0133	449	0.0022
Phase I	120	325	216(368)	378	0.0135	665	0.0078
Phase II	20	380	272(–)	382	0.0145	660	0.0107
Phase IIIa	105	350	246(–)	359	0.0144	542	0.0100
Phase IIIb	70	390	262(–)	374	0.0154	633	0.0105
Phase IV	112	410	265(–)	403	0.0163	636	0.0106
Phase V	145	450	345(440)	414	0.0175	627	0.0128
Quenching	0	≈10	63(−17)	384	0.0156	607	0.0127

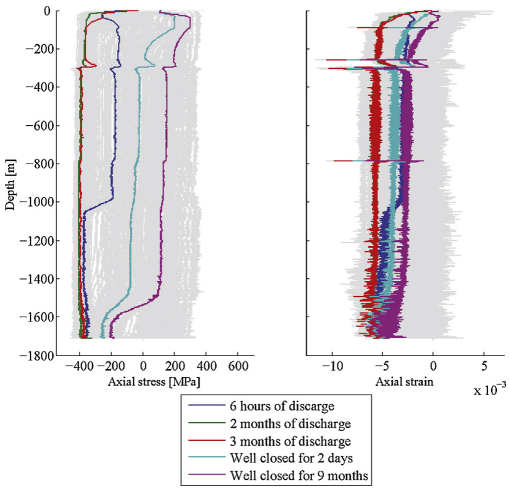

Fig. 23. Axial stress and total axial strain of the production casing in discharge phase II.

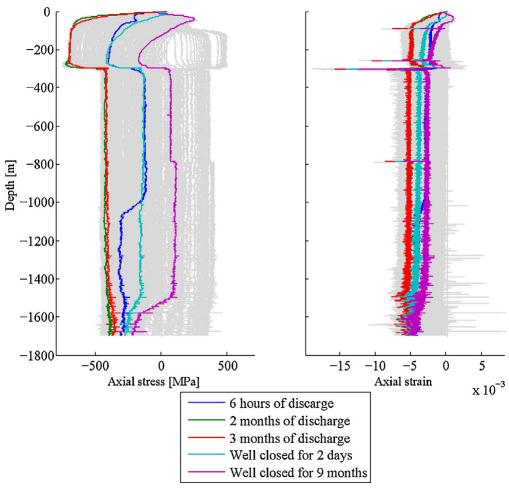

Fig. 24. Axial stress and total axial strain of the anchor casing in discharge phase II.

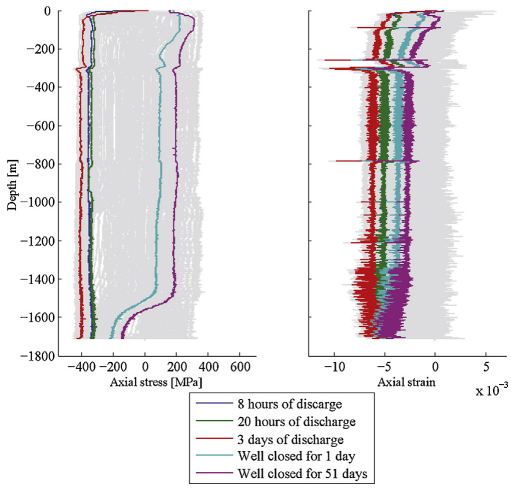

Fig. 25. Axial stress and total axial strain of the production casing in discharge phase IV.

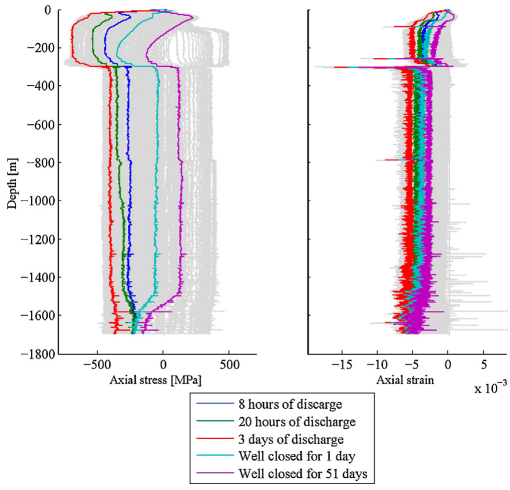

Fig. 26. Axial stress and total axial strain of the anchor casing in discharge phase IV.

is clearly observed at the locations of casing shoes of external casings. This is for example seen in Fig. 21 where the shoe of one of the intermediate casing at 785 m results in stress change in the production casing at that depth. Change in axial stress with depth is also directly connected to the temperature distribution down the well. This is clearly observed during the warm-up of the well, see Fig. 19, where the thermal load results in a thermal compressive stress which resembles the temperature load displayed in Fig. 7. The strain concentration in the production casing at a depth near 290 m, is however, caused by the thickness change in the external anchor casing at that depth. This is seen as a sharp notch in the plotted strain throughout the load history of the well. The stress and strain distribution in each casing is therefore governed by several factors, e.g. material properties, thickness changes, locations of casing shoes of neighboring casings, surface friction and change in temperature/pressure distribution down the well with time.

During discharge, see Fig. 27, the results show that the wellbore temperature change abruptly generates compressive stress in the production casing which is reduced in the shallow regions as the external casings heat up. Initially, the reverse is seen in the anchor casing, see Fig. 28, where the stress increases slowly before reaching a maximum and is then relaxed similarly when the external casings warm up. This also indicates that the casings external to the production casing are somewhat protected against abrupt temperature changes inside the wellbore, provided that cementing in between is adequate.

During quenching, see Fig. 29, the production casing which is initially in compression generates high tensile stresses. Modeling the quenching procedure in greater detail is a subject for further

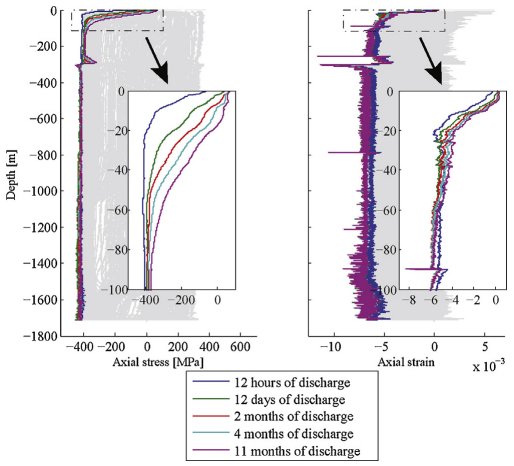

Fig. 27. Axial stress and total axial strain of the production casing in discharge phase V.

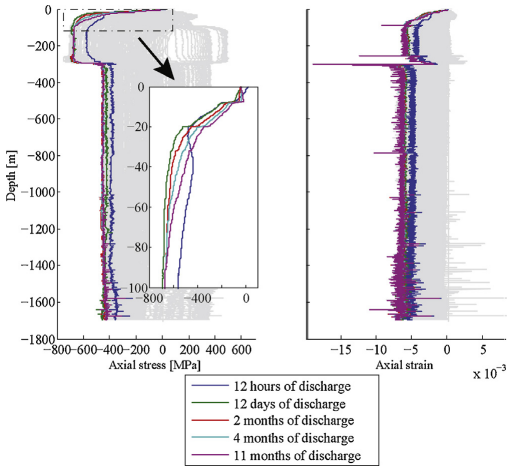

Fig. 28. Axial stress and total axial strain of the anchor casing in discharge phase V.

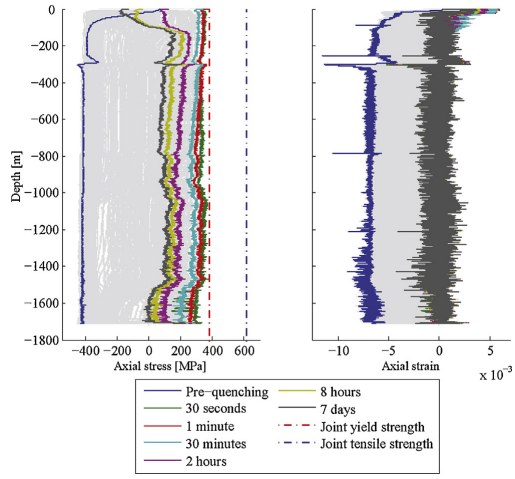

Fig. 29. Quenching. Axial stress and total axial strain of the production casing during quenching of the well.

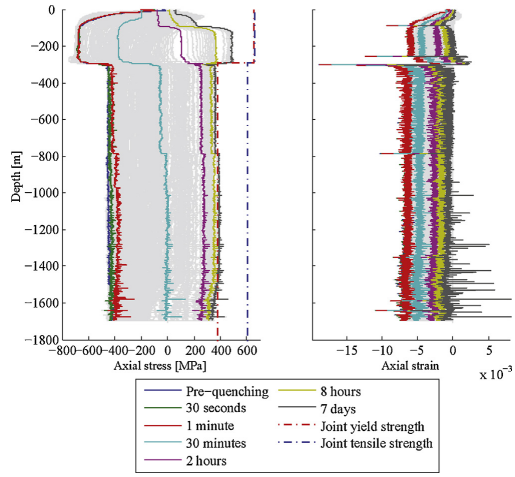

Fig. 30. Quenching. Axial stress and total axial strain of the anchor casing during quenching of the well.

analysis. A connection to a transient wellbore flow model might also be an interesting subject for further study. In the analysis, indications of the coupling ruptures that were found at depths of 356 m and 505 m are inconclusive and appear to be at arbitrary locations. There is however, an indication of the failure at 300 m, which is likely caused by a change in thickness of the external casing near that depth. Similar to the compressive stress that forms during discharges, during quenching the tensile stress in the production casing forms rapidly and the stress in the anchor casing changes slowly from compressive to tensile as the casing cools down, see Fig. 30. The tensile stresses that are produced in the anchor casing stay below the joint tensile strength of the couplings. At the transition between casing material and thickness at depth at 290 m, the tensile stress reaches the joint yield strength of the lower casing section but elsewhere the stress is lower.

Further studies might include modeling cement imperfections and analyzing the effect of production casing failures on outer casings. But failures of the production casing, e.g. coupling ruptures and collapses, would lead to increased local stresses in the outer casings. The cyclic stress and strain results show how the material behaves during the load history of the well. The predicted strain in the production casing that forms during quenching is however below the rupture strain of a new K55 material. Strength reduction due to factors such as corrosion, stress relaxation and creep, which all might have a great effect in this case are however difficult to estimate. When the well was shut-in, condensate was formed in the well. Since the shut-in periods were lasting for several weeks up to 4 months, corrosion effects such as pitting and hydrogen embrittlement might have weakened the material. Compressive stress relaxation as seen in cyclic thermal load tests by Maruyama et al. (1990) could result in higher subsequent tensile stresses than the model predicts and creep might also have greater effect on the

rupture strength of the casing than previously expected. These considerations are a subject for future studies. The results from this analysis forms a basis for further studies of casing design for deep geothermal wells.

5. Summary and conclusions

In this paper, a nonlinear finite-element model of IDDP-1 is presented and the results are compared to wellhead displacement data. The model results show that location of casing shoes and casing thickness changes affect stress and strain formations in neighboring casings and could cause local problems due to cyclic strain hardening and production of large local strains. The results illustrate that the production casing is subjected to abrupt temperature changes during the operation history and the anchor casing is protected, provided that the thermal insulation of the concrete in between is sound. The results also illustrate that after 8 h of quenching large thermal gradients still exist between casings and that slower cooling would be ideal if possible in these critical situations. The results demonstrate how the model can be used for transient load history analysis. A simpler load history can however be used to reveal structural risks during the design phase of casing programs for wells. This could involve material selection, aiding with casing program design and well operation planning, e.g. determining an adequate warm-up periods before discharges and developing a quenching scenario with the objective of minimizing stresses and strains in the casings.

Acknowledgements

This work was financially supported by the University of Iceland Research Fund, the Technology Development Fund at RANNIS – The Icelandic Centre for Research, the Innovation Center Iceland, Landsvirkjun Energy Research Fund, and GEORG – Geothermal Research Group. Their support is much appreciated. The authors would also like to thank Reykjavik Energy, HS Orka, Landsvirkjun, Iceland Drilling, Iceland GeoSurvey and Mannvit for providing data and useful information for the development of the work presented here. The authors would additionally like to thank Landsvirkjun for providing data and open discussion on the IDDP-1 well.

References

Axelsson, G., Egilson, T., Gylfadóttir, S.S., 2014. Modelling of temperature conditions near the bottom of well IDDP-1 in Krafla, Northeast Iceland. Geothermics 49, 49–57.

Björnsson, G., Steingrímsson, B., Ásgrímur Guðmundsson, 1990. Krafla – Hola KG-25 – Upphitun og upphafsástand (in Icelandic). Technical Report OS90052/JHD-30 B. Orkustofnun (National Energy Authority).

Elders, W.A., Fridleifsson, G., Bignall, G., 2012. Saga report no 9. IDDP-ICDP Workshop.

Elders, W.A., Friðleifsson, G., Pálsson, B., 2014. Iceland deep drilling project: the first well, IDDP-1, drilled into magma. Geothermics 49, 1.

Hólmgeirsson, S., Ásgrímur Guðmundsson, Pálsson, B., Árni Báasson, H., Ingason, K., þórhallsson, S., 2010. Drilling operations of the first Iceland deep drilling well (IDDP). In: Proceedings World Geothermal Congress 2010, Bali, Indonesia, 25–29 April.

Ingason, K., Kristjánsson, V., Einarsson, K., 2014. Design and development of the discharge system of IDDP-1. Geothermics 49, 58–65.

Kaldal, G.S., Jonsson, M.T., Palsson, H., Karlsdottir, S.N., 2015. Structural modeling of the casings in high temperature geothermal wells. Geothermics 55, 126–137.

Karlsdottir, S.N., Thorbjornsson, I.O., 2009. High Temperature Geothermal Wells – Center of Excellence in Iceland – Phase I: Corrosion Testing of Steel in High Temperature Geothermal Wells in Iceland. Technical Report for RANNIS (The Icelandic Centre for Research), in Icelandic.

Maruyama, K., Tsuru, E., Ogasawara, M., Inoue, Y., Peters, E.J., 1990. An experimental study of casing performance under thermal cycling conditions. SPE Drill. Eng. 5, 156–164.

Paul, J.D., Hoppe, R., Appel, F., 2016. On the Bauschinger effect in TiAl alloys. Acta Mater. 104, 101–108.

Phan, L.T., Carino, N.J., 2000. Fire performance of high strength concrete: research needs. In: Proceedings of ASCE/SEI Structures Congress 2000, Philadelphia, USA.

Pálsson, B., Hólmgeirsson, S., Guðmundsson, Bóasson, H., Ingason, K., Sverrisson, H., Thórhallsson, S., 2014. Drilling of the well IDDP-1. Geothermics 49, 23–30.

Thórhallsson, S., Pálsson, B., Hólmgeirsson, S., Ingason, K., Matthíasson, M., Bóasson, H., Sverrisson, H., 2014. Well design for the Iceland deep drilling project (IDDP). Geothermics 49, 16–22.

Paper VIII

Structural Analysis of the Casings in Deep Geothermal Wells

Gunnar Skúlason Kaldal[1,2], Magnús Þ. Jónsson[1], Halldór Pálsson[1], Sigrún Nanna Karlsdóttir[1]

[1]Faculty of Industrial Engineering, Mechanical Engineering and Computer Science, University of Iceland, Hjarðarhagi 2-6, 107 Reykjavík, Iceland
[2]ÍSOR – Iceland GeoSurvey, Grensásvegi 9, 108 Reykjavík, Iceland

Abstract

With recent increasing interest in drilling deep geothermal wells in order to produce from higher enthalpy heat sources than before, the strength of the casing becomes one of the most limiting factors. Casing failures include collapse or partial collapse (bulges) and tensile ruptures if wells are allowed to cool down or are killed by pumping water into them. Structural impact of large temperature and pressure changes remains one of the challenges to be solved for utilization of deep geothermal wells. Thermal expansion of materials, degradation of structural properties at elevated temperatures, corrosion and cyclic loads are of particular concern as well as determining how many thermal cycles casings can go through before failure occurs. A nonlinear structural finite-element model of the cased section of high temperature geothermal well is presented and discussed here. The purpose of the model is to evaluate the structural integrity of casings when subjected to large temperature and pressure loads. The model can be used further to evaluate well designs and material selections for deep geothermal wells.
Keywords: Casings, structural analysis, finite-element method, thermal loads, deep drilling

*email: gsk@isor.is

Introduction

This paper provides an overview of structural modeling of casings in high temperature geothermal wells. Structural integrity of high temperature geothermal wells is important for utilization and safety concerns on the surface. During each drilling phase, steel casings are run in hole and cemented externally, until the last phase where the production section of the well is drilled. This is done to control wells during drilling, seal off unwanted feed-zones and the last casing, the production casing, acts as a pipe allowing the geothermal fluid (water and/or steam) to flow to the surface. In most cases, a perforated liner is placed in the production section to avoid formation collapse. Above the liner is the cased section of the well, which is a layered structure of multiple cemented casings. The structure is initially relatively cold, i.e. during drilling and cementing, compared to the hot conditions during production of

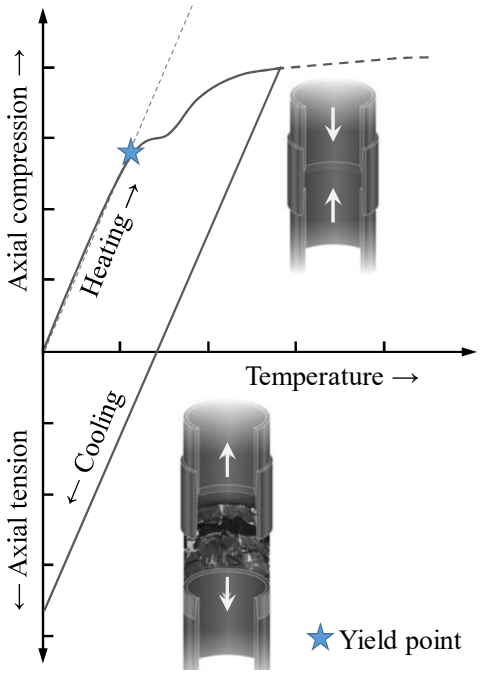

Figure 1. Concept diagram describing how plastic strain that forms in axial compression can result in axial tension during cooling. Adopted from a diagram by **(Rahman & Chilingarian, 1995)**.

(two-phase or pure) steam. As cement sets and hardens after cementing jobs for each casing, its temperature distribution down the well provides initial conditions for subsequent thermal stresses that form as the well warms up. In high-temperature geothermal wells (T>200°C at 1000 m depth) stresses which generate due to thermal expansion driven by the temperature change between an initially cold well to a producing well, typically reach beyond the yield point of the commonly used casing material, API (American Petroleum Institute) grade K55. As stresses go past the yield strength, plastic permanent strains are produced in the casings. Depending on the magnitude of these plastic strains, some wells, specially the hotter ones, cannot be cooled down again without causing casing failure. In such cases, plastic strains that build up in axial compression (hot well) lead to axial tensile load when the casing cools down again. Figure 1 illustrates this phenomenon, where plastic strains created in compression lead to high tensile stresses when the casing cools down again. Casing failure of tensile rupture of the casing normally occurs in the casing near couplings (first thread groove) or in the threads themselves. In casing design, guidelines acknowledge that axial tension leads to reduced collapse resistance of casings. However, as standards are developed for the oil & gas industry where casings are anchored at the casing shoe with cement and not cemented over their full length as in geothermal wells, failures as a result axial compressive loads are assumed to be on the form of Euler buckling (or helical buckling) where the casing string buckles laterally. Casings in geothermal wells have no means to displace laterally due to the cement support, instead high compressive stresses and strains are formed which can as with tension reduce their collapse resistance.

The Finite-Element Method (FEM) models shown in this paper have been created to evaluate stresses and strains in casings due to pressure and temperature changes in wells.

Load history of casings

Casings are cold-drawn seamless steel pipes. Thickness tolerance of such pipes is -12.5% (API, 2005), meaning that for a 9 5/8" 47 lb/ft casing that is specified with thickness of 12 mm, it may be 12 mm on one side and 10.5 mm on the other. Heat treatments are used to relieve residual stresses present in the material due to non-uniform cooling during manufacturing. Residual stresses and non-circular geometry (ovality, eccentricity and wall thickness irregularity) can significantly lower the collapse resistance of casings. Material properties, i.e. yield strength and shape of the stress-strain curve, and residual stresses also affect collapse resistance (ISO/TR, 2007).

While casings are run-in-hole, the highest axial tensile stress occurs at the topmost coupling, which essentially holds up the whole casing string before it is cemented. Buoyancy and friction between the casing, centralizers and the wellbore lower the axial force on top.

Thermal stresses form in casings as wells warm up, which magnitudes are controlled by the temperature difference ΔT at each location as well as the (time dependent) thermal gradient through the layered casing structure. The initial conditions are different between wells, and depend on formation temperature, feed zones that are closed off with cement, cooling from drilling and the time the well has been cooled. In many cases, depending on feed zones, drilling time, etc., wells heat up faster downhole as the formation temperature increases with depth. In cases where the cement sets at such temperature conditions, the highest ΔT (from cementing conditions to production) is uppermost in the well. This does however not mean that the highest compressive stresses form at the wellhead. At the surface there is freedom for displacement, both because of the design of the wellhead, if it includes an expansion spool, and due to less

restricted displacement as the surface can displace upwards. Wellheads are known to move upwards as wells warm-up, sometimes called wellhead growth. This is in some cases very evident during discharge initiation, where the temperature uppermost in the well changes quickly, whereas deeper in the well lower ΔT is seen. When drilling has been problematic and the wellbore has been cooled for a long period, ΔT can be similar at the wellhead and deeper in the well, as the cement sets before the well heats up. The positive side of higher setting temperatures is that less stresses form during production. The down side is that if cement sets at too high temperature, cooling due to further drilling can de-bond the casing from the cement as it contracts, creating a micro-annulus.

As discussed in the introduction, compressive stresses form in the casing as the well warms up and plastic strains form in the most common material used, API grade K55. Using the next higher grade L80 postpones the problem and plastic strains will occur as well. Using the specified minimum yield strength of K55 and L80, 379 MPa and 552 MPa (API, 2005), onset of plastic strains is at around 150°C and 200°C, for K55 and L80, respectively (using a thermal expansion coefficient of 13μm/(m°C) and Young's modulus of 205 GPa). This however does not tell the whole story as stress-strain characteristics can influence collapse resistance. For a work hardening material such as K55 it has been shown that the API collapse equation applies only for small axial tensile stresses and that the measured collapse resistance is significantly higher than those predicted by the API equation (Maruyama, et al., 1990). They show that due to the work hardening characteristics of grade K55 casing, it may be superior to higher-grade casing for thermal well service where high residual axial tensile stresses may be present.

Field study and FEM analysis

In this study, wellhead displacement monitoring during discharge initiation is used to validate a FEM model of the cased section of a high-temperature geothermal well (Kaldal, et al., 2015). Figure 2 shows temperature and elevation measurement locations on the wellhead of well HE-46, located in Sleggjubeinsdalur near Hellisheiði power plant.

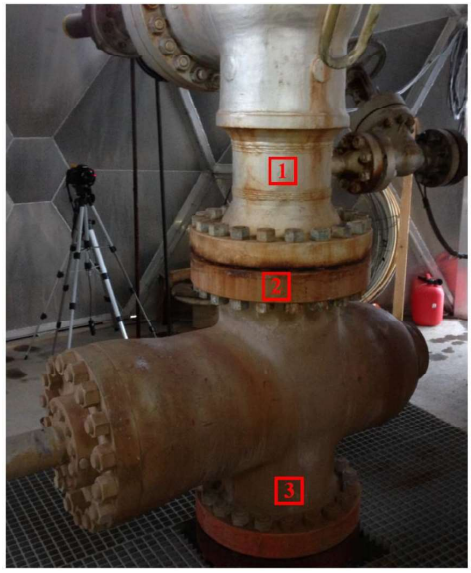

Figure 2. Locations for temperature measurements during discharge initiation of well HE-46, located in Sleggjubeinsdalur near Hellisheiði power plant. Location [2] shows where elevation measurements were taken for the wellhead.

The ANSYS Parametric Design Language (APDL) is used to construct the models. Included are temperature dependent material properties, including stress-strain curves for casing materials, for determining formation of plastic strain, and thermal expansion coefficients. Other material properties include; Young's modulus, Poisson's ratio, density, thermal conductivity, specific heat and compressive strength of cement. Kinematic hardening material model is used for the casings and the compressive strength of cement is included by using a bi-linear material model.

Boundary conditions of the model are at the rock formation outer boundary and bottom where displacements are constrained. Initial conditions of the rock formation is the

estimated formation temperature and cementing temperature distribution for all casings, which need to be defined for each specific case. Transient thermal analyses include load steps such as cooling due to drilling, thermal recovery where wells heat-up over a period of weeks to months, discharge initiation, discharge and well shut-in. Initial conditions for the structural modeling are the formation overburden pressure and residual axial load in casings from casing run-in. Transient thermal results are then used as temperature load in the structural analysis, where displacements, stresses and strains (elastic and permanent plastic strain) are analyzed.

Results

Wellhead displacement

Wellhead measurements, i.e. temperature, pressure and elevation changes during discharge initiation were taken for several wells including the case studied here, well HE-46.

Temperature changes, shown in Figure 3, are similar for two separate discharges, conducted in years 2011 and 2013. Wellhead pressure, measured for the 2011 discharge, is initially 37.5 bar-g and after discharge initiation (at 13:16 o'clock on graph), it lowers and stabilizes at 18 bar-g. In 2013 the wellhead pressure was initially 48 bar and after discharge initiation it stabilized at 16 bar-g.

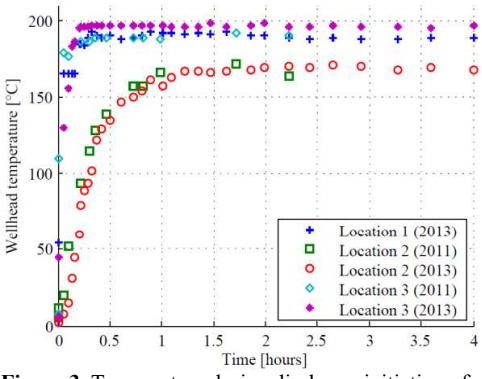

Figure 3. Temperature during discharge initiation of well HE-46, measurement locations are shown in Figure 2 **(Kaldal, et al., 2012) (Kaldal, et al., 2015)**.

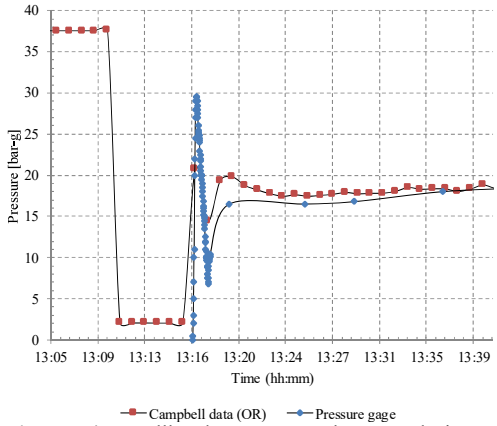

Figure 4. Wellhead pressure changes during discharge initiation (well opened at time 13:16). Campbell data (taken at 1 min intervals) shows initial pressure of 37.5 bar-g. Note that lowering in pressure in Campell data before discharge is due to closing of control valve and both pressure gauges are behind it **(Kaldal, et al., 2012) (Kaldal, et al., 2015)**.

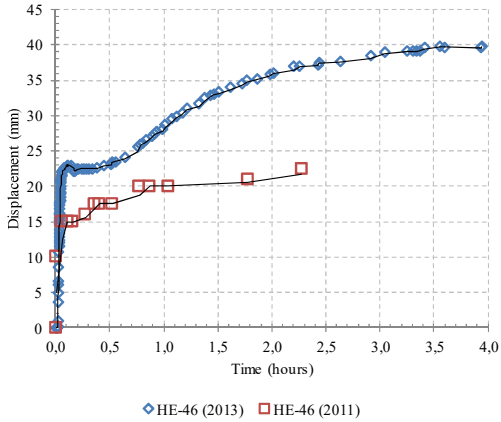

Figure 5. Measured displacement of the wellhead of two separate discharges of well HE-46 in years 2011 and 2013 **(Kaldal, et al., 2012) (Kaldal, et al., 2015)**.

Measured wellhead displacements for the two separate discharges, shown in Figure 5, differ by 15 mm after 2 h of discharge. In 2013, wellhead displacement measured 37 mm and in 2011, it was 22 mm, in both cases after 2 h of discharge.

DOI: 10.3384/ecp17138391

FEM results

During installation while casings are run in hole, wells are kept full of water or mud and the casing is filled with water. Depending on the situation, a buoyancy force and friction counteracts the casing's self weight. The largest tensile forces should occur at the top of the casing that hangs in the well. A buttress-threaded connection (BTC) is modeled. Assuming no buoyancy or friction, i.e. casing hanging in air, stresses forms in the threads of the connections as is shown in Figure 6.

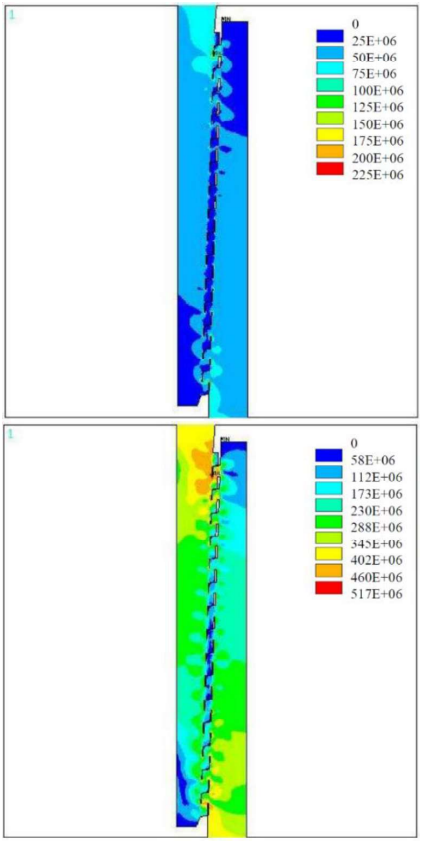

Figure 6. Von Mises stress (Pa) of buttress threaded connection (BTC) during installation assuming 700 m (top) and 5000 m (bottom) casing hanging from the connection in free in air. For API K55 grade casings the minimum yield strength is 379 MPa **(API, 2005)**.

Two cases are taken, conventional 700 m casing and extreme 5000 m casing. assuming 9 5/8" 47 lb/ft casing. In the former, the stresses are below yield of any API casing grade, but for the latter, stresses above yield occur in the area of the casing where the first threads are located. This implies a risk zone of casing failure due to axial tension.

After drilling, and warm-up, wells are flow tested. A simulation of flow test of well HE-46 results in wellhead displacement of 30 mm after 2 hours of discharge, whereas the measured value was at 36 mm (Figure 7). The modeled wellhead displacement, shown in Figure 8, shows that the production casing slides slightly inside the wellhead due to thermal expansion.

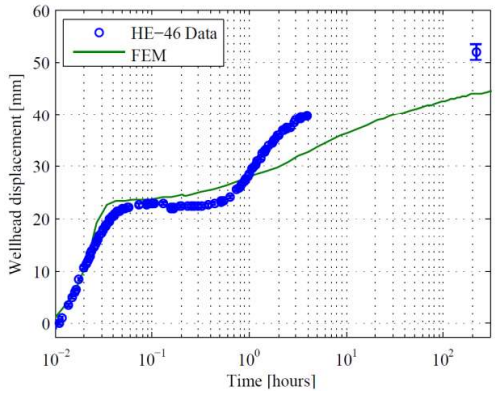

Figure 7. Measured displacement during discharge (2013 data) and modeled displacement in green **(Kaldal, et al., 2015)**.

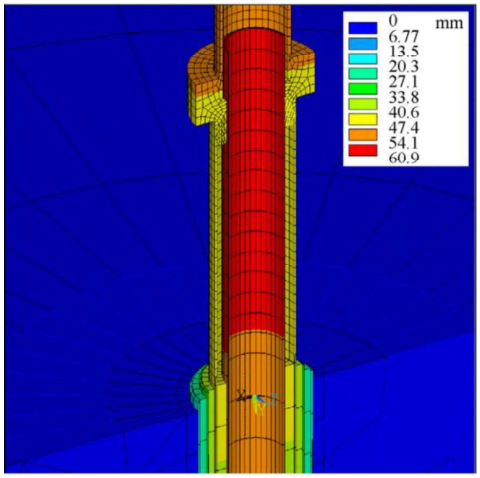

Figure 8. Modeled wellhead displacement due to thermal expansion of casings, also shown in Figure 7 **(Kaldal, et al., 2015)**.

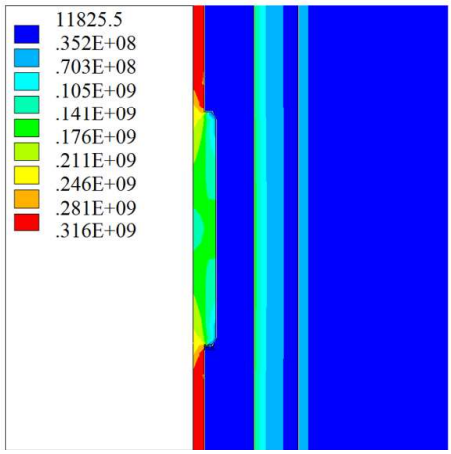

Figure 9. Modeling of casings during discharge shows high compressive stresses forming near couplings, which anchor the casing in the cement **(Kaldal, et al., 2015)**.

Deeper in the well, where the casings are more constrained than at the surface, discharge initiation results in compressive stresses forming due to thermal expansion as the well heats up. Figure 9 shows compressive stresses in the production casing near a simplified connection, illustrating how the casing is anchored at the couplings in the cement. In this case, the treads are not modeled and therefore lower stresses are seen in the coupling.

Modeling shows high stresses forming in the cement at these anchoring locations as the production expands. Figure 10 shows modeling of stresses near the uppermost coupling of the production casing as it displaces upwards. Stresses above the compressive strength (27 MPa) of the cement occurs at the top of the coupling. After the compressive strength is reached, the cement deforms according to its defined bi-linear material curve, explaining higher stresses.

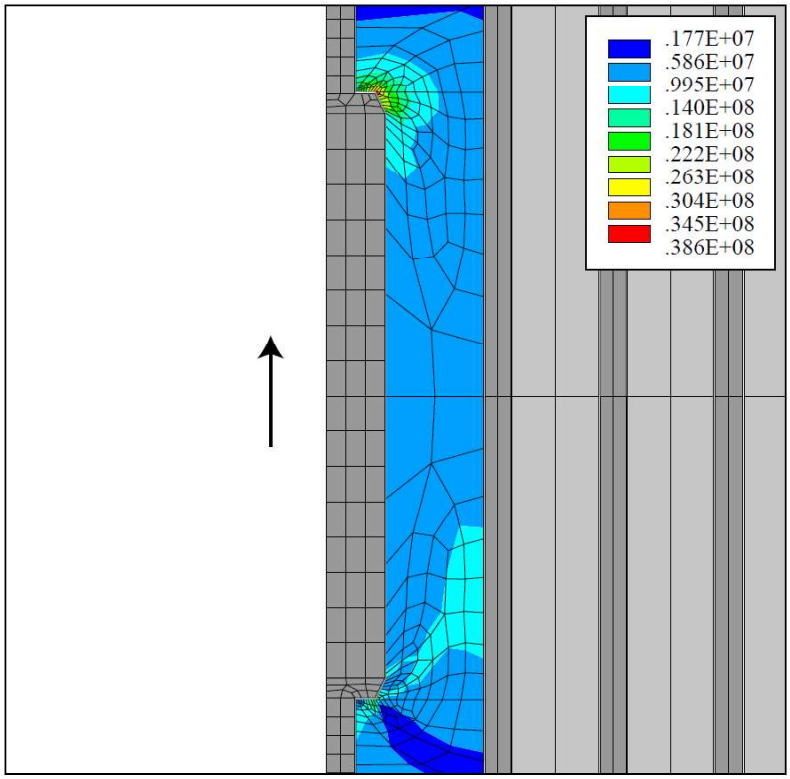

Figure 10. As wells heat up, high stresses develop in cement near the couplings that anchor the thermally expanding production casing in the cement (casings and simplified coupling shown in dark gray and external concrete shown in gray).

Modeling of casing collapse due to annular pressure, i.e. due to expansion of water in cement/annulus during discharge, shows that cement support has vital effect on the casing's collapse form (Figure 11). Casings without cement support collapse completely, but with the support the collapse is less severe. A small defect is included on the external surface of the casing for introducing instability to the model to allow buckling. Figure 12 shows that the collapse resistance of the un-cemented casing is much less than that of the cemented casing.

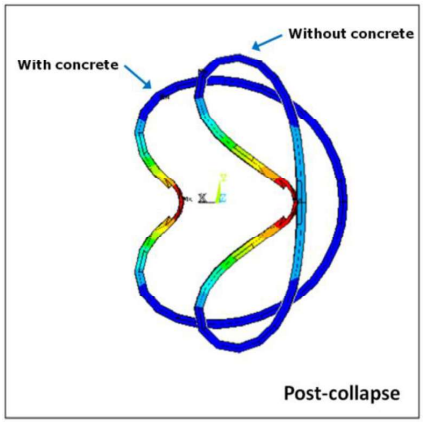

Figure 11. Collapse form of casing with and without external cement structural support **(Kaldal, et al., 2013)**.

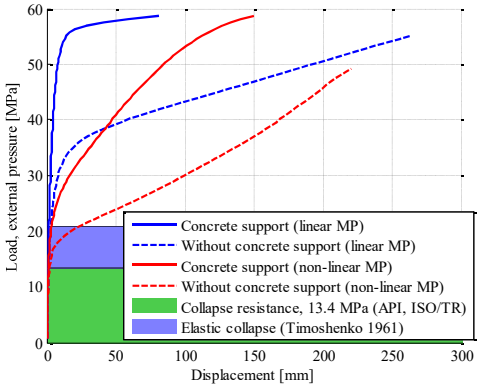

Figure 12. Modeled collapse of casings shows increased collapse resistance with cement structural support **(Kaldal, et al., 2013)**.

Discussion

Measurements of wellhead displacement during discharge initiation was used to validate results from a FEM model of the cased section of a high-temperature geothermal well. Although temperature monitoring of well HE-46 showed similar values, two separate discharges (two years apart) show different outcome in wellhead displacement. The cause of this unclear, but many factors could influence the displacement, e.g. T and P wellbore conditions can be different although wellhead conditions are similar, constraints of the wellhead might be different as two years are between measurements, the wellhead might be less constrained in the latter case due to cement cracking near the top.

In FEM analysis of threaded casing/coupling connection, the highest stresses occur in the area of the casing where the first threads are located. Casing failures of tensile ruptures have been seen at this location in wells that were quenched by pumping cold water into them. In another case, in well IDDP-1 in Iceland, where premium connections were used, the threads of the casing were swept off due to high shear force in the threads.

The models show that the casings are anchored at the couplings that stand out into the cement. Therefore, higher stresses are seen in the cement nearby couplings.

According to the FEM results, collapse resistance of casings increases when cement is present in the annulus, and the collapse form is less severe than for non-cemented casings, that completely collapse together.

Conclusions

Nonlinear FEM structural modeling of casings in high-temperature geothermal wells was presented. As most wells experience temperature change that leads to thermal stresses above the yield strength of casing materials commonly used, API grades K55, L80 and T95, plasticity needs to be considered. This is addressed by

DOI: 10.3384/ecp17138391

defining nonlinear material stress-strain curves, and using multilinear kinematic hardening material model. Modeling such as this requires knowledge about the structure, its initial conditions and loads in the form of temperature and pressure changes. Load history is therefore important, to fully understand the structure's response to loads. For drilling deeper wells to challenging pressures and temperatures and assuring a lasting well, the structural design needs to be carefully considered to include all aspects of the design. Including material challenges of strength reduction at elevated temperatures, thermal expansion, corrosion and embrittlement, wellhead pressure class. Modeling such as shown here provides an excellent tool for evaluating stresses and strains for future well designs.

Acknowledgement

This PhD work was financially supported by the University of Iceland research fund, the Technology Development Fund at RANNIS - The Icelandic Centre for Research, the Innovation Center Iceland, Landsvirkjun Energy Research Fund, and GEORG - Geothermal Research Group. Their support is greatly appreciated. The authors would like to thank Reykjavik Energy, HS Orka, Landsvirkjun, Iceland Drilling, ÍSOR - Iceland GeoSurvey, Mannvit and the Innovation Center Iceland for providing data and useful discussion and information for the work presented here.

References

API, 2005. *API Standard 5CT (ISO 11960:2004) Specification for Casing and Tubing.* 8th ed. Washington: American Petroleum Institute.

ISO/TR, 2007. *ISO/TR 10400, Petroleum and natural gas industries - equations and calculations for the properties of casing, tubing, drill pipe and line pipe used as casing or tubing.* Geneva: ISO copyright office.

Kaldal, G. S., Jonsson, M. T., Palsson, H. & Karlsdottir, S. N., 2012. *Thermal and Structural Analysis of the Casings in a High Temperature Geothermal Well During Discharge.* s.l., Thirty-Seventh Workshop on Geothermal Reservoir Engineering, Stanford University, Stanford, California, January 30 - February 1, 2012.

Kaldal, G. S., Jonsson, M. T., Palsson, H. & Karlsdottir, S. N., 2013. *Collapse analysis of the casing in high temperature geothermal wells.* Stanford, California, s.n.

Kaldal, G. S., Jonsson, M. T., Palsson, H. & Karlsdottir, S. N., 2015. *Structural Analysis of Casings in High Temperature Geothermal Wells in Iceland.* Melbourne, Australia, World Geothermal Congress 2015.

Kaldal, G. S., Jonsson, M. T., Palsson, H. & Karlsdottir, S. N., 2015. Structural modeling of the casings in high temperature geothermal wells. *Geothermics,* Volume 55, pp. 126-137.

Kaldal, G. S., Jonsson, M. T., Palsson, H. & Karlsdottir, S. N., 2016. Structural modeling of the casings in the IDDP-1 well: Load history analysis. *Geothermics,* pp. 1-11.

Maruyama, K. et al., 1990. An Experimental Study of Casing Performance Under Thermal Cycling Conditions. *SPE,* pp. 156-164.

Rahman, S. S. & Chilingarian, G. V., 1995. *Casing design theory and practice.* Amsterdam - Lausanne - New York - Oxford - Shannon - Tokyo: Elsevier.